The Prediction of Coarse Aggregate Performance by Micro-Deval and Other Soundness, Strength, and Intrinsic Particle Property Tests

by

Alexander Paul Lang, B.S.

Thesis

Presented to the Faculty of the Graduate School of

The University of Texas at Austin

in Partial Fulfillment

of the Requirements

for the Degree of

Master of Science in Engineering

The University of Texas at Austin

May 2006

The Prediction of Coarse Aggregate Performance by Micro-Deval and Other Soundness, Strength, and Intrinsic Particle Property Tests

Approved by
Supervising Committee:

David W. Fowler

John J. Allen

Dedication

To my friends and family.

Acknowledgements

I would like to Dr. David Fowler and Dr. John Allen to presenting me with an opportunity to participate in this research project. Their continuous guidance and advice over the course of the project proved crucial to its successful progress and completion.

Additionally, I would like to express my gratitude to Peter Range for his continuous hard work and dedication, which made the successful and timely completion of work on this project possible.

Without the help of highly skilled individuals working at the Materials Testing Laboratory at the Pickle Research Center, this research would not have been possible. Therefore, I would like to thank Mike Rung, David Whitney, and Kerry Rothenbach for their willingness to share technical expertise related to test setup and execution. In addition, I would like to thank Arnoud Thibonnier and Rachel Lute, who help carry out the necessary testing.

Furthermore, I would like to express my gratitude to all DOT representatives who contributed their valuable time and knowledge in determining field performance information. In particular, I would like to thank Michael Crenshaw and Texas Department of Transportation for sharing their technical expertise as well as the use of their testing equipment, as well as Chris Rogers of Ontario Department of Transportation for their invaluable guidance and advice.

Finally, I would like to thank my family for their support and assistance without which this would not have been possible.

April 28, 2006

Abstract

The Prediction of Coarse Aggregate Performance by Micro-Deval and Other Soundness, Strength, and Intrinsic Particle Property Tests

Alexander Paul Lang, M.S.E.

The University of Texas at Austin, 2006

Supervisor: David W. Fowler

This research project concentrated on determining whether or not a correlation existed between laboratory aggregate tests and observed aggregate field performance. For this purpose, aggregate samples were collected from the majority of the U.S. states as well as several Canadian provinces and subjected to a variety of strength, soundness, and intrinsic particle property tests. Additionally, performance data on the aggregates was obtained by contacting multiple DOT's where aggregates were in use in several categories – hot-mix asphalt, portland cement concrete, base course, and open-graded friction course. Numerical and qualitative analyses were performed to evaluate the success of separating good performers from fair and poor performers using the micro-Deval test alone as well as the micro-Deval test combined with another test. Furthermore, attempts were made to determine if a correlation exists between any two tests.

Table of Contents

List of Tables

List of Figures

Chapter 1: Introduction

1.1 NECESSITY OF PROJECT

As the supply of high quality aggregates diminishes, the need to accurately distinguish between poor-performing aggregates and good-performing aggregates is growing at a highly increasing pace. Therefore, a test or a combination of several tests is needed to accurately qualify an aggregate within its intended usage environment. As the result, numerous studies have been performed by various transportation agencies within the United States as well as Canada to evaluate the effectiveness of micro-Deval in correctly identifying field performance of various aggregates.

The published results thus far have been mixed – several agencies showed that micro-Deval is an excellent performance predictor while others found no such conclusions could be drawn. Since the transportation industry, which heavily relies on aggregates for road construction, is vital to a country's economic growth and prosperity, a clear need exists to evaluate the effectiveness of micro-Deval as a performance predictor. Furthermore, if micro-Deval is determined to be a good qualification test, limits on the losses should be determined as well. Thus, a comprehensive international study is necessary to accomplish the above objectives.

1.2 PRIMARY PROJECT OBJECTIVES

International Center for Aggregate Research (ICAR) has initiated ICAR Project 507 to evaluate the effectiveness of micro-Deval in predicting aggregate field performance. Furthermore, the project strives to determine if better performance prediction is possible using micro-Deval in combination with another test. To

accomplish these tasks, a suite of strength and soundness tests was carried out. While the primary goal is to study micro-Deval and micro-Deval with another test combinations, investigations will be carried out on all two-test combinations of tests conducted during this research project to determine if another two-test combination would be able to predict aggregate performance better. Finally, correlations will be studied to determine how well one test results can be used to predict another test result, if at all possible.

1.3 SCOPE OF THE PROJECT

To ensure national acceptance of the research results, a comprehensive suite of aggregates was necessary to obtain. To accomplish this task, all departments of transportation within the United States as well as all Canadian provinces were contacted to participate in the study by providing aggregates and their observed field performance data. The vast majority responded, resulting in 117 sources representing various mineralogical and geological spectrums. More importantly, however, attempts were made to ensure sufficient number of good-performing aggregates as well as poor-performing aggregates to produce meaningful results.

Upon reception of aggregates at the Pickle Research Center at the University of Texas at Austin, the following tests were performed on all sources according to current ASTM and AASHTO specifications: micro-Deval, magnesium sulfate soundness, Canadian freeze-thaw soundness, L.A. abrasion, aggregate crushing value, aggregate crushing value (saturated, surface-dry), absorption, specific gravity (bulk, saturated surface-dry, apparent), particle shape factor determination, and percent fractured. Appropriate departments of transportation (DOT's) were then contacted to obtain field performance information within the following major uses: hot-mix asphalt, Portland cement concrete, base course, and open-graded friction course. Qualitative and

quantitative analyses were then performed to evaluate how well micro-Deval as well as various two-test combinations can predict field performance within each application. Finally, tests correlations were studied using all aggregates regardless of aggregate performance in the field.

Chapter 2: Performance Analysis for Hot-Mix Asphalt Aggregates

2.1 Success Rate Comparison of Individual Tests

Literature review indicated that micro-Deval has proven to be a good predictor of performance. To test this assertion, performance graphs were created and are included in the Appendix A, where the performance of aggregates was divided into three categories - good, fair, and poor. The following sections will analyze the results by computing how well the micro-Deval test can separate the good performances from the fair and poor performers compared to other tests carried out during this research project. Both qualitative and quantitative analysis will be carried out. Additionally, conclusions will be drawn on whether or not micro-Deval in combination with another test can improve the overall success rate of the prediction.

Figure 2.1 represents the performance spread of all aggregates used in hot-mix

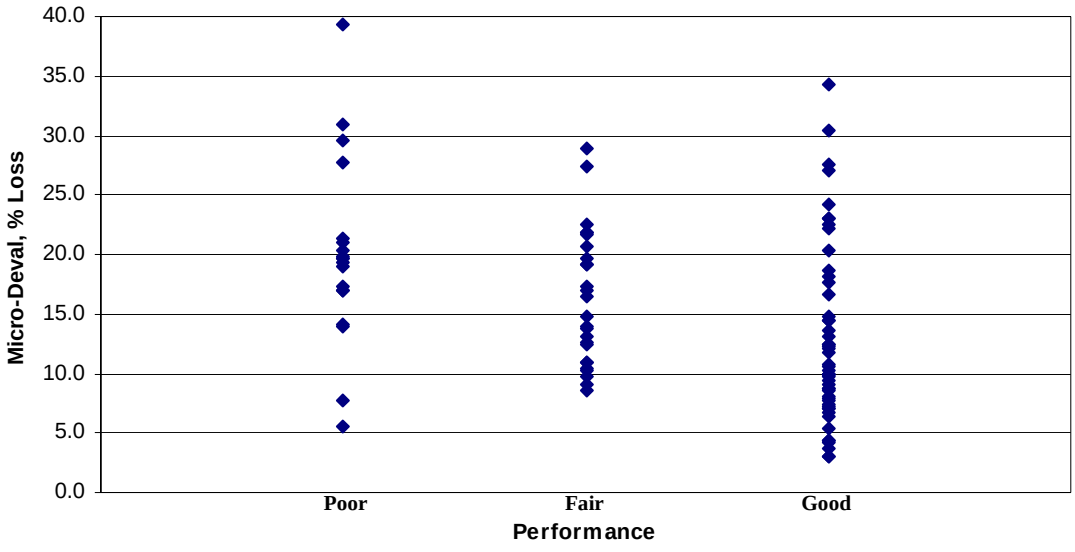

Figure 2.1: Micro-Deval vs. Performance

asphalt and tested using micro-Deval. As the plot demonstrates, all values lie below 40% micro-Deval loss. There is considerable scatter within each category. However, higher densities are observed between 5 and 15% for good performers, 9 and 15% for fair performers, and 17 to 22% for poor performers. To test how well micro-Deval can separate good performers from fair and poor aggregates, a micro-Deval threshold value was varied in Microsoft Excel 2003, with correct percentage predictions computed for each trial value for good, fair, and poor aggregates. A weighted percentage of the three was computed as well to see how good the prediction is overall. Table 2.1 provides the key values to demonstrate how the overall percentage first increases and then decreases

Table 2.1: Micro-Deval Success Rate

TRIAL NUMBER	MD Value	GOOD	FAIR	POOR	OVERALL
1	7%	17%	100%	95%	55%
2	8%	31%	100%	90%	61%
3	11%	54%	73%	90%	66%
4	12%	56%	73%	90%	67%
5	13%	63%	65%	90%	69%
6	14%	67%	54%	85%	67%
7	17%	75%	42%	70%	65%
8	18%	77%	38%	65%	64%
9	20%	81%	27%	40%	58%
10	21%	83%	23%	30%	56%

as the micro-Deval threshold value is increased. Thus, it can be concluded that micro-Deval alone can separate the good aggregates from the fair and poor sources with the maximum overall success rate of 69%.

Magnesium sulfate testing was carried out in an attempt to measure the aggregates' resistances to freeze-thaw cycles. Figure 2.2 demonstrates the results when performance is plotted against test values for all aggregates used in hot-mix asphalt.

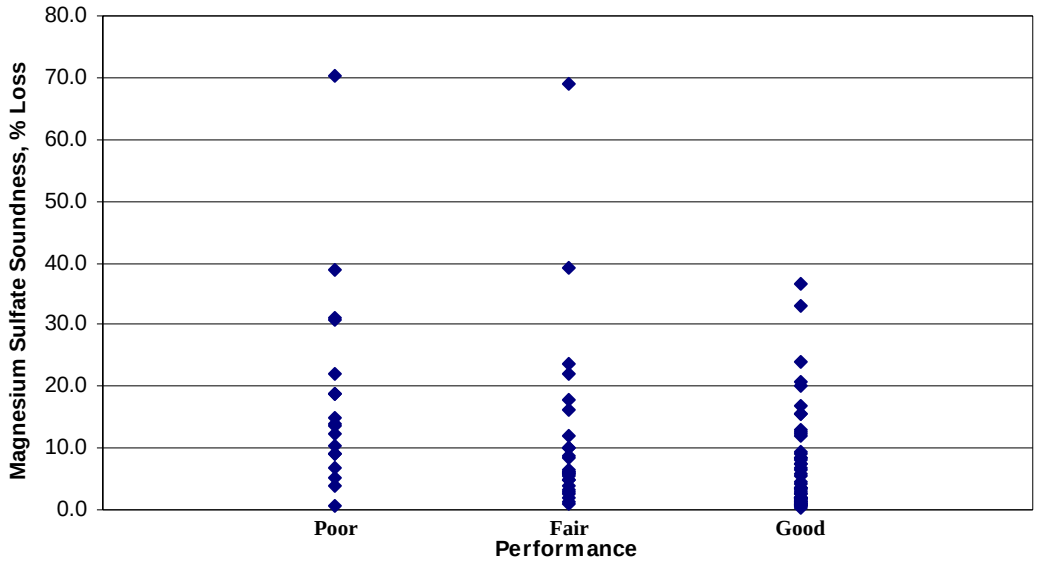

Figure 2.2: Magnesium Sulfate Soundness vs. Performance

As the figure demonstrates, considerable scatter is present within each performance category. Such behavior is not unexpected since large variations in test results were observed within each source during magnesium sulfate testing. Generally, all good performers fall below the 40% loss mark with considerably higher point density in the 0 to 10% range. Fair performers are more widely spread out between losses of 0 and 70% with noticeably higher point density in the 0 to 7.5% range. Poor performers are even more widely spread out between losses of 0 and 70%, but the region with higher point density has moved up to approximately 10 to 15%. Table 2.2 provides a summary of quantitative analysis that was performed to assess the success rate of the test. As the table demonstrates, the highest overall success rate achieved is 64%, which is lower that that achieved by micro-Deval test alone.

Table 2.2: MSS Success Rate					
TRIAL NUMBER	MSS Value	GOOD	FAIR	POOR	OVERALL
1	2%	35%	88%	90%	60%
2	4%	52%	73%	85%	64%
3	8%	67%	42%	75%	62%
4	10%	77%	27%	65%	61%
5	12%	79%	23%	60%	60%
6	16%	88%	23%	40%	61%
7	20%	92%	15%	30%	59%
8	24%	96%	8%	25%	58%
9	34%	98%	8%	15%	57%
10	40%	100%	4%	10%	56%

L.A. abrasion values were then analyzed, and its performance graph is shown in Figure 2.3. Once again, considerable scatter is present within each category. Higher

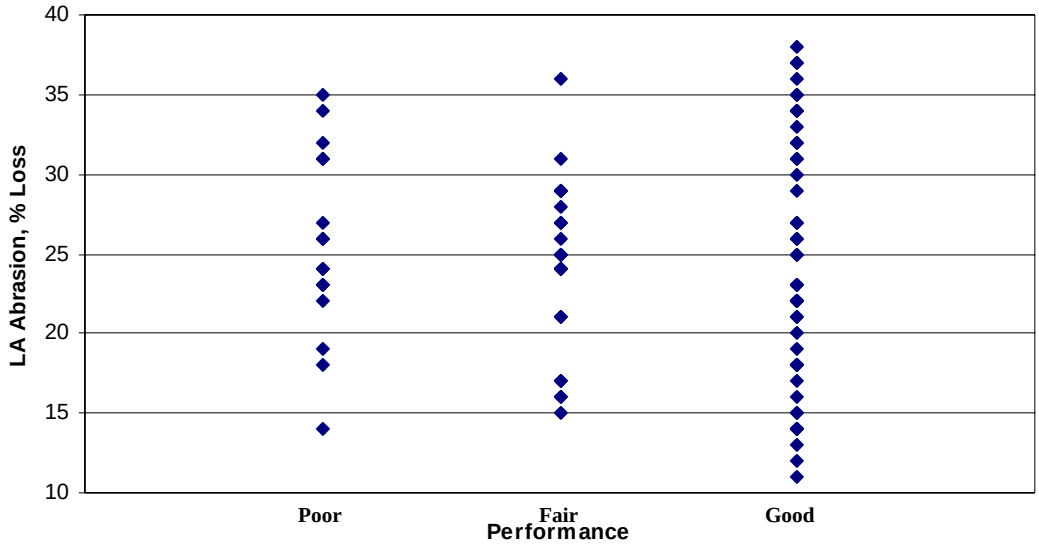

Figure 2.3: L.A. Abrasion vs. Performance

densities are observed for fair performers between 19 and 28% and for poor performers between 22 and 23%. Once again, Microsoft Excel 2003 was utilized to test the entire

L.A. abrasion loss range to observe how the overall success percentage changes as the threshold value is slowly increased. Key points are shown in Table 2.3 to demonstrate

Table 2.3: LAA Success Rate

TRIAL NUMBER	LAA Value	GOOD	FAIR	POOR	OVERALL
1	12%	4%	100%	100%	49%
2	14%	13%	100%	95%	53%
3	19%	31%	81%	85%	55%
4	20%	33%	81%	85%	56%
5	22%	46%	73%	80%	60%
6	23%	52%	73%	70%	61%
7	24%	52%	58%	60%	55%
8	25%	56%	46%	60%	54%
9	28%	63%	31%	45%	51%
10	29%	65%	19%	45%	49%

the progression behavior - the success rate is first observed to increase and then decrease. The maximum success percentage is observed at a value of 61% for the L.A. abrasion loss of 23%. Thus, it can be concluded that the L.A. abrasion test is less accurate in correctly separating the aggregates than the micro-Deval test.

Literature review indicated that the Canadian freeze-thaw test should provide good prediction performance. Figure 2.4 provides the performance separation graph for all aggregates tested in this research project. It should be noted that all aggregates suffered relatively small losses, with a maximum of 15% suffered by a good-performing material. Scattering of data is observed for each performance category, but greater densities can be observed between 1 and 4% for good performers, 1.5 and 3.5% for fair performers, and 6 and 7.5% for poor performers.

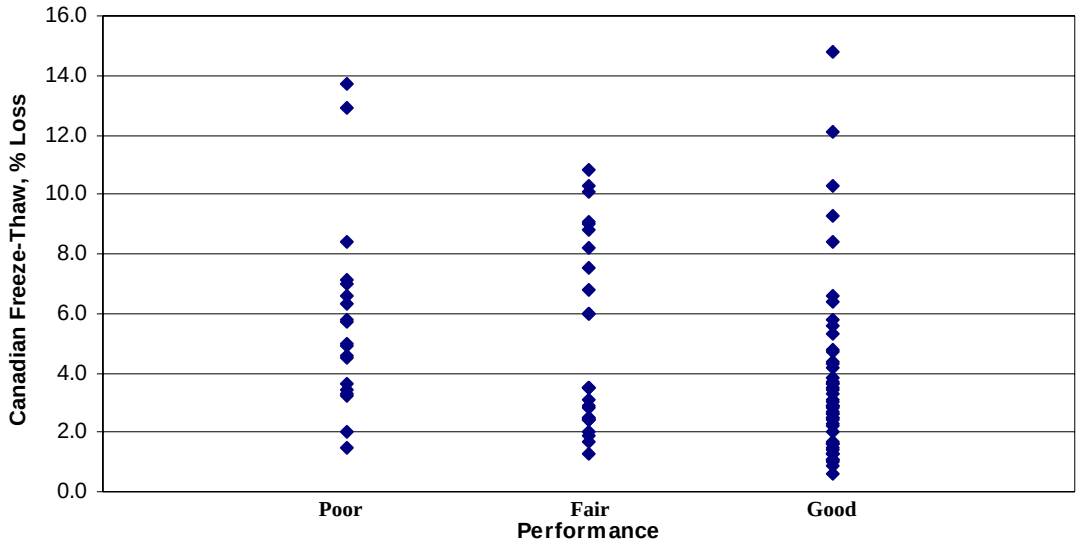

Figure 2.4: Canadian Freeze-Thaw Soundness vs. Performance

To quantitatively assess the success rate of the test's prediction, Microsoft Excel 2003 was utilized as before by varying the loss value for the entire range in one percent increments. Table 2.4 shows the key points to demonstrate how the overall percentage

Table 2.4: CFT Success Rate

TRIAL NUMBER	CFT Value	GOOD	FAIR	POOR	OVERALL
1	1%	6%	100%	100%	50%
2	2%	31%	85%	90%	57%
3	3%	56%	58%	90%	63%
4	5%	83%	42%	50%	65%
5	6%	87%	35%	40%	63%
6	7%	90%	31%	25%	61%
7	8%	90%	27%	20%	59%
8	10%	94%	12%	15%	56%
9	11%	96%	0%	15%	54%
10	14%	98%	0%	5%	53%

first increases and then decreases as we increase the test loss value. The peak overall success rate is 65%, and it is attained at the Canadian freeze-thaw loss value of 5%. Hence, it can be concluded that while the Canadian freeze-thaw test is a better predictor of performance than the L.A. abrasion test, it is nonetheless worse than the micro-Deval test.

Aggregate crushing value test measures the strength of the material as it is subjected to compressive force in a confined environment. Figure 2.5 indicates that the crushing values for all sources lie between 10 and 35%. Good performers are uniformly spread out between 12 and 31%; fair performers lie between 14 and 30% with slightly higher point density observed in the 19 to 27.5% range; fair performers are scattered relatively uniformly between about 15 and 34%.

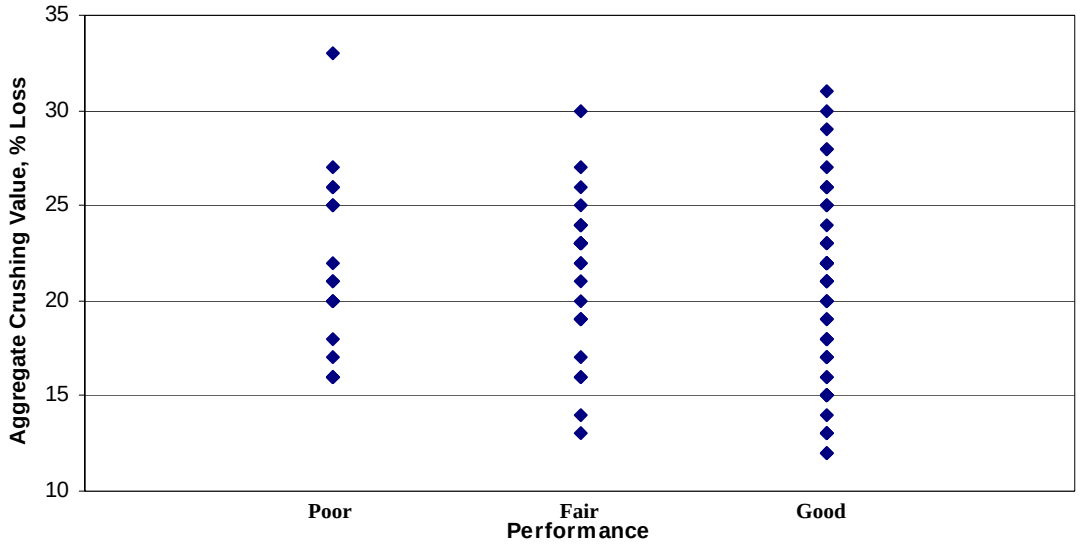

Figure 2.5: Aggregate Crushing Value vs. Performance

Quantitative analysis was performed on the data by varying the percent loss from 10 to 35% to determine the maximum overall success rate of the test to separate good performers from poor and fair aggregates. Table 2.5 outlines the key points to emphasize the fact that the overall success percentage first increases and then decreases.

Table 2.5: ACV Success Rate

TRIAL NUMBER	ACV	GOOD	FAIR	POOR	OVERALL
1	11%	0%	100%	100%	47%
2	12%	4%	100%	100%	49%
3	13%	10%	96%	100%	51%
4	16%	27%	85%	85%	54%
5	17%	33%	81%	80%	55%
6	18%	38%	81%	75%	57%
7	22%	69%	54%	40%	59%
8	23%	75%	27%	40%	55%
9	28%	92%	4%	15%	53%
10	29%	94%	4%	15%	54%

The maximum success rate is 59%, and it is reached at a loss value of 22%. Hence, it is clear that the aggregate crushing value test is not as accurate as the micro-Deval test.

Aggregate crushing value (SSD) test is very similar to the previously-discussed crushing value test except for the fact that the aggregate pores are saturated with water prior to the material being subjected to compression. Figure 2.6 shows the spread of points by the performance criterion. As the figure indicates, all good performers lie between 9 and 45% with much higher density between 11 and 30%. Fair performers lie between 12 and 32% with higher density observed between 18 and 28%. Poor performers show the greatest spread with values ranging between 0 and 50%, but higher density is observed between 15 and 23%.

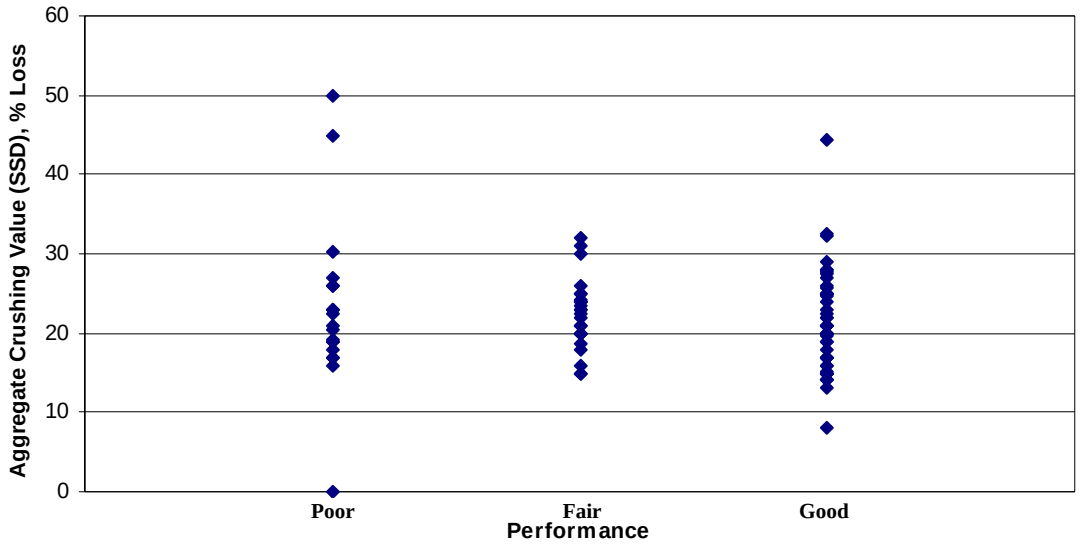

Figure 2.6: Aggregate Crushing Value (SSD) vs. Performance

Table 2.6 shows ten points that demonstrate the fluctuations in the overall success

Table 2.6: WCV Success Rate

TRIAL NUMBER	WCV	GOOD	FAIR	POOR	OVERALL
1	8%	2%	100%	100%	48%
2	13%	4%	100%	100%	49%
3	16%	23%	88%	100%	56%
4	17%	29%	88%	89%	57%
5	20%	50%	69%	63%	58%
6	23%	67%	46%	37%	55%
7	27%	85%	12%	21%	52%
8	32%	94%	0%	16%	53%
9	38%	98%	0%	16%	55%
10	51%	100%	0%	5%	54%

percentage value as the loss percentage is gradually increased. The maximum is observed to be 58% and occurs for the loss value of 20.0%. Considering the maximum

micro-Deval success rate, it can be concluded that the micro-Deval test is a better predictor of performance.

Absorption properties of aggregates influence the material behavior during the exposure to freeze-thaw cycling. Hence, it is necessary to look at the absorption versus performance graph for possible trends. As Figure 2.7 demonstrates, good performers are spread out throughout the range of 0 to 6% with high density between 0 and 2.2%.

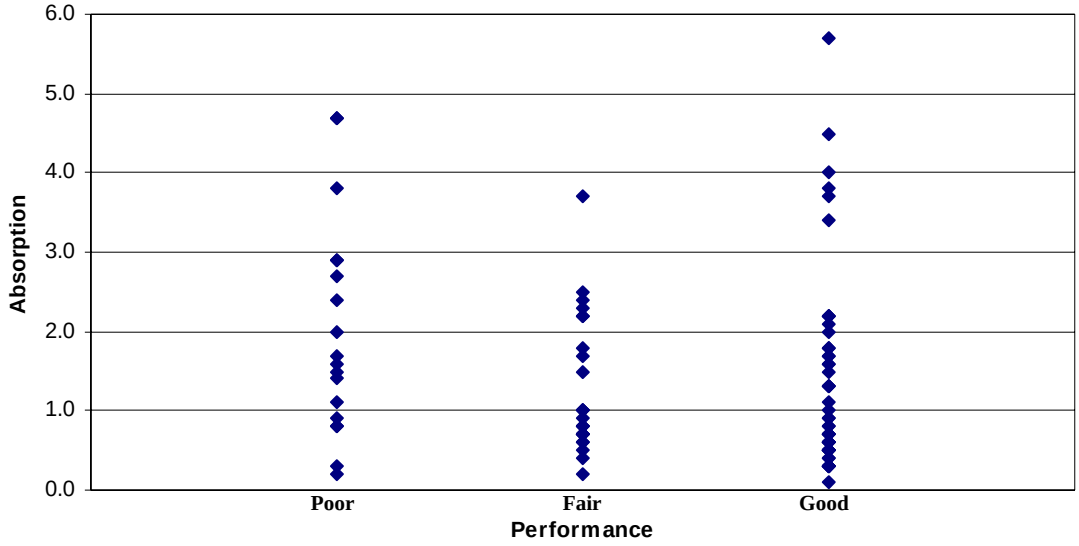

Figure 2.7: Absorption vs. Performance

Fair performers are scattered between 0 and 3.8% with high point densities between 0 and 1% as well as 2.1 and 2.5%. Poor performers are spread out between 0 and 4.8% with slightly higher density towards the bottom of the spectrum. Table 2.7 displays ten key points to demonstrate the fluctuations in the overall prediction success rate. The maximum overall success percentage of 58% is achieved at an absorption capacity of 0.5%. However, this overall success rate is still lower than that of the micro-Deval test.

Table 2.7: Absorption Success Rate					
TRIAL NUMBER	**ABS**	**GOOD**	**FAIR**	**POOR**	**OVERALL**
1	0.50%	33%	88%	84%	58%
2	1.00%	62%	35%	63%	55%
3	1.50%	71%	31%	47%	56%
4	2.00%	85%	23%	32%	57%
5	2.50%	88%	4%	26%	53%
6	3.00%	88%	4%	16%	51%
7	3.50%	90%	4%	16%	52%
8	4.00%	96%	0%	16%	54%
9	4.50%	98%	0%	16%	55%
10	5.50%	98%	0%	5%	53%

Three different specific gravities were computed from the measurements taken during specific gravity testing – bulk specific gravity, saturated surface-dry specific gravity, as well as the apparent specific gravity. All three exhibit identical trends, and therefore, only bulk specific gravity graph is discussed below. All three graphs are included in Appendix A. Figure 2.8 demonstrates that most good performers lie between the bulk specific gravities of 2.25 and 3 with higher density observed between 2.5 and 2.75. Fair performers are scattered between the bulk specific gravities of 2.4 and 2.9 with higher density observed between 2.58 and 2.67. Poor performers are widely spread out between bulk specific gravity values of 2.2 and 2.9 with slightly higher density towards the middle of the spectrum.

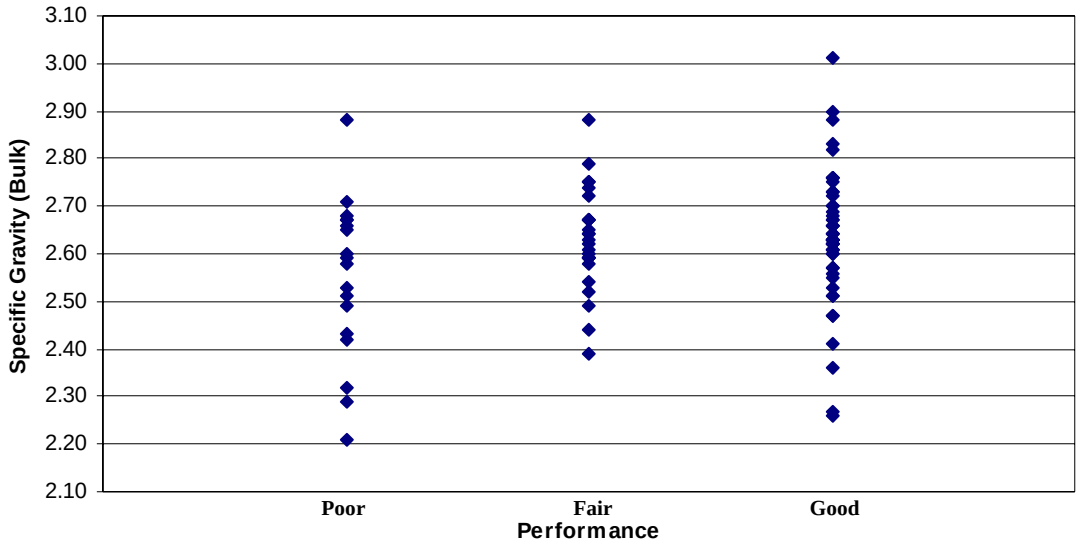

Figure 2.8: Specific Gravity (Bulk) vs. Performance

Table 2.8 demonstrates the trend of the computed overall success percentage as

Table 2.8: SG (Bulk) Success Rate

TRIAL NUMBER	SG(BULK)	GOOD	FAIR	POOR	OVERALL
1	2.10%	0%	100%	100%	47%
2	2.20%	0%	100%	95%	46%
3	2.30%	4%	100%	79%	45%
4	2.40%	6%	96%	68%	43%
5	2.50%	12%	88%	58%	41%
6	2.60%	29%	58%	37%	38%
7	2.70%	77%	23%	5%	48%
8	2.80%	90%	4%	5%	50%
9	2.90%	98%	0%	5%	53%
10	3.10%	100%	0%	5%	54%

the bulk specific gravity value is gradually increased. The maximum success percentage is 54%. During similar numerical analysis of saturated surface-dry specific gravity and

apparent specific gravity, maximum overall success value of 54% was observed as well, which is lower then the previously-computed micro-Deval overall success rating.

Particle shape factor is a measure of angularity of an aggregate, a property that could have a considerable impact on the performance of the material in the field. Figure 2.9 displays the results when performance is plotted against the particle shape factor.

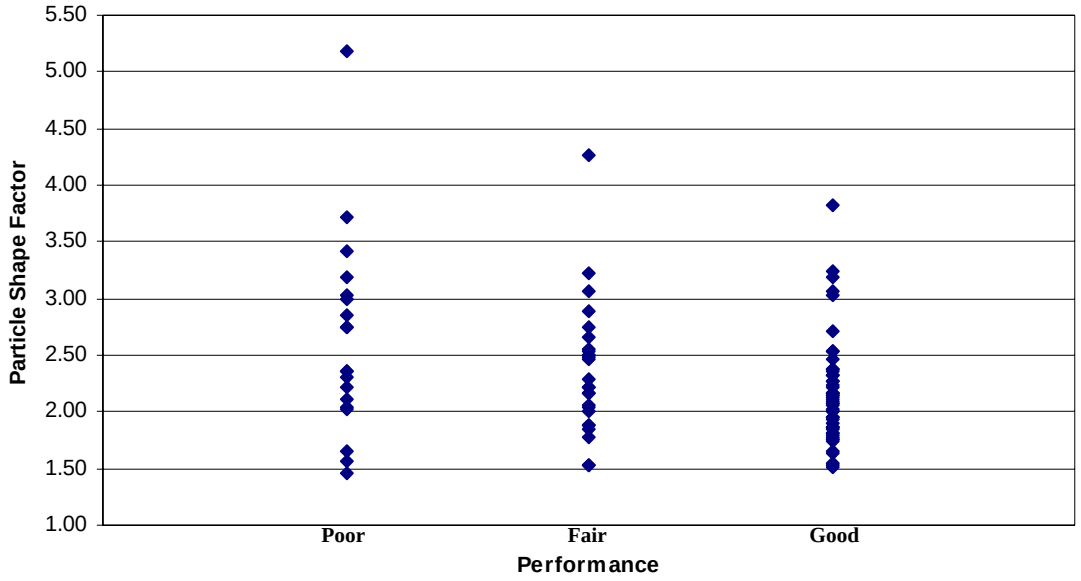

Figure 2.9: Particle Shape Factor vs. Performance

As the figure indicates, good performers lie in the range of 1.5 to 4 with noticeably higher density in the lower spectrum − values ranging between 1.5 and 2.5. Fair performers are more uniformly scattered between particle shape factors of 1.5 and 4.5 with slightly higher density between 1.75 and 2.25. The scatter is even higher for poor performers with values ranging between 1.75 and 5.25, and slightly higher density is apparent toward the bottom of the spectrum. Table 2.9 shows the calculations carried out to quantitatively assess the effectiveness of the test at separating the aggregates. Overall maximum success rate is 58%, a value considerably lower than that of the micro-Deval test.

Table 2.9: PSF Success Rate

TRIAL NUMBER	PSF	GOOD	FAIR	POOR	OVERALL
1	1.00%	0%	100%	100%	47%
2	1.50%	0%	100%	90%	45%
3	2.00%	40%	73%	85%	58%
4	2.50%	85%	31%	45%	62%
5	3.00%	90%	12%	25%	56%
6	3.50%	98%	4%	15%	56%
7	4.00%	100%	4%	10%	56%
8	4.50%	100%	0%	10%	55%
9	5.00%	100%	0%	10%	55%
10	5.50%	100%	0%	5%	54%

Computations for percentages of fractured particles in each source were carried out during the research project. Data were recorded for two cases – particles with one or more fractured faces and particles with two or more fractured faces. Figures 2.10 and 2.11 graphically summarize the findings. Furthermore, Tables A.1 and A.2 in the Appendix A provide the same information summarized in a table format. From Figure 2.10, it is clear that material in all three performance criteria was mostly fractured. Fair performers have the least scatter of values that lie between 70 and 100% while both fair and good performers have values ranging between 0 and 100% with higher densities at the top of the spectrums.

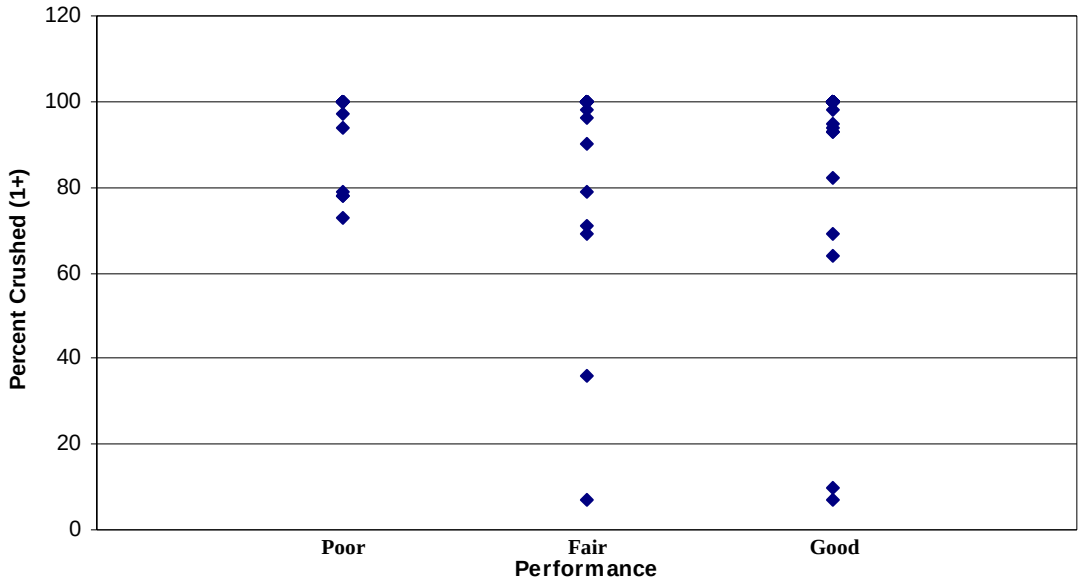

Figure 2.10: Percent Crushed (1+) vs. Performance

Table 2.10 quantitatively assesses the effectiveness of the test. The maximum overall success percentage is 54%, a value significantly smaller than that of the micro-Deval test.

Table 2.10: %Crushed (1+) Success Rate

TRIAL NUMBER	%Crushed (1+)	GOOD	FAIR	POOR	OVERALL
1	10.00%	4%	96%	100%	48%
2	20.00%	4%	96%	100%	48%
3	30.00%	4%	96%	100%	48%
4	40.00%	4%	92%	100%	47%
5	50.00%	4%	92%	100%	47%
6	60.00%	4%	92%	100%	47%
7	70.00%	8%	88%	95%	47%
8	80.00%	8%	81%	70%	40%
9	90.00%	10%	77%	75%	41%
10	100.00%	100%	0%	5%	54%

Figure 2.11 provides the graphical summary for the test where particles with two or more fractured faces were counted. The results are similar to those of the one fractured face analysis. However, greater scatters are observed for poor performers, which now lie between 60 and 100%.

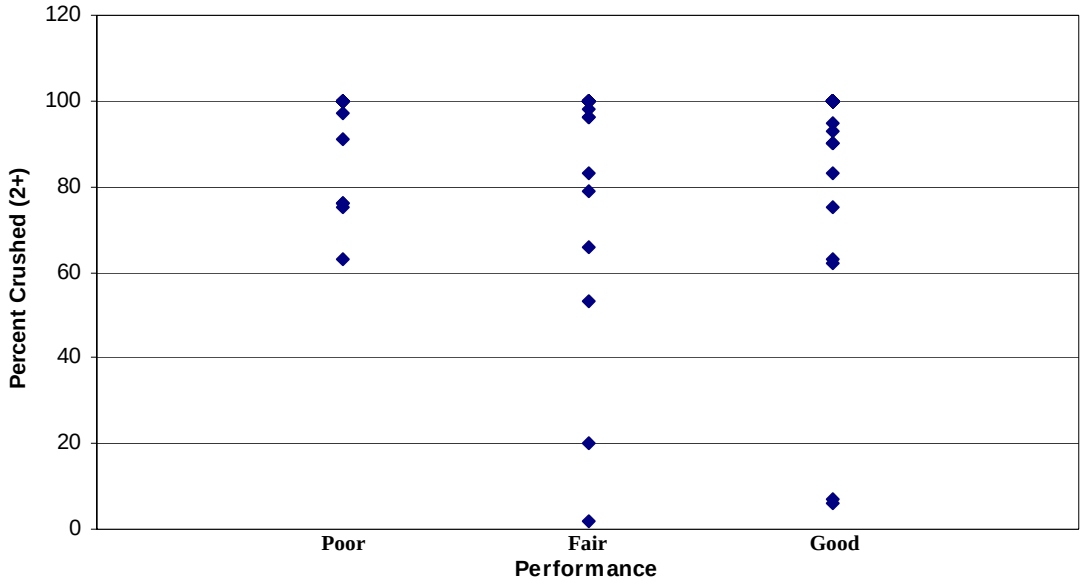

Figure 2.11: Percent Crushed (2+) vs. Performance

Both good and fair performers are scattered throughout the entire range of 0 to 100% with slightly higher point concentrations around 100%. Table 2.11 provides quantitative analysis summary. The observed maximum overall success percentage is 54% as in the previous case of only one fractured face analysis. Thus, it can be concluded that the percent fractured test is not as good of a performance predictor as the micro-Deval test regardless whether one or two fractured faces are counted.

Table 2.11: %Crushed (2+) Success Rate					
TRIAL NUMBER	%Crushed (2+)	GOOD	FAIR	POOR	OVERALL
1	10.00%	4%	96%	100%	48%
2	20.00%	4%	92%	100%	47%
3	30.00%	4%	92%	100%	47%
4	40.00%	4%	92%	100%	47%
5	50.00%	4%	92%	100%	47%
6	60.00%	4%	88%	95%	45%
7	70.00%	8%	85%	95%	46%
8	80.00%	10%	81%	70%	41%
9	90.00%	15%	77%	75%	44%
10	100.00%	100%	0%	5%	54%

2.2 SUCCESS RATE COMPARISON OF TWO-TEST COMBINATIONS INVOLVING MICRO-DEVAL

One of the main goals of this research project was to identify whether or not micro-Deval in combination with another test would be able to predict performance better than if it was used alone. Literature review suggested that a quadrant could be identified on a graph where the majority of good performers would lie. Hence, in the following sections, micro-Deval will be plotted against every other test conducted during this research project. Within each graph, a quadrant will be identified, if possible, within which mostly good performers will lie while all poor and fair performers will lie outside of it. Percentages will be computed to quantitatively assess how well the two-test combination can separate the good, poor, and fair performers. Weighted overall success percentage will be computed for each plot as well. Multiple trials will be carried out to try to optimize the overall success percentage by changing the borders of the quadrant.

Finally, conclusions will be drawn on whether or not better classifications can be achieved using a particular combination as opposed to the micro-Deval test alone.

Figure 2.12 represents the results when the micro-Deval test is plotted against the L.A. abrasion test. From the plot, it can be observed that good performers tend to congregate towards the lower-left corner.

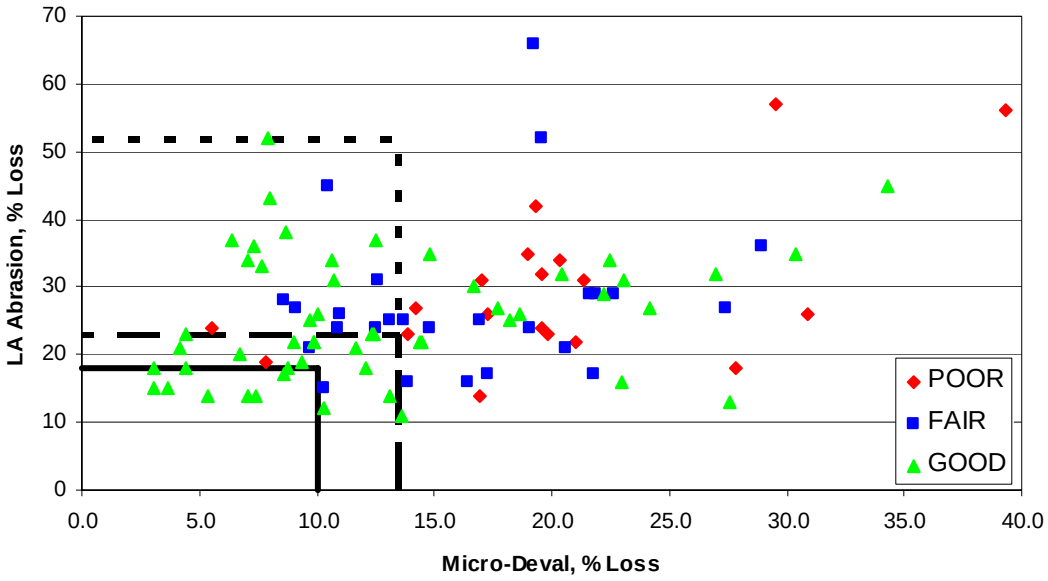

Figure 2.12: L.A. Abrasion vs. Micro-Deval

To quantitatively assess the additional information gained from the L.A. abrasion test, numerous trials were carried out by changing the position of the borders of the quadrant. Table 2.12 summarizes the general trends observed when the borders were moved to the right or to the top, with Trial 3 being the optimal quadrant position obtained through extensive trial and error process. In the table, the value for quadrant success percentage is computed by calculating the number of good points within the quadrant and dividing it by the total number of points within the quadrant. The value of good percentage is computed by dividing the number of good points within the quadrant by the total number

of good points. Similarly, fair percentage is computed by dividing the number of fair points within the quadrant by the total number of fair performers, and poor percentage is computed by dividing the number of poor performers within the quadrant by the total number of poor performers. Finally, overall success percentage is the weighted average of good, poor, and fair percentages.

Table 2.12: LAA and MD Success Rate

TRIAL NUMBER	1	2	3
LAA	18	23	52
MD	10	13.5	13.5
QUADRANT	100%	88%	74%
GOOD	17%	42%	65%
FAIR	100%	92%	62%
POOR	100%	95%	90%
OVERALL	56%	66%	69%

Hence, the table values provide a measure of successful aggregate qualification for a two-test combination, where higher quadrant and overall percentages indicate better aggregate qualification performance. Thus, Table 2.12 shows that an overall success rate of 69% can be achieved but at the expense of the quadrant percentage. Furthermore, as the quadrant is expanded, the percentage of good aggregates accurately predicted increases significantly while the percentages for the fair and poor aggregates decrease. Therefore, it can be concluded that combining micro-Deval with L.A. abrasion test does not yield better results than using the micro-Deval test alone, which can achieve 69% success rate on its own as discussed in the previous section.

The literature review indicated that micro-Deval and Canadian freeze-thaw tests combination provides good results for aggregate separation. Since magnesium sulfate soundness test is intended to measure aggregate's resistance to freeze-thaw, similar

results were expected. Figure 2.13 demonstrates the results of micro-Deval and magnesium sulfate soundness being included on the same plot.

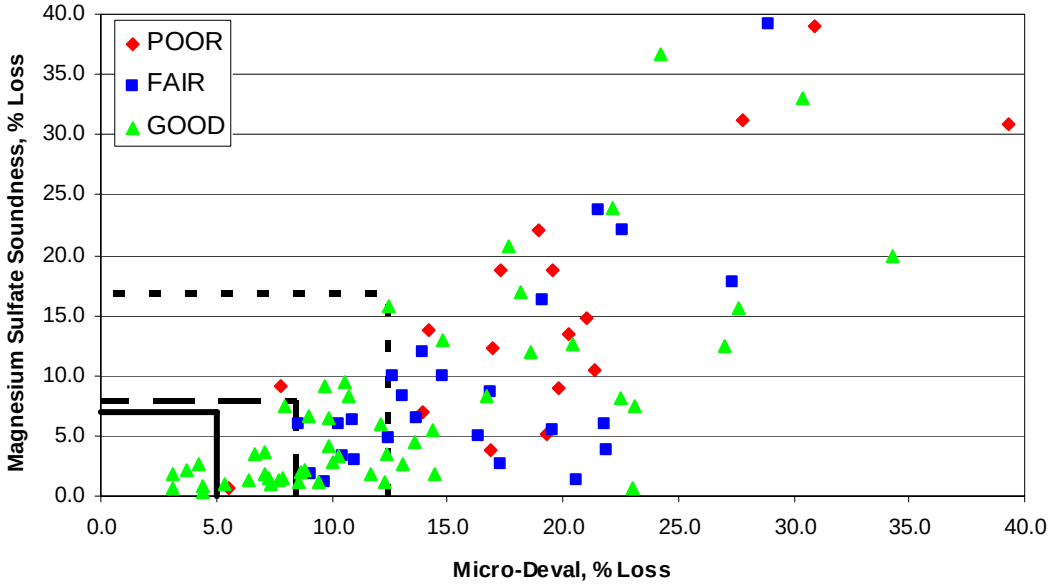

Figure 2.13: Magnesium Sulfate Soundness vs. Micro-Deval

As the figure demonstrates, considerable scatter was observed. However, good performers seem to congregate in the lower-left quadrant. Once again, quantitative analysis was performed, and the findings are summarized in Table 2.13.

Table 2.13: MSS and MD Success Rate

TRIAL NUMBER	1	2	3
MSS	7	8	17
MD	5	8.5	12.5
QUADRANT	100%	94%	77%
GOOD	12%	31%	63%
FAIR	100%	100%	69%
POOR	100%	95%	90%
OVERALL	53%	62%	70%

Three trials are outlined to provide an overview of quadrant expansion progression in an attempt to increase the overall success rate. As the quadrant is expanded further to the right and to the top, quadrant success rate decreases. However, the overall success rate of 70% becomes possible. This is a slight improvement upon the 69% overall success rate that can be achieved by micro-Deval alone.

As previous discussion indicated, the Canadian freeze-thaw test is one of the better tests to separate good performers from fair and poor aggregates. Furthermore, the literature review indicated that the combination of micro-Deval and Canadian freeze-thaw tests produced better predictions than using each test alone. Figure 2.14 displays the results when micro-Deval is plotted against Canadian freeze-thaw. The three quadrants outlined in the plot represent the results of numerous trials in an attempt to optimize overall prediction success percentage. During the first attempt, outlined by the solid line, only

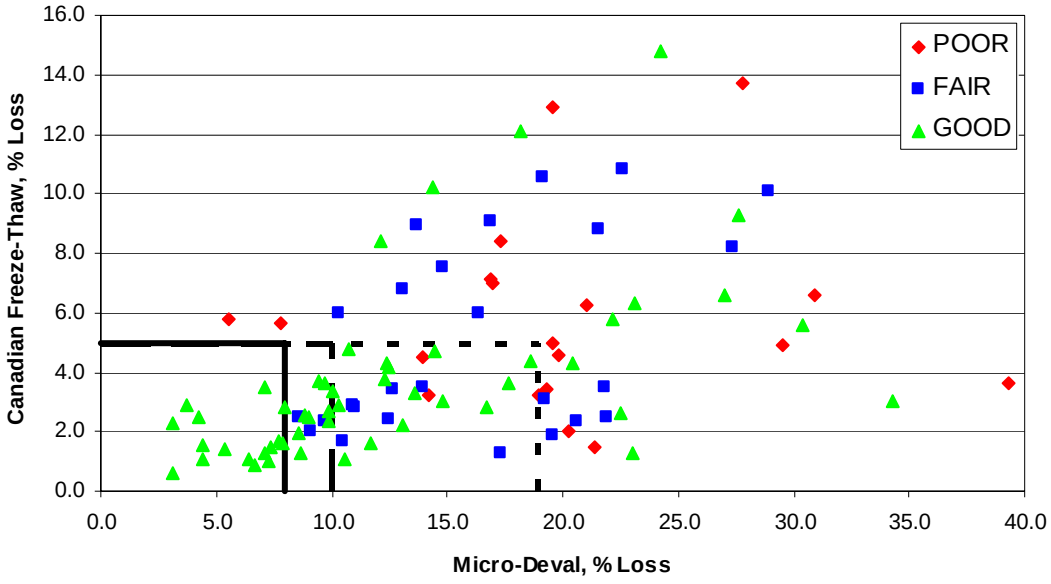

Figure 2.14: Canadian Freeze-Thaw vs. Micro-Deval

good performers were included in the quadrant, resulting in an overall success rate of 63%. By including several fair sources into the quadrant area, an overall success rate of 69% can be achieved. By further extending the border to the right, the overall percentage increases to the maximum value of 73%. Numerical results for the three trials are summarized in Table 2.14. As the table indicates, the overall success rate is achieved

Table 2.14: CFT and MD Success Rate

TRIAL NUMBER	1	2	3
CFT	5	5	5
MD	8	10	19
QUADRANT	100%	89%	75%
GOOD	31%	48%	75%
FAIR	100%	88%	62%
POOR	100%	100%	85%
OVERALL	63%	69%	73%

at the expense of decreasing fair and poor prediction success rates as well as the quadrant prediction success rate. Thus, it can be concluded that the additional information provided by the Canadian freeze-thaw test is quite significant as its inclusion in the analysis leads to the higher overall success rate than that of using the micro-Deval test alone.

Figure 2.15 represents the results when micro-Deval losses are plotted against aggregate crushing value losses.

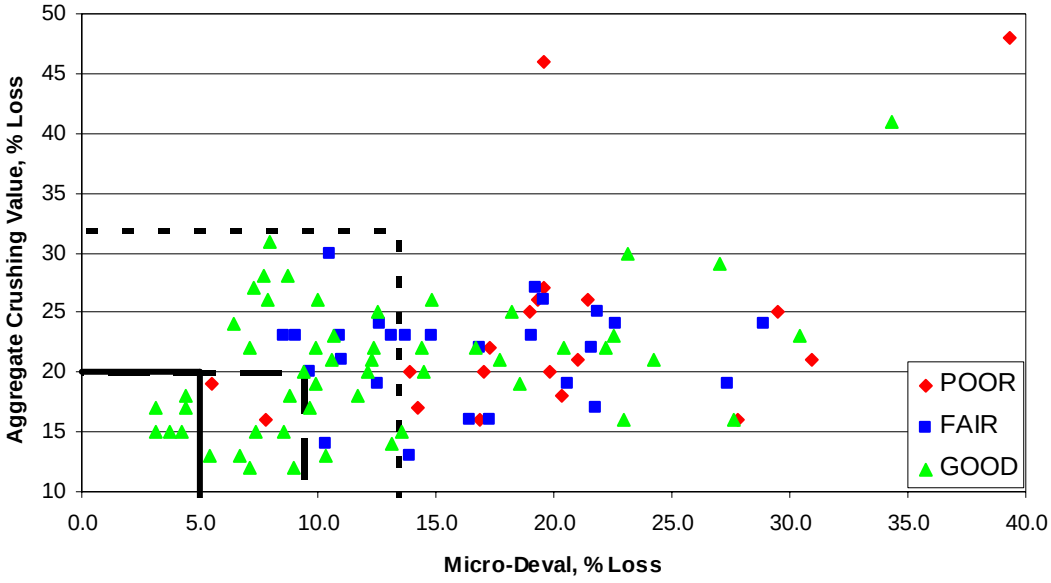

Figure 2.15: Aggregate Crushing Value vs. Micro-Deval

For the first trial, the quadrant was chosen so that only good performers would fall into the area. Overall success rate of 53% is achieved in this case but only 12% of good aggregates overall are classified correctly. The quadrant was then expanded by slowly increasing the micro-Deval loss value. The newly-enclosed area now contains several poor sources, but the overall success rate increases to 59% with the improvement of good performer prediction to 27%. By further expanding the quadrant to the right and upwards, the overall success rate increases to 69%. During this process, the quadrant prediction percentage falls significantly as does the percentage for fair prediction. However, 65% of good performers now fall into the quadrant. Thus, it can be concluded that aggregate crushing value test does not provide any useful additional information to increase the overall success rate since micro-Deval alone produces a 69% success rate.

Table 2.15: ACV and MD Success Rate			
TRIAL NUMBER	**1**	**2**	**3**
ACV	20	20	32
MD	5	9.5	13.5
QUADRANT	100%	88%	74%
GOOD	12%	27%	65%
FAIR	100%	100%	62%
POOR	100%	90%	90%
OVERALL	53%	59%	69%

Since the aggregate crushing value (SSD) test is very similar to the aggregate crushing value test, similar results were expected and observed during the data analysis. Figure 2.16 shows the plotted results with three curves outlining the outcomes as the

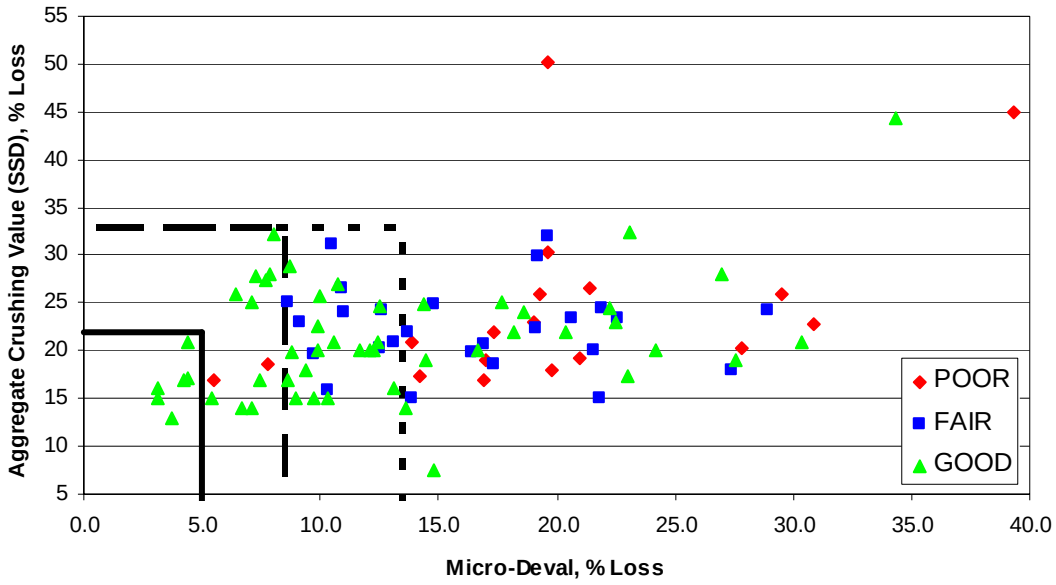

Figure 2.16: Aggregate Crushing Value (SSD) vs. Micro-Deval

quadrant borders were expanded. Table 2.16 provides numerical summary for the trials data. During the first trial, only good performers are included in the quadrant area. Even

though 59% overall success rate is achieved, only 12% of good sources overall are counted. As the quadrant is allowed to expand to the right, two poor sources are included in the quadrant, hence reducing its success rating to 88%. However, more good

Table 2.16: WCV and MD Success Rate

TRIAL NUMBER	1	2	3
WCV	22	33	33
MD	5	8.5	13.5
QUADRANT	100%	88%	73%
GOOD	12%	31%	65%
FAIR	100%	100%	62%
POOR	100%	89%	89%
OVERALL	53%	61%	69%

performers overall are now included (31% of all good aggregates), and the overall success rate increases to 61%. Upon further quadrant expansion, the quadrant success rate continues to decline to 73% as more fair performers now fall into it, and fair performance success rate falls significantly to 62%. Overall success rate increases to 69%, however, and 65% of good performers now fall into the quadrant. Numerous trials were carried out during quantitative analysis, and 69% shown in Trial #3 is the maximum achieved overall success rate. Thus, it can be concluded that saturated, surface-dry aggregate crushing value test produces results very similar to those of the regular crushing value test, and hence no significant improvements are made to the overall success rate of 69% obtained through the use of the micro-Deval test alone.

Figure 2.17 represents the results obtained by plotting micro-Deval losses and absorption capacities of the aggregates on the same plot. Additionally, quadrant assessment information is summarized in Table 2.17.

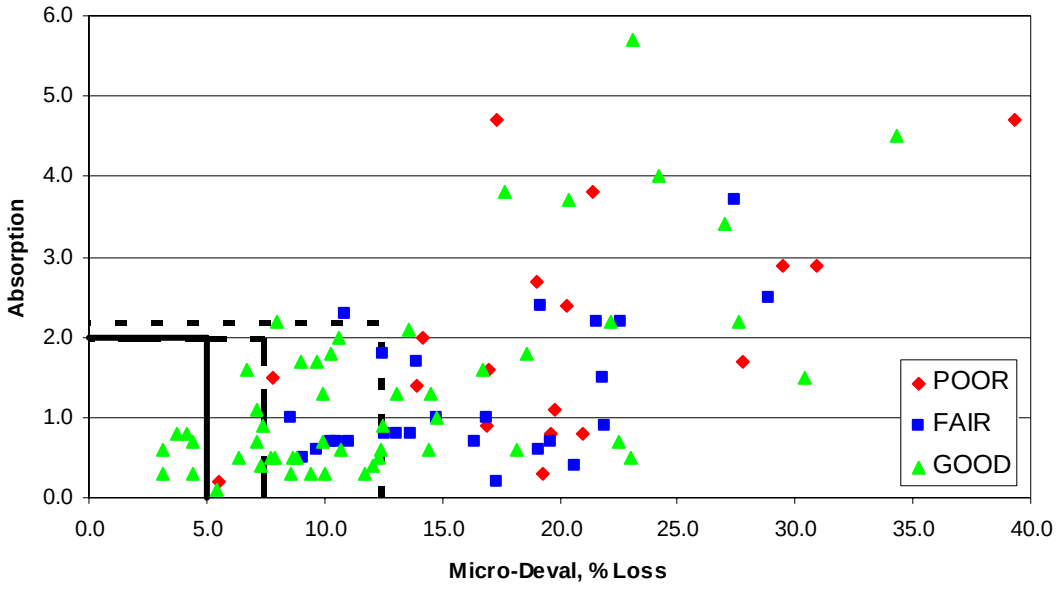

Figure 2.17: Absorption vs. Micro-Deval

The first trial represents the results obtained by including only good performers within the quadrant, resulting in 52% success rate, but only 10% of all good points fall within the quadrant. By expanding the quadrant boundary to the right, both poor sources success rate and the quadrant success rate decrease,

Table 2.17: ABS and MD Success Rate

TRIAL NUMBER	1	2	3
ABS	2	2	2.2
MD	5	7.5	12.5
QUADRANT	100%	92%	78%
GOOD	10%	23%	62%
FAIR	100%	100%	73%
POOR	100%	95%	89%
OVERALL	52%	58%	70%

but the percent of good points falling within the area increases to 92% and the overall success rate improves to 58%. By further expanding the area to the right and slightly upward, the maximum overall success rate of 70% is observed. However, as expected, since more fair sources now fall into the quadrant, its success rate as well as fair aggregates success rates fall significantly. Thus, it can be concluded that the addition of absorption data to the micro-Deval data increases the prediction success rate very slightly to 70% as compared to 69% achieved by micro-Deval alone.

Based on the data collected during the research project, three specific gravity values were computed – bulk specific gravity, saturated surface-dry specific gravity, and apparent specific gravity. Only bulk specific gravity plotted against micro-Deval is discussed here since the data for all three forms the exact same scatter patterns, but the readers is encouraged to refer to the Appendix B for the specific gravity graphs. Figure 2.18 shows the results after numerous trials were carried out aimed at optimizing the overall success rate.

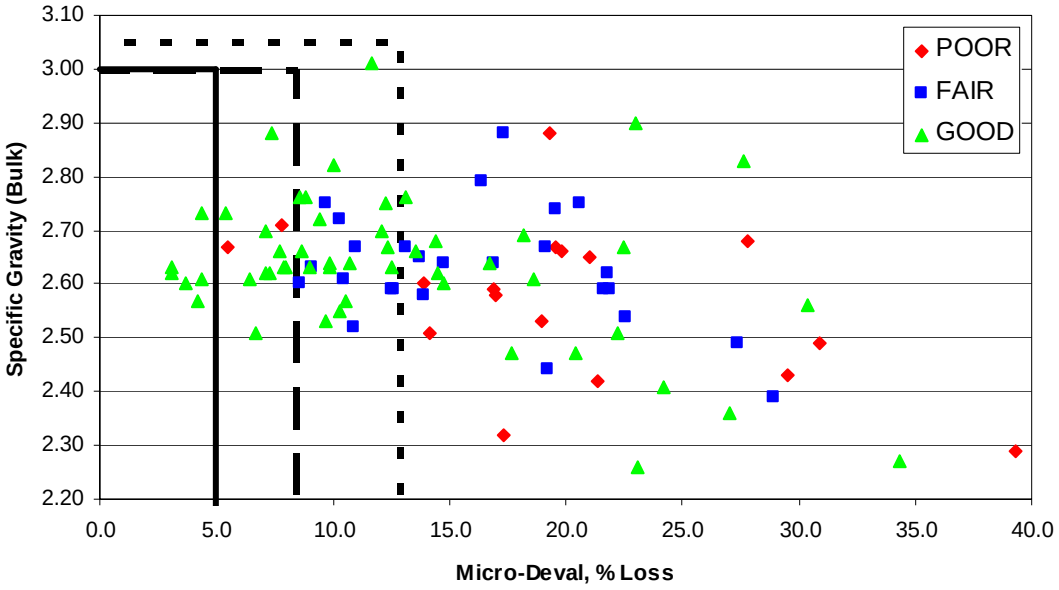

Figure 2.18: Specific Gravity (Bulk) vs. Micro-Deval

Table 2.18 provides the numerical summary of the trials data. During the first trial, only good performers are included in the quadrant, resulting in 52% success rate, but only 10% of good performers fall into the area. Upon expansion of the quadrant to the right, several poor points fall into the quadrant area, resulting in quadrant success rate decreasing to 88%, but the overall success rate increases to 60%, and now 29% of good

Table 2.18: SG(Bulk) and MD Success Rate

TRIAL NUMBER	1	2	3
SG(BULK)	3	3	3.1
MD	5	8.5	13
QUADRANT	100%	88%	74%
GOOD	10%	29%	62%
FAIR	100%	100%	65%
POOR	100%	89%	89%
OVERALL	52%	60%	68%

performers fall into the square. The maximum success rate of 68% is observed during Trial #3 but at the expense of fair sources success rate decreasing from 100% to 65% and quadrant success rate falling significantly to 74%. Thus, it is clear that the addition of specific gravity information does not improve our predictions results at all compared to using the micro-Deval test alone.

Particle shape factor provides information about the degree of angularity of aggregate particles. Figure 2.19 demonstrates the final results after numerous trials were carried out in an attempt to optimize the overall success rate. Table 2.19 provides numerical summary for the key steps in the trial process. The first trial again is intended to have the quadrant contain good performers only.

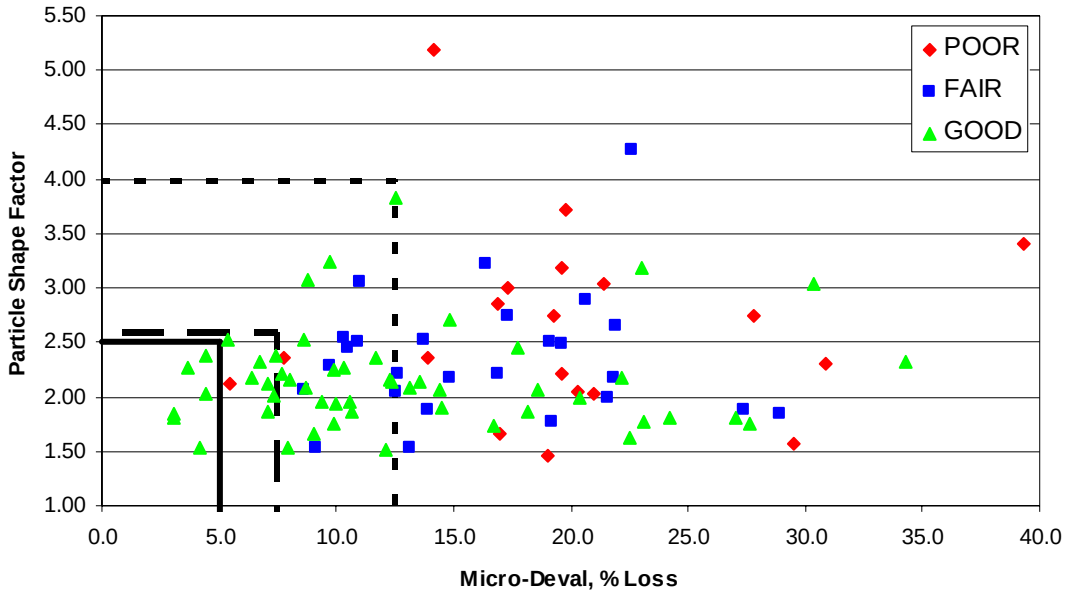

Figure 2.19: Particle Shape Factor vs. Micro-Deval

The overall success rate of 53% is achieved in this case, but only 12% of all good performers are included in the quadrant area. By expanding the quadrant to the right, the overall success rate increases to 59% with 25% of good performers falling into the quadrant area. Further gains are possible at the expense of quadrant success rate decrease by expanding the area. Trial #3 represents the optimal quadrant size to achieve the

Table 2.19: PSF and MD Success Rate

TRIAL NUMBER	1	2	3
PSF	2.5	2.6	4
MD	5	7.5	12.5
QUADRANT	100%	93%	77%
GOOD	12%	25%	63%
FAIR	100%	100%	69%
POOR	100%	95%	90%
OVERALL	53%	59%	70%

highest possible overall success rate of 70%. This result leads to the inclusion of 63% of good performers into the quadrant area but significant decreases in quadrant success rate as well as fair sources success rate. Thus, it can be concluded that very slight improvement to prediction success rate is observed by including particle shape factor information to that of the micro-Deval test alone.

Figure B.11 and Figure B.12 in Appendix B demonstrates the results of plotting micro-Deval losses and percent crushed results on the same plot. As the graphs indicate, no clear data groupings are evident, and hence no further statistical analysis is possible. Thus, it can be concluded that percent crushed tests, one crushed face or two crushed faces, do not provide any additional information.

2.3 SUCCESS RATE COMPARISON OF OTHER RELEVANT TWO-TEST COMBINATIONS

During this research project, a series of two-dimensional graphs was created where every test was plotted against every other test. This series of graphs is included in the Appendix B. Every graph was carefully examined in an attempt to find out whether or not meaningful quadrants could be drawn in as was done in the micro-Deval case. The results of this inspection lead to the conclusion that only two other test combinations produced meaningful quadrant divisions: Canadian freeze-thaw versus aggregate crushing value graph produced and magnesium sulfate soundness versus particle shape factor. Both graphs are discussed in this section.

Figure 2.20 shows the plot of aggregate crushing value versus Canadian freeze-thaw losses. Once again, a statistical analysis was performed as before to evaluate how well the good aggregates could be separated. Results of this analysis are summarized in Table 2.20.

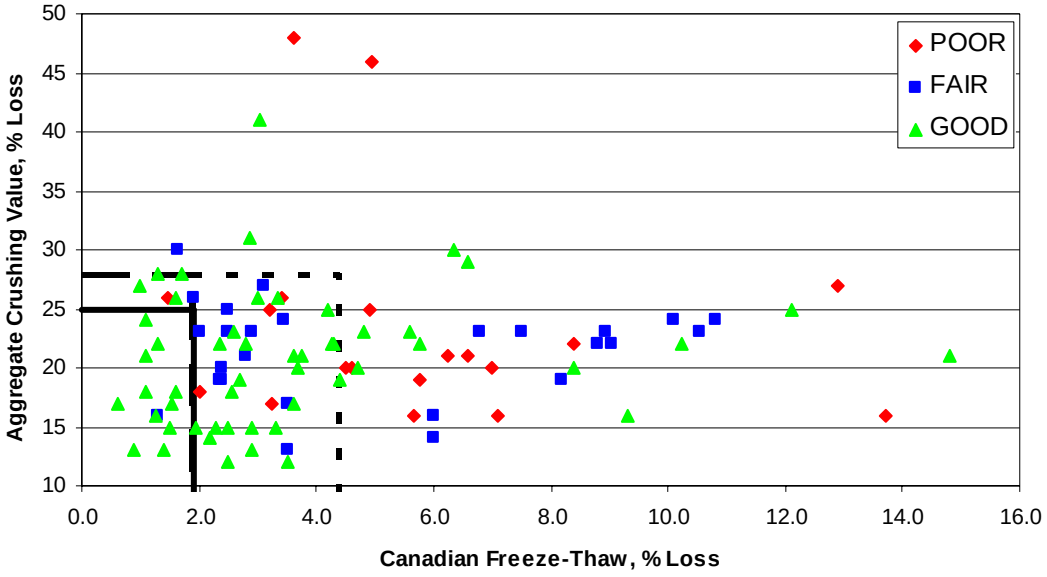

Figure 2.20: Aggregate Crushing Value vs. Canadian Freeze-Thaw

As the graph data show, higher overall success rate was achieved at the expense of decreasing quadrant success rate. While the decreases in success rates for fair and poor performers are not very significant, they do increase significantly in order to achieve the maximum overall success rate of 67%. However, the increase in the success rate of good performers is quite significant to justify the decreases in fair and poor success rates.

Table 2.20: ACV and CFT Success Rate

TRIAL NUMBER	1	2	3
ACV	25	28	28
CFT	1.9	1.9	4.4
QUADRANT	92%	83%	67%
GOOD	21%	29%	75%
FAIR	96%	92%	46%
POOR	100%	95%	75%
OVERALL	57%	59%	67%

Generally, however, the maximum overall success rate achieved by aggregate crushing value and Canadian freeze-thaw tests is not as good as that achieved through the use of the micro-Deval test in combination with other tests.

Figure 2.21 provides the graph of particle shape factor versus magnesium sulfate soundness.

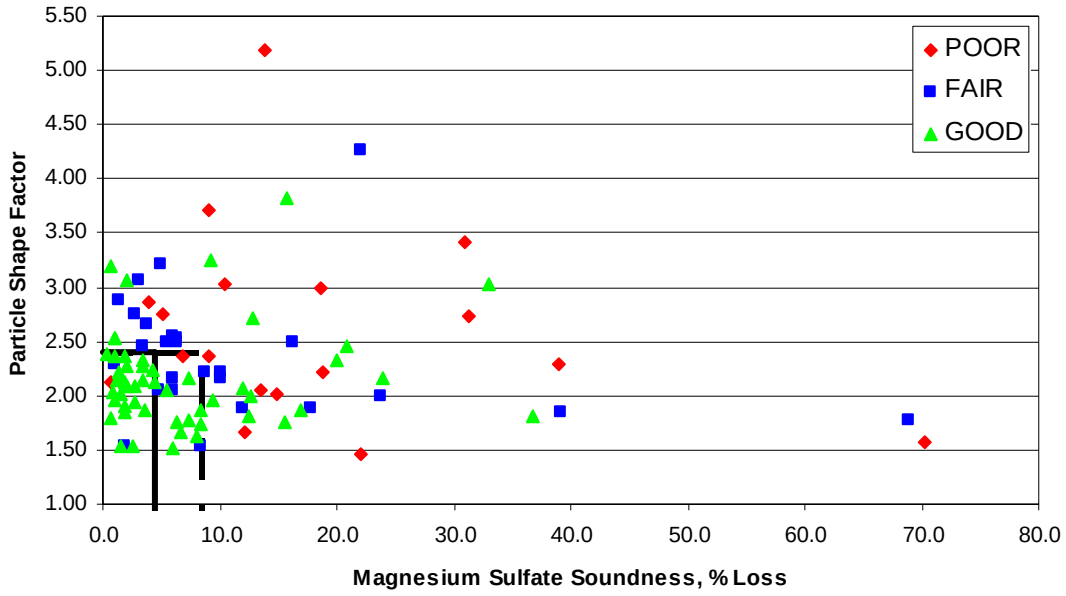

Figure 2.21: Particle Shape Factor vs. Canadian Freeze-Thaw

The quantitative analysis performed on this graph is summarized in Table 2.21 below.

Table 2.21: PSF and MSS Success Rate

TRIAL NUMBER	1	2
PSF	2.4	2.4
MSS	4.5	8.5
QUADRANT	89%	81%
GOOD	48%	65%
FAIR	92%	77%
POOR	95%	90%
OVERALL	69%	73%

As the table demonstrates, by expanding the quadrant slightly to the right and to the top, the quadrant success rate decreases by 8%. However, the overall success rate increases to 73% - a notable improvement to the success rate of 69% achieved by micro-Deval test alone. Thus, it can once again be concluded that freeze-thaw performance evaluation provides significant information to successful identify aggregate performance in the field.

2.4 RESULTS SUMMARY AND CONCLUSIONS

Table 2.22 below provides the summary of the statistical analysis performed for hot-mixed asphalt aggregates. The first column represents the success rates obtained when only one test is used to separate the good-performing aggregates. The second column provides the success rate of a two-test combination with one of the tests being

Table 2.22: HMA Success Rates Summary

	TEST ALONE	MICRO-DEVAL COMBINATION
MICRO-DEVAL	69%	NOT APPLICABLE
MAGNESIUM SULFATE SOUNDNESS	64%	70%
L.A. ABRASION	61%	69%
CANADIAN FREEZE-THAW	65%	73%
AGGREGATE CRUSHING VALUE	59%	69%
AGGREGATE CRUSHING VALUE (SSD)	58%	69%
ABSORPTION	58%	70%
SPECIFIC GRAVITY (BULK)	54%	68%
PARTICLE SHAPE FACTOR	58%	70%
PERCENT CRUSHED (1+)	54%	NOT APPLICABLE
PERCENT CRUSHED (2+)	54%	NOT APPLICABLE

the micro-Deval test. As the data considering one test only illustrate, the highest success rate percentage was achieved using the micro-Deval test, which was followed by the Canadian freeze-thaw test. These conclusions are supportive of the conclusions drawn by

previous research projects outlined in the literature review section. The data in the second column indicate that success rates could be improved from the highest of 69% by using micro-Deval alone to 73% overall success rate by using micro-Deval and Canadian freeze-thaw tests together. This result is in line with research performed by Chris Rogers, et al, who concluded that better classification results are obtained by combining Canadian freeze-thaw test data with micro-Deval test data. Thus, it is the conclusion of this research project team that micro-Deval represents the best single-test prediction performance while the combination of micro-Deval and Canadian freeze-thaw tests represents the best two-test combination for performance classification of aggregates used in the hot-mix asphalt.

Chapter 3: Performance Analysis for Base Course Aggregates

3.1 Success Rate Comparison of Individual Tests

A considerable number of aggregates studied in this research project were also used in base courses throughout the United States and Canada. Hence, attempts will be made to determine the prediction success rate of the tests performed in this research study for aggregates used in base courses. However, it should be noted that the vast majority of the aggregates are good performers. Only two fair performers and three poor performers were identified by participating DOTs. Therefore, the analysis procedure used for hot-mixed asphalt aggregates cannot be directly applied in this situation.

The overall success rate cannot be considered the determining factor in evaluating the prediction success rate of a test alone since the highest percentage will be obtained at a threshold value such that all good sources fall below it regardless of where fair and poor sources lie. However, the quadrant quantitative analysis previously performed does provide meaningful information for two-test combinations and will be used. Base course performance graphs for each test are provided in Appendix C if the reader should choose to study them. Thus, the following sections will provide qualitative and quantitative analysis for two-test combinations and attempt to draw conclusions as to which two-test combination provides the highest prediction success rate.

3.2 Success Rate Comparison of Two-Test Combinations Involving Micro-Deval

Two-test combinations were studied in this research project by plotting the results of every test against every other test. The resulting graphs are provided in Appendix D. In this section, only the plots involving micro-Deval will be quantitatively as well as

qualitatively analyzed since the main purpose of this research project is to evaluate the effectiveness of predictions using micro-Deval. As previously discussed, due to only two fair and three poor performers present, close attention must now be paid to the quadrant success rate with secondary importance placed on computed overall success rate. Nevertheless, conclusions can be drawn on the extent of successful aggregate qualification produced by micro-Deval in combination with another test versus micro-Deval alone.

Figure 3.1 demonstrates the results of micro-Deval plotted versus magnesium sulfate soundness results. Additionally, Table 3.1 summarizes the

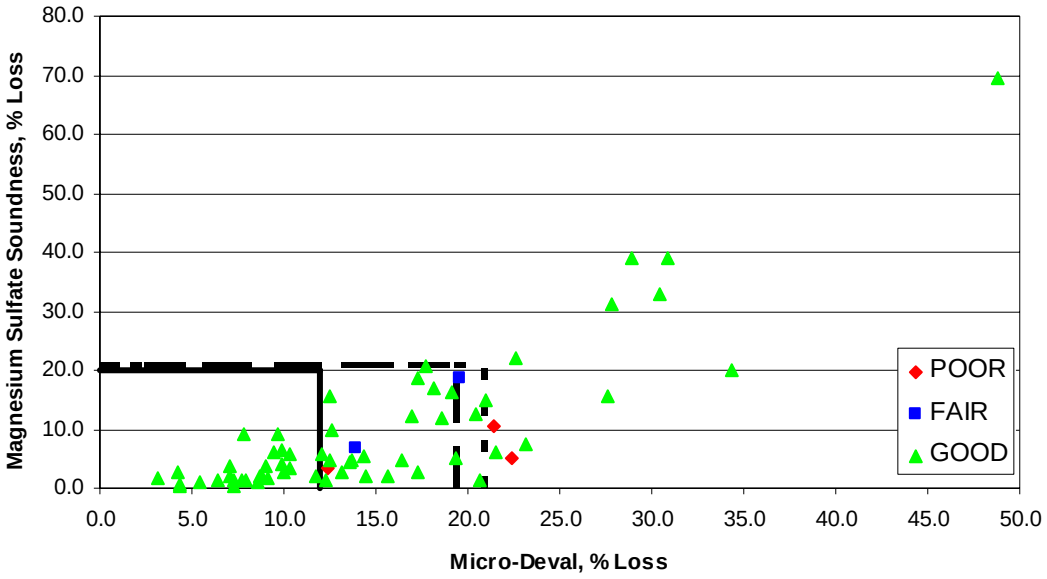

Figure 3.1: Magnesium Sulfate Soundness vs. Micro-Deval

results of the performed quantitative analysis using Microsoft Excel 2003. As the data illustrate, the overall success rate can be significantly increased by expanding the quadrant laterally to the right. Trial #3 represents the highest overall success rate achieved through extensive trial and error process. More importantly, however, the

Table 3.1: MSS and MD Success Rate			
TRIAL NUMBER	**1**	**2**	**3**
MSS	20	21	21
MD	12	19.5	21
QUADRANT	100%	96%	94%
GOOD	44%	78%	83%
FAIR	100%	50%	0%
POOR	100%	67%	67%
OVERALL	48%	77%	80%

quadrant success rate only falls 6% throughout the process, with 94% success rate in the optimal situation. However, although 83% of good performers are included at this point, none of the fair performers are identified correctly. Overall, it can be concluded that micro-Deval in addition to magnesium sulfate provide good prediction results.

Figure 3.2 demonstrates the results of micro-Deval losses plotted against L.A. abrasion losses. Three quadrants were attempted to optimize the overall performance as

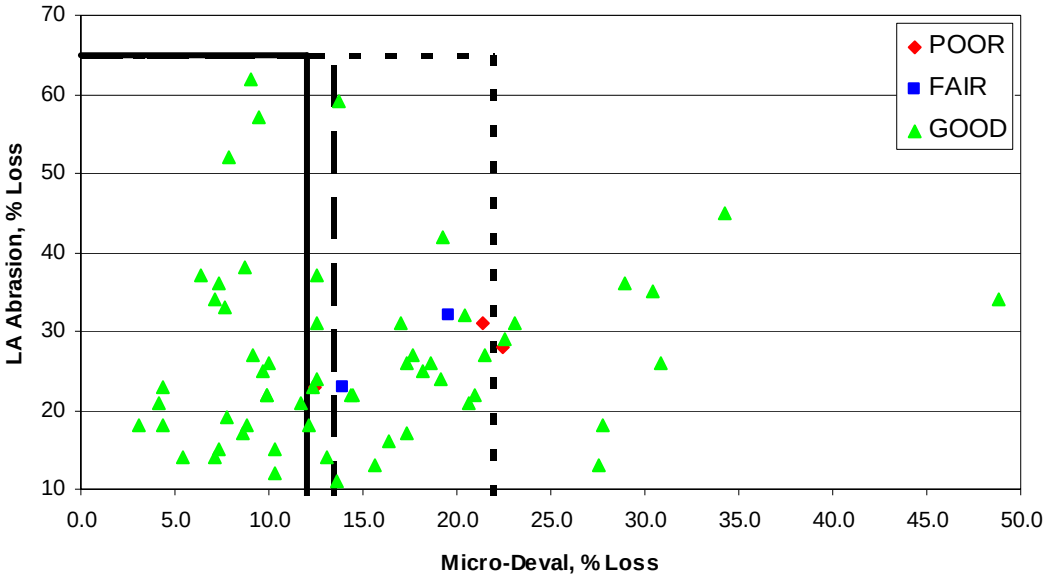

Figure 3.2: L.A. Abrasion vs. Micro-Deval

well as show how quadrant success rate changes as the quadrant is expanded to the right. The results are summarized in Table 3.2. As the data illustrate, a maximum overall success rate of 80% can be achieved using micro-Deval loss of 22% and L.A. abrasion loss of 65%. The reader should note that the quadrant success rate, which is more

Table 3.2: LAA and MD Success Rate

TRIAL NUMBER	1	2	3
LAA	65	65	65
MD	12	13.5	22
QUADRANT	100%	97%	93%
GOOD	44%	54%	85%
FAIR	100%	100%	0%
POOR	100%	67%	33%
OVERALL	48%	56%	80%

important in our analysis due to very few poor and fair sources present, decreases as overall success rate increases. However, the decrease for each consecutive trial are very low, with the maximum difference of 7% between Trial #1 and Trial #3, which represents the maximum overall success rate. Thus, the final quadrant success rate is 93% and, although relatively high, is less than the 94% achieved through micro-Deval and magnesium sulfate soundness combination. Additionally, although 85% of good sources are fall within the quadrant, none of the fair sources are identified correctly.

Figure 3.3 demonstrates the results of Canadian freeze-thaw test plotted against micro-Deval losses. Quantitative analysis is performed using Microsoft Excel 2003, and

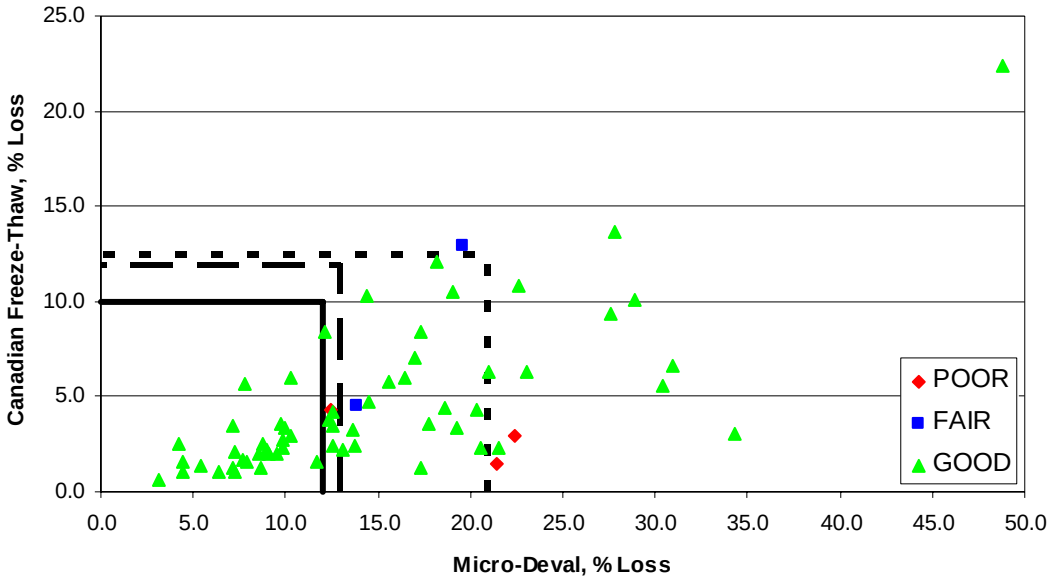

Figure 3.3: Canadian Freeze-Thaw vs. Micro-Deval

the results are summarized in Table 3.3. Since both magnesium sulfate soundness and Canadian freeze-thaw tests measure the aggregate resistance to freeze-thaw cycles, similar results were expected. Moreover, due to extremely high test variability observed

Table 3.3: CFT and MD Success Rate

TRIAL NUMBER	1	2	3
CFT	10	12	12.5
MD	12	13	21
QUADRANT	100%	97%	96%
GOOD	44%	53%	83%
FAIR	100%	100%	50%
POOR	100%	67%	67%
OVERALL	48%	55%	81%

during magnesium sulfate testing, greater success rates were expected. As Table 3.3 indicates, the expectations are substantiated by the computed data. The maximum overall success rate of 81% is achieved as shown in Trial #3 but at the expense of decreasing quadrant success rate. However, to achieve the optimal overall success rate, the quadrant success rate is only reduced by 4% to 96%, which is better than 94% observed through utilization of micro-Deval and magnesium sulfate soundness data. Thus, this combination produces the highest overall success rate thus far of 81% while also achieving the highest quadrant success rate of 96%.

Figure 3.4 and Table 3.4 summarize the results of aggregate crushing value losses plotted against micro-Deval losses. The results demonstrate that the maximum overall

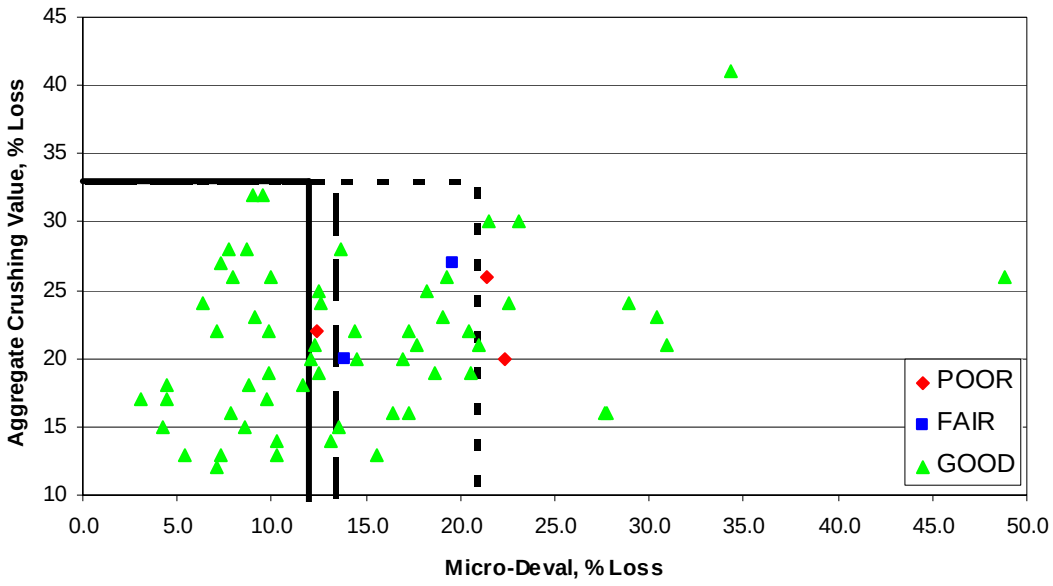

Figure 3.4: Aggregate Crushing Value vs. Micro-Deval

success rate of 80% is achieved through this two-test combination as shown by Trail #3. Furthermore, quadrant success rate of 94% is achieved in the same trial as well, indicating that optimal results are achieved at the expense of only 6% decrease in the

quadrant success rate. Although the success rates are not as high as those achieved through Canadian freeze-thaw and micro-Deval combination, they are still quite high and indicate that useful information is gained through the usage of this two-test combination.

Table 3.4: ACV and MD Success Rate

TRIAL NUMBER	1	2	3
ACV	33	33	33
MD	12	13.5	21
QUADRANT	100%	97%	94%
GOOD	44%	54%	83%
FAIR	100%	100%	0%
POOR	100%	67%	67%
OVERALL	48%	56%	80%

The plot of saturated, surface-dry aggregate crushing value test versus micro-Deval is shown in Figure 3.5.

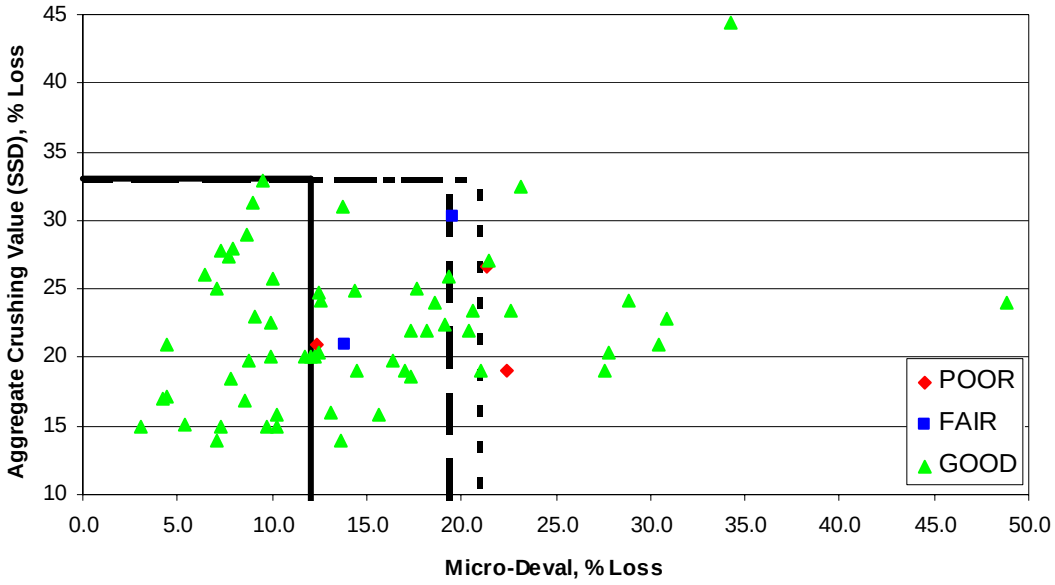

Figure 3.5: Aggregate Crushing Value (SSD) vs. Micro-Deval

Since the test is very similar to the aggregate crushing value test previously analyzed, similar results were expected. Table 3.5 summarizes the results of the quantitative analysis carried out on the plot data. Both the quadrant success rate of 94% and overall

Table 3.5: WCV and MD Success Rate

TRIAL NUMBER	1	2	3
WCV	33	33	33
MD	12	19.5	21
QUADRANT	100%	96%	94%
GOOD	44%	78%	83%
FAIR	100%	50%	0%
POOR	100%	67%	67%
OVERALL	48%	77%	80%

success rate of 80% are identical to that of aggregate crushing value and micro-Deval combination despite the different trial course of action taken. Thus, it can be concluded that this combination does not provide any more information than the previously-discussed aggregate crushing value and micro-Deval combination.

Figure 3.6 provides the results of incorporation micro-Deval and absorption information on the same plot. Quantitative analysis carried out using Microsoft Excel 2003 is summarized in Table 3.6. At micro-Deval loss of 22% and absorption capacity of 6%, the overall success rate of 80% is achieved while the quadrant success rate is 93%. However, at Trial #3 which represents the optimal solution for the overall success rate as well as the quadrant success rate, none of the fair aggregates are identified correctly and only one poor source is identified as poor. Thus, it can be concluded that the combination does provide useful information but it is not as high as achieved by other tests.

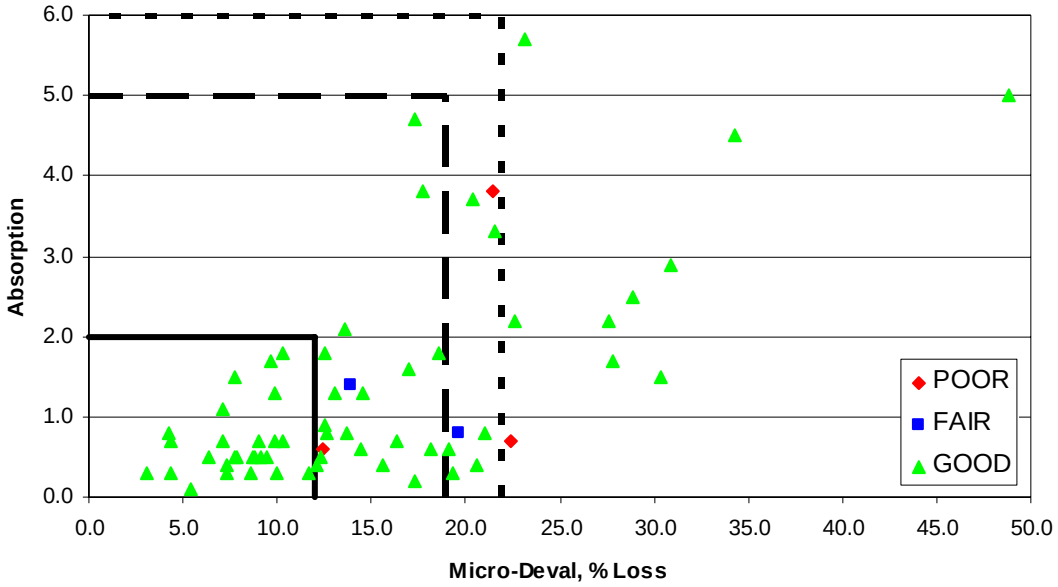

Figure 3.6: Absorption vs. Micro-Deval

Table 3.6: ABS and MD Success Rate

TRIAL NUMBER	1	2	3
ABS	2	5	6
MD	12	19	22
QUADRANT	100%	96%	93%
GOOD	44%	75%	85%
FAIR	100%	50%	0%
POOR	100%	67%	33%
OVERALL	48%	73%	80%

Bulk specific gravity, saturated surface dry specific gravity, as well as apparent specific gravity were computed during this research project, and the graphs for all three are included in Appendix D. However, all three exhibit identical results and only bulk specific gravity versus micro-Deval is shown in Figure 3.7 as well as further analyzed with Table 3.7 providing a summery of the quantitative analysis. As the table

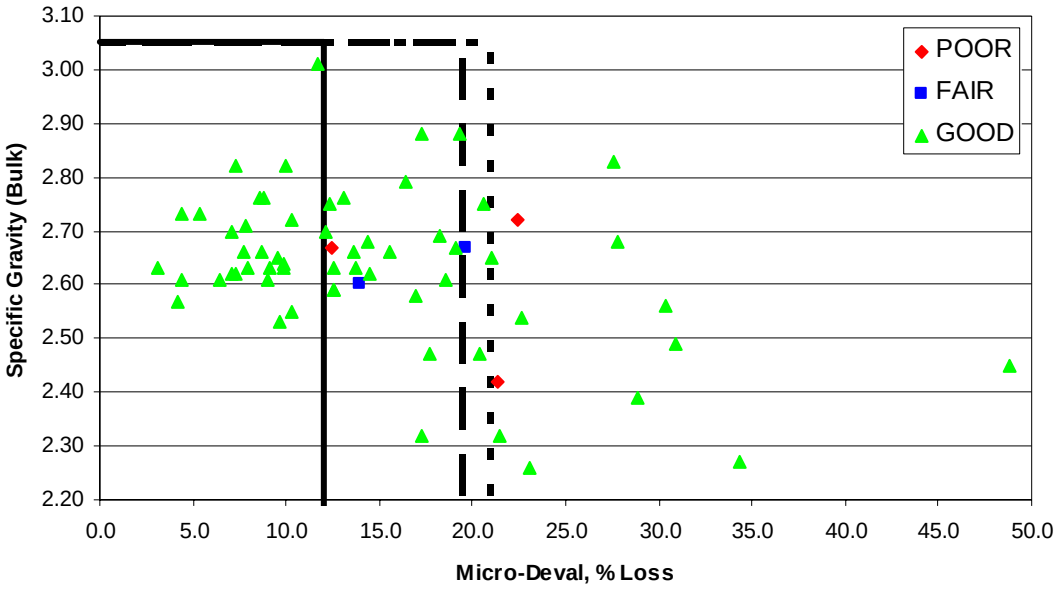

Figure 3.7: Specific Gravity (Bulk) vs. Micro-Deval

indicates, the highest overall success rate achieved is once again 80%, and the highest quadrant success rate is 93%. Once again, a very high success rate of 85% of good sources is achieved in the optimal solution while none of the fair sources

Table 3.7: SG (Bulk) and MD Success Rate

TRIAL NUMBER	1	2	3
SG(BULK)	3.05	3.05	3.05
MD	12	19.5	21
QUADRANT	100%	96%	94%
GOOD	44%	78%	83%
FAIR	100%	50%	0%
POOR	100%	67%	67%
OVERALL	48%	77%	80%

are identified correctly and only one poor sources is qualified as such. Thus, it can be concluded that this two-test combination provides useful information although not as much as previously-discussed micro-Deval and Canadian freeze-thaw tests combination.

The results of particle shape factor and micro-Deval are shown in Figure 3.8 and summarized in Table 3.8. As the data demonstrate, the same overall success

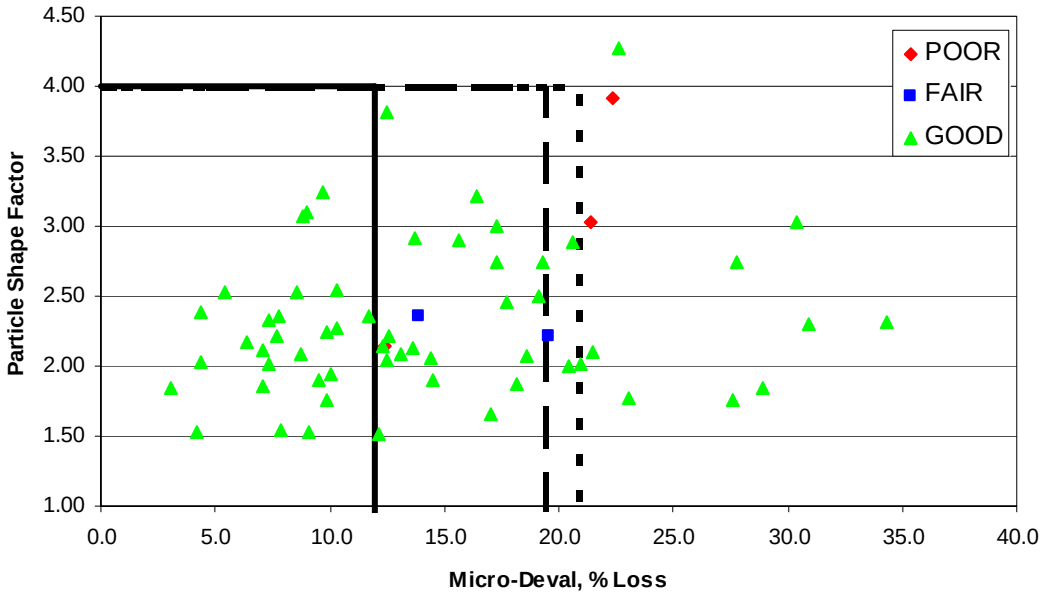

Figure 3.8: Particle Shape Factor vs. Micro-Deval

rate of 80% was achieved. However, this two-test combination also provides the highest quadrant success rate observed thus far of 94%. Although none of the fair sources are identified correctly, 83% of good sources are and more importantly two of the three poor sources are identified correctly as well. Thus, it can be concluded that the information provided by this combination is quite significant.

Table 3.8: PSF and MD Success Rate			
TRIAL NUMBER	**1**	**2**	**3**
PSF	4	4	4
MD	12	19.5	21
QUADRANT	100%	96%	94%
GOOD	44%	78%	83%
FAIR	100%	50%	0%
POOR	100%	67%	67%
OVERALL	48%	77%	80%

3.3 SUCCESS RATE COMPARISON OF OTHER RELEVANT TWO-TEST COMBINATIONS

Since every test was plotted against every other test carried out during this research project, it was necessary to visually inspect all graphs and perform qualitative analysis on those graphs that visual inspection identified as possibly having a high quadrant success rate. Only the following combinations exhibited the possibility of meaningful quadrant division:

- Aggregate crushing value and L.A. abrasion
- Particle shape factor and L.A. abrasion
- Particle shape factor and Canadian freeze-thaw

Quantitative analysis was performed on those three graphs according to the procedure previously described. However, in each situation, it was determined that the optimal solution lies when all points lie within the quadrant. Hence, no useful information for comparison purposes can be extracted for the three plots.

3.4 RESULTS SUMMARY AND CONCLUSIONS

Table 3.9 provides a summary of the discussion above. As the data illustrate, all two-test combinations had very similar overall success rates with the maximum of 81% being achieved by micro-Deval and Canadian freeze-thaw combination.

Table 3.9: BC Success Rates Summary

	OVERALL SUCCESS RATE	QUADRANT SUCCESS RATE
MAGNESIUM SULFATE SOUNDNESS	80%	94%
L.A. ABRASION	80%	93%
CANADIAN FREEZE-THAW	81%	96%
AGGREGATE CRUSHING VALUE	80%	94%
AGGREGATE CRUSHING VALUE (SSD)	80%	94%
ABSORPTION	80%	93%
SPECIFIC GRAVITY (BULK)	80%	93%
PARTICLE SHAPE FACTOR	80%	94%

This test combination also represents the highest quadrant success rate of 96%. All other tests had the same overall success rate of 80%. Four two-test combinations had a quadrant success rate of 94% while three had a quadrant success rate of 93%. Although the data illustrate that better information can be gained by certain two-test combinations, more research is necessary where fair and poor sources are represented more evenly.

Chapter 4: Test Correlations Analysis

4.1 Correlations Analysis Overview

One of the objectives of this research project was to determine if any correlations could be drawn between any two tests conducted in the study. To accomplish this task, test results of one test were plotted against test results of another test, regardless of performance rating, according to the matrix shown in Table 4.1, where a shaded

Table 4.1: Correlations Graphs

	MD	MSS	LAA	CFT	ACV	ACV (SSD)	ABS	SG (BULK)	SG (SSD)	SG (APP)
MSS	■									
LAA	■	■								
CFT	■	■	■							
ACV	■	■	■	■						
ACV (SSD)	■	■	■	■	■					
ABS	■	■	■	■	■	■				
SG (BULK)	■	■	■	■	■	■	■			
SG (SSD)	■	■	■	■	■	■	■	■		
SG (APP)	■	■	■	■	■	■	■	■	■	
PSF	■	■	■	■	■	■	■	■	■	■

rectangle indicates that the graph was plotted. Additionally, all graphs are included in the Appendix E. Once the graphs were created, correlation analysis was performed on each one to measure the strength of the association between numerical variables by performing linear regression analysis. In cases where no linear relationship clearly existed, logarithmic, polynomial, power, and exponential regression analyses were performed using Microsoft Excel 2003. During the analysis, the coefficient of determination R^2,

which measures the proportion of variation that is explained by the independent variable X in the regression model, was computed according to the following formula:

$$r^2 = \frac{SSR}{SST} = \frac{regression\_sum\_of\_squares}{total\_sum\_of\_squares}$$

where SST measures the variation of the Y-values around their mean Y and SSR explains the variation attributable to the relationship between X and Y. Finally, correlation coefficient can be computed by taking the square root of the R^2 value. Since it is common in research practice to report the coefficient of determination value, R^2 will be used throughout this report for comparison and analysis purposes.

Upon recommendation of Dr. Zhanmin Zhang of the University of Texas at Austin whose expertise lies in the area of statistical analysis within the field of Civil Engineering, R^2 values were computed for three cases:

1. The complete data set with no outliers eliminated.
2. The data set with 99.7% of the values retained and outliers eliminated based on the assumption of normal population distribution and using the interval of $\mu \pm 3*\sigma$, where μ is the sample mean and σ is the sample standard deviation.
3. The data set with 95% of the values retained and outliers eliminated based on the assumption of normal population distribution and using the interval of $\mu \pm 2*\sigma$, where once again μ is the sample mean and σ is the sample standard deviation.

The complete data set analysis is discussed in Section 4.2, while Case 2 is described in Section 4.3, and Case 3 is discussed in Section 4.4.

4.2 COMPLETE DATA SET REGRESSION ANALYSIS

During this analysis, the complete data set was used for each test with no outliers eliminated to improve R^2 values. Only the graphs where significant correlations were found will be discussed below, but the entire graph set is included in Appendix E. Additionally, Appendix H includes Microsoft Excel tables used to produce the graphs. Table 4.2 provides a summary of R^2 values for each graph plotted in this analysis. The values provided within the table are the highest possible R^2 obtained using linear, logarithmic, second-degree polynomial, power, and exponential regression analysis techniques. The reader should refer to Appendix E for the equations of the best-fit curves that resulted in the highest possible R^2 value.

Table 4.2: Summary of Coefficients of Determination for the Complete Data Set

	MD	MSS	LAA	CFT	ACV	ACV (SSD)	ABS	SG (BULK)	SG(SSD)	SG(APP)
MSS	0.536									
LAA	0.116	0.179								
CFT	0.320	0.389	0.041							
ACV	0.220	0.124	0.650	0.012						
ACV (SSD)	0.196	0.080	0.487	0.005	0.836					
ABS	0.401	0.536	0.075	0.147	0.141	0.134				
SG (BULK)	0.172	0.311	0.171	0.031	0.167	0.172	0.647			
SG (SSD)	0.114	0.247	0.180	0.020	0.161	0.169	0.492	0.975		
SG (APP)	0.012	0.079	0.168	0.009	0.122	0.133	0.140	0.744	0.854	
PSF	0.037	0.013	0.000	0.004	0.033	0.028	0.004	0.009	0.011	0.011

According to statistical analysis, only R^2 values above approximately 0.60 can indicate a notable correlation between two variables. Hence, values greater than 0.60 are

highlighted in Table 4.2. One of the graphs showing a correlation is aggregate crushing value test plotted against L.A. abrasion test. The graph is shown in Figure 4.1.

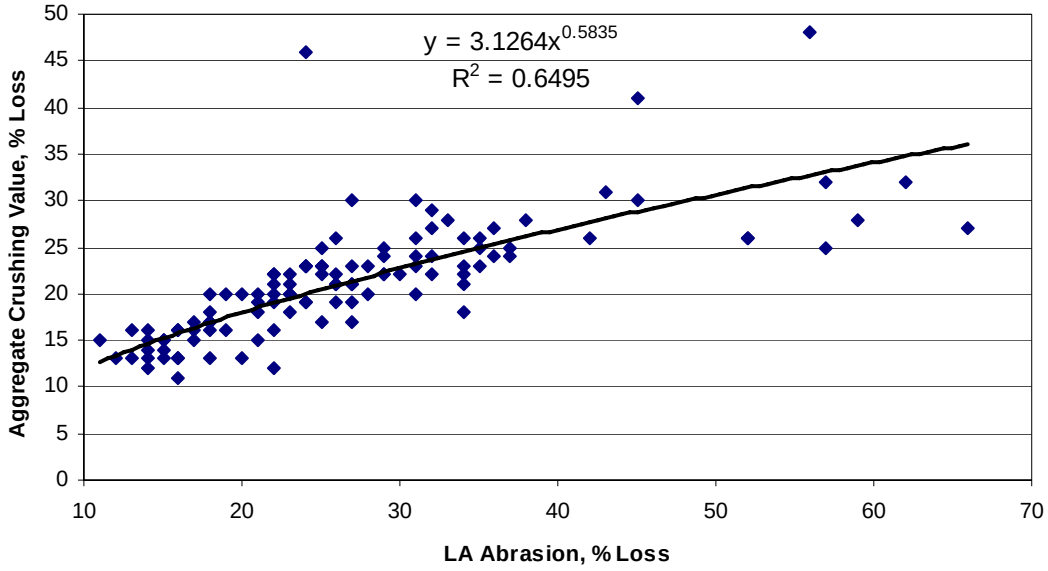

Figure 4.1: L.A. Abrasion vs. Aggregate Crushing Value

As the graph demonstrates, a coefficient of determination of 0.65 was obtained using exponential regression analysis. A correlation was expected in this case since both tests measure aggregate strength to a certain extent – aggregate crushing value test does this directly by subjecting the material to slow crushing pressure in a dry condition while the L.A. abrasion test subjects the aggregate to repeated impact by large steel balls. However, statisticians consider a relationship strong when the R^2 value is greater than approximately 0.75. Hence, the correlation is worth noting but is not very strong in this case.

A strong linear correlation was observed when aggregate crushing value test was plotted against aggregate crushing value (saturated, surface dry). Figure 4.2 illustrates

the strong relationship with the R^2 value of 0.84. This behavior was expected since the two tests are very similar in their procedures with the only difference in the

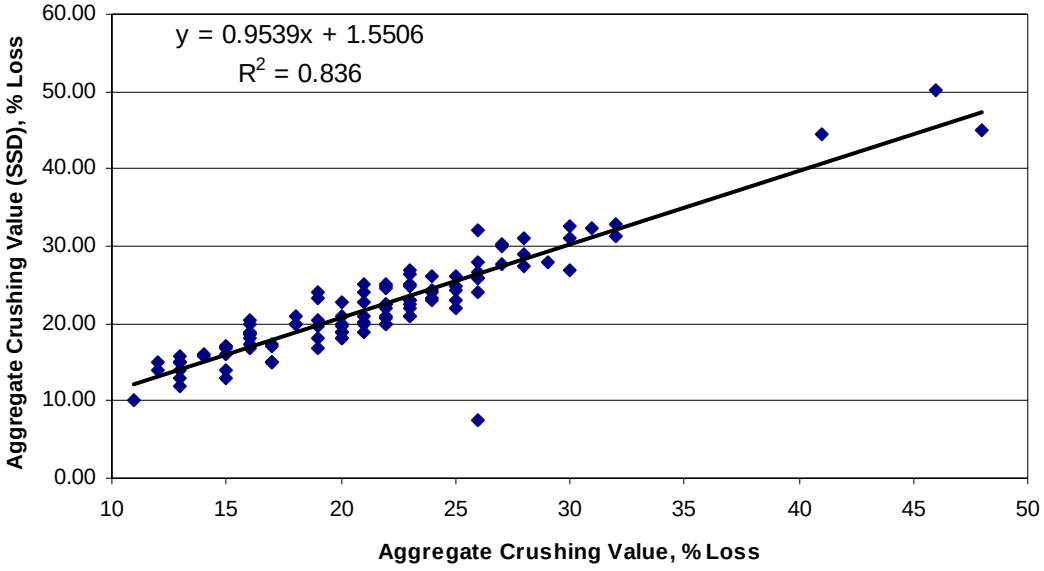

Figure 4.2: Aggregate Crushing Value (SSD) vs. Aggregate Crushing Value

fact that testing of the aggregate is done when the pores are saturated and the surface is dry in the latter case.

A notable correlation was observed when absorption was plotted against bulk specific gravity as Figure 4.3 indicates. During the regression analysis, the highest possible value of R^2 obtained was 0.65, which indicated that a relationship exists. However, statistically it is not a significant one since the value is less than 0.75, and hence it can be concluded that the correlation between the two tests is not strong.

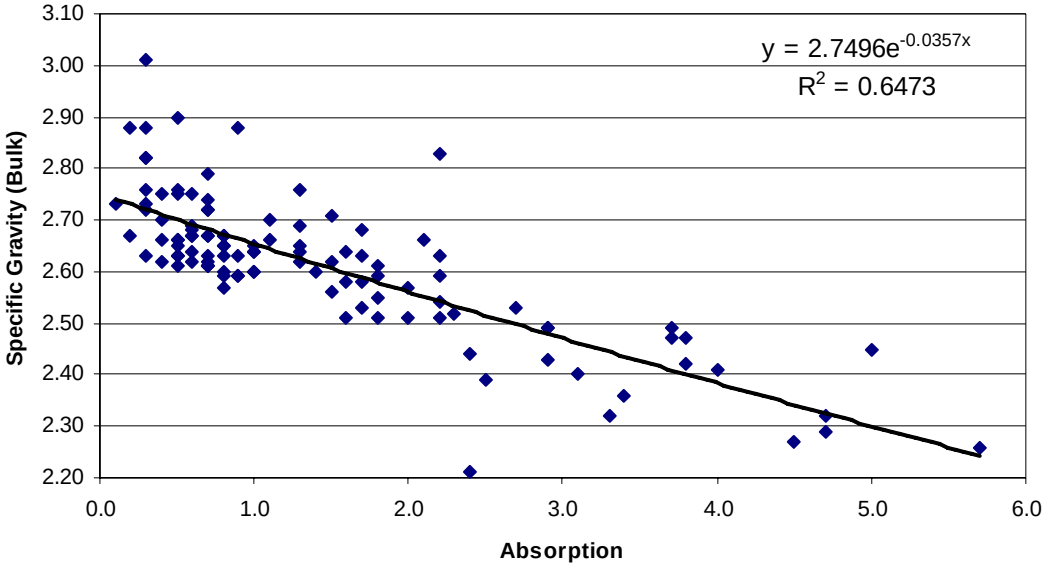

Figure 4.3: Specific Gravity (Bulk) vs. Absorption

A strong correlation was expected when bulk specific gravity was plotted against saturated, surface-dry specific gravity. The plot is shown in Figure 4.4.

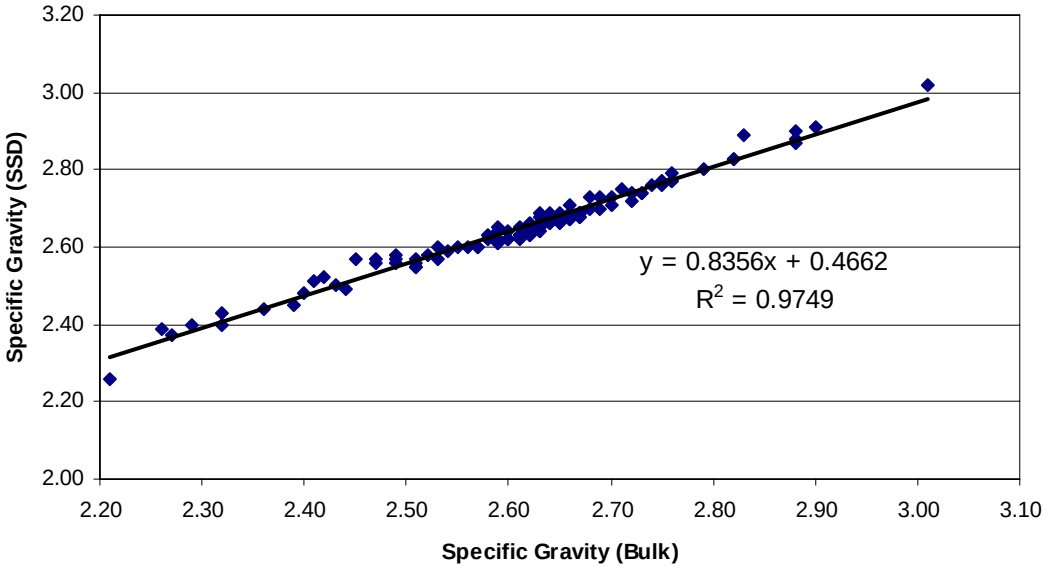

Figure 4.4: Specific Gravity (SSD) vs. Specific Gravity (Bulk)

Regression analysis showed that the linear relationship produces the highest R^2 value of 0.97. As the coefficient of determination indicates, the relationship is very strong, and hence, it can be recommended that the value of one test can be predicted using the equation of the line given in Figure 4.4.

A similar behavior was observed when bulk specific gravity was plotted against apparent specific gravity. As Figure 4.5 indicates, the coefficient of determination of 0.74 is high and is achieved when quadratic curve is used. Thus, it can be concluded that

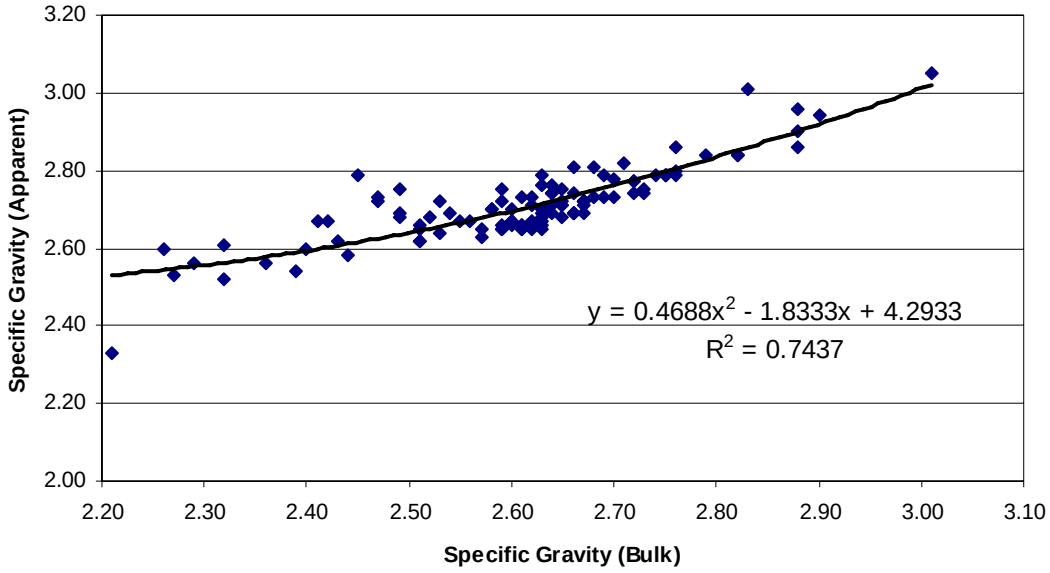

Figure 4.5: Specific Gravity (Apparent) vs. Specific Gravity (Bulk)

the relationship is strong, and the two tests can be correlated using the equation provided in Figure 4.5 with relatively high certainty.

Another notable correlation was noted when apparent specific gravity was plotted against saturated, surface-dry gravity as shown in Figure 4.6. A coefficient of determination of 0.85 was obtained when quadratic curve was used in the regression analysis. Using linear regression analysis produced similarly high value of the

coefficient of determination. The R^2 value is close to 1.0 and hence the correlation is strong when the curve shown in Figure 4.6 is used to correlate the two tests.

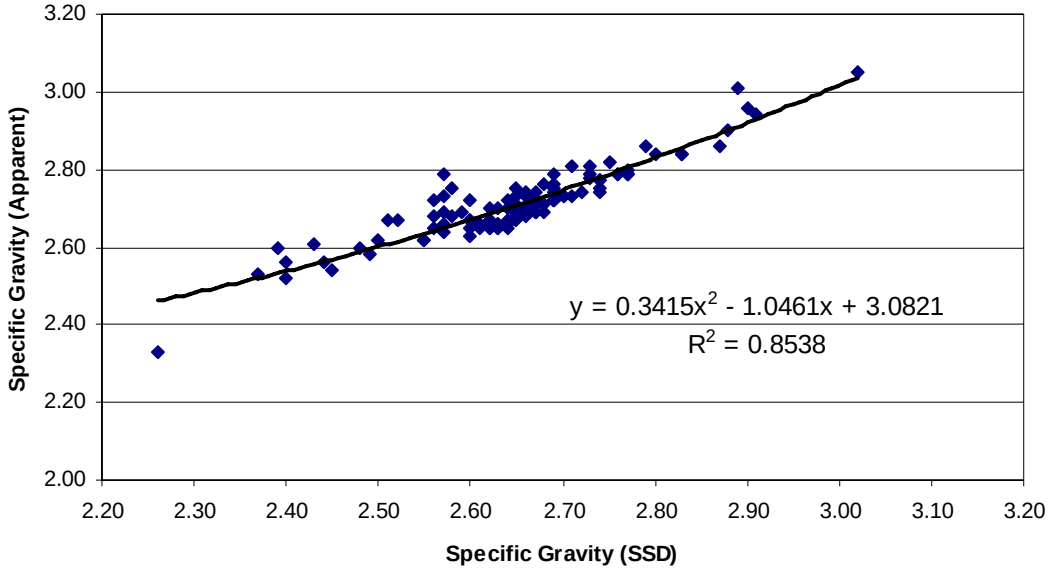

Figure 4.6: Specific Gravity (Apparent) vs. Specific Gravity (SSD)

Unfortunately, no other tests showed notably strong correlations. In particular, micro-Deval did not correlate well with any of the tests. Interestingly, an R^2 value of only 0.12 was observed between L.A. abrasion and micro-Deval tests indicating that no correlation exists between the two tests even though both tests subject the aggregates to impact by steel balls. A possible explanation for this behavior could lie in the fact that the aggregate pores are saturated with water in micro-Deval testing while the aggregate is completely dry when tested in the L.A. abrasion machine. Furthermore, no correlation was observed between magnesium sulfate soundness and Canadian freeze-thaw tests despite the fact that both measure aggregate resistance to freeze-thaw cycles. One possible explanation for such behavior lies in the extremely large test data variations observed during magnesium sulfate testing for each source. Additionally, analysis

showed that the particle shape factor cannot be correlated to any of the tests carried out during this study as computed R^2 values are extremely low.

4.3 PARTIAL DATA SET REGRESSION ANALYSIS I

During computations of R^2 values, outliers carry an extremely negative impact. A presence of only a few outliers can reduce the value of the coefficient of determination significantly. Hence, using the assumption of normal population distribution, some outliers can be eliminated by including points only within the range of $\mu \pm 3 * \sigma$, where μ is the data set mean and σ is the sample standard deviation. Using this procedure, 99.7% of the data points will still be included and some extreme outliers will be eliminating. Thus, a correlation will be more readily seen as the R^2 values should be higher if a correlation exists but was previously disguised by the presence of outliers.

Using Microsoft Excel 2003, the data for each test were analyzed and outliers eliminated as described above. A complete set of graphs was then produced and is included in Appendix F. Additionally, Appendix H includes Microsoft Excel tables showing which points were eliminated based on the prescribed criteria. Table 4.3 provides a summary of maximum R^2 values obtained using linear, logarithmic, second-degree polynomial, power, and exponential regression analysis techniques. The reader should refer to Appendix F for the equations of the best-fit curves that resulted in the highest possible R^2 values.

Table 4.3: Summary of Coefficients of Determination for the Partial Data Set I

	MD	MSS	LAA	CFT	ACV	ACV (SSD)	ABS	SG (BULK)	SG (SSD)	SG (APP)
MSS	0.565									
LAA	0.122	0.129								
CFT	0.223	0.393	0.045							
ACV	0.171	0.074	0.704	0.011						
ACV (SSD)	0.154	0.032	0.571	0.015	0.748					
ABS	0.330	0.528	0.063	0.120	0.011	0.036				
SG (BULK)	0.211	0.279	0.151	0.031	0.068	0.148	0.623			
SG (SSD)	0.190	0.218	0.163	0.019	0.095	0.116	0.503	0.978		
SG (APP)	0.132	0.088	0.135	0.009	0.091	0.120	0.147	0.722	0.831	
PSF	0.029	0.001	0.006	0.007	0.014	0.021	0.064	0.041	0.040	0.043

As Table 4.3 demonstrates, no significant changes in R^2 values were observed indicating that the very extreme outliers do no influence the data significantly. One R^2 change worth noting did occur for the L.A. abrasion test vs. aggregate crushing value test since the R^2 value increased from 0.65 to 0.71 indicating that the relationship between the two tests is statistically important and should be noted.

4.4 PARTIAL DATA SET REGRESSION ANALYSIS II

Second data reduction was performed on including only the values that lie in the range of $\mu \pm 2*\sigma$ for each test, where once again μ is the sample mean and σ is the sample standard deviation. Using this method, 95% of the original data are included within calculations of R^2 value. It should be noted, however, that upon performing data reduction, R^2 values are not going to necessarily increase since it is possible that outliers

positively contribute to the computed R^2 value and removing them will reduce the coefficient of determination. The computations were carried out using linear, logarithmic, second-degree polynomial, power, and exponential regression analysis techniques. The entire graph set is contained in Appendix G, and Microsoft Excel tables showing which points were eliminated to obtain the graphs are included in Appendix H. The results are summarized in Table 4.4.Avoid using "below"--redundant

Table 4.4: Summary of Coefficients of Determination for the Partial Data Set II

	MD	MSS	LAA	CFT	ACV	ACV (SSD)	ABS	SG (BULK)	SG (SSD)	SG (APP)
MSS	0.452									
LAA	0.107	0.157								
CFT	0.232	0.320	0.068							
ACV	0.171	0.070	0.701	0.017						
ACV (SSD)	0.190	0.047	0.613	0.025	0.857					
ABS	0.270	0.469	0.041	0.119	0.005	0.002				
SG (BULK)	0.166	0.212	0.126	0.025	0.040	0.020	0.555			
SG (SSD)	0.174	0.170	0.089	0.034	0.035	0.019	0.465	0.969		
SG (APP)	0.123	0.088	0.090	0.002	0.084	0.103	0.116	0.667	0.795	
PSF	0.010	0.033	0.022	0.002	0.005	0.031	0.063	0.064	0.067	0.054

As the table indicates, the only notable improvement in the R^2 value is evident for aggregate crushing value test (saturated, surface-dry) versus L.A. abrasion test. However, the R^2 value is only 0.61 indicating that the relationship is weak. Such behavior was expected since a significant relationship was observed between L.A. abrasion and aggregate crushing value test, and aggregate crushing value test is closely related to the aggregate crushing value (SSD) test.

4.5 RESULTS SUMMARY AND CONCLUSIONS

Statistical analyses were performed on test data to determine if correlations existed between any two tests performed in this research project regardless of performance. Consequently, two data reductions were performed in an attempt to find any correlations previously disguised by the presence of outliers and hence negatively impacting the computed R^2 values. The following conclusions can be drawn:

1. Micro-Deval did not have statistically significant correlations to any other tests.
2. The following pairs of tests were found to have significant correlations: L.A. abrasion and aggregate crushing value, L.A. abrasion and aggregate crushing value (saturated, surface-dry), aggregate crushing value and aggregate crushing value (saturated, surface-dry), absorption and bulk specific gravity, bulk specific gravity and saturated surface-dry specific gravity, bulk specific gravity and apparent specific gravity, as well as saturated surface-dry specific gravity and apparent specific gravity.
3. Upon performing data reduction, the significance level of the following relationships increased: L.A. abrasion and aggregate crushing value, L.A. abrasion and aggregate crushing value (SSD), as well as aggregate crushing value and aggregate crushing value (SSD).
4. Magnesium sulfate soundness test did not correlate well to Canadian freeze-thaw test since the maximum obtained R^2 value was 0.39.
5. Particle shape factor test had extremely low R^2 values and hence did not correlate at all to any of the tests carried out during this research.

Chapter 5: Summary and Future Research

5.1 PROJECT SUMMARY

Due to excellent communication between numerous transportation agencies within the United States and Canada, an international study was possible and carried out to investigate the effectiveness of micro-Deval and other tests in successfully qualifying future field performance of an aggregate based on laboratory test data. During the material collection stage of the project, successful attempts were made to obtain aggregates representing diverse mineralogical backgrounds as well as various field performance. Upon reception of 117 sources, the following laboratory tests were carried out on each one: micro-Deval, magnesium sulfate soundness, L.A. abrasion, Canadian freeze-thaw soundness, aggregate crushing value, aggregate crushing value (SSD), absorption, specific gravity (bulk, saturated surface dry, apparent), particle shape factor determination, and percent fractured test.

Four major uses of aggregates were studied – hot-mix asphalt, portland cement concrete, base course, and open-graded friction course. Within each use category, prediction success rates were studied for micro-Deval alone as well as two-test combinations involving micro-Deval. Furthermore, investigations into all other two-test combinations were carried out. Finally, a test correlation study was performed to determine if any correlations existed between the tests conducted during this research project in an attempt to determine if laboratory results of one test can be used to predict test results of another test.

This thesis presented the results of hot-mix asphalt and base course uses while portland cement and open-graded friction course findings are provided in a thesis by Range to be submitted to the University of Texas at Austin in May 2006. Consequently,

both theses will be combined and published as a single final report presented by the International Center for Aggregate Research in August 2006.

5.2 CONCLUSIONS

Within hot-mix asphalt application category, micro-Deval proved to be the best single-test indicator of performance with the overall success rate of 69%. It was followed by Canadian freeze-thaw soundness with the overall success rate of 65% and magnesium sulfate soundness with the overall success rate of 64%. Further prediction improvements were obtained by combining micro-Deval and Canadian freeze-thaw test data, resulting in the overall success rate of 73%. Similar results were obtained within base course application materials. Both micro-Deval and Canadian freeze-thaw proved to be the best single-test performance indicators, each having the overall success rate of 81%. Further improvements were obtained by combing micro-Deval and Canadian freeze-thaw data, resulting in the overall success rate of 96%.

Additionally, regression analysis showed that micro-Deval did not correlate well to any other test carried out during this research project. However, statistically significant correlations were observed between the following pairs of tests: L.A. abrasion and aggregate crushing value, L.A. abrasion and aggregate crushing value (saturated, surface-dry), aggregate crushing value and aggregate crushing value (saturated, surface-dry), absorption and bulk specific gravity, bulk specific gravity and saturated surface-dry specific gravity, bulk specific gravity and apparent specific gravity, as well as saturated surface-dry specific gravity and apparent specific gravity. Remarkably, magnesium sulfate soundness test did not correlate well to Canadian freeze-thaw test since the maximum obtained R^2 value was only 0.39. Furthermore, the particle shape factor test

had extremely low R^2 values and hence did not correlate at all to any of the tests carried out during this research.

5.3 NEED FOR FUTURE RESEARCH

Two important aspects of this research project require further study that could result in gaining of additional useful information. The first feature that requires further attention is the need to include more poor and fair sources within base course category. Only two fair and three poor sources were available in this study, and hence, prediction success rate comparison of micro-Deval to other tests alone was not possible. However, if more poor and fair sources can be obtained to achieve a balance between the numbers of fair, poor, and good sources, it will become possible to verify the patterns observed during hot-mix asphalt category study.

The second aspect requiring further attention is the need to obtain greater field performance information from participating transportation agencies. For the purposes of this research study, field performance of aggregates was separated into three major categories of poor, fair, or good based on a formal survey created by ICAR 507 research team. While such category division was sufficient to successfully conduct the analysis, it is possible that better results or more useful information can be gained if the performance can be divided into more specific categories by dedicating a considerably greater amount of time investigating actual field performance based on a much more detailed criteria than that used in this research study.

Appendix A: One Test Only Field Performance Graphs for Hot-Mix Asphalt Aggregates

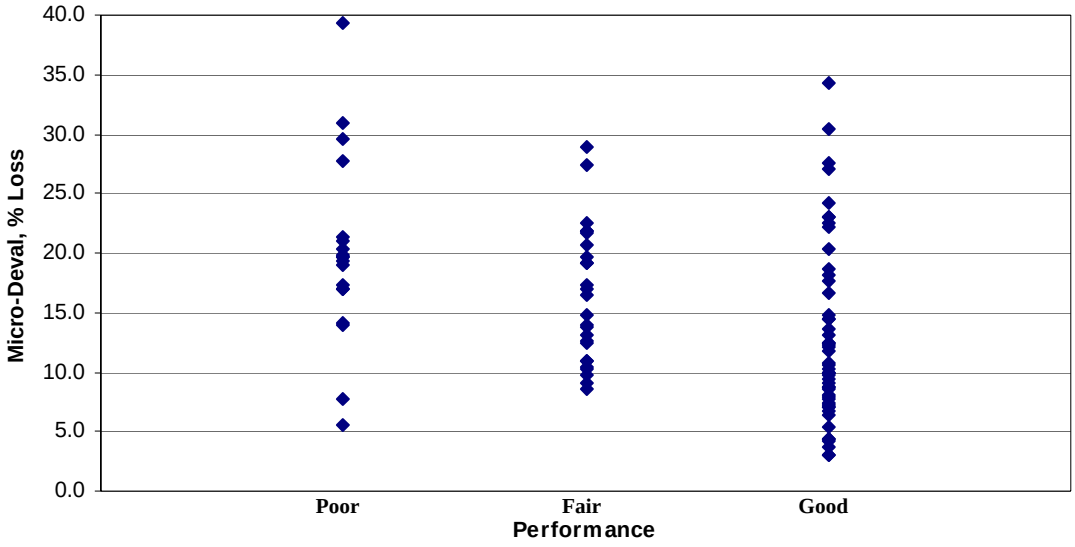

Figure A.1: Micro-Deval vs. Performance

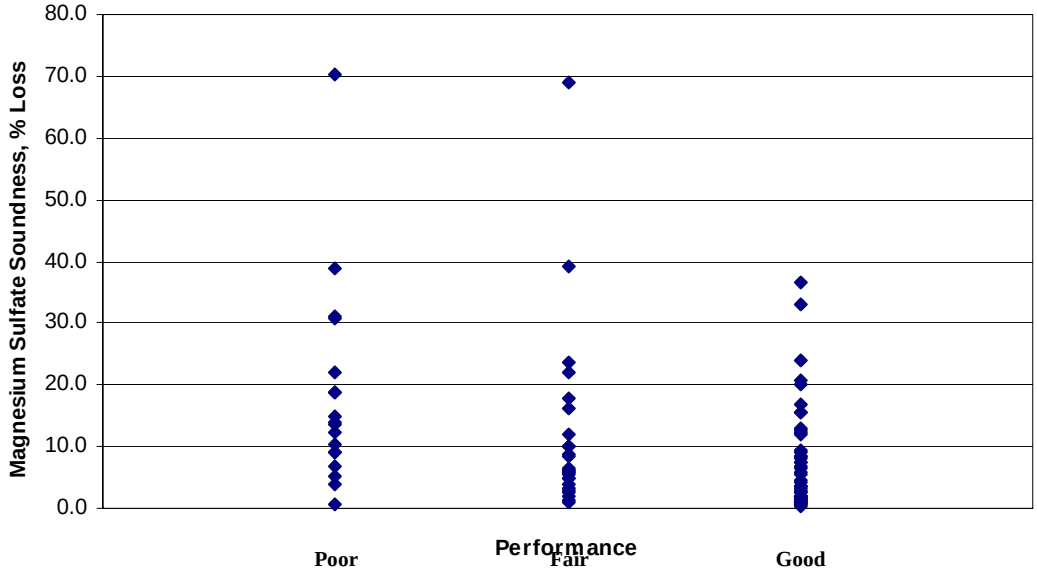

Figure A.2: Magnesium Sulfate Soundness vs. Performance

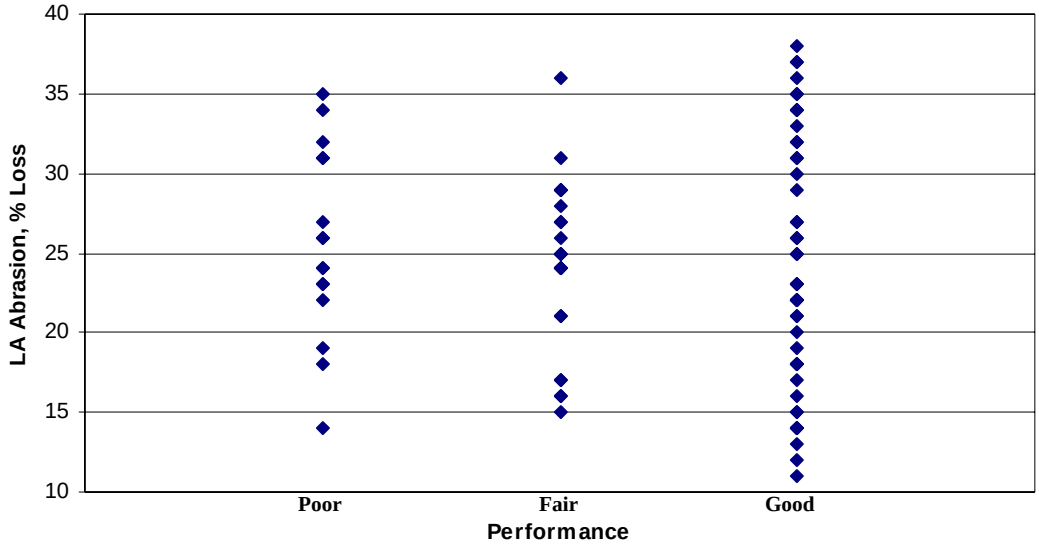

Figure A.3: L.A. Abrasion vs. Performance

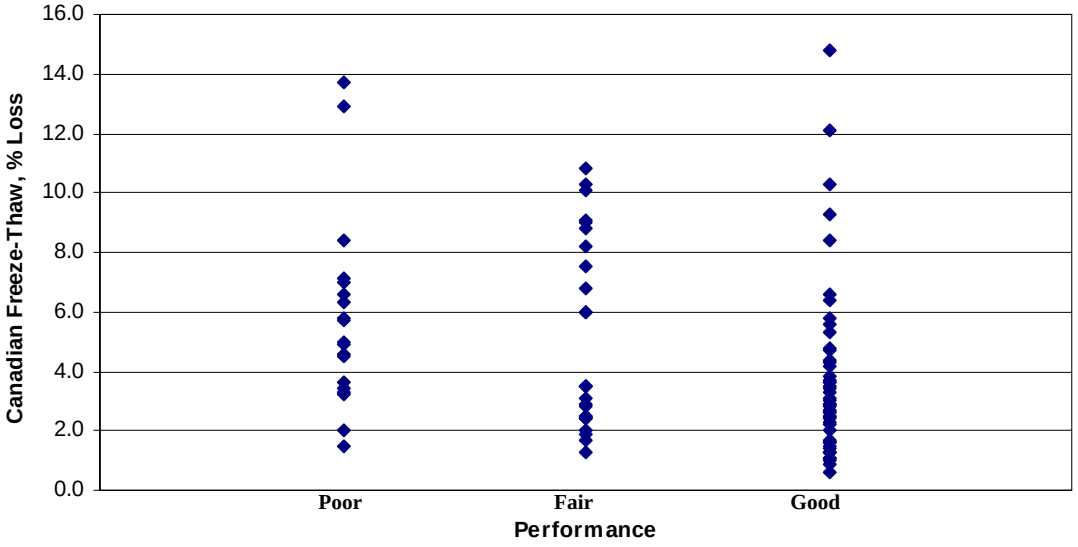

Figure A.4: Canadian Freeze-Thaw Soundness vs. Performance

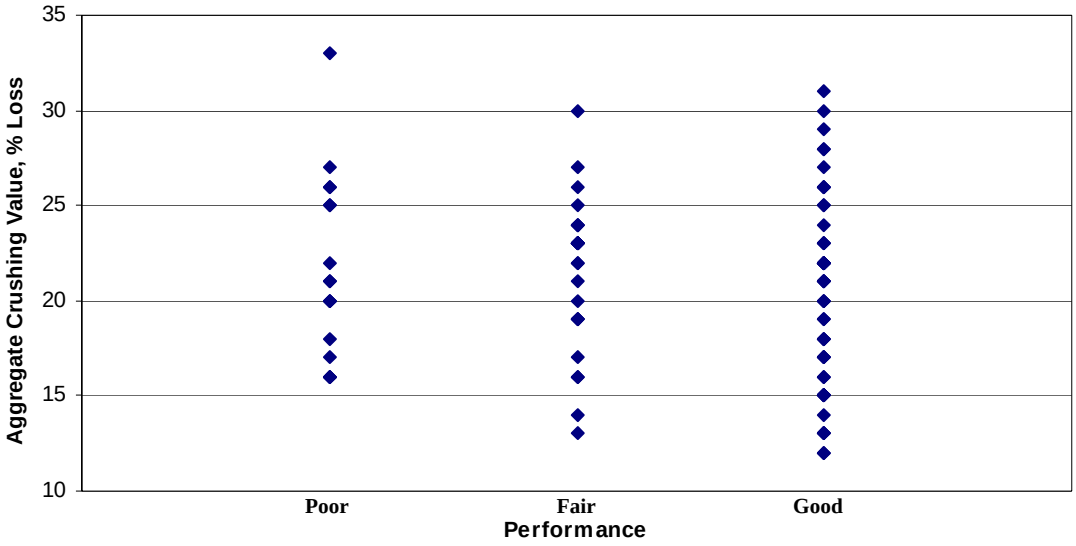

Figure A.5: Aggregate Crushing Value vs. Performance

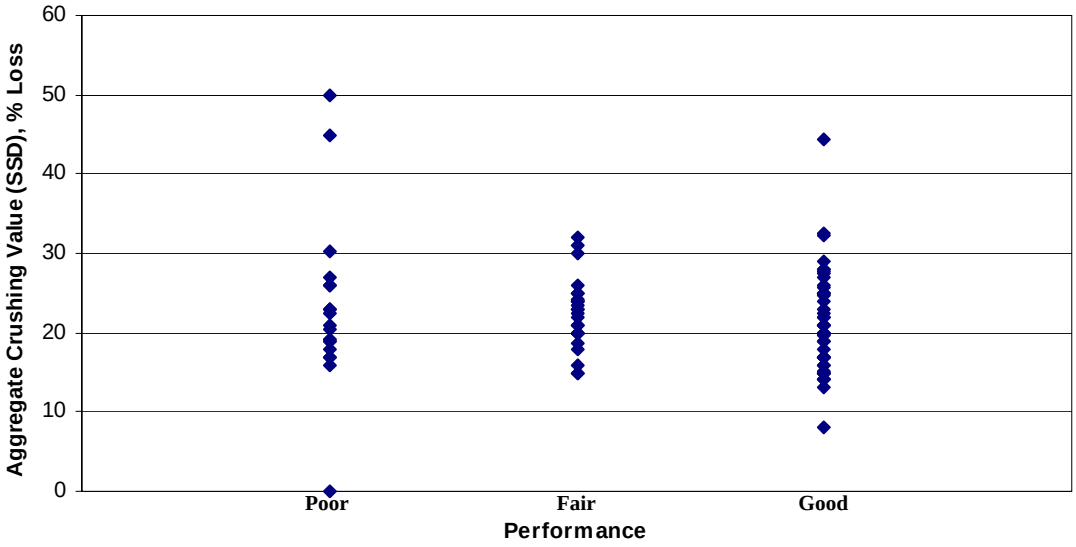

Figure A.6: Aggregate Crushing Value (SSD) vs. Performance

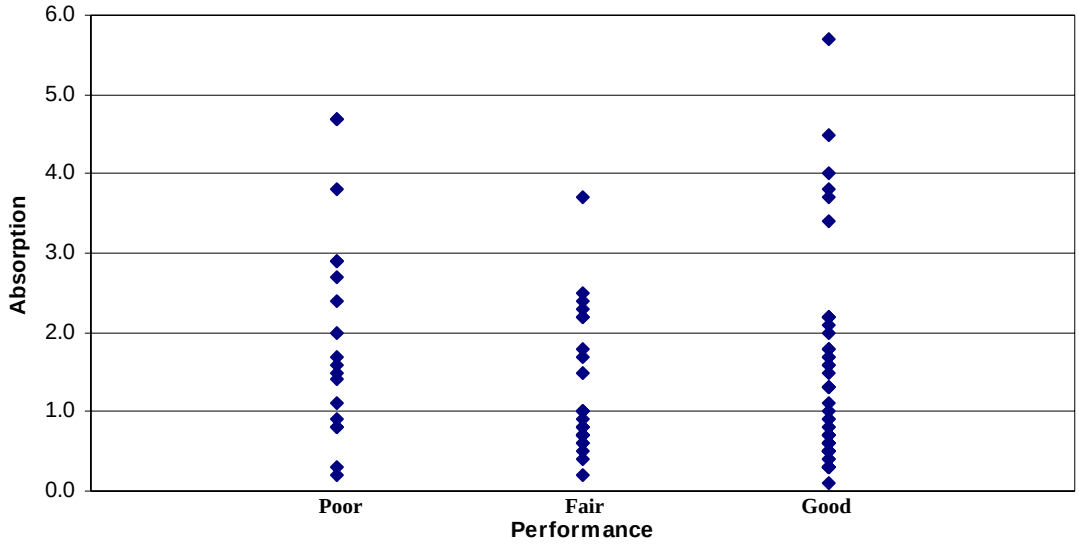

Figure A.7: Absorption vs. Performance

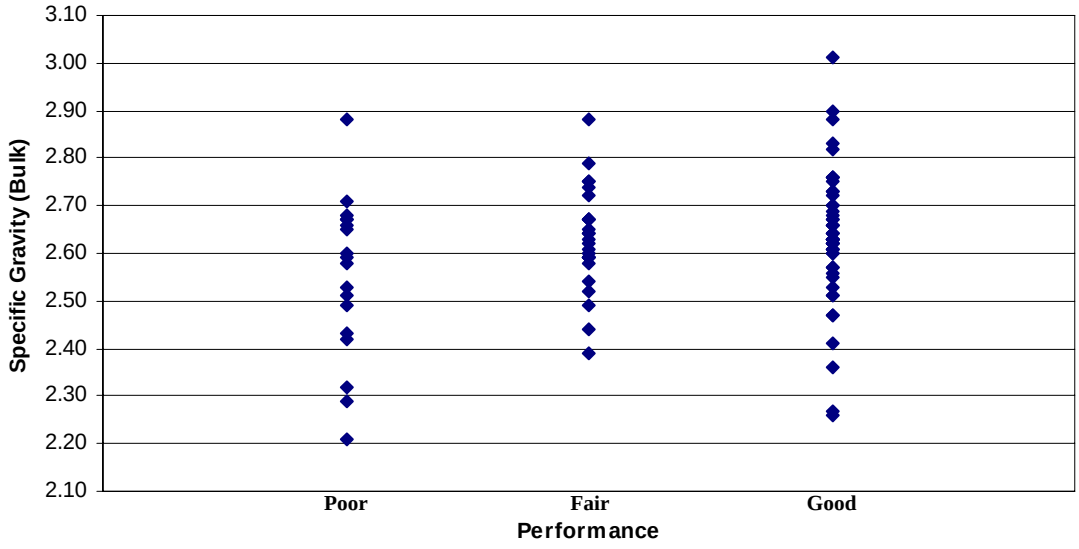

Figure A.8: Specific Gravity (Bulk) vs. Performance

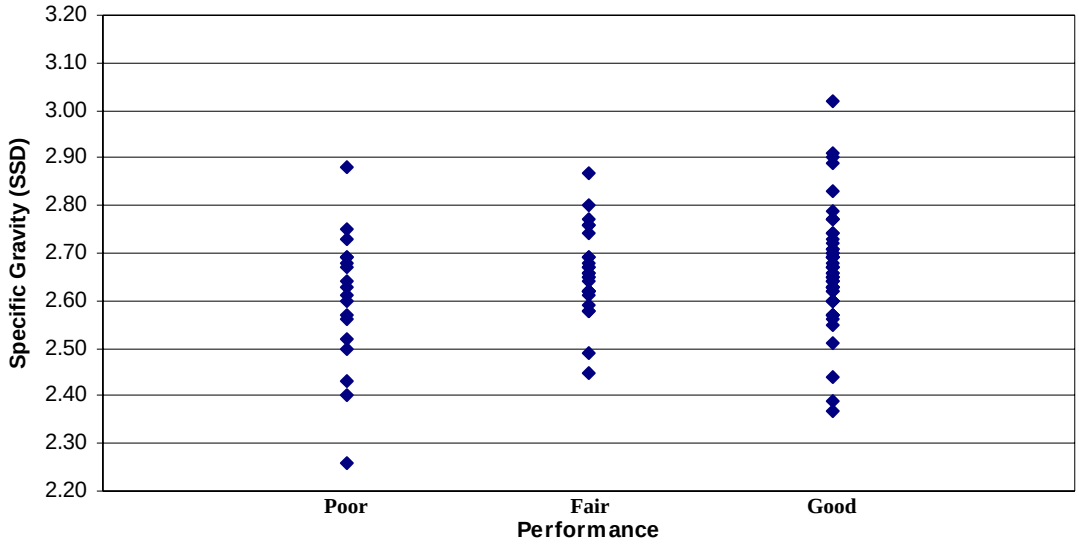

Figure A.9: Specific Gravity (SSD) vs. Performance

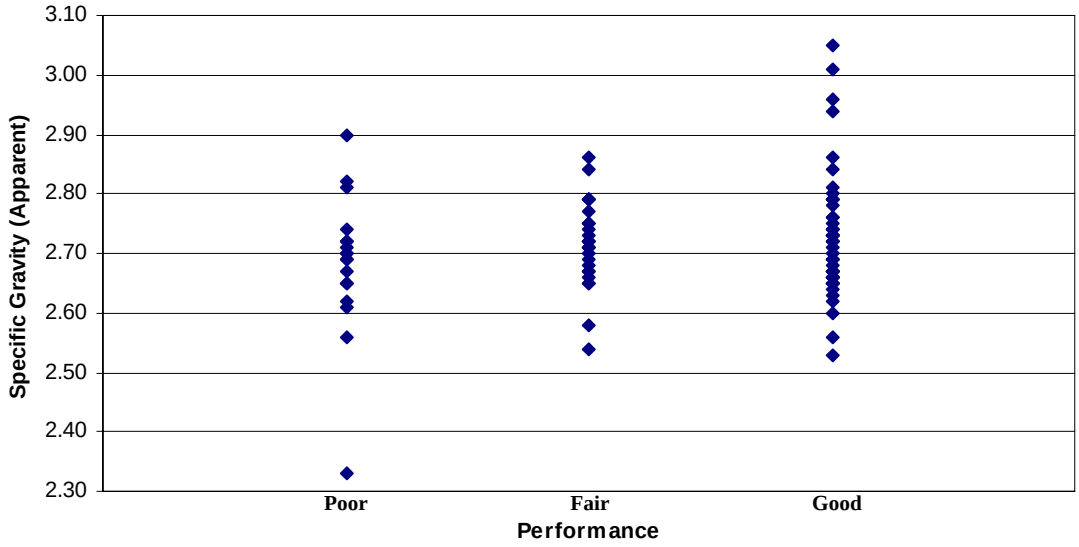

Figure A.10: Specific Gravity (Apparent) vs. Performance

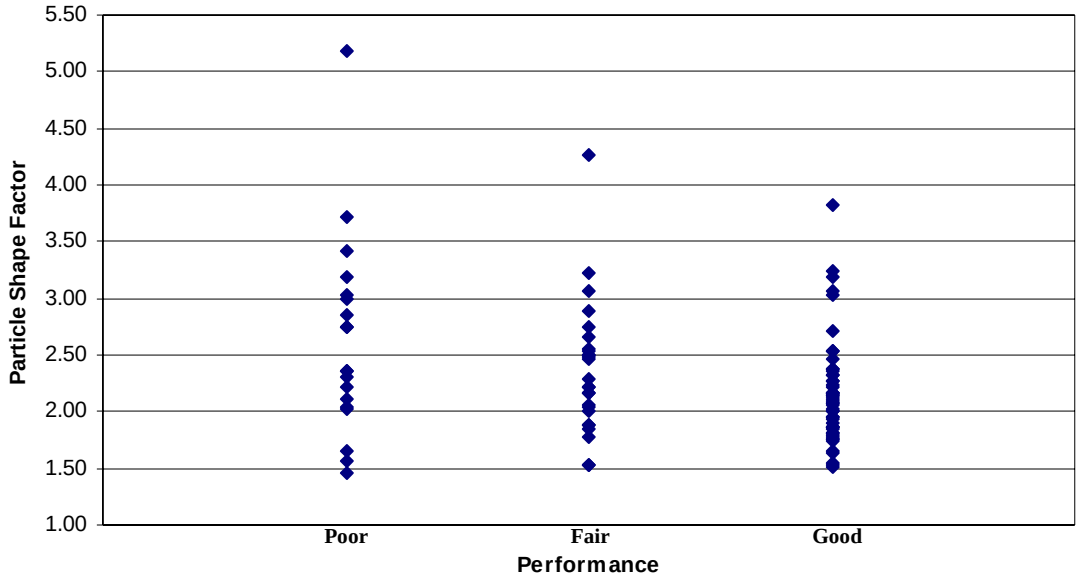

Figure A.11: Particle Shape Factor vs. Performance

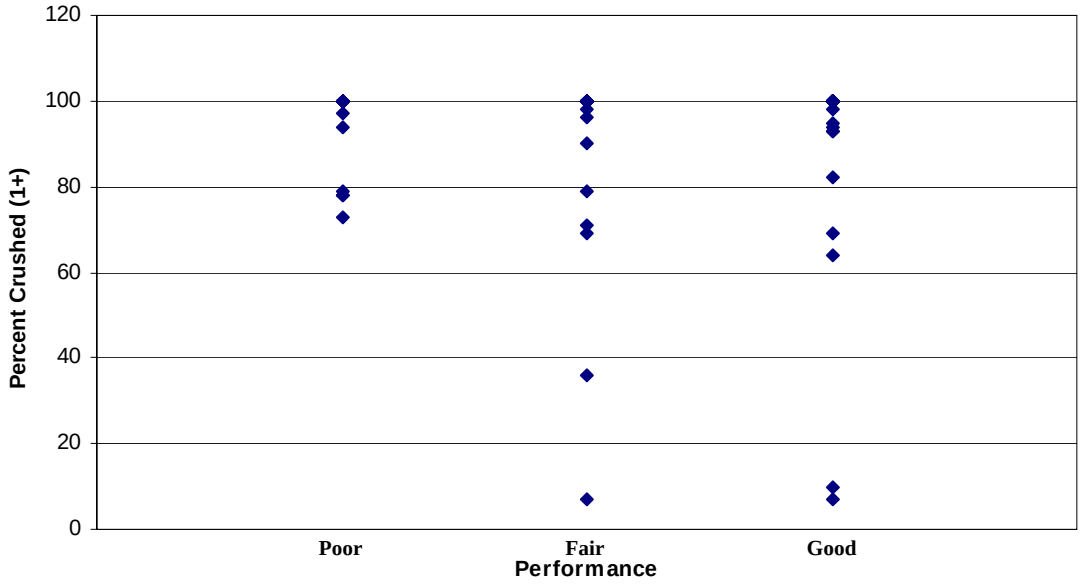

Figure A.12: Particle Shape Factor vs. Performance

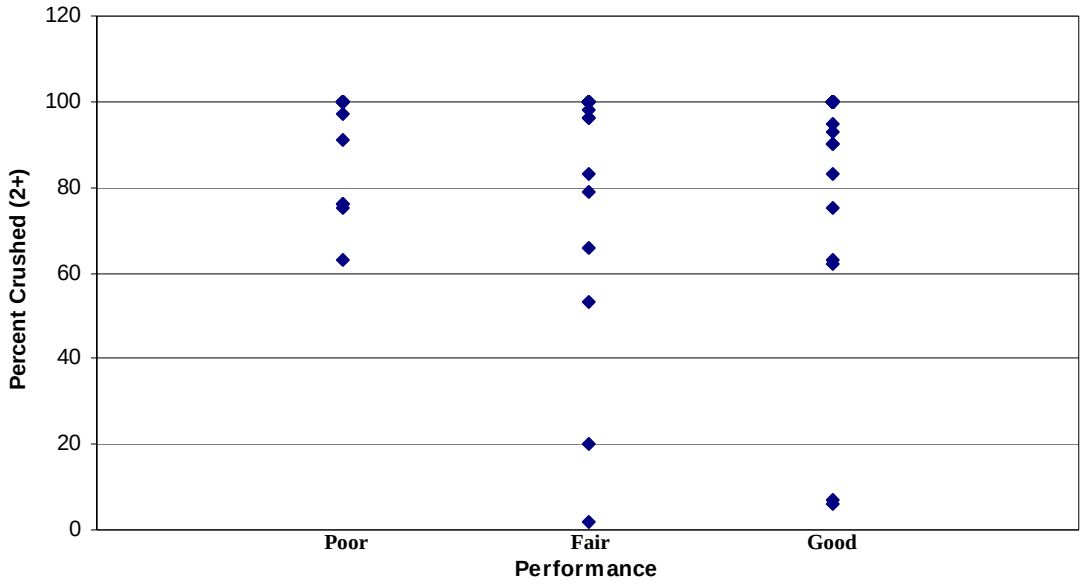

Figure A.13: Particle Shape Factor vs. Performance

	Fractured Particles (1 or more sides)								
	POOR		FAIR		GOOD		Overall %		
% of total	number	overall %	number	overall %	number	overall %	POOR	FAIR	GOOD
100	14	70%	18	69%	42	81%	19%	24%	57%
90 - 99	2	10%	3	12%	5	10%	20%	30%	50%
80 - 89	0	0%	0	0%	1	2%	0%	0%	100%
70 - 79	4	20%	2	8%	0	0%	67%	33%	0%
60 - 69	0	0%	1	4%	2	4%	0%	33%	67%
50 - 59	0	0%	0	0%	0	0%	0%	0%	0%
40 - 49	0	0%	0	0%	0	0%	0%	0%	0%
30 - 39	0	0%	1	4%	0	0%	0%	100%	0%
20 - 29	0	0%	0	0%	0	0%	0%	0%	0%
10 - 19	0	0%	0	0%	1	2%	0%	0%	100%
0 - 10	0	0%	1	4%	1	2%	0%	50%	50%

Table A.1: Percent Fractured Particles (1 or more sides)

	Fractured Particles (2 or more sides)								
	POOR		FAIR		GOOD		Overall %		
% of total	number	overall %	number	overall %	number	overall %	POOR	FAIR	GOOD
100	14	70%	17	65%	42	81%	19%	23%	58%
90 - 99	2	10%	3	12%	4	8%	22%	33%	44%
80 - 89	0	0%	1	4%	1	2%	0%	50%	50%
70 - 79	3	15%	1	4%	1	2%	60%	20%	20%
60 - 69	1	5%	1	4%	2	4%	25%	25%	50%
50 - 59	0	0%	1	4%	0	0%	0%	100%	0%
40 - 49	0	0%	0	0%	0	0%	0%	0%	0%
30 - 39	0	0%	0	0%	0	0%	0%	0%	0%
20 - 29	0	0%	1	4%	0	0%	0%	100%	0%
10 - 19	0	0%	0	0%	0	0%	0%	0%	0%
0 - 10	0	0%	1	4%	2	4%	0%	33%	67%

Table A.2: Percent Fractured Particles (2 or more sides)

Appendix B: Two-Test Combination Field Performance Graphs for Hot-Mix Asphalt Aggregates

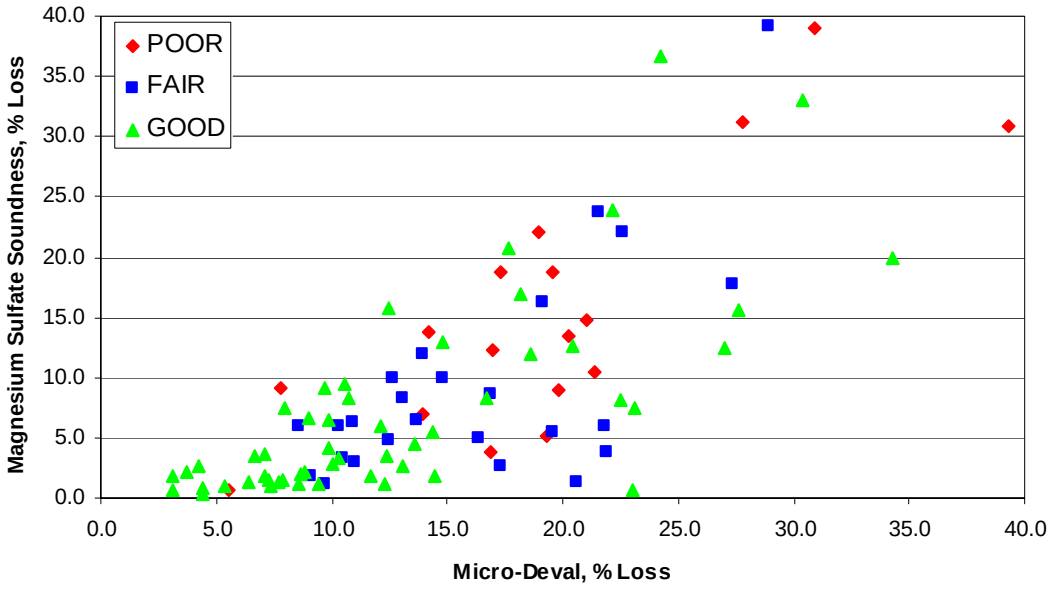

Figure B.1: Magnesium Sulfate Soundness vs. Micro-Deval

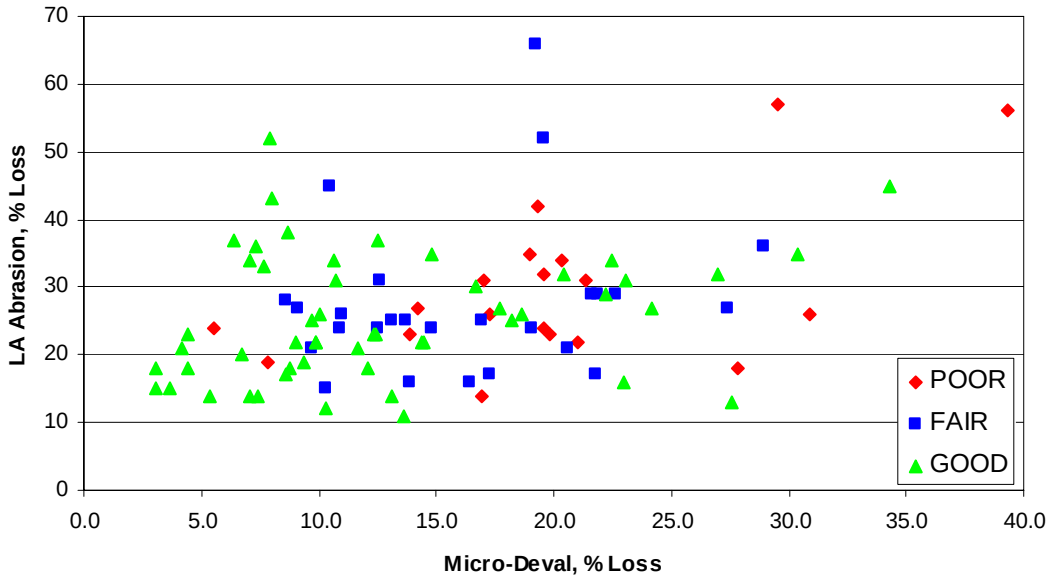

Figure B.2: L.A. Abrasion vs. Micro-Deval

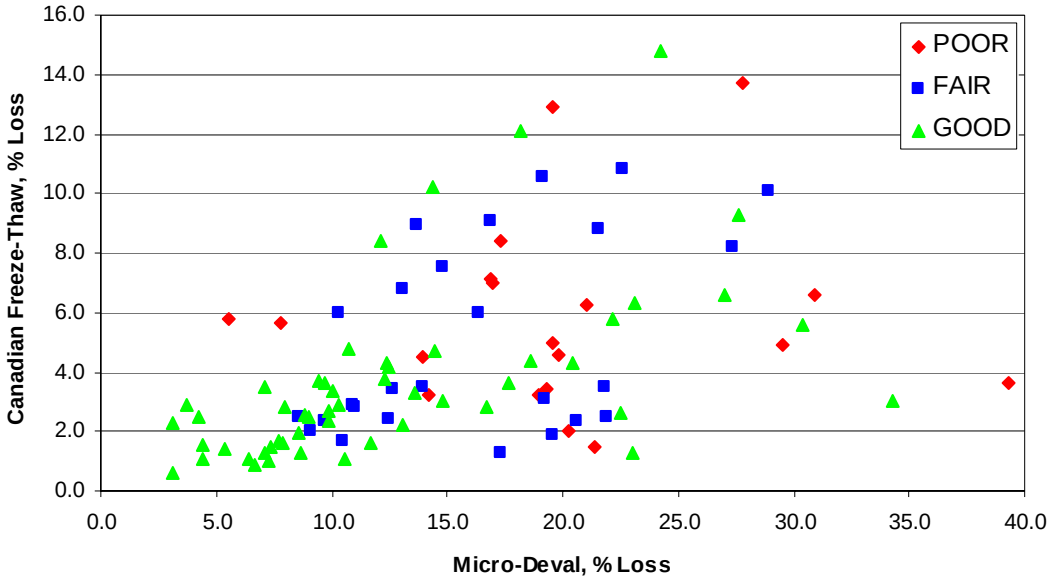

Figure B.3: Canadian Freeze-Thaw Soundness vs. Micro-Deval

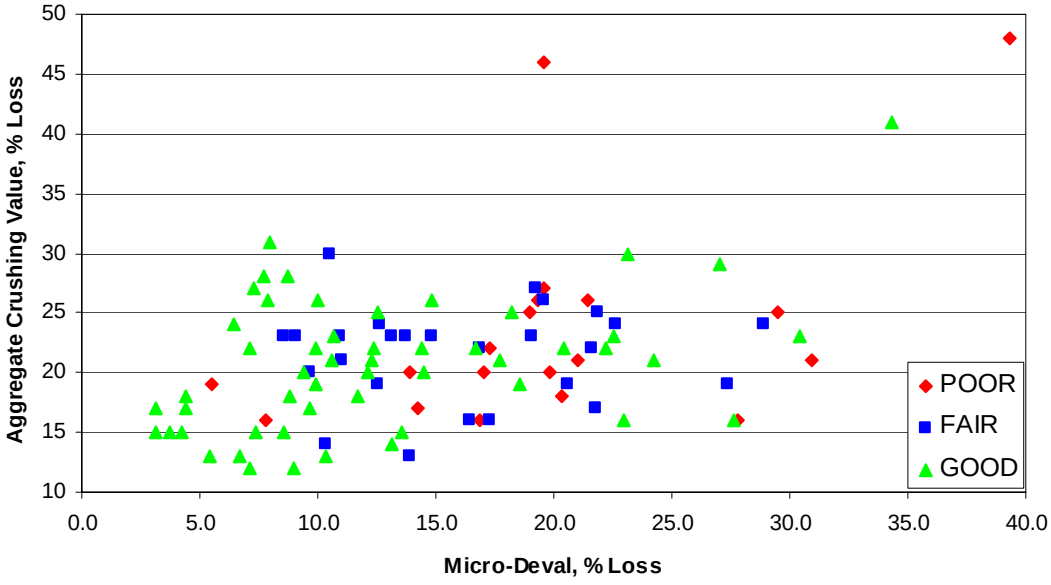

Figure B.4: Aggregate Crushing Value vs. Micro-Deval

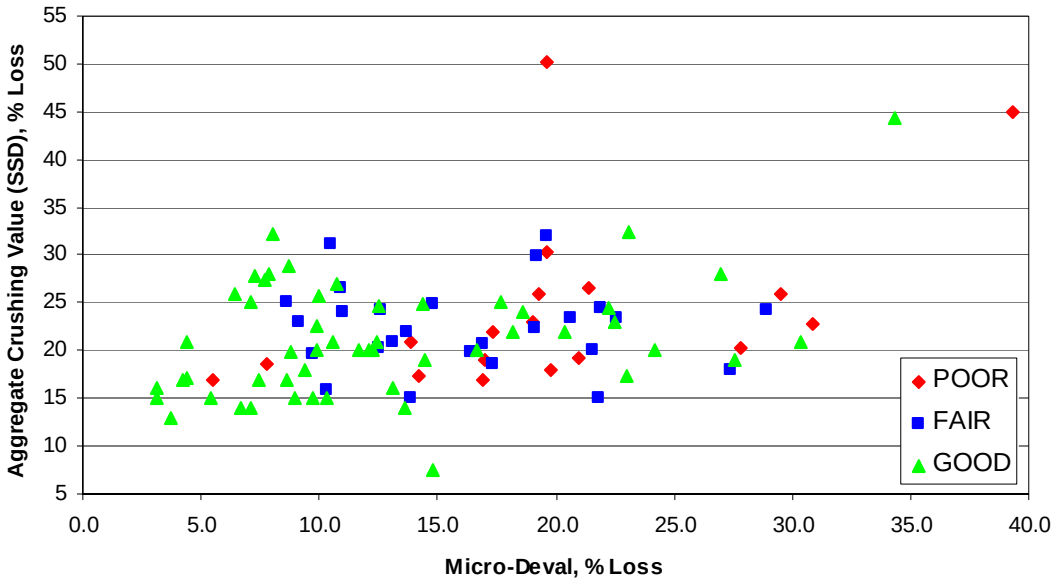

Figure B.5: Aggregate Crushing Value (SSD) vs. Micro-Deval

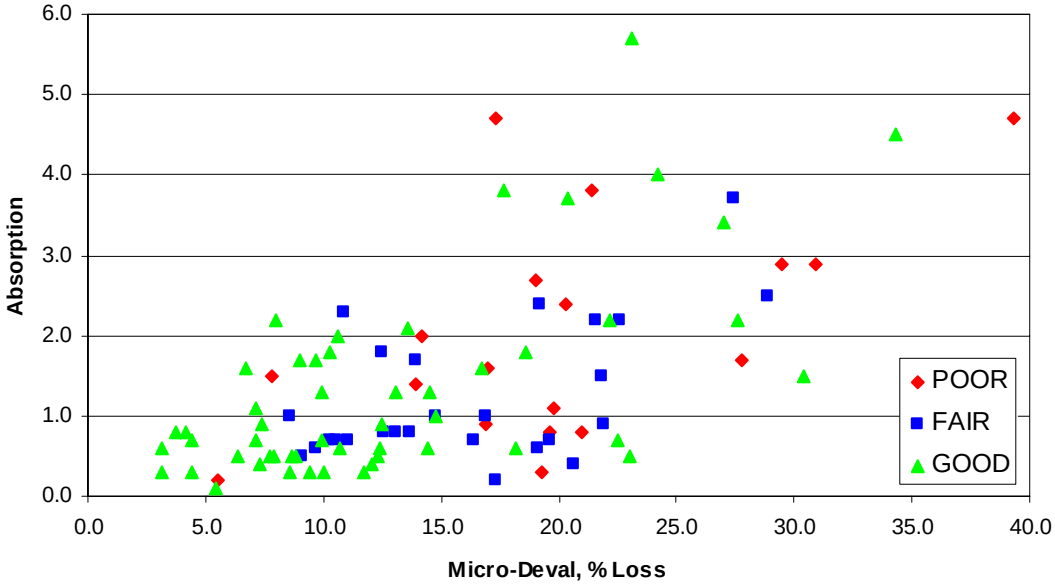

Figure B.6: Absorption vs. Micro-Deval

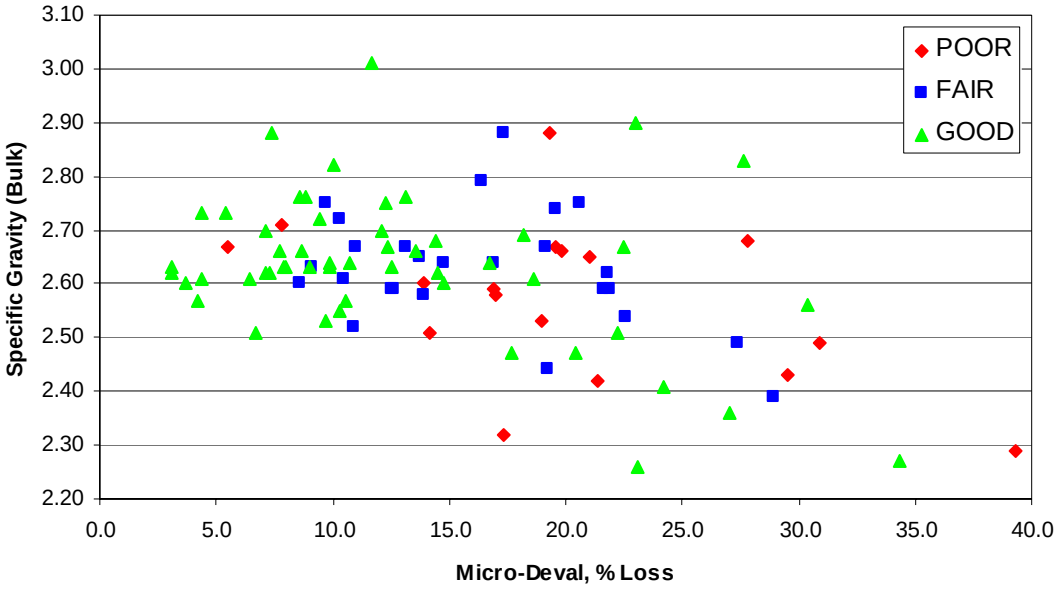

Figure B.7: Specific Gravity (Bulk) vs. Micro-Deval

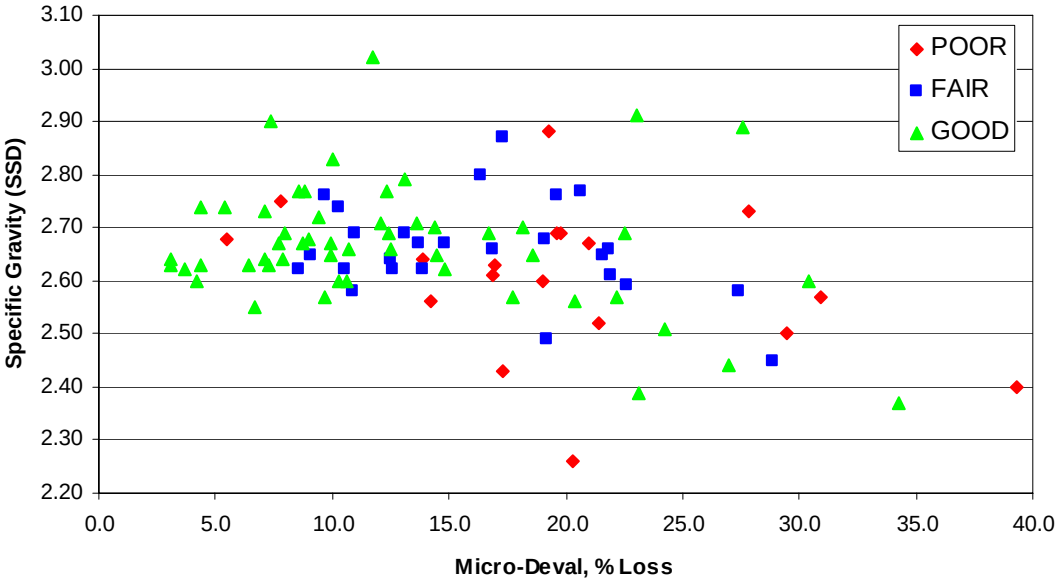

Figure B.8: Specific Gravity (SSD) vs. Micro-Deval

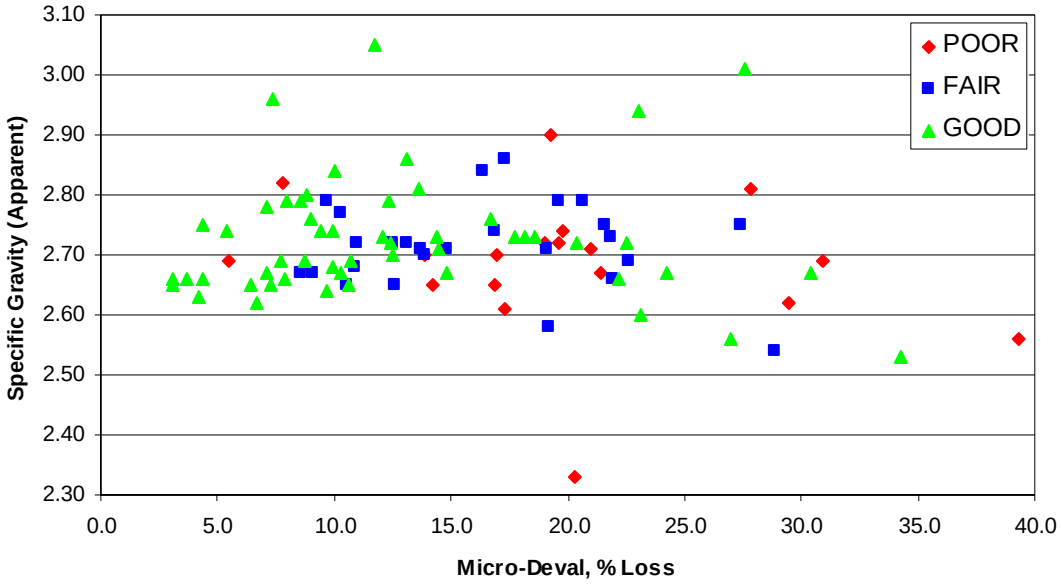

Figure B.9: Specific Gravity (Apparent) vs. Micro-Deval

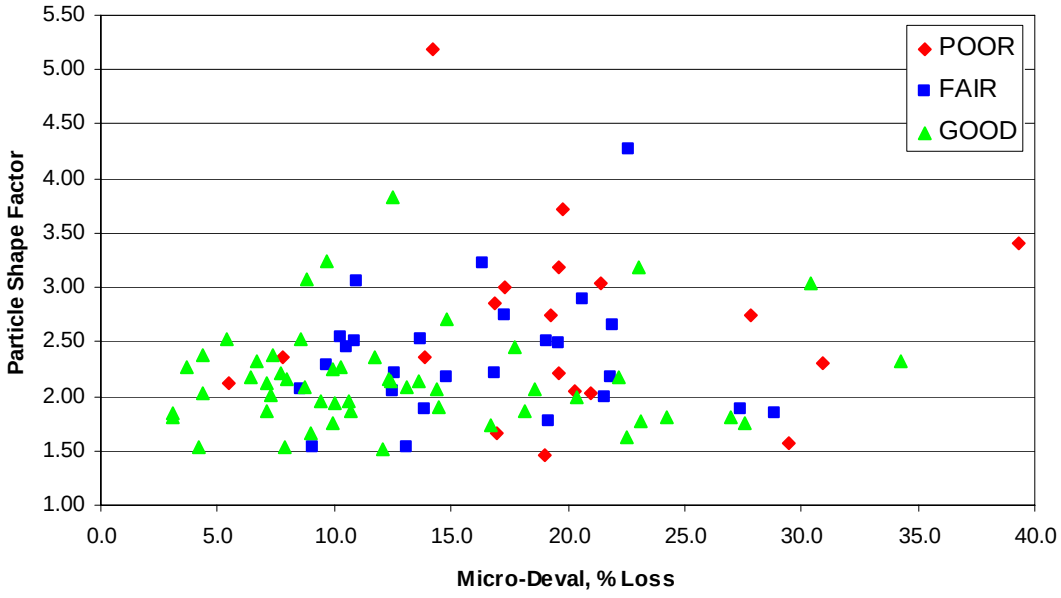

Figure B.10: Particle Shape Factor vs. Micro-Deval

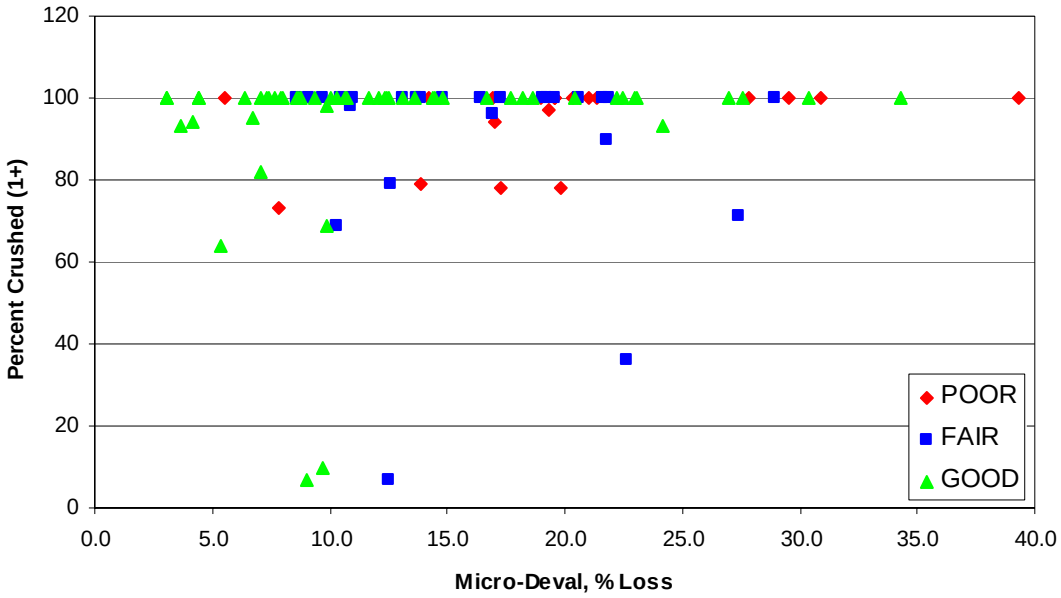

Figure B.11: Percent Crushed (1+ Sides) vs. Micro-Deval

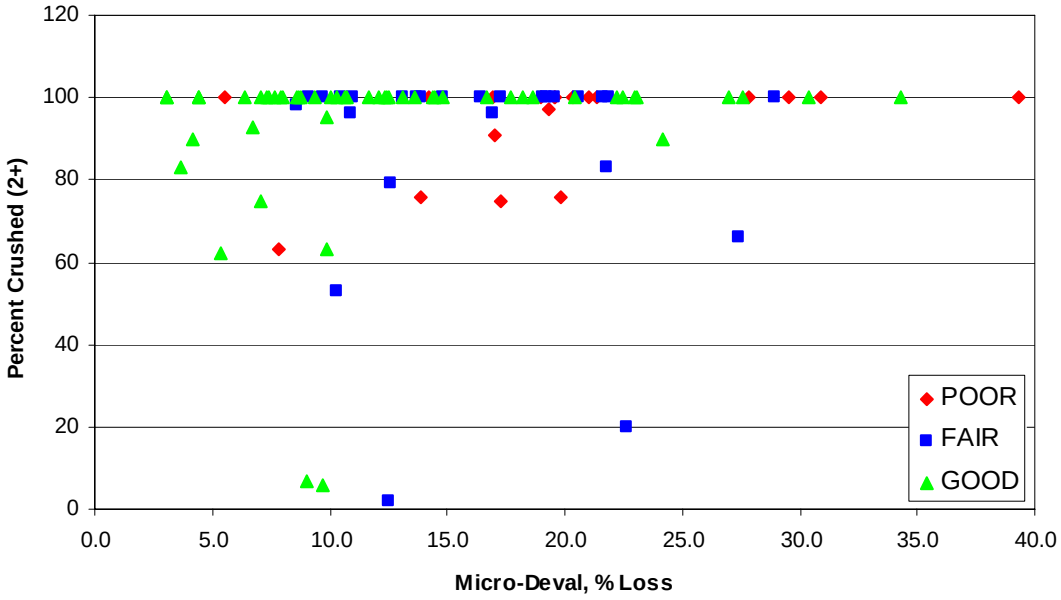

Figure B.12: Percent Crushed (2+ Sides) vs. Micro-Deval

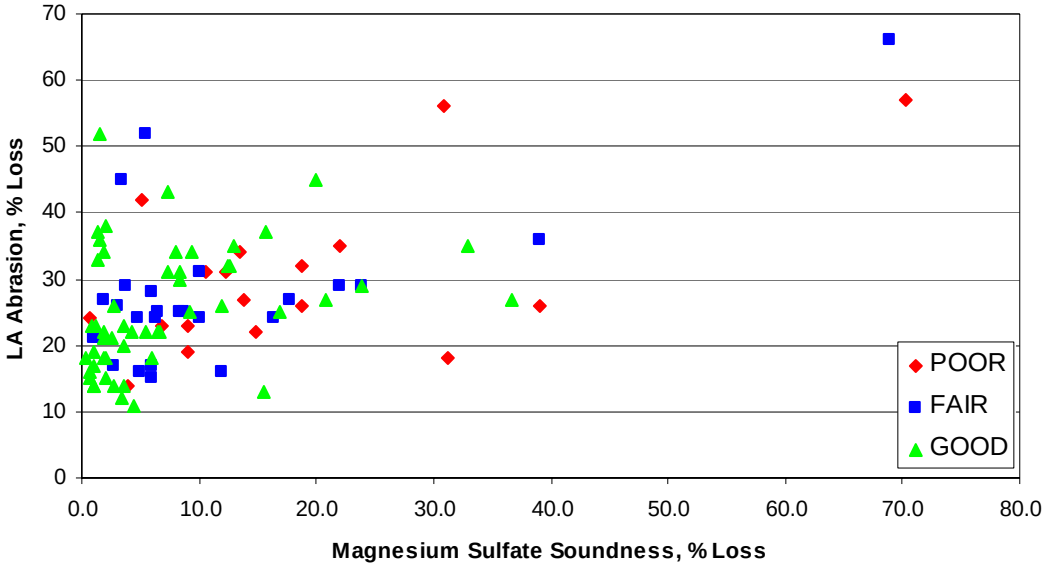

Figure B.13: L.A. Abrasion vs. Magnesium Sulfate Soundness

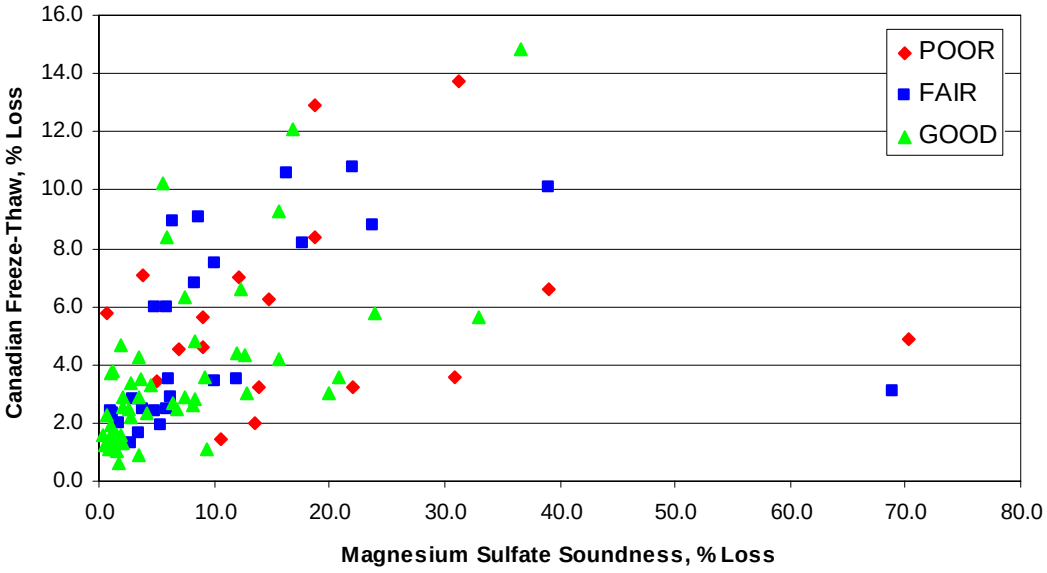

Figure B.14: Canadian Freeze-Thaw Soundness vs. Magnesium Sulfate Soundness

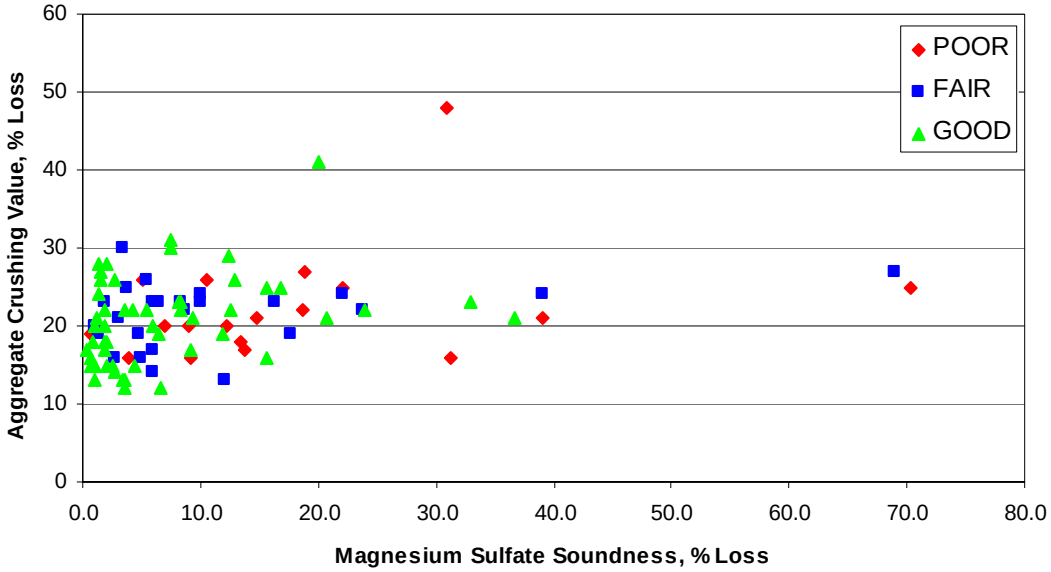

Figure B.15: Aggregate Crushing Value vs. Magnesium Sulfate Soundness

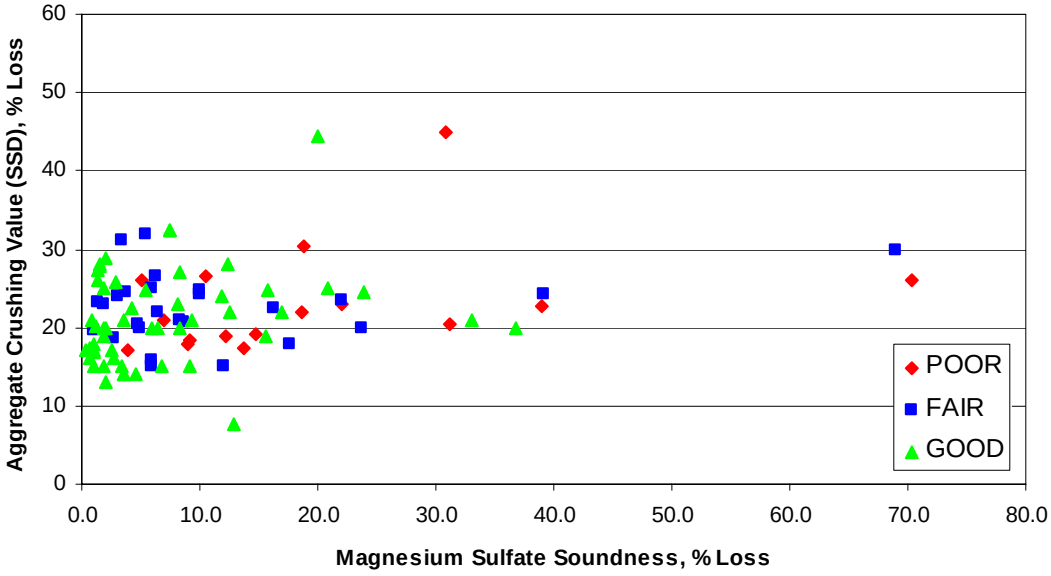

Figure B.16: Aggregate Crushing Value (SSD) vs. Magnesium Sulfate Soundness

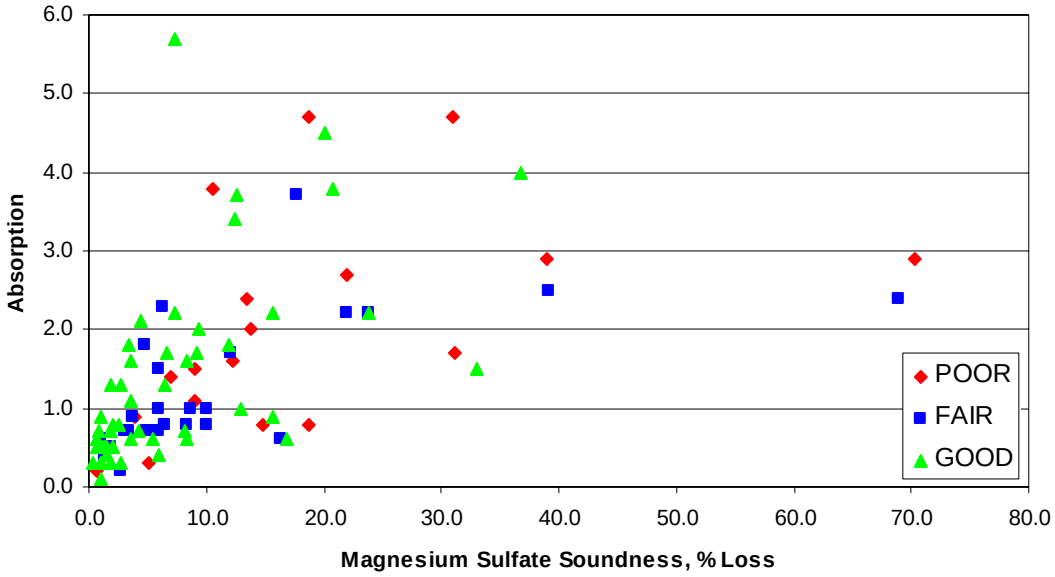

Figure B.17: Absorption vs. Magnesium Sulfate Soundness

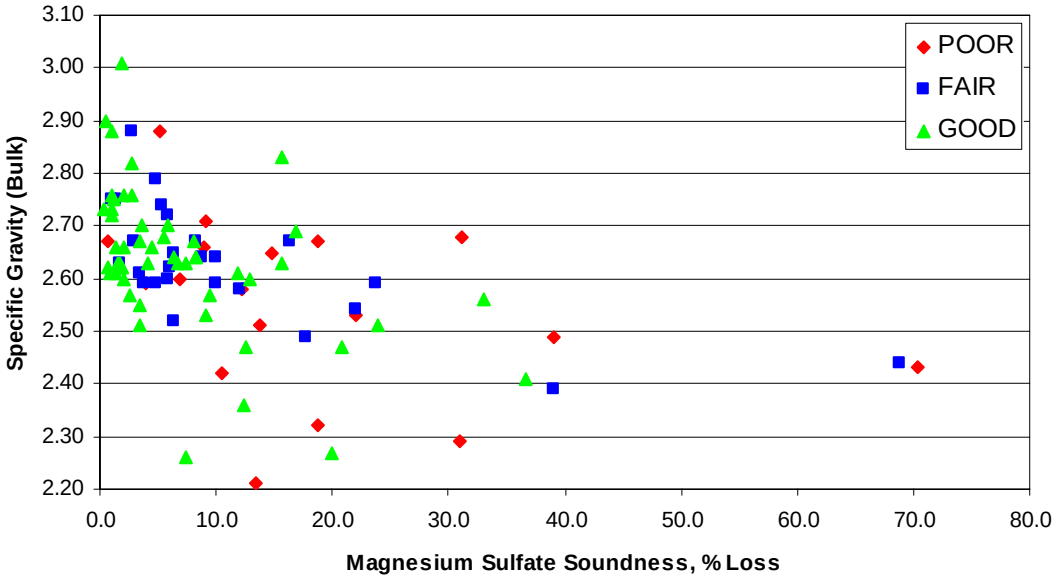

Figure B.18: Specific Gravity (Bulk) vs. Magnesium Sulfate Soundness

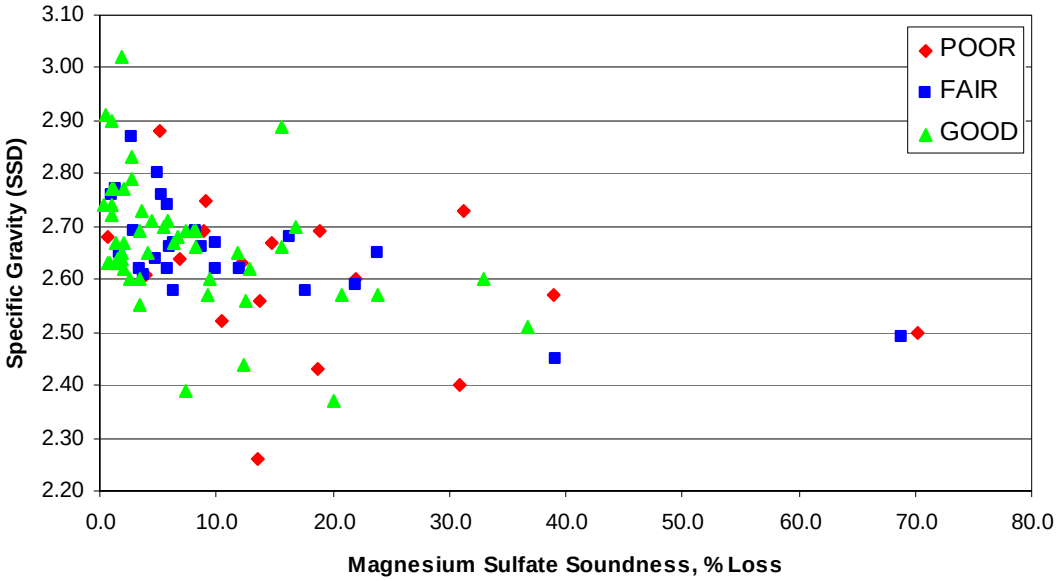

Figure B.19: Specific Gravity (SSD) vs. Magnesium Sulfate Soundness

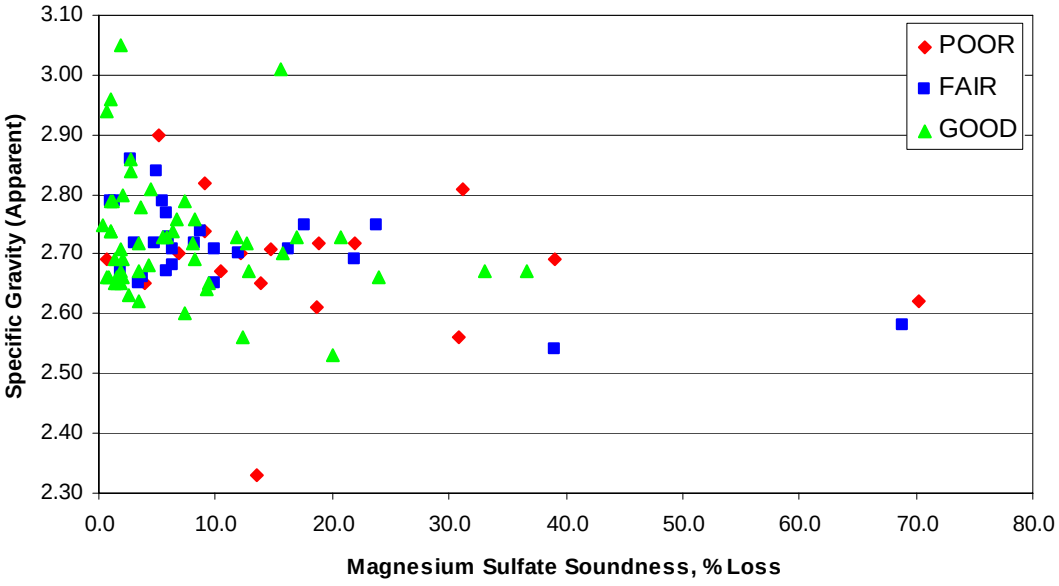

Figure B.20: Specific Gravity (Apparent) vs. Magnesium Sulfate Soundness

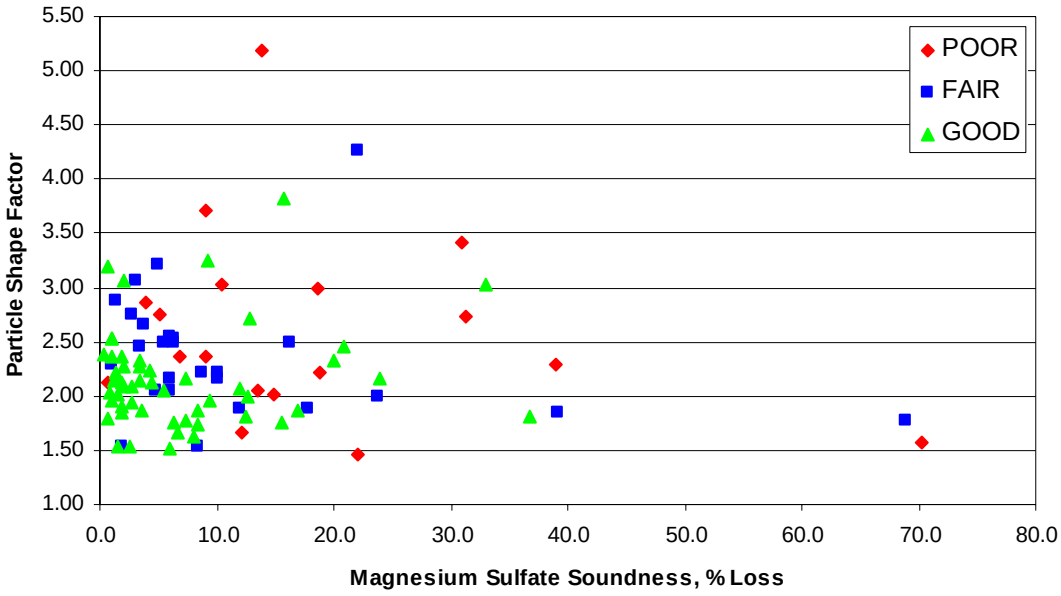

Figure B.21: Particle Shape Factor vs. Magnesium Sulfate Soundness

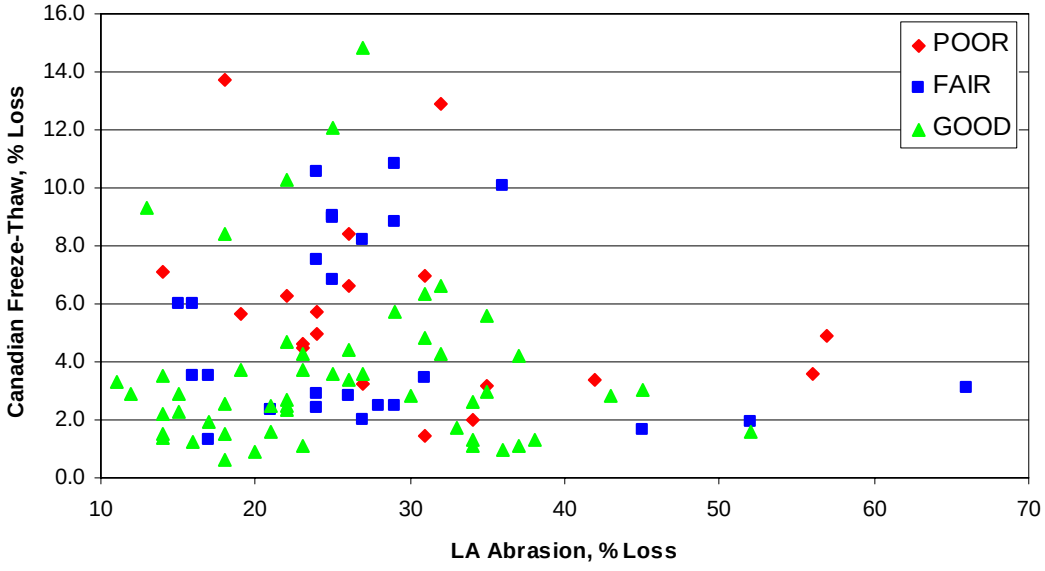

Figure B.22: Canadian Freeze-Thaw Soundness vs. L.A. Abrasion

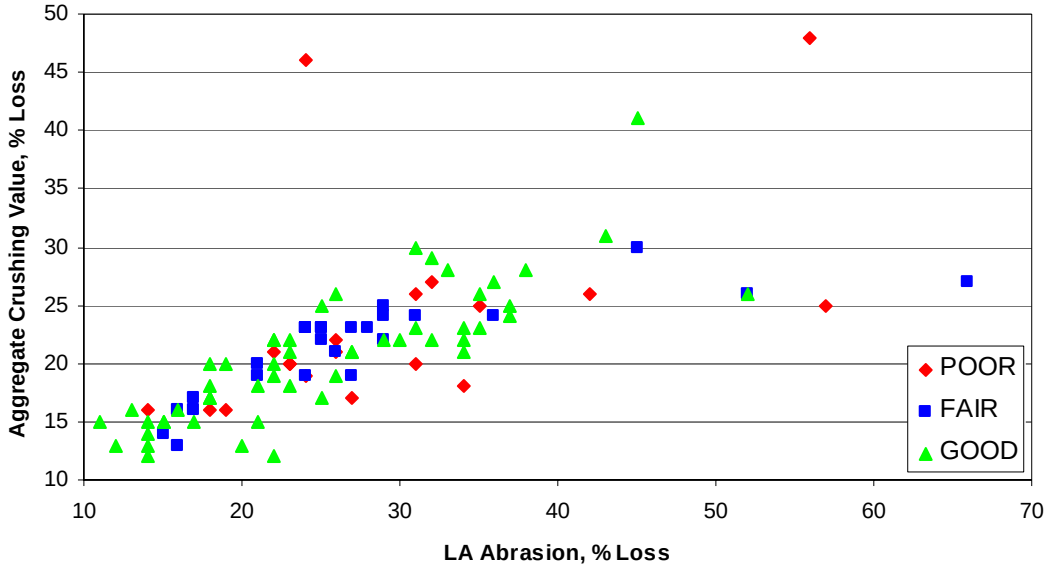

Figure B.23: Aggregate Crushing Value vs. L.A. Abrasion

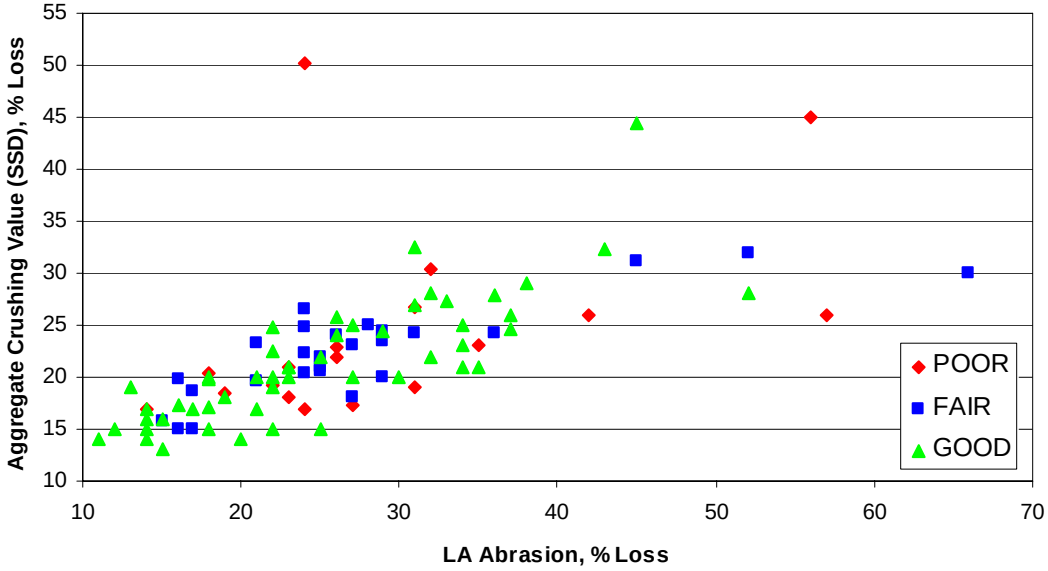

Figure B.24: Aggregate Crushing Value (SSD) vs. L.A. Abrasion

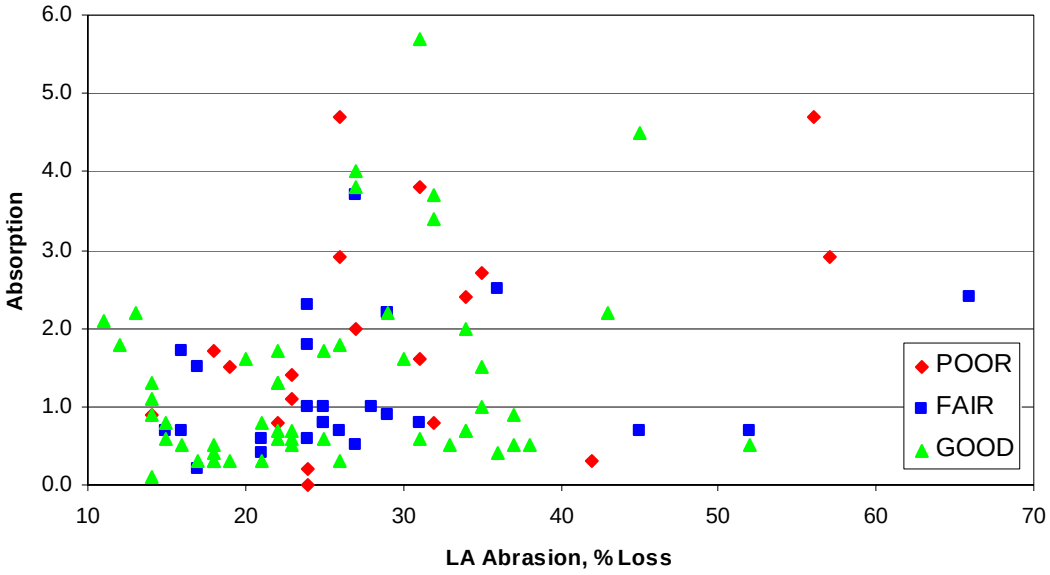

Figure B.25: Absorption vs. L.A. Abrasion

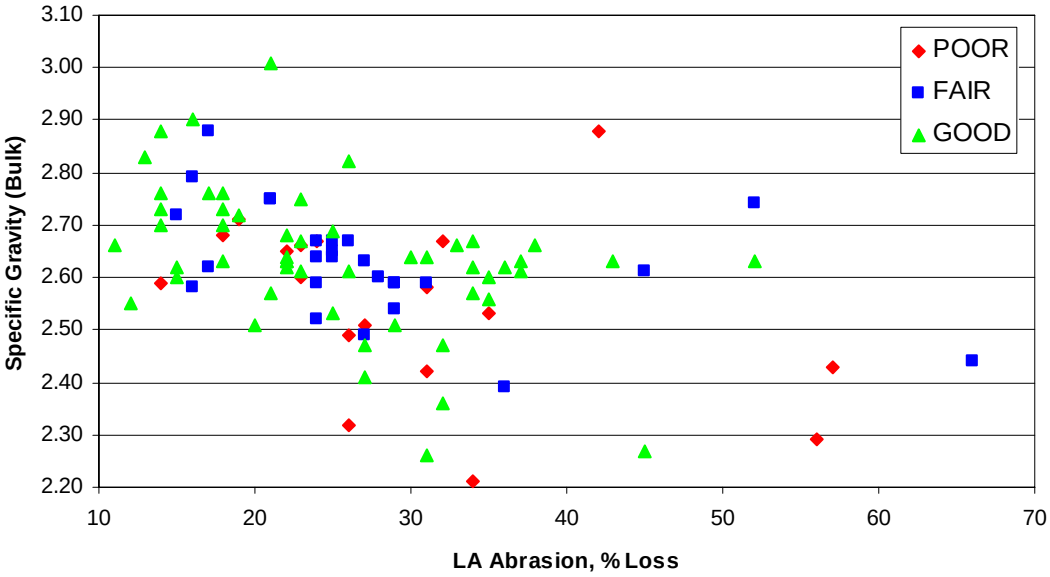

Figure B.26: Specific Gravity (Bulk) vs. L.A. Abrasion

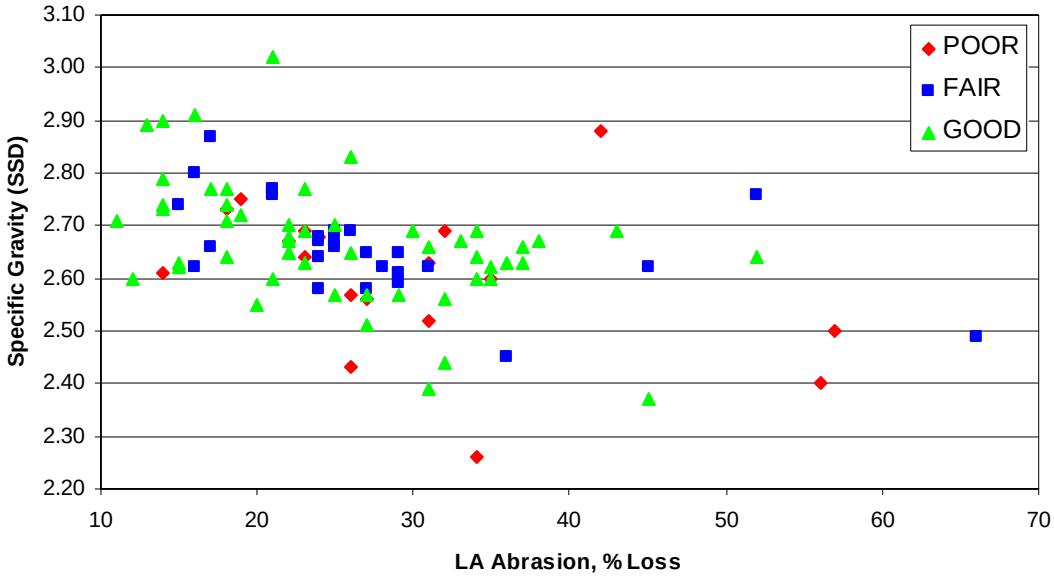

Figure B.27: Specific Gravity (SSD) vs. L.A. Abrasion

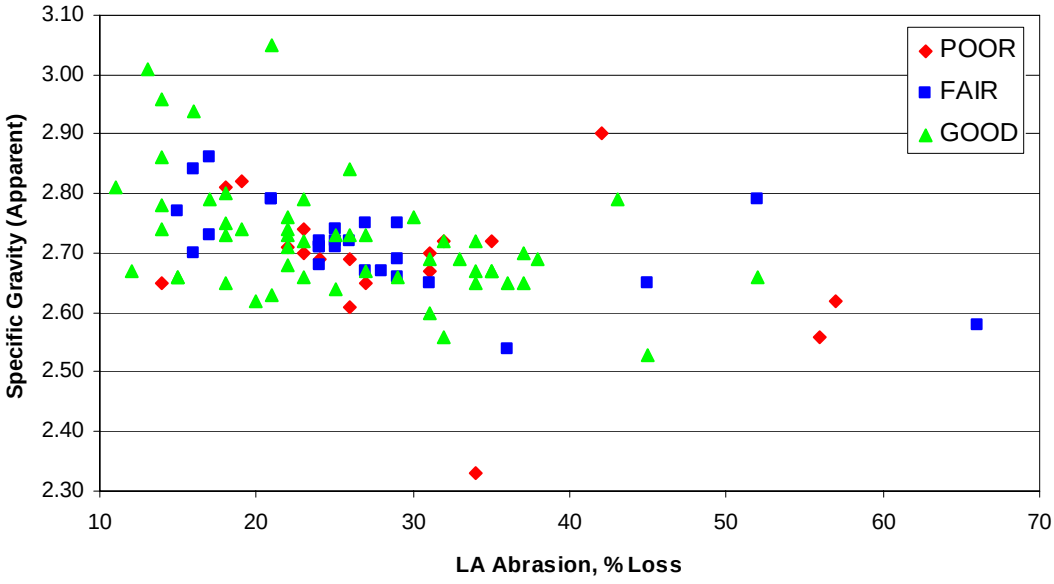

Figure B.28: Specific Gravity (Apparent) vs. L.A. Abrasion

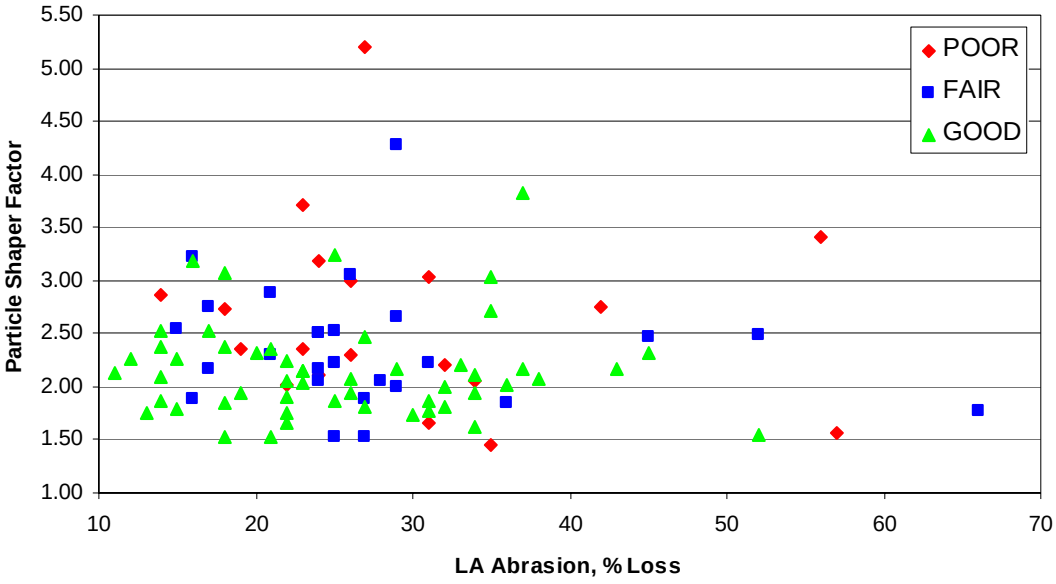

Figure B.29: Particle Shape Factor vs. L.A. Abrasion

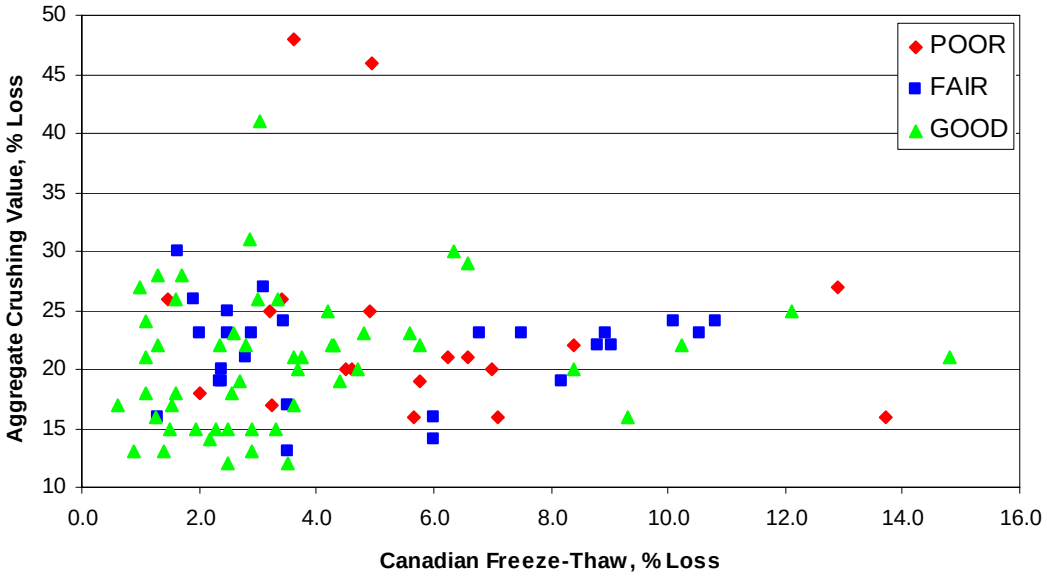

Figure B.30: Aggregate Crushing Value vs. Canadian Freeze-Thaw Soundness

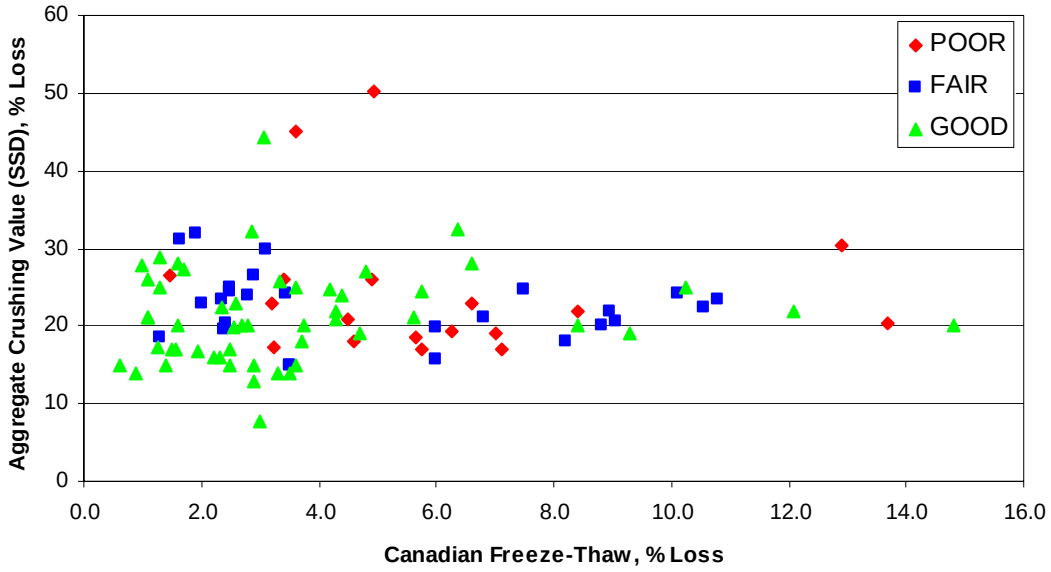

Figure B.31: Aggregate Crushing Value (SSD) vs. Canadian Freeze-Thaw Soundness

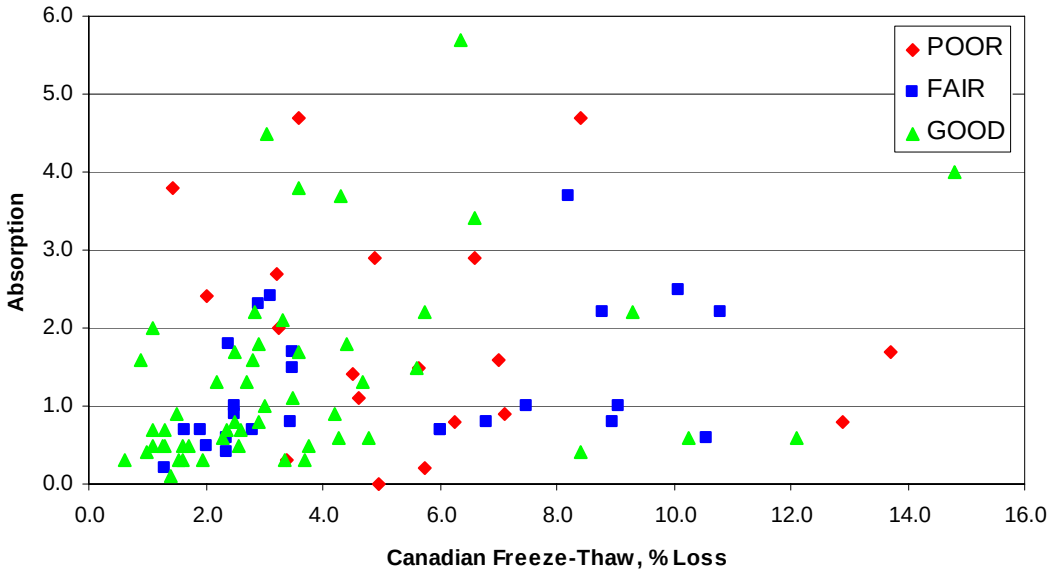

Figure B.32: Absorption vs. Canadian Freeze-Thaw Soundness

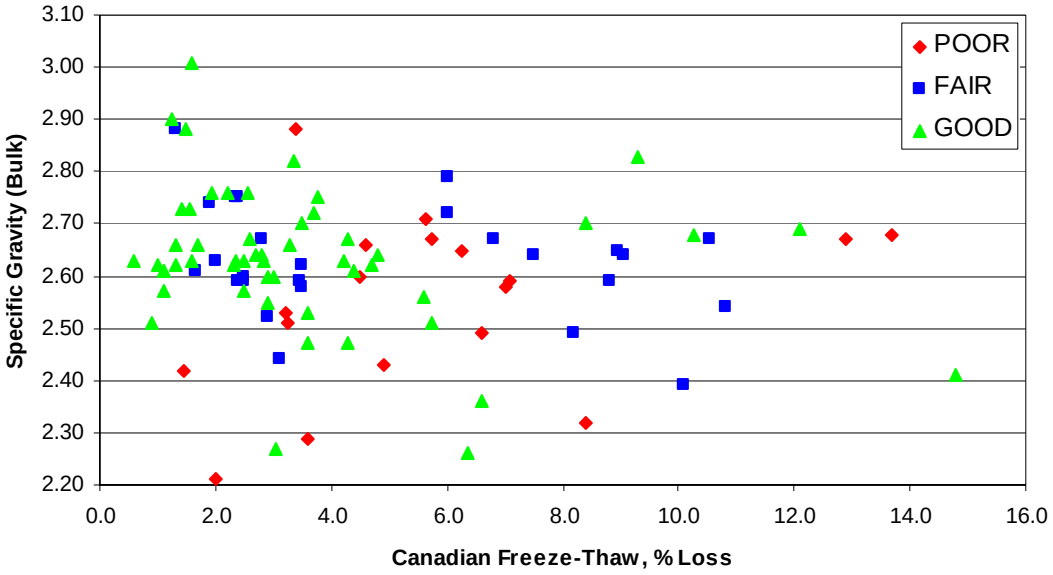

Figure B.33: Specific Gravity (Bulk) vs. Canadian Freeze-Thaw Soundness

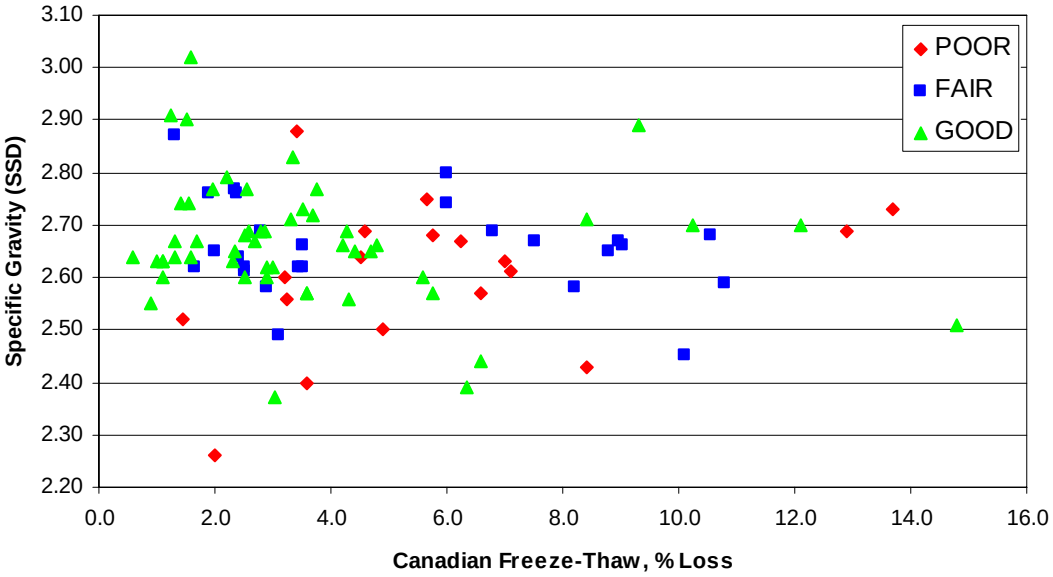

Figure B.34: Specific Gravity (SSD) vs. Canadian Freeze-Thaw Soundness

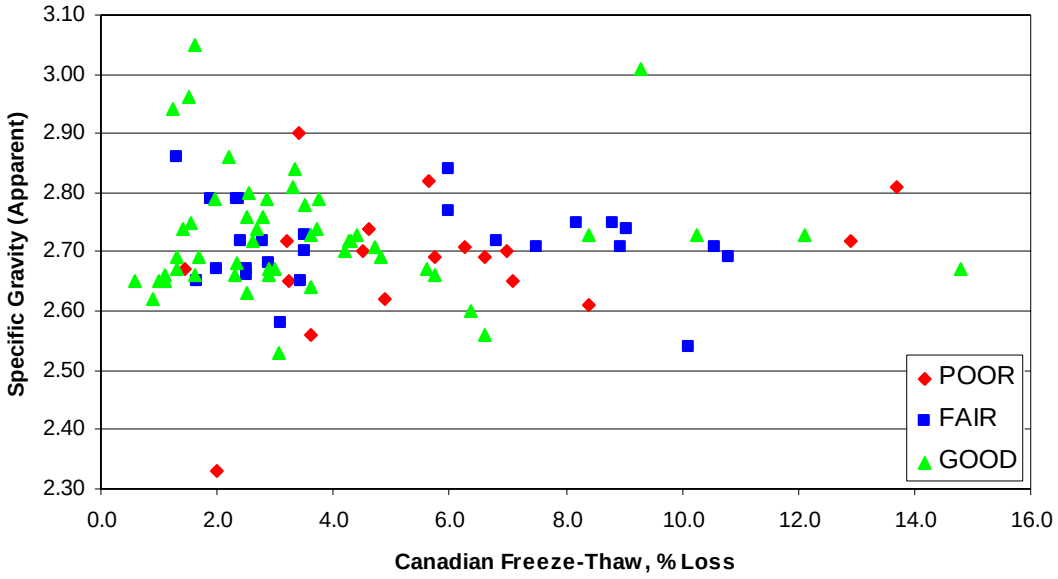

Figure B.35: Specific Gravity (Apparent) vs. Canadian Freeze-Thaw Soundness

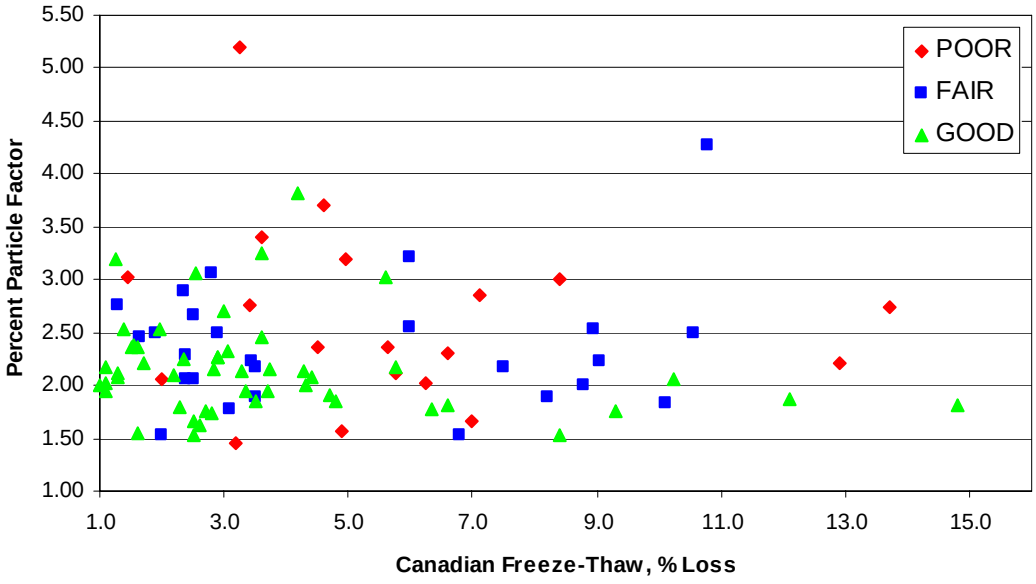

Figure B.36: Particle Shape Factor vs. Canadian Freeze-Thaw Soundness

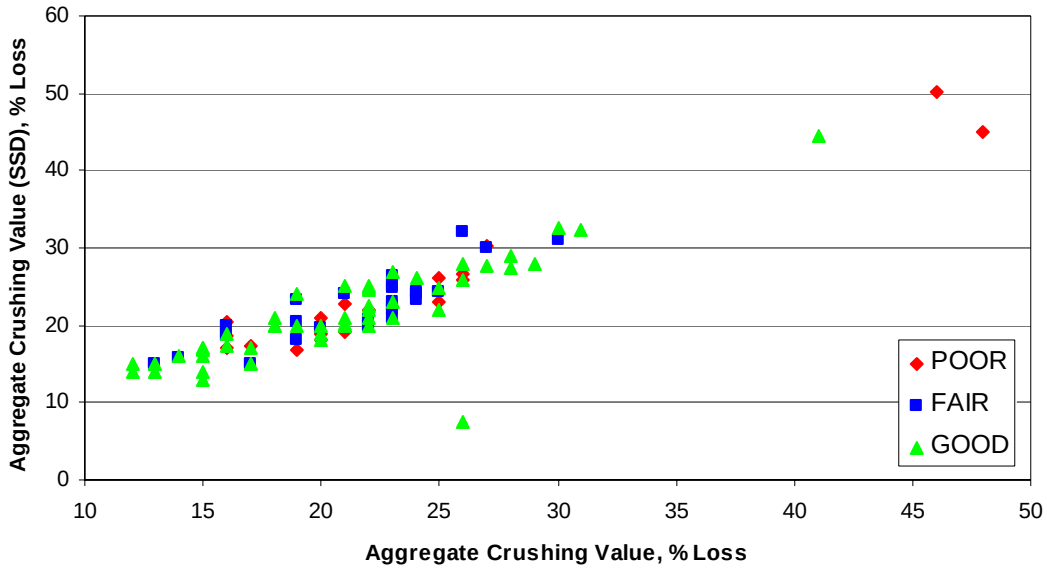

Figure B.37: Aggregate Crushing Value (SSD) vs. Aggregate Crushing Value

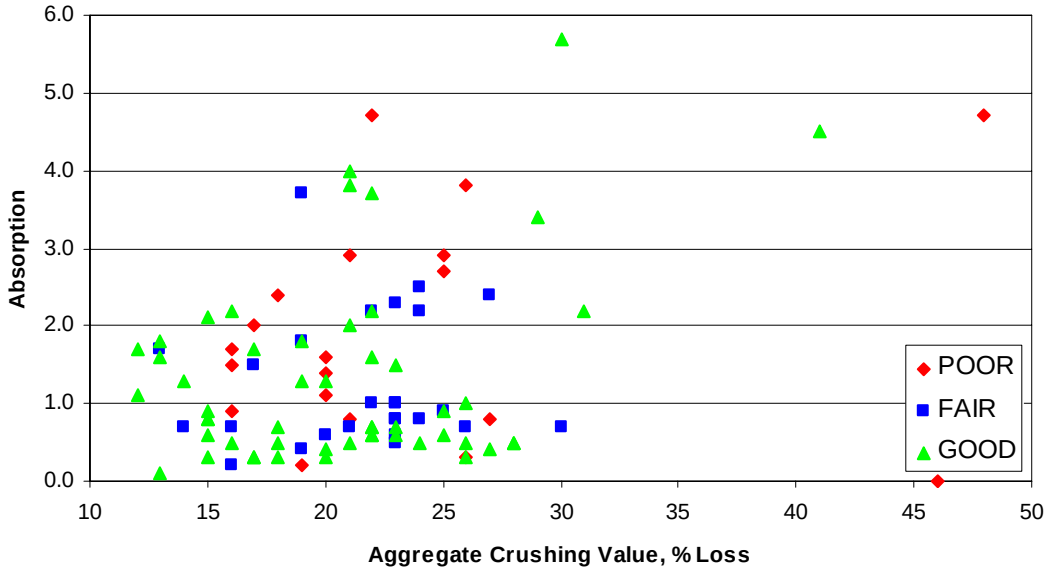

Figure B.38: Absorption vs. Aggregate Crushing Value

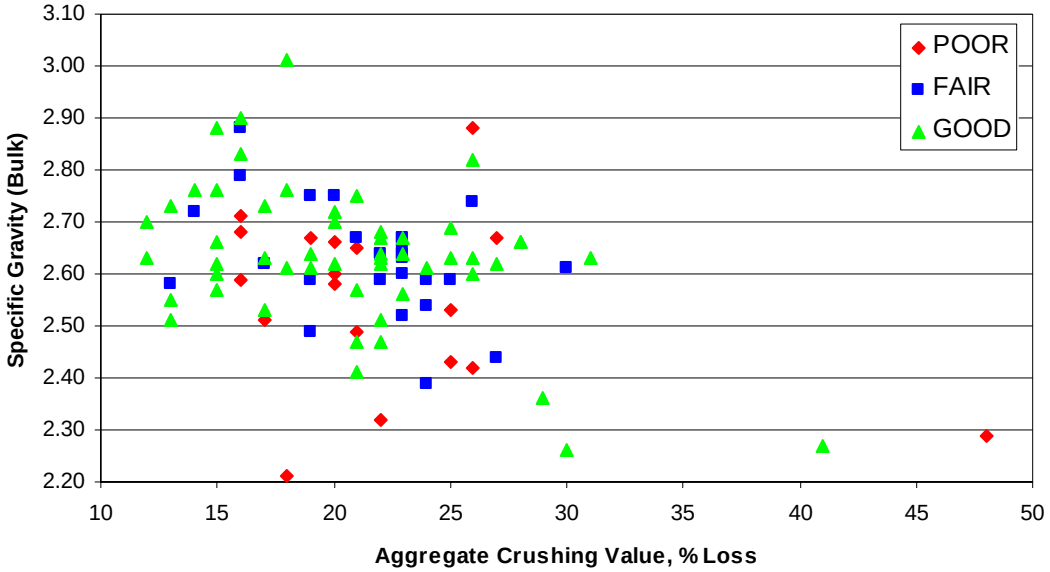

Figure B.39: Specific Gravity (Bulk) vs. Aggregate Crushing Value

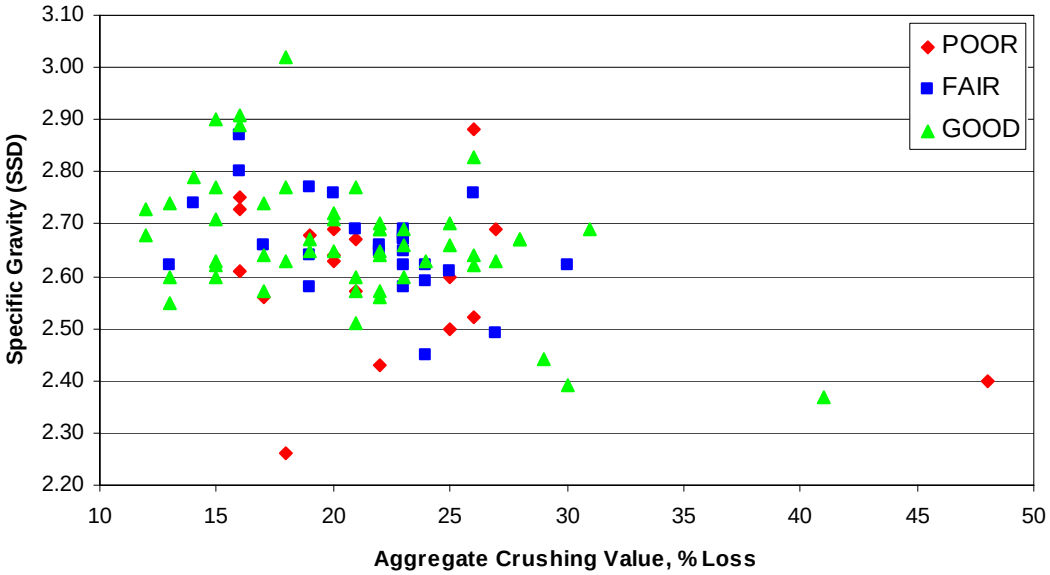

Figure B.40: Specific Gravity (SSD) vs. Aggregate Crushing Value

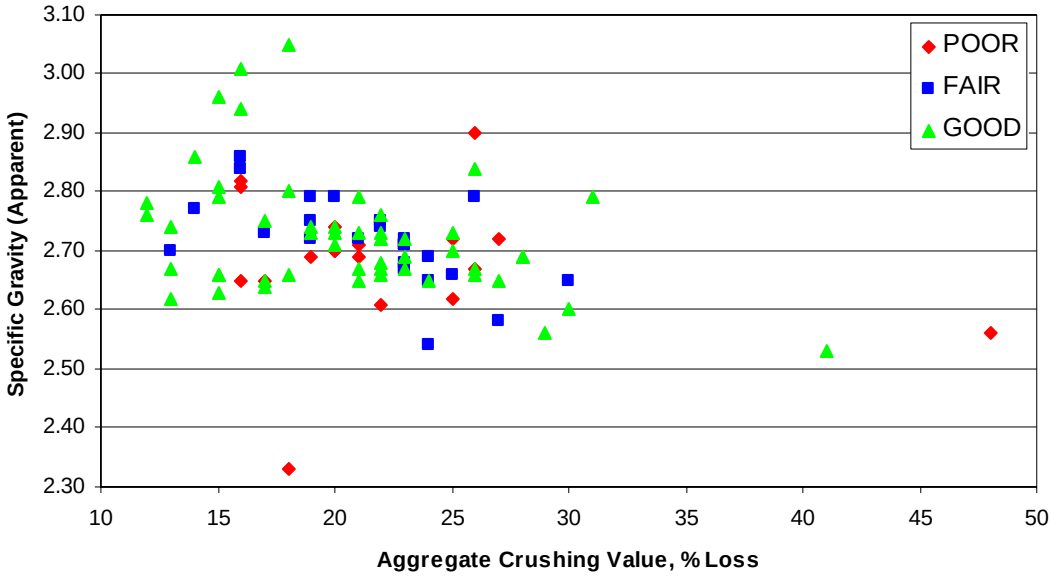

Figure B.41: Specific Gravity (Apparent) vs. Aggregate Crushing Value

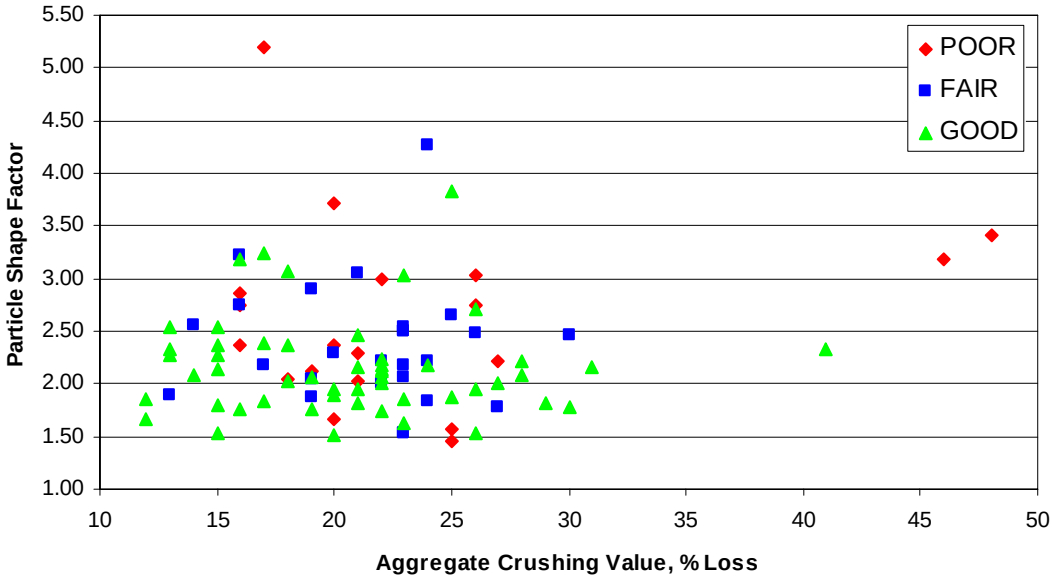

Figure B.42: Particle Shape Factor vs. Aggregate Crushing Value

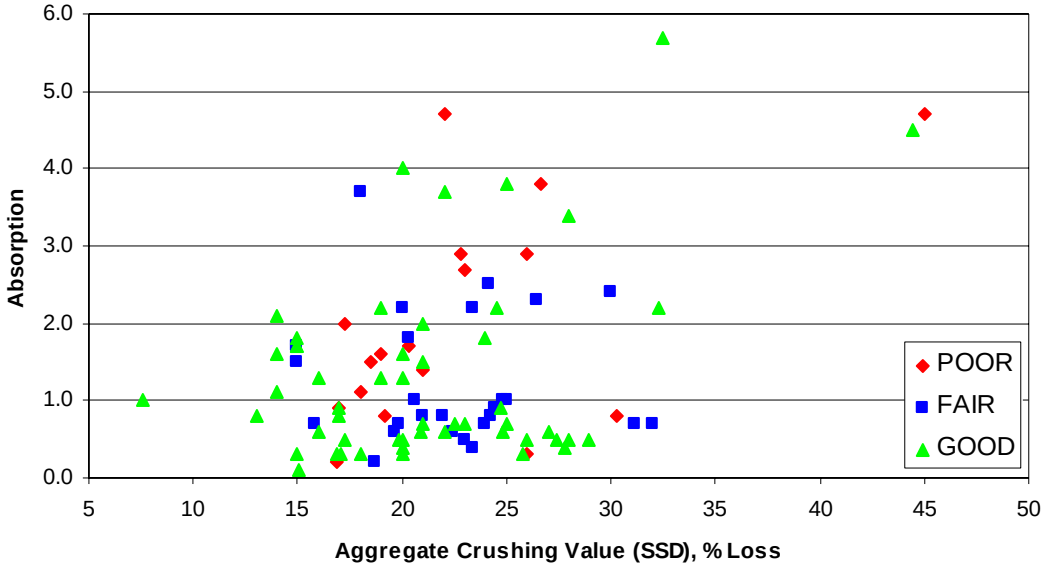

Figure B.43: Absorption vs. Aggregate Crushing Value (SSD)

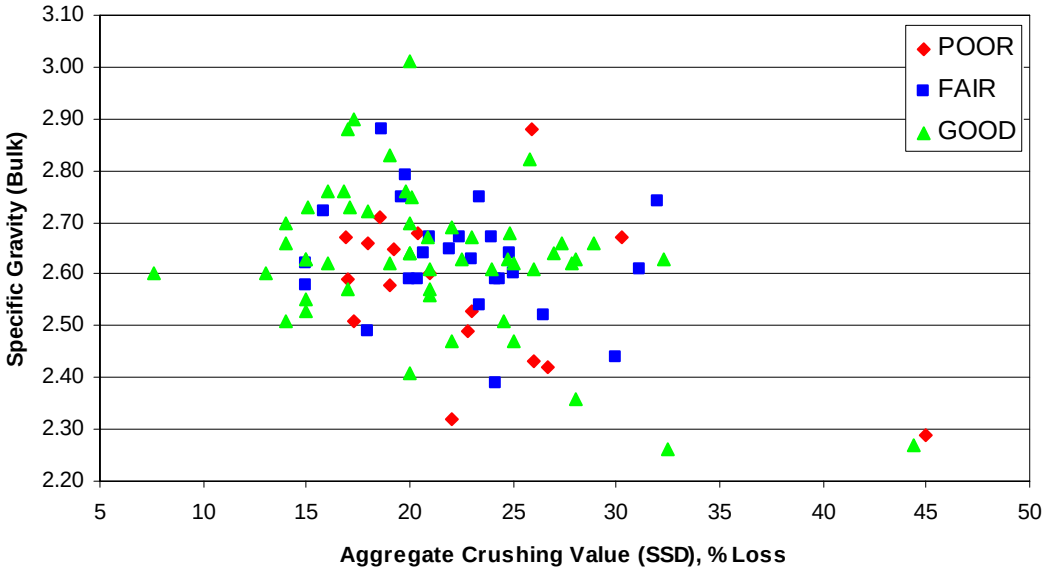

Figure B.44: Specific Gravity (Bulk) vs. Aggregate Crushing Value (SSD)

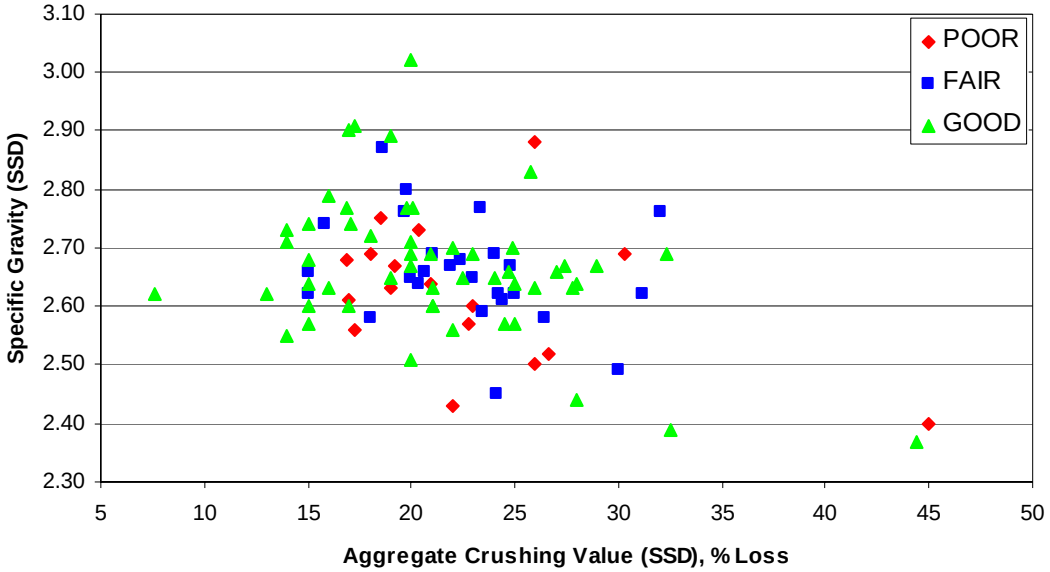

Figure B.45: Specific Gravity (SSD) vs. Aggregate Crushing Value (SSD)

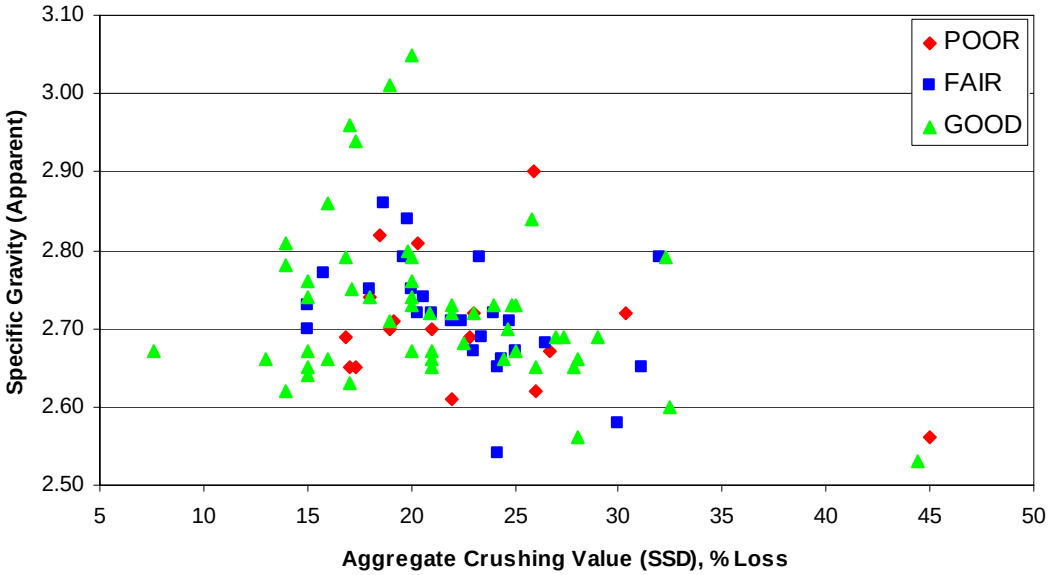

Figure B.46: Specific Gravity (Apparent) vs. Aggregate Crushing Value (SSD)

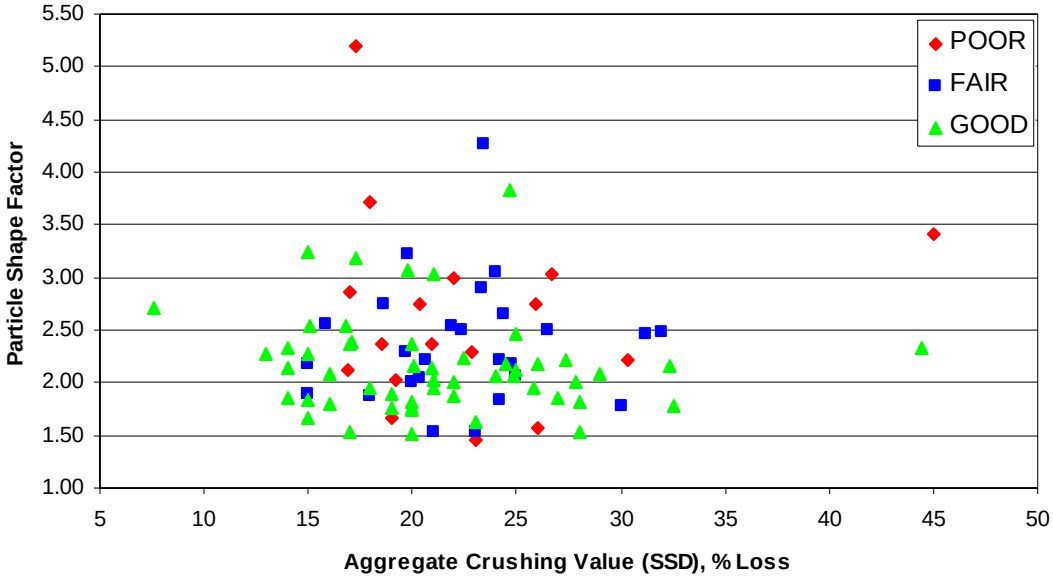

Figure B.47: Particle Shape Factor vs. Aggregate Crushing Value (SSD)

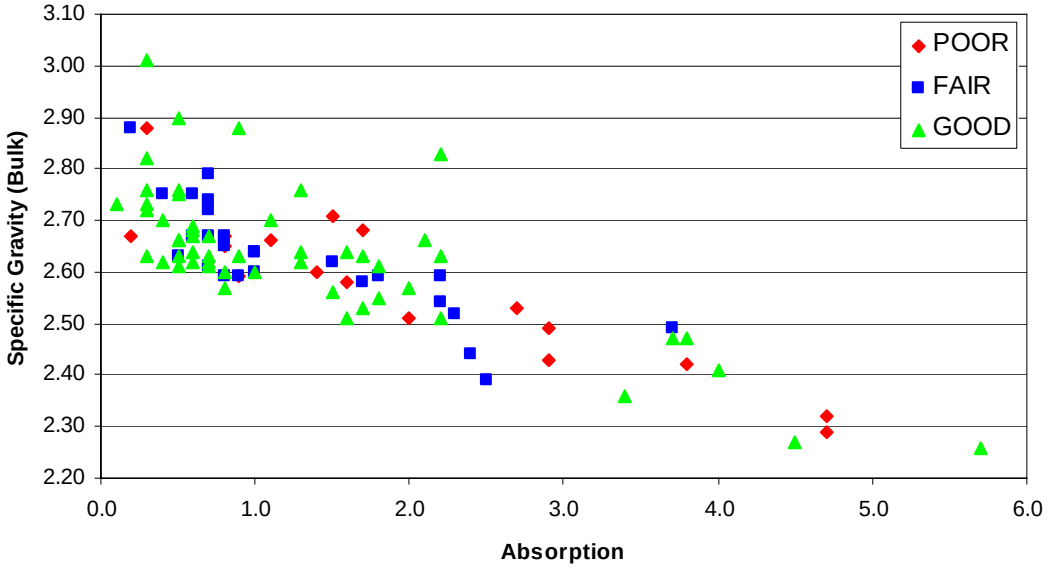

Figure B.48: Specific Gravity (Bulk) vs. Absorption

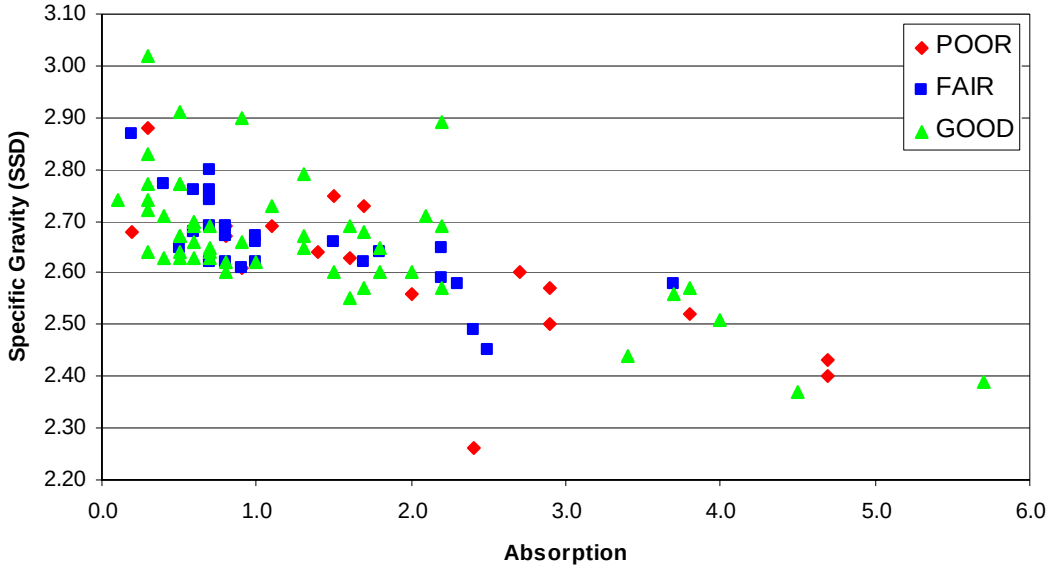

Figure B.49: Specific Gravity (SSD) vs. Absorption

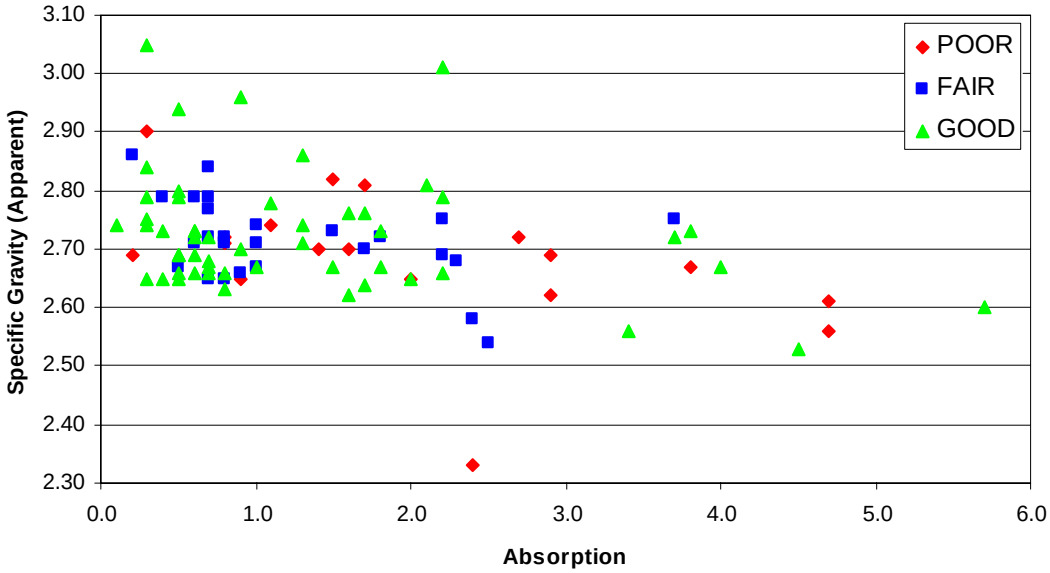

Figure B.50: Specific Gravity (Apparent) vs. Absorption

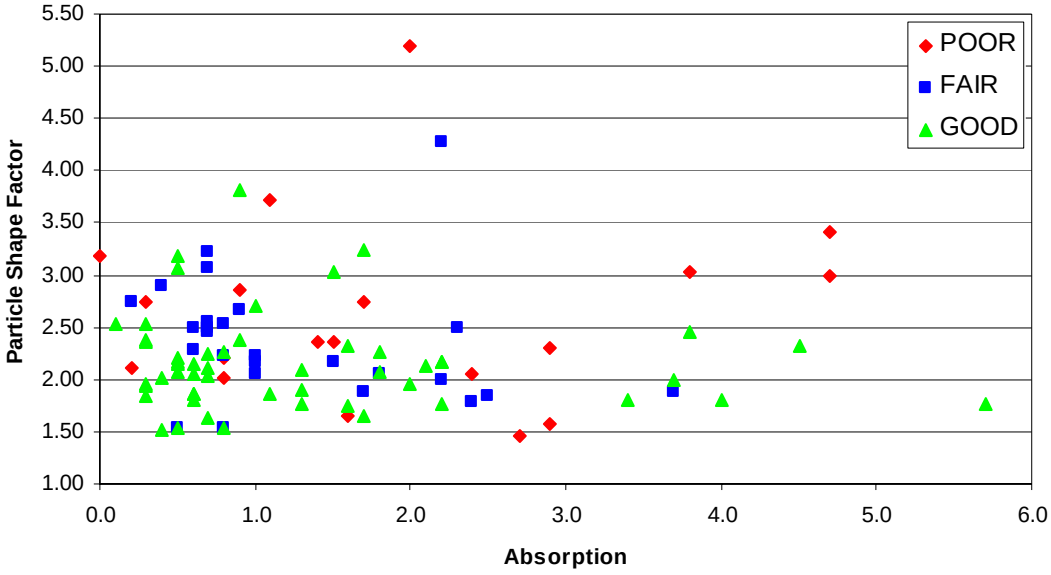

Figure B.51: Particle Shape Factor vs. Absorption

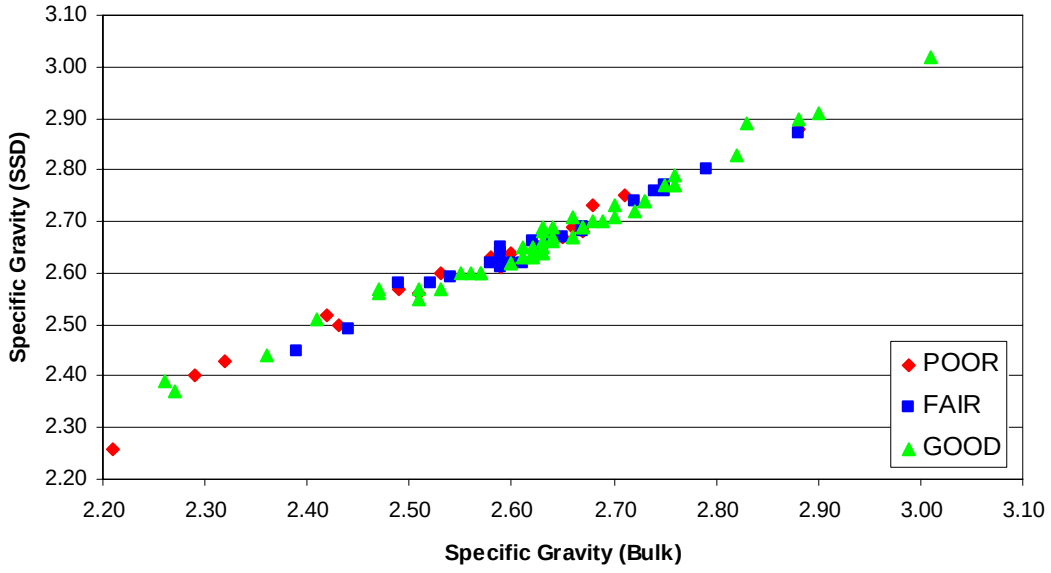

Figure B.52: Specific Gravity (SSD) vs. Specific Gravity (Bulk)

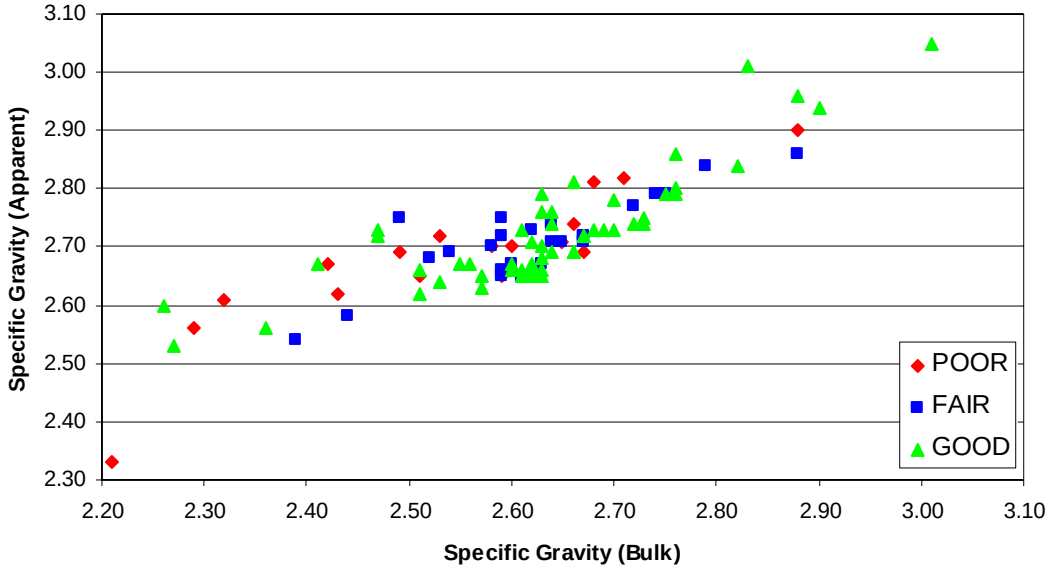

Figure B.53: Specific Gravity (Apparent) vs. Specific Gravity (Bulk)

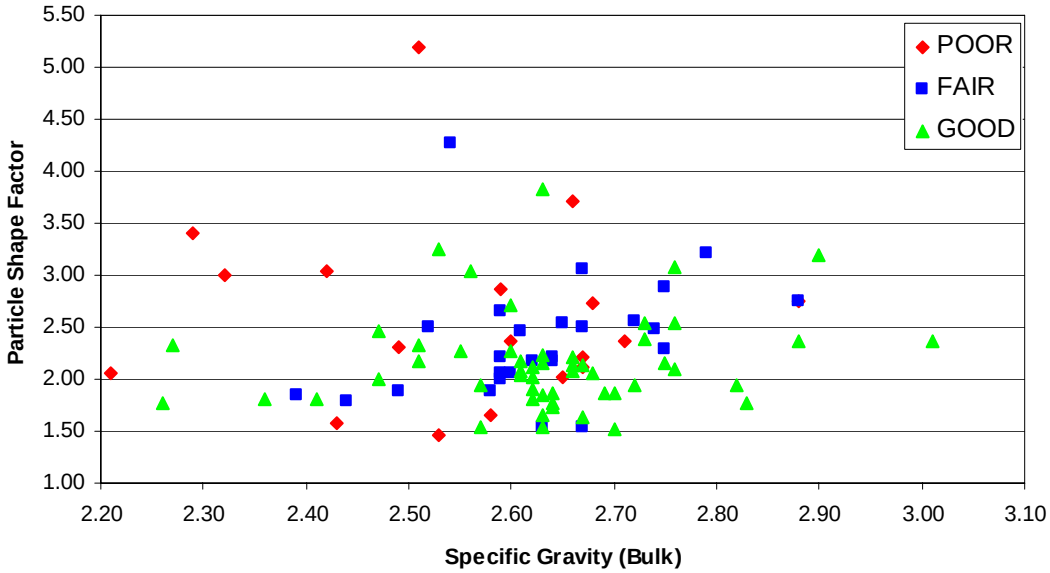

Figure B.54: Particle Shape Factor vs. Specific Gravity (Bulk)

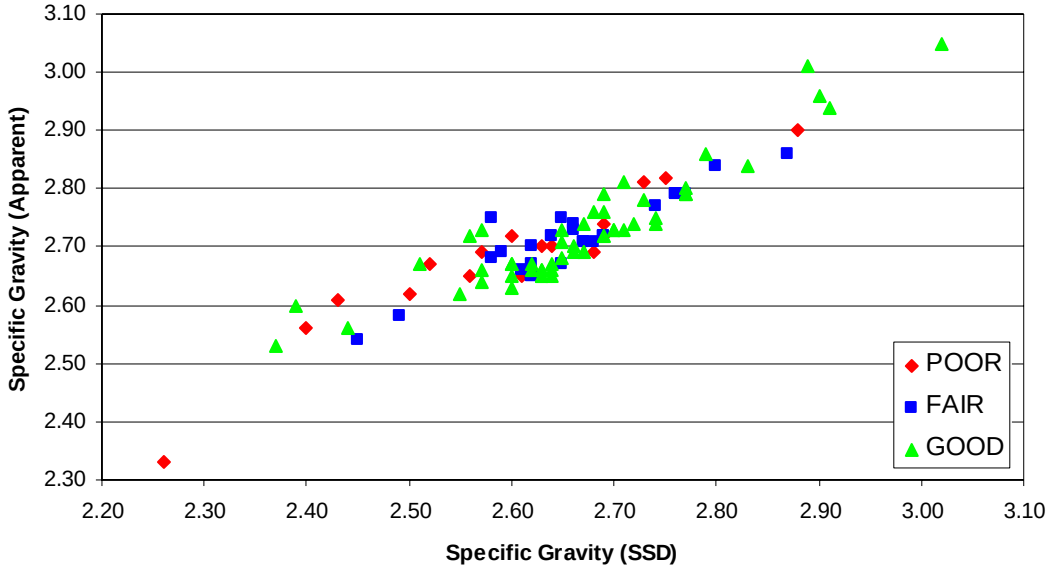

Figure B.55: Specific Gravity (Apparent) vs. Specific Gravity (SSD)

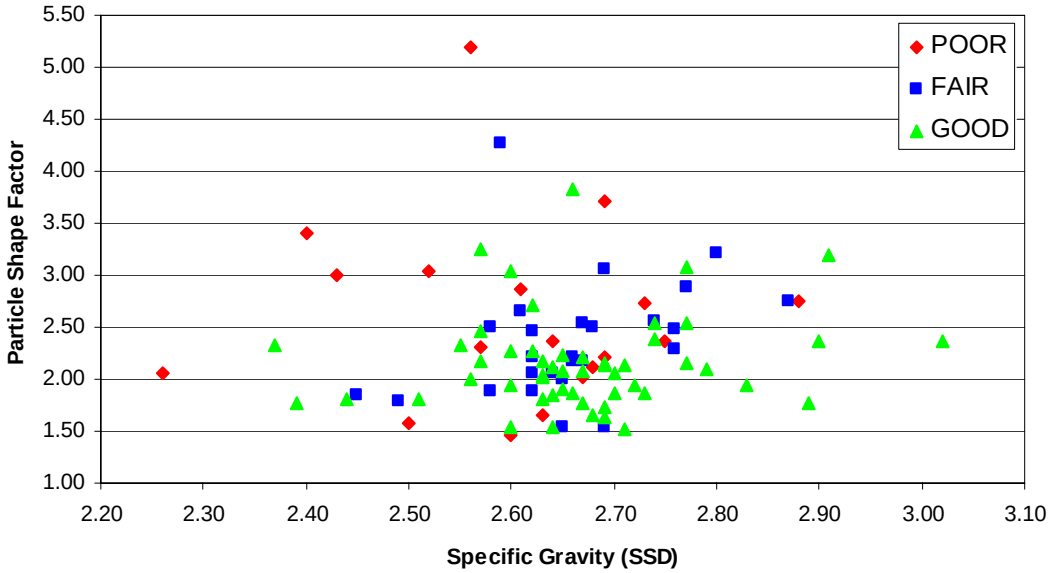

Figure B.56: Particle Shape Factor vs. Specific Gravity (SSD)

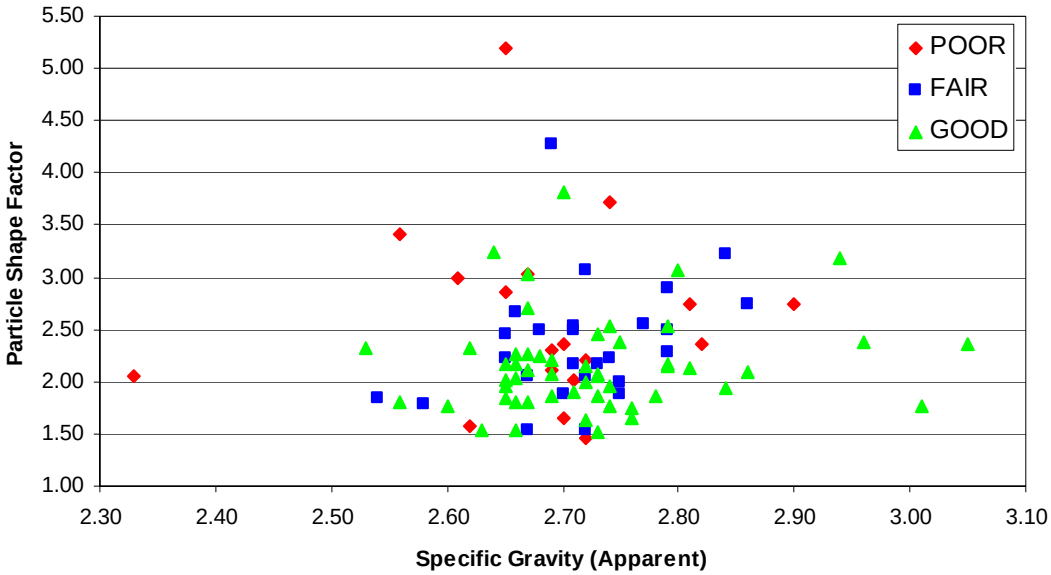

Figure B.57: Particle Shape Factor vs. Specific Gravity (Apparent)

Appendix C: One Test Only Field Performance Graphs for Base Course Aggregates

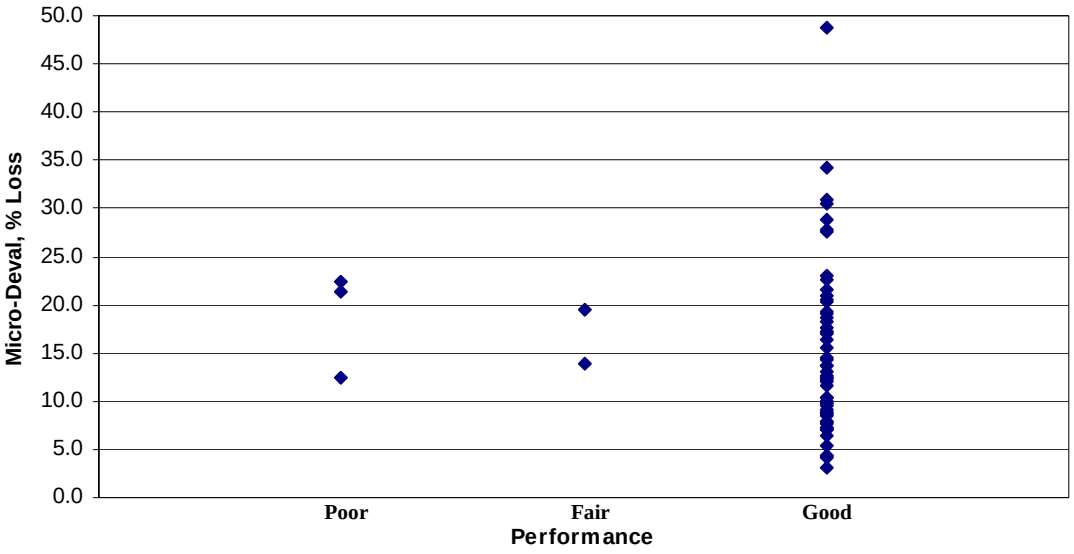

Figure C.1: Micro-Deval vs. Performance

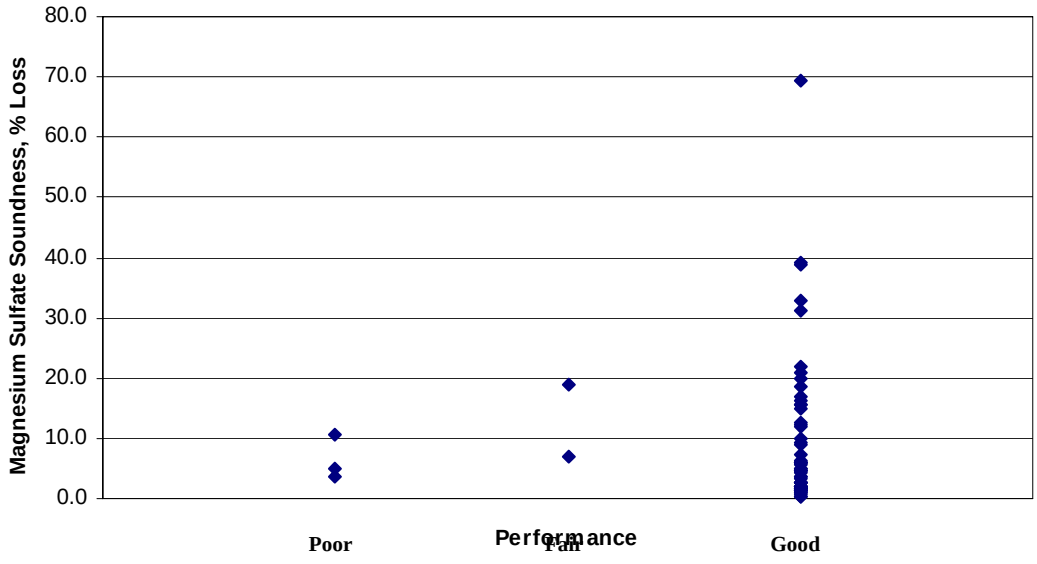

Figure C.2: Magnesium Sulfate Soundness vs. Performance

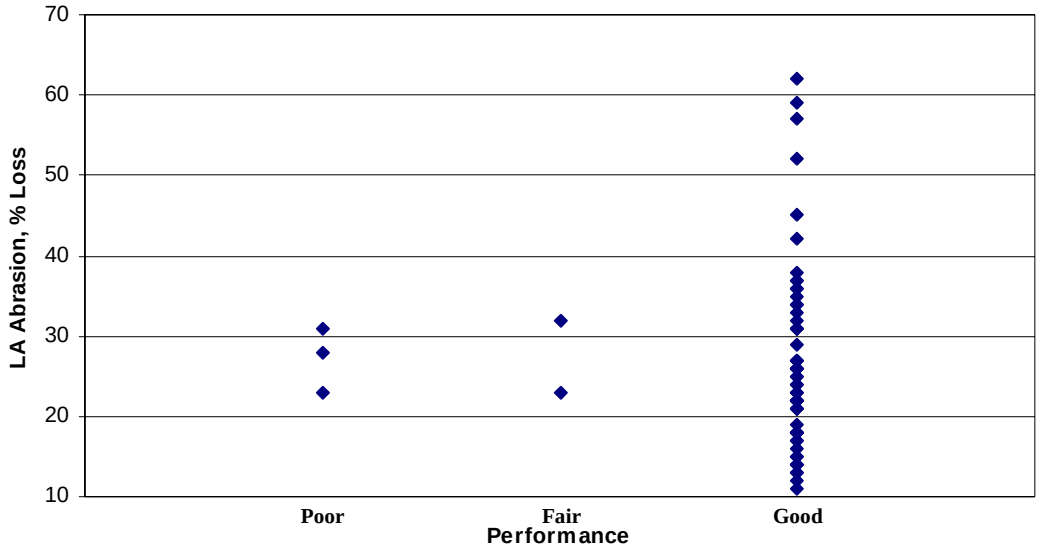

Figure C.3: L.A. Abrasion vs. Performance

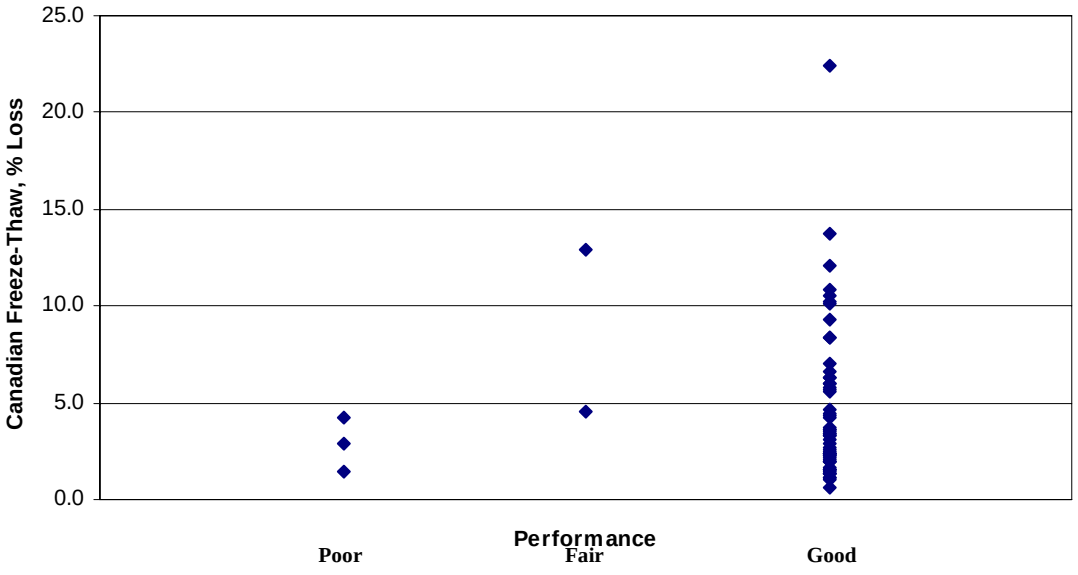

Figure C.4: Canadian Freeze-Thaw Soundness vs. Performance

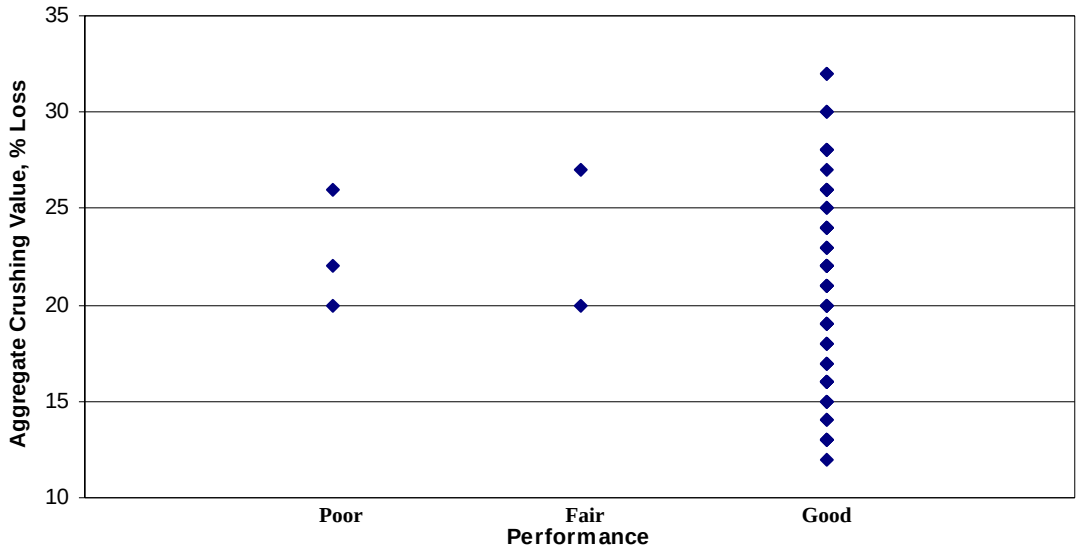

Figure C.5: Aggregate Crushing Value vs. Performance

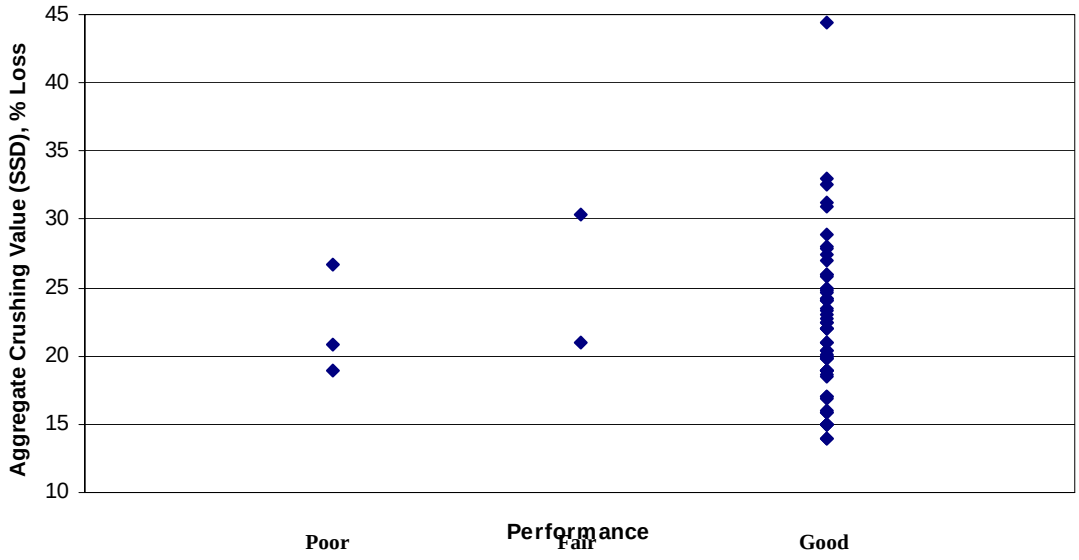

Figure C.6: Aggregate Crushing Value (SSD) vs. Performance

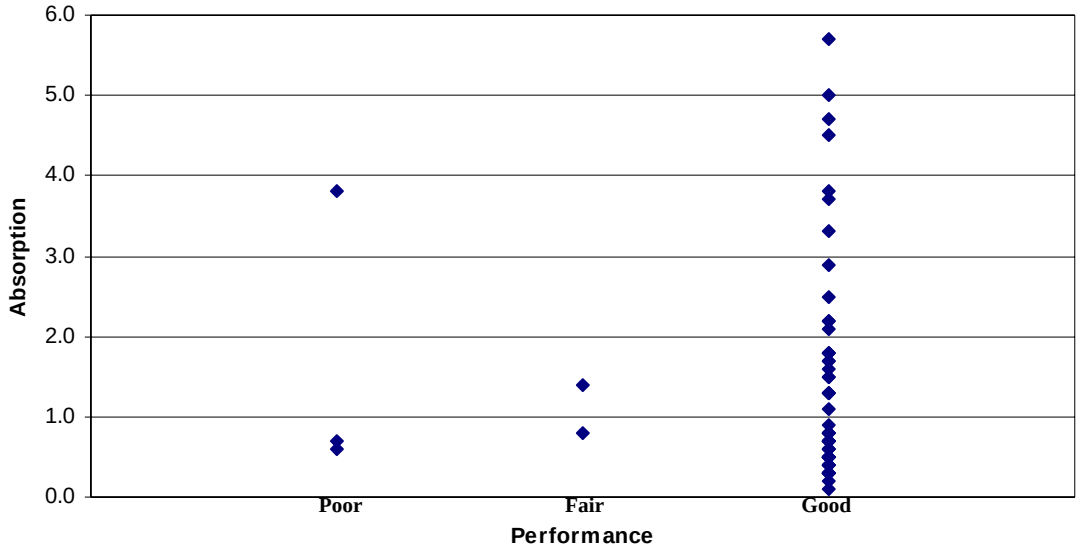

Figure C.7: Absorption vs. Performance

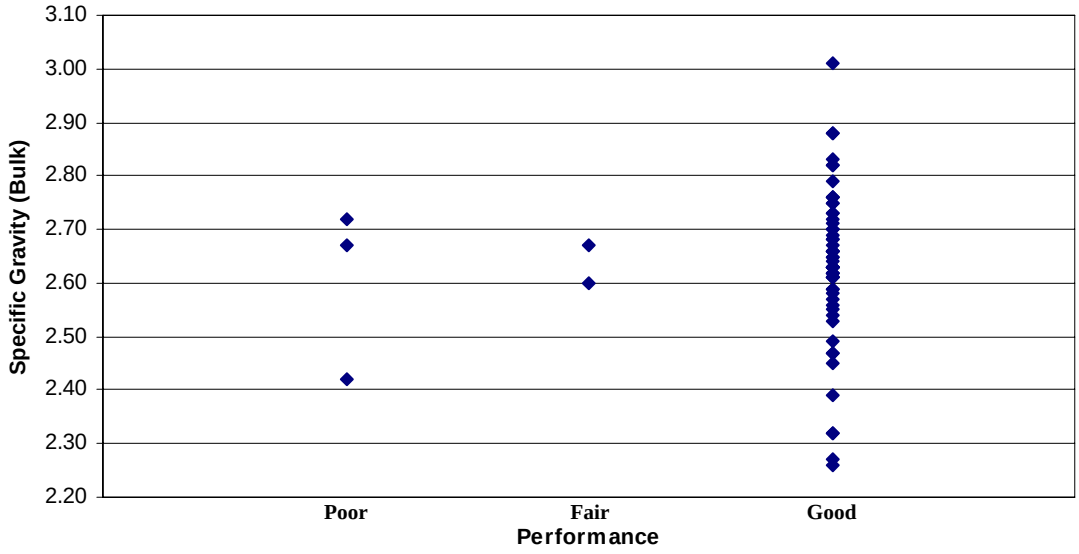

Figure C.8: Specific Gravity (Bulk) vs. Performance

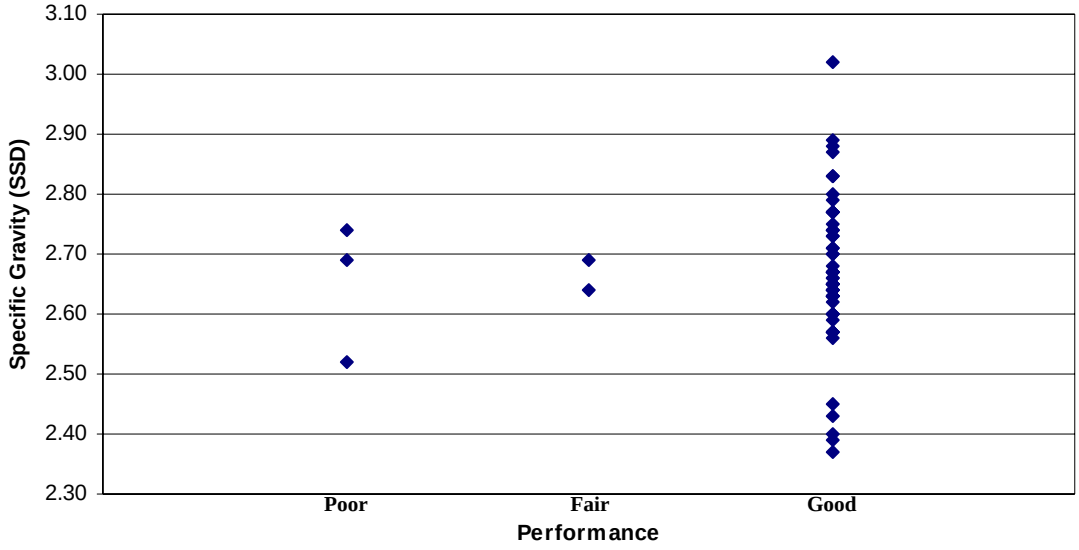

Figure C.9: Specific Gravity (SSD) vs. Performance

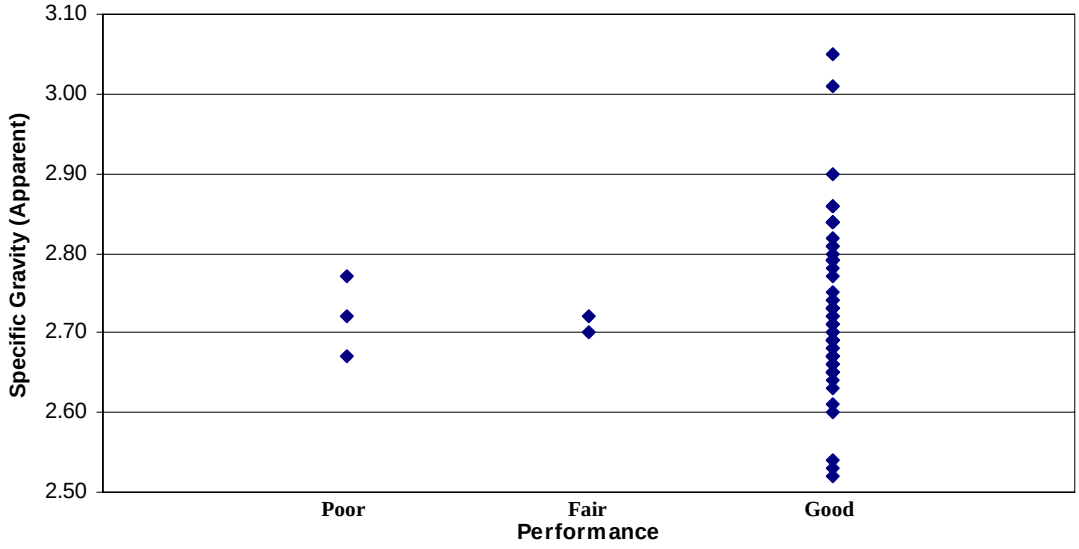

Figure C.10: Specific Gravity (Apparent) vs. Performance

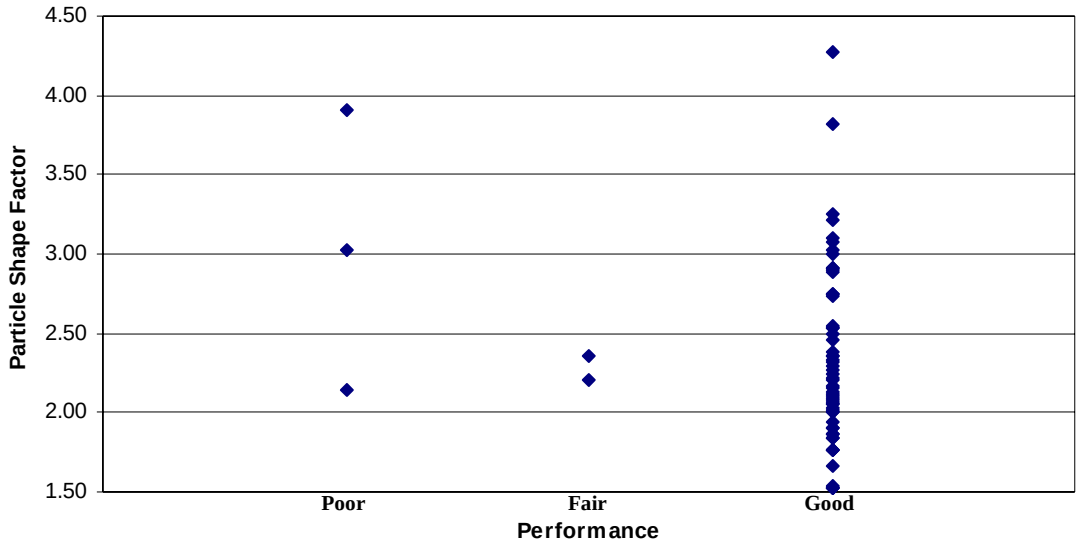

Figure C.11: Particle Shape Factor vs. Performance

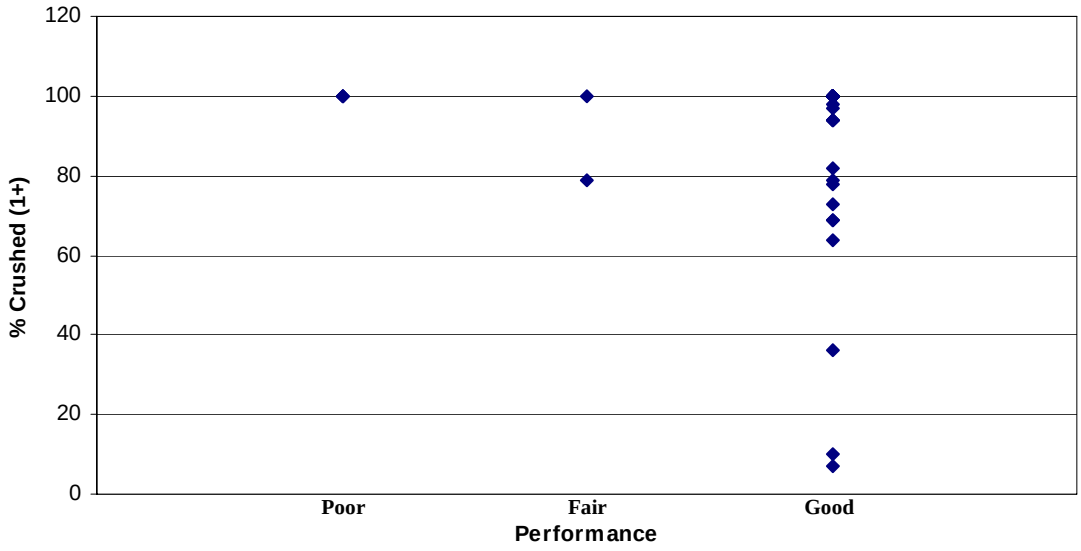

Figure C.12: Particle Shape Factor vs. Performance

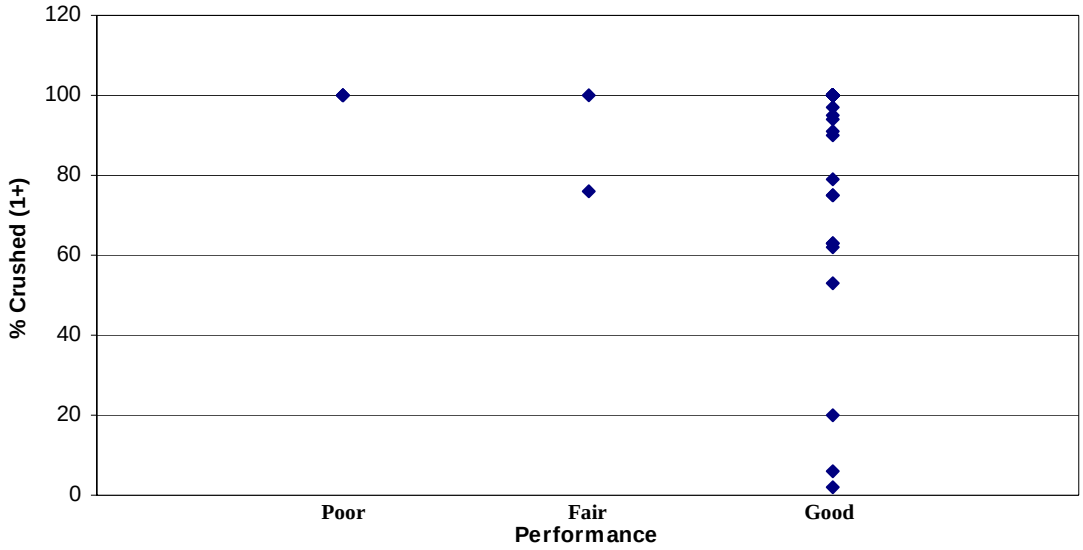

Figure C.13: Particle Shape Factor vs. Performance

	Fractured Particles (1 or more sides)								
	POOR		FAIR		GOOD		Overall %		
% of total	number	overall %	number	overall %	number	overall %	POOR	FAIR	GOOD
100	4	100%	1	50%	44	75%	8%	2%	90%
90 - 99	0	0%	0	0%	5	8%	0%	0%	100%
80 - 89	0	0%	0	0%	1	2%	0%	0%	100%
70 - 79	0	0%	1	50%	3	5%	0%	25%	75%
60 - 69	0	0%	0	0%	3	5%	0%	0%	100%
50 - 59	0	0%	0	0%	0	0%	0%	0%	0%
40 - 49	0	0%	0	0%	0	0%	0%	0%	0%
30 - 39	0	0%	0	0%	1	2%	0%	0%	100%
20 - 29	0	0%	0	0%	0	0%	0%	0%	0%
10 - 19	0	0%	0	0%	1	2%	0%	0%	100%
0 - 10	0	0%	0	0%	1	2%	0%	0%	100%

Table C.1: Percent Fractured Particles (1 or more sides)

	Fractured Particles (2 or more sides)								
	POOR		FAIR		GOOD		Overall %		
% of total	number	overall %	number	overall %	number	overall %	POOR	FAIR	GOOD
100	4	100%	1	50%	44	75%	8%	2%	90%
90 - 99	0	0%	0	0%	5	8%	0%	0%	100%
80 - 89	0	0%	0	0%	0	0%	0%	0%	0%
70 - 79	0	0%	1	50%	3	5%	0%	25%	75%
60 - 69	0	0%	0	0%	3	5%	0%	0%	100%
50 - 59	0	0%	0	0%	1	2%	0%	0%	100%
40 - 49	0	0%	0	0%	0	0%	0%	0%	0%
30 - 39	0	0%	0	0%	0	0%	0%	0%	0%
20 - 29	0	0%	0	0%	1	2%	0%	0%	100%
10 - 19	0	0%	0	0%	0	0%	0%	0%	0%
0 - 10	0	0%	0	0%	2	3%	0%	0%	100%

Table C.2: Percent Fractured Particles (2 or more sides)

Appendix D: Two-Test Combination Field Performance Graphs for Base Course Aggregates

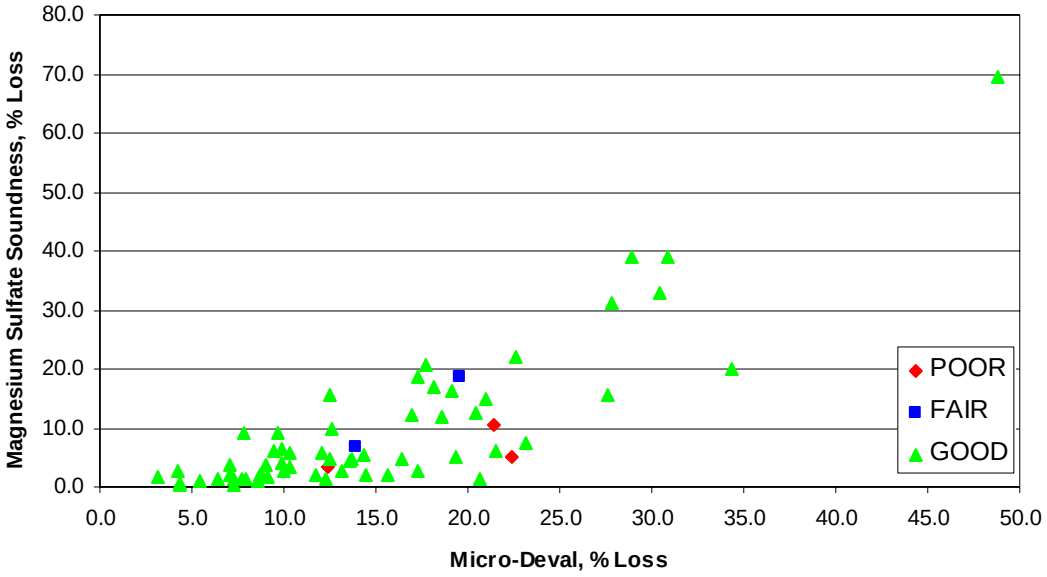

Figure D.1: Magnesium Sulfate Soundness vs. Micro-Deval

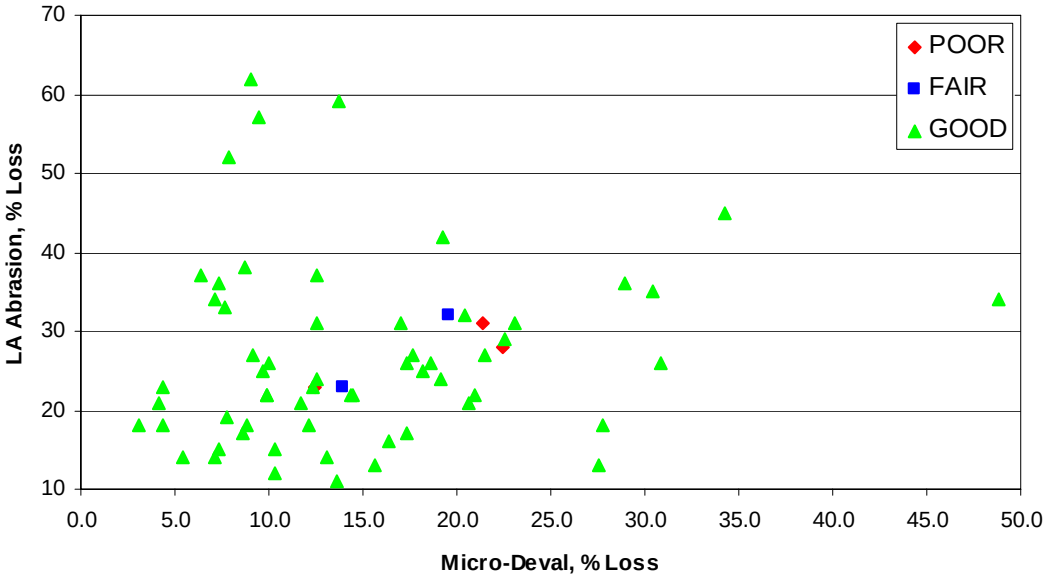

Figure D.2: L.A. Abrasion vs. Micro-Deval

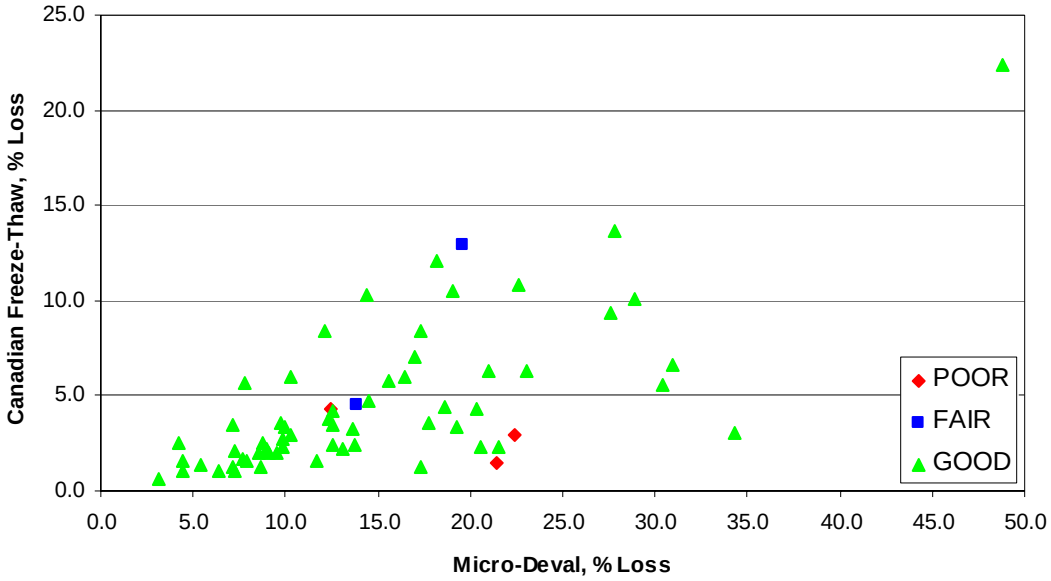

Figure D.3: Canadian Freeze-Thaw Soundness vs. Micro-Deval

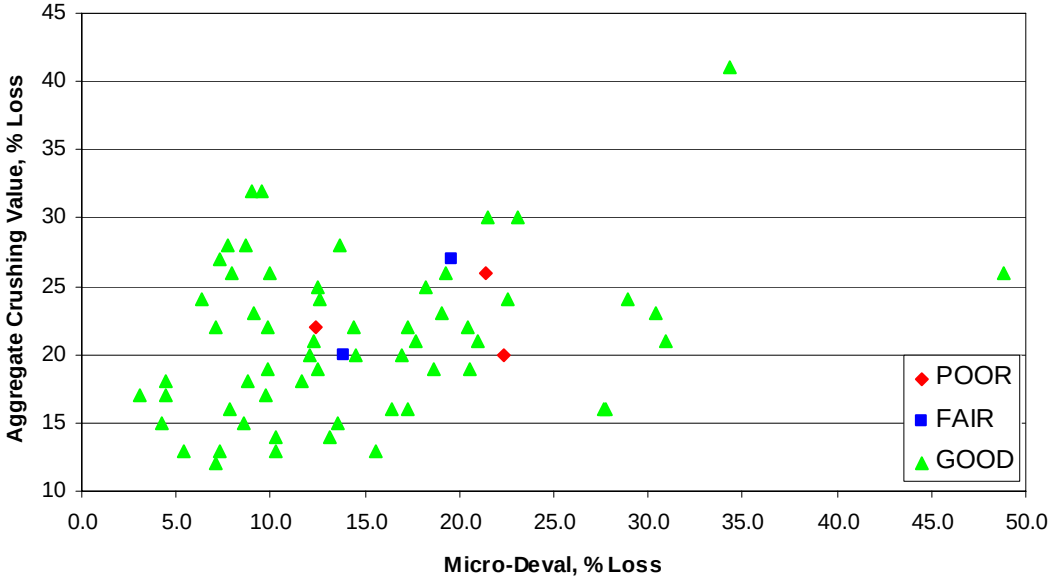

Figure D.4: Aggregate Crushing Value vs. Micro-Deval

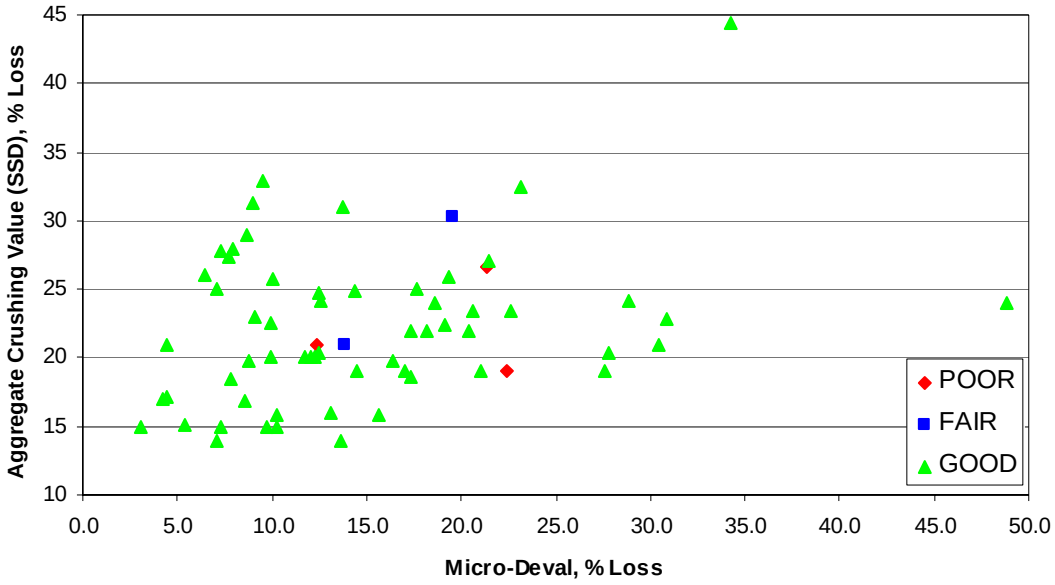

Figure D.5: Aggregate Crushing Value (SSD) vs. Micro-Deval

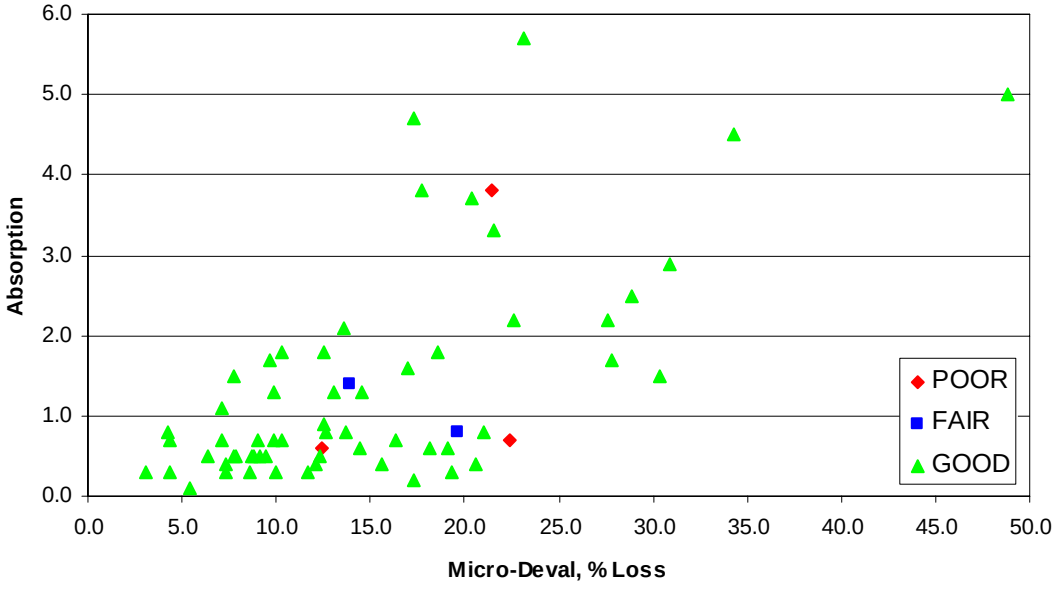

Figure D.6: Absorption vs. Micro-Deval

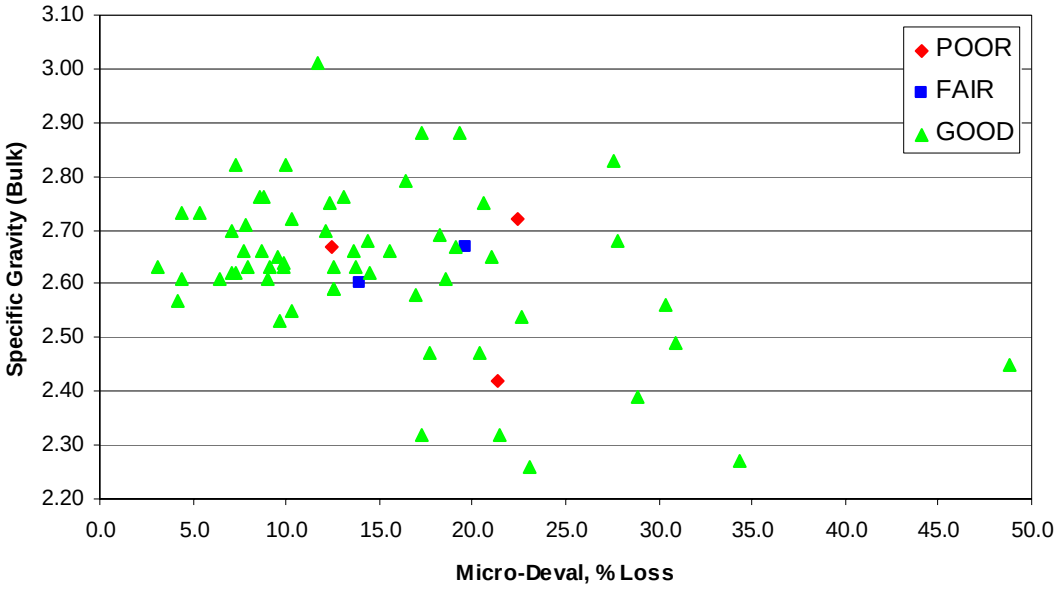

Figure D.7: Specific Gravity (Bulk) vs. Micro-Deval

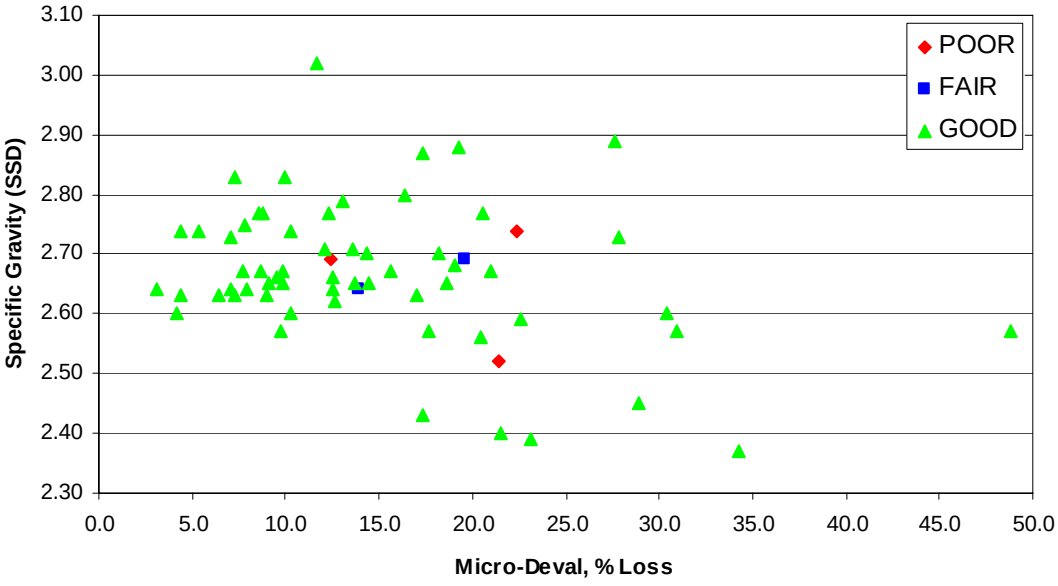

Figure D.8: Specific Gravity (SSD) vs. Micro-Deval

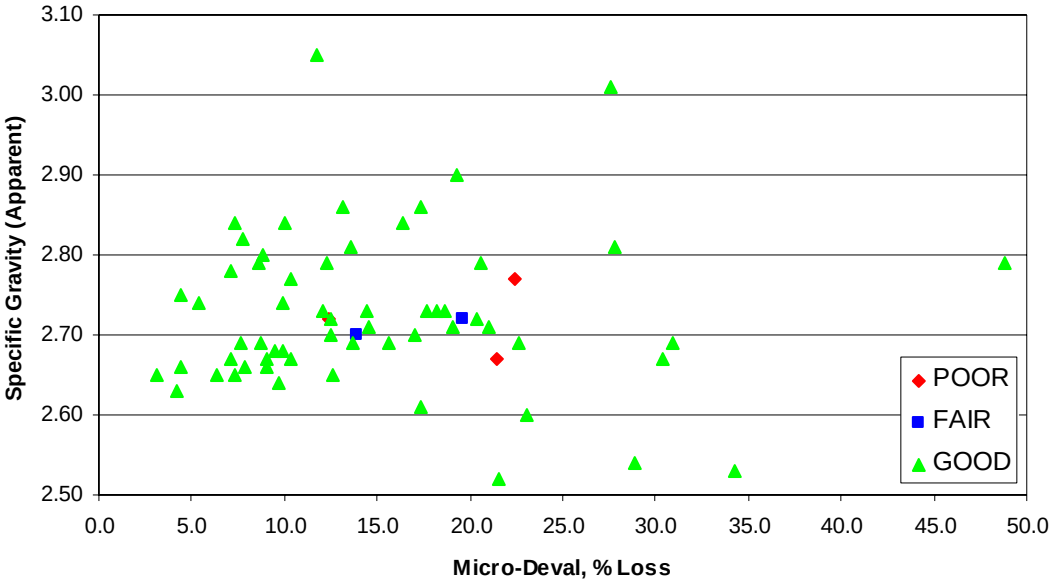

Figure D.9: Specific Gravity (Apparent) vs. Micro-Deval

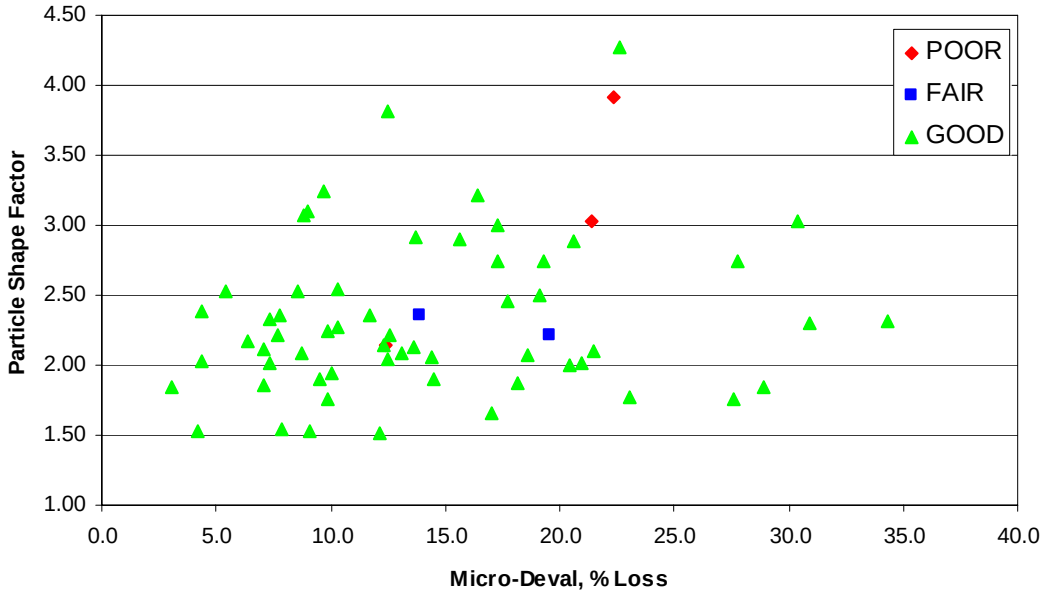

Figure D.10: Particle Shape Factor vs. Micro-Deval

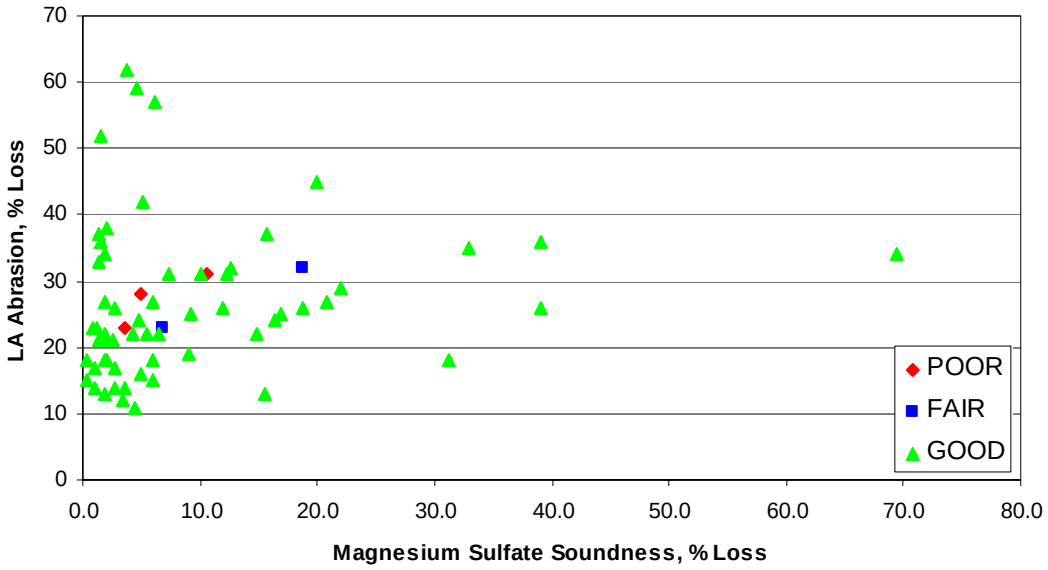

Figure D.11: L.A. Abrasion vs. Magnesium Sulfate Soundness

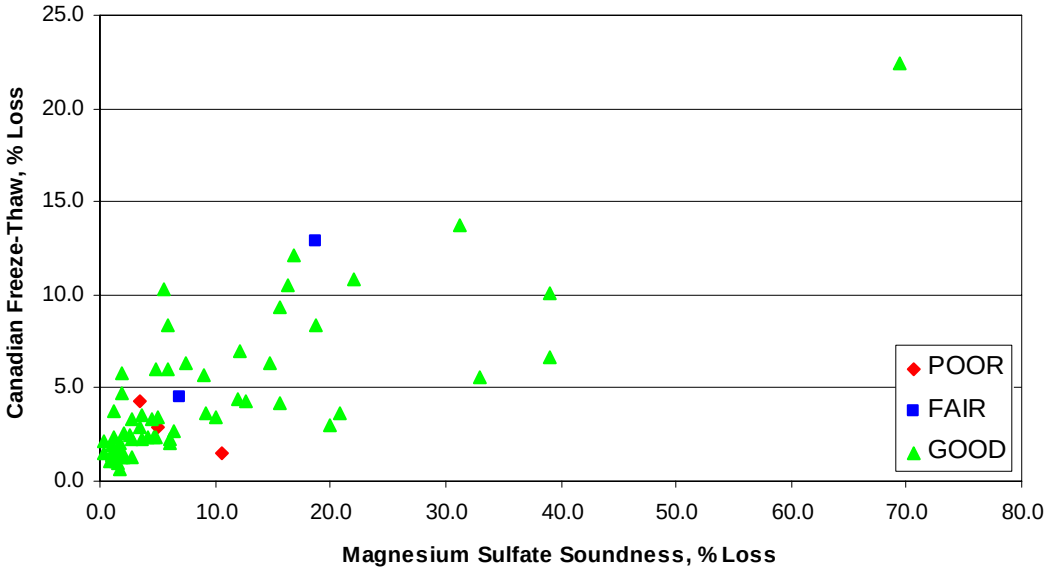

Figure D.12: Canadian Freeze-Thaw Soundness vs. Magnesium Sulfate Soundness

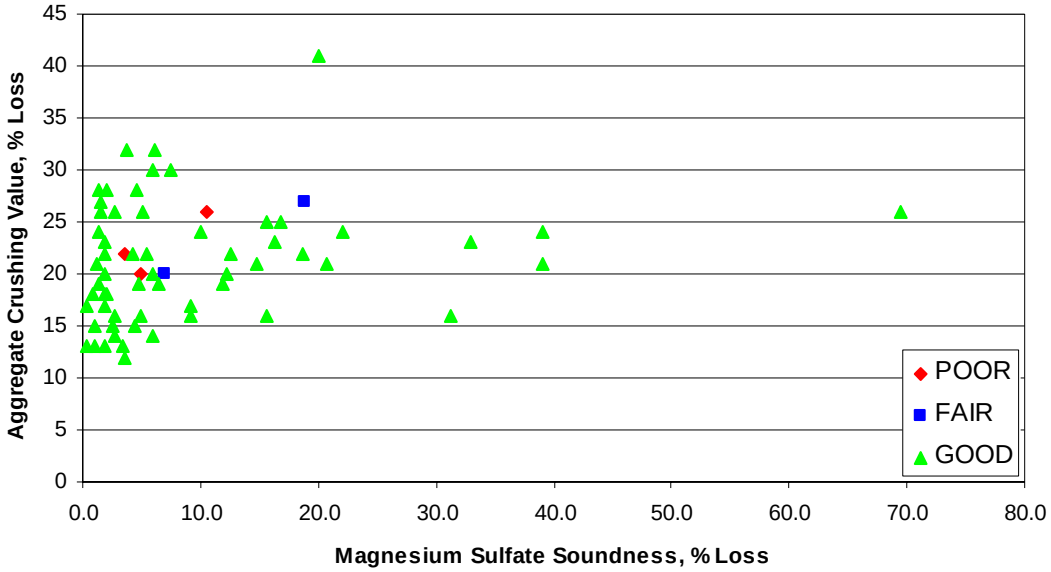

Figure D.13: Canadian Freeze-Thaw Soundness vs. Magnesium Sulfate Soundness

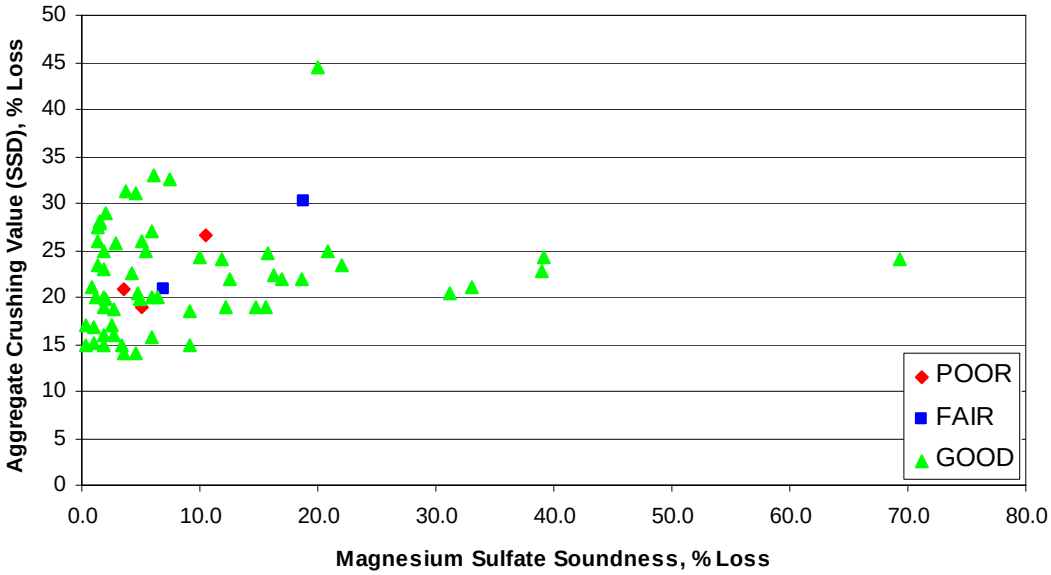

Figure D.14: Canadian Freeze-Thaw Soundness vs. Magnesium Sulfate Soundness

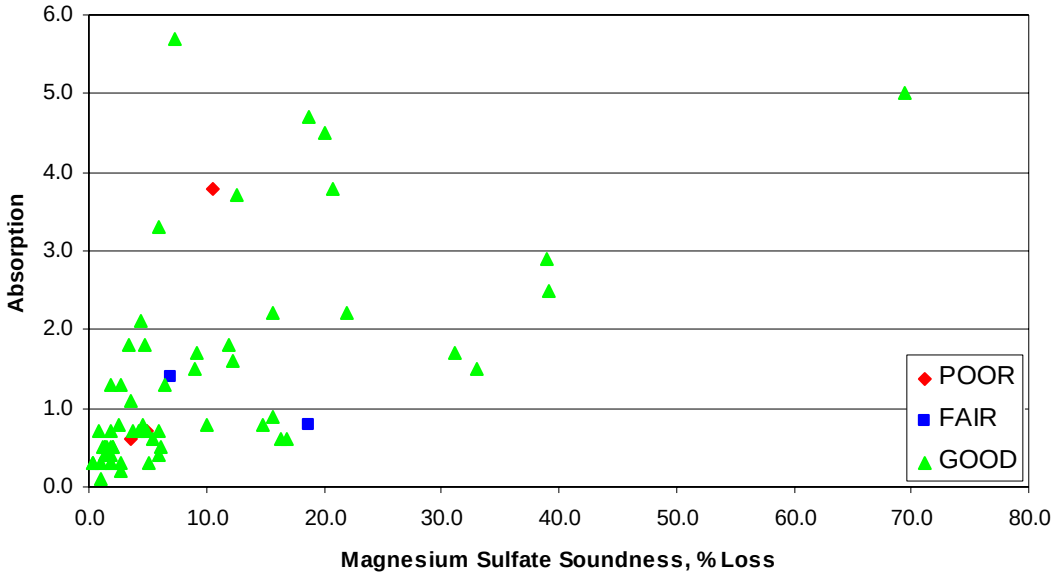

Figure D.15: Absorption vs. Magnesium Sulfate Soundness

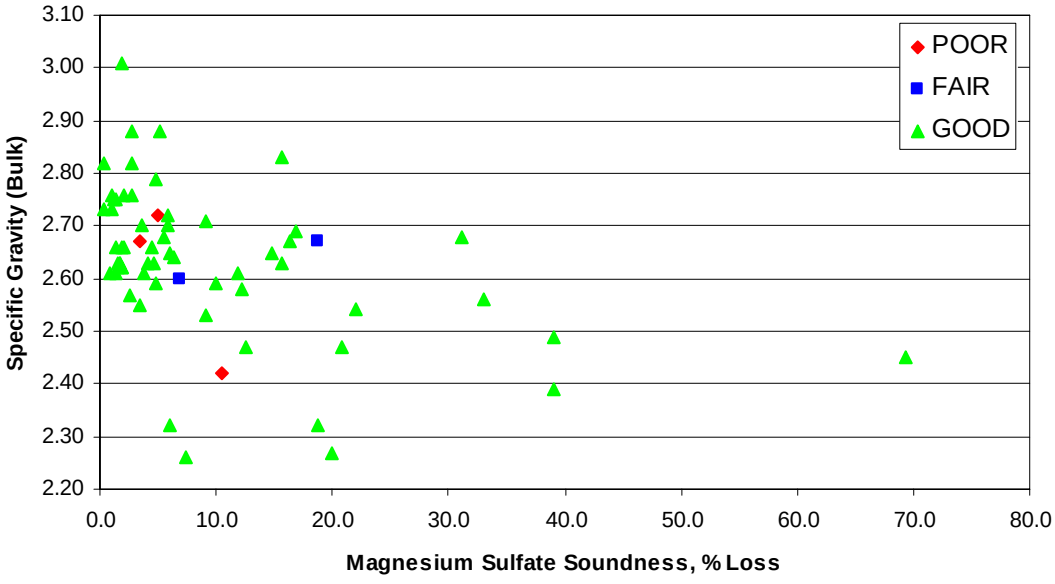

Figure D.16: Specific Gravity (Bulk) vs. Magnesium Sulfate Soundness

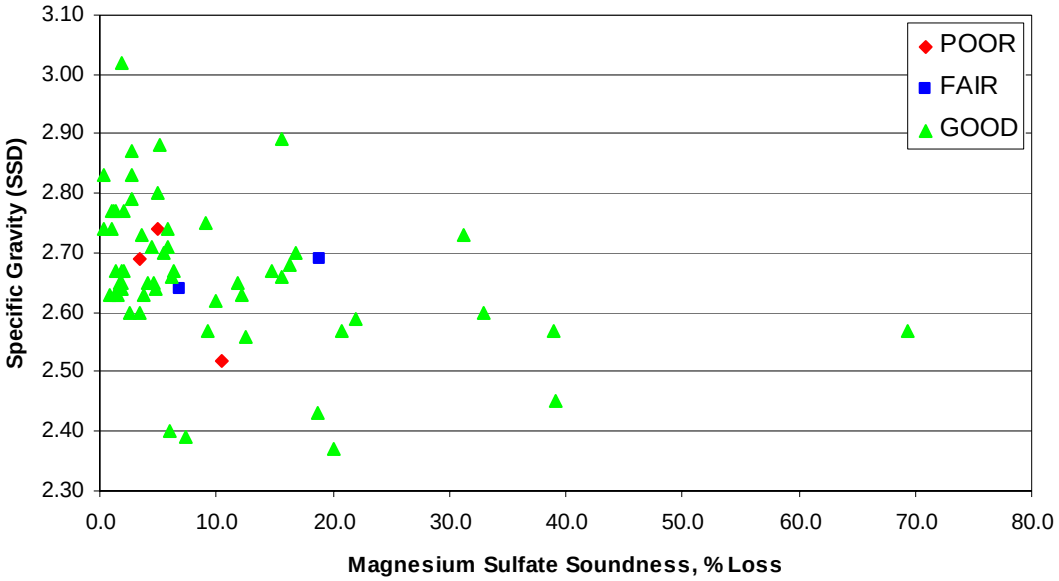

Figure D.17: Specific Gravity (SSD) vs. Magnesium Sulfate Soundness

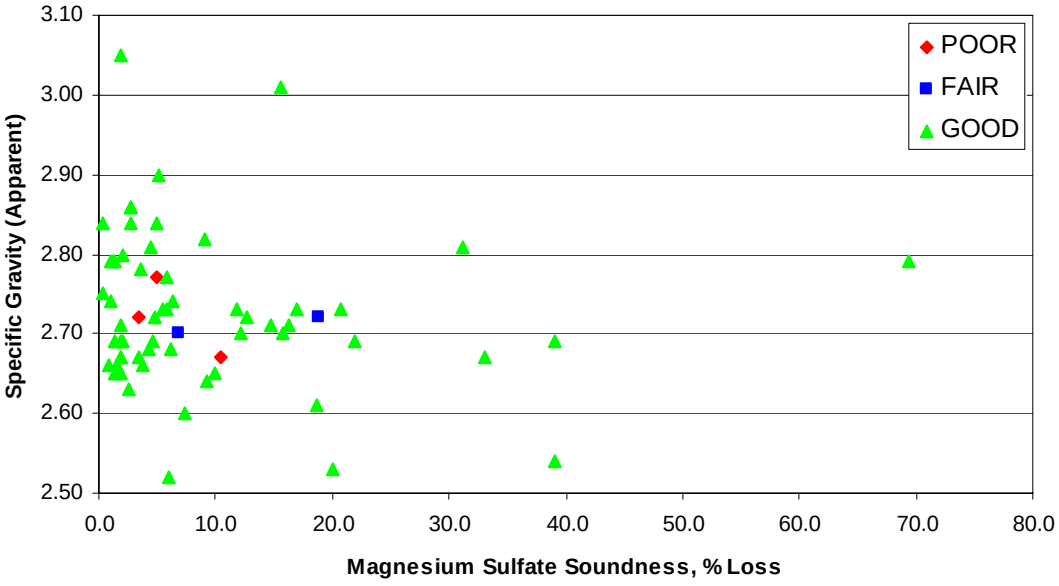

Figure D.18: Specific Gravity (Apparent) vs. Magnesium Sulfate Soundness

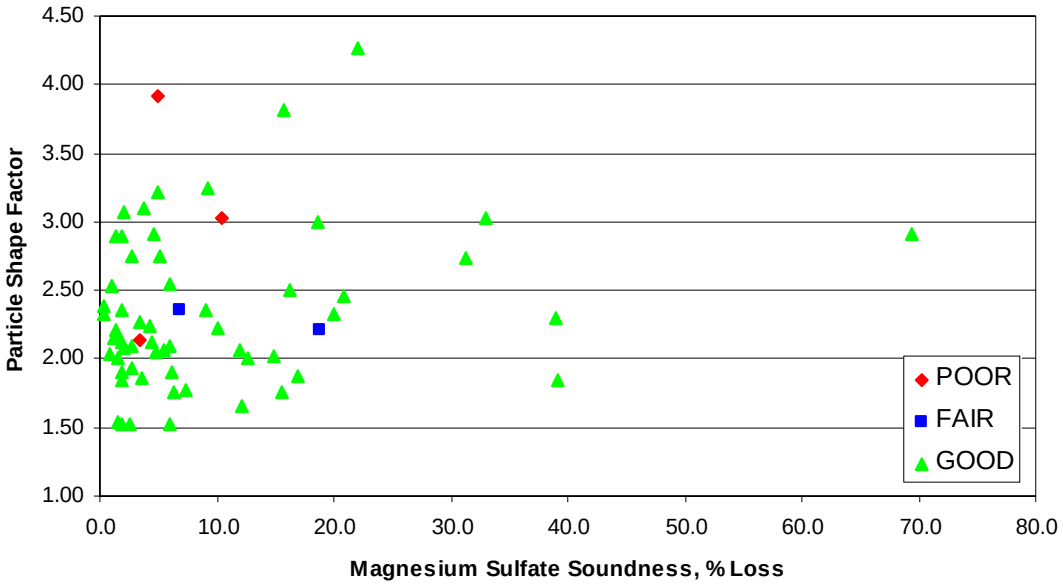

Figure D.19: Particle Shape Factor vs. Magnesium Sulfate Soundness

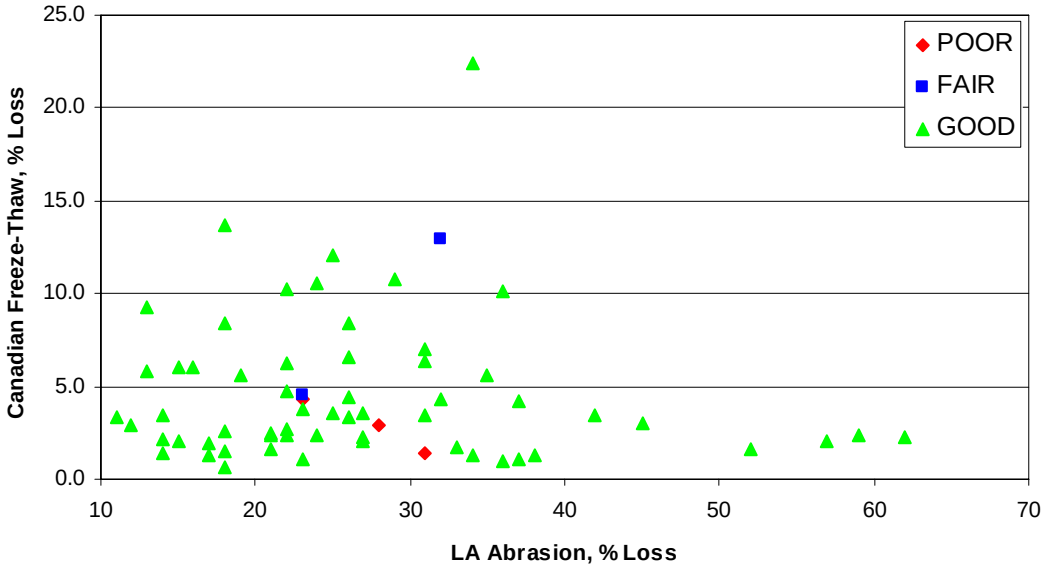

Figure D.20: Canadian Freeze-Thaw Soundness vs. L.A. Abrasion

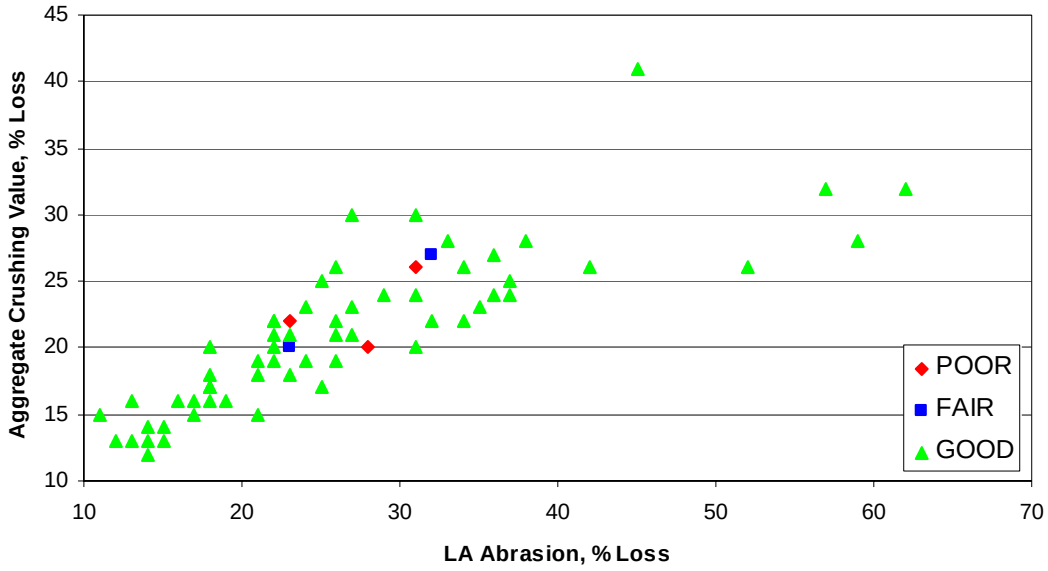

Figure D.21: Aggregate Crushing Value vs. L.A. Abrasion

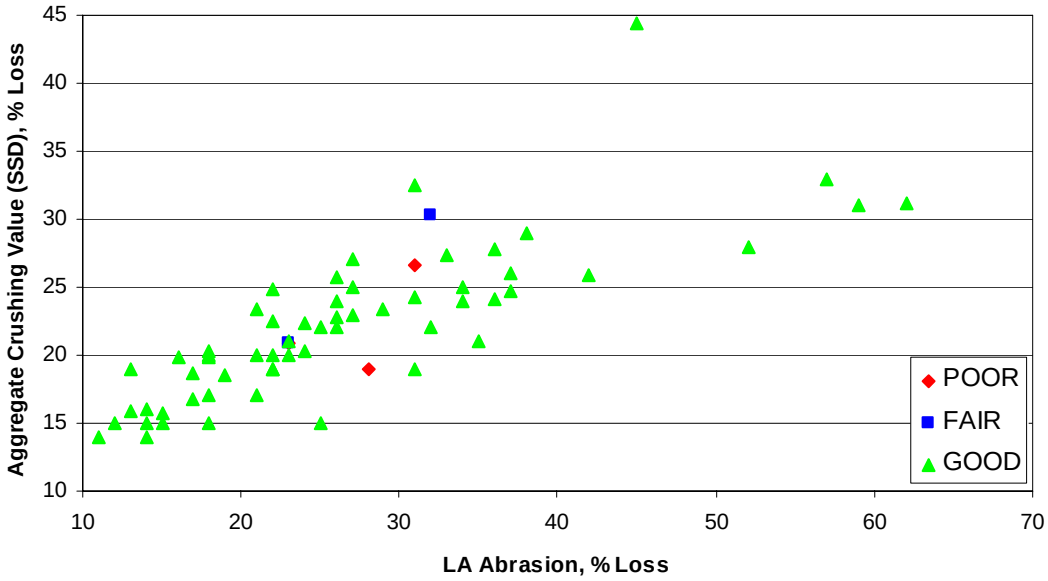

Figure D.22: Aggregate Crushing Value vs. Micro-Deval

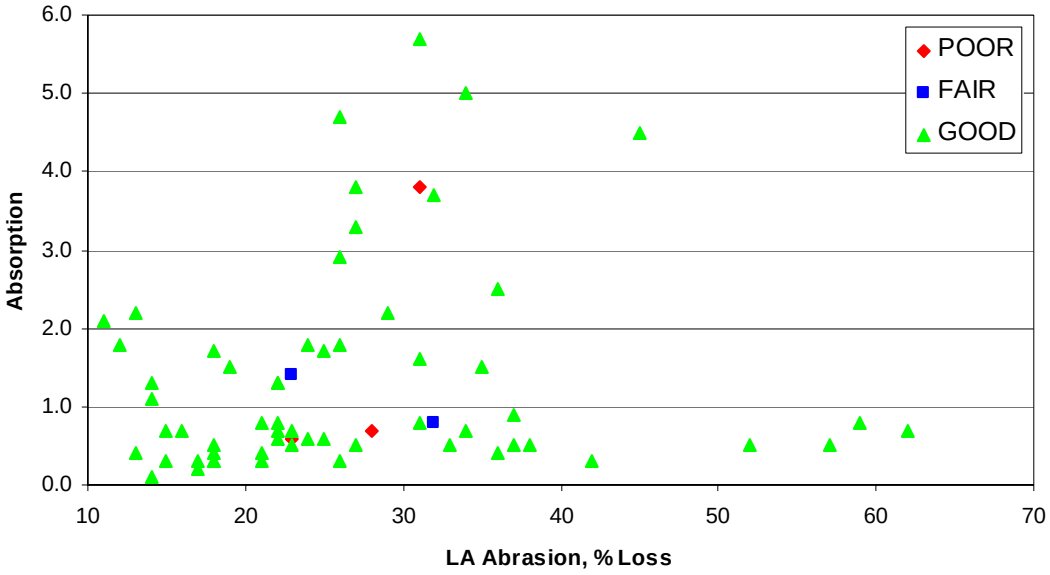

Figure D.23: Absorption vs. L.A. Abrasion

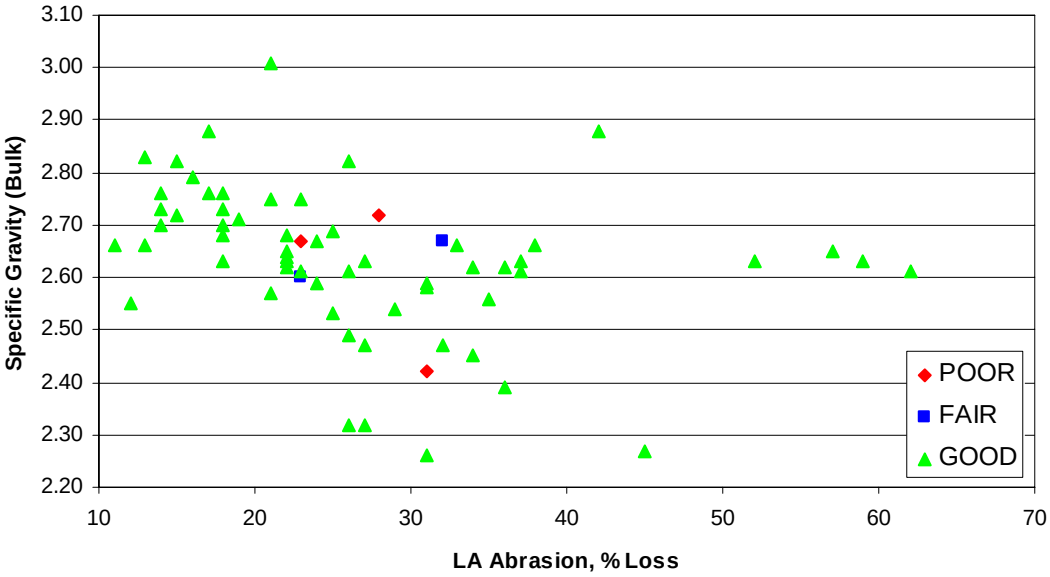

Figure D.24: Specific Gravity (Bulk) vs. L.A. Abrasion

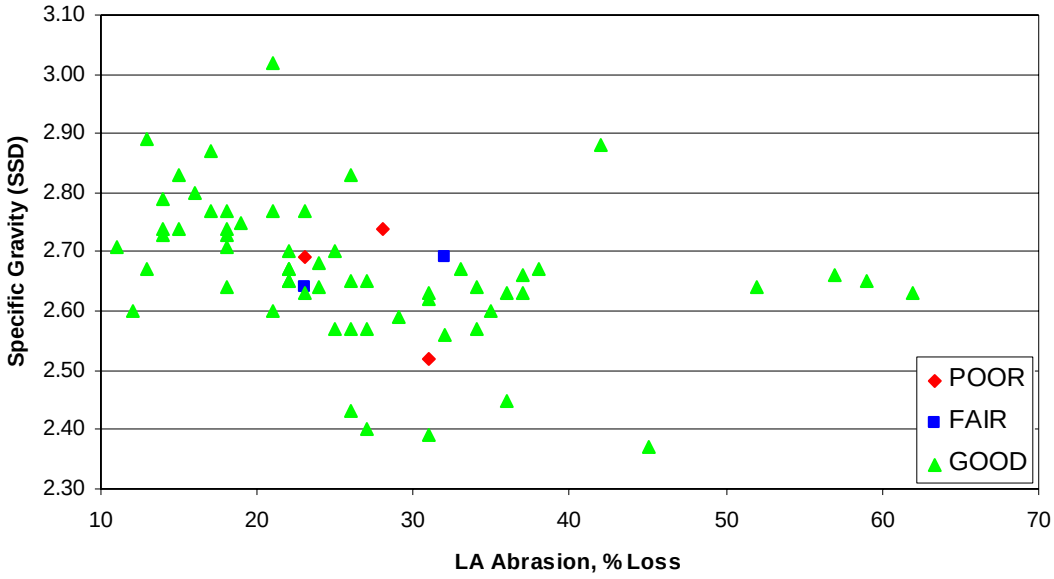

Figure D.25: Specific Gravity (SSD) vs. L.A. Abrasion

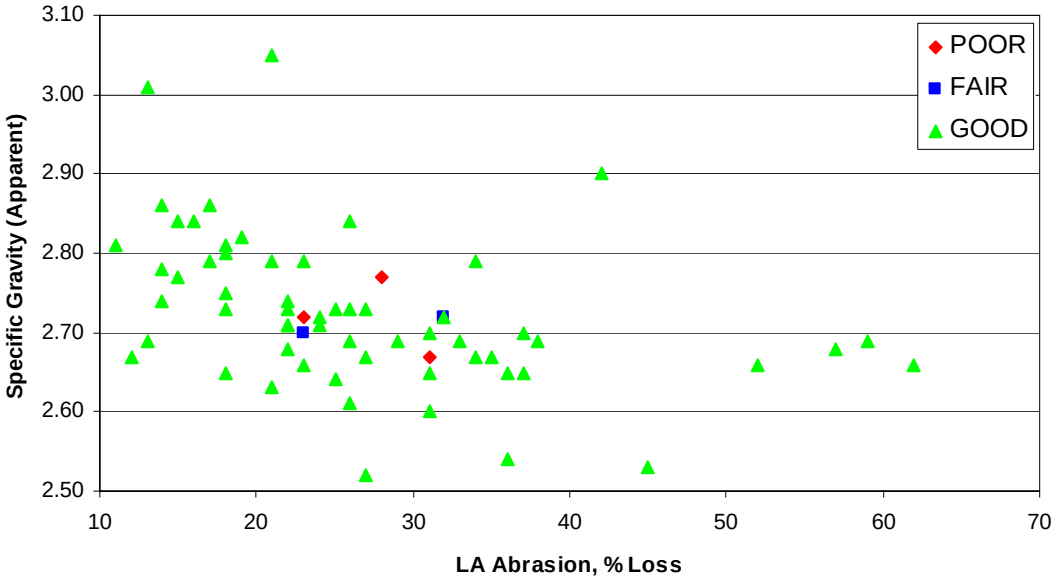

Figure D.26: Specific Gravity (Apparent) vs. L.A. Abrasion

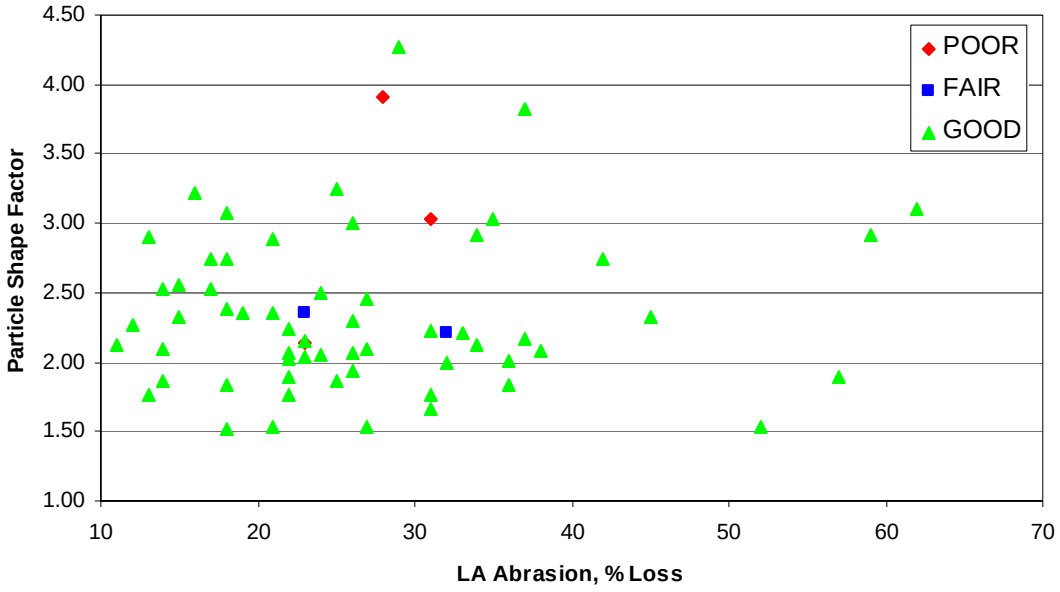

Figure D.27: Particle Shape Factor vs. L.A. Abrasion

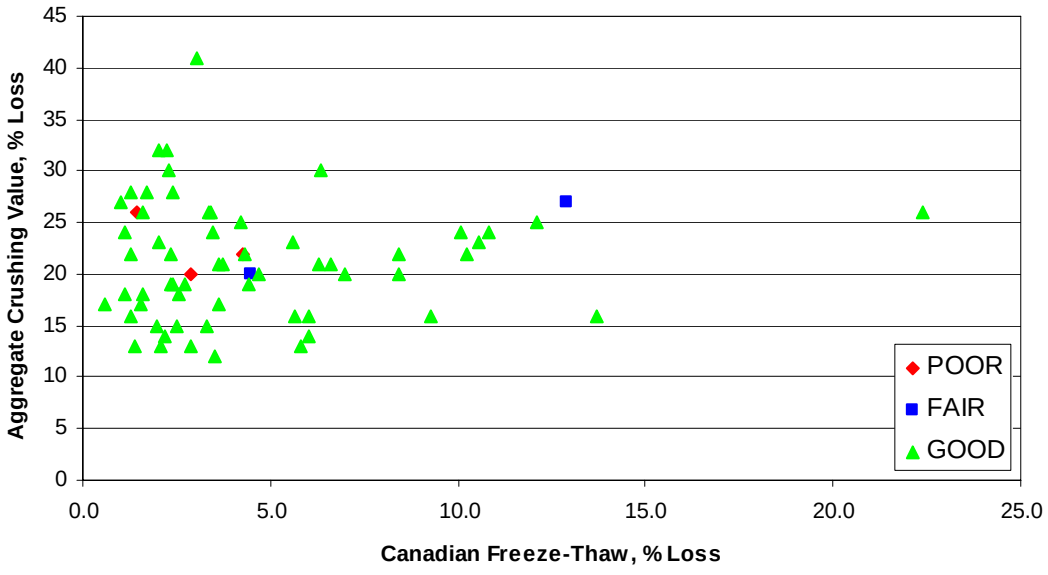

Figure D.28: Aggregate Crushing Value vs. Canadian Freeze-Thaw Soundness

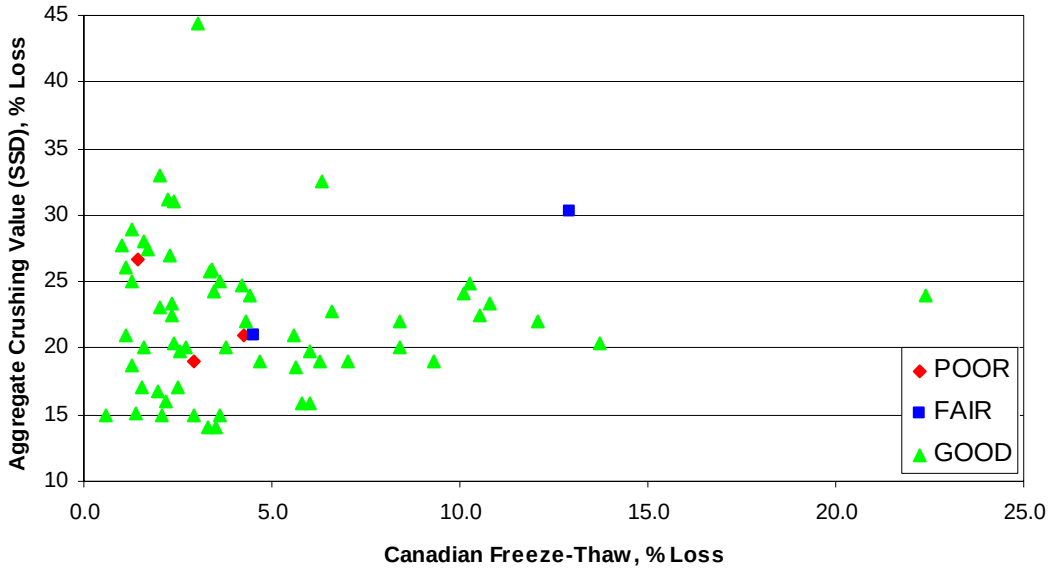

Figure D.29: Aggregate Crushing Value (SSD) vs. Canadian Freeze-Thaw Soundness

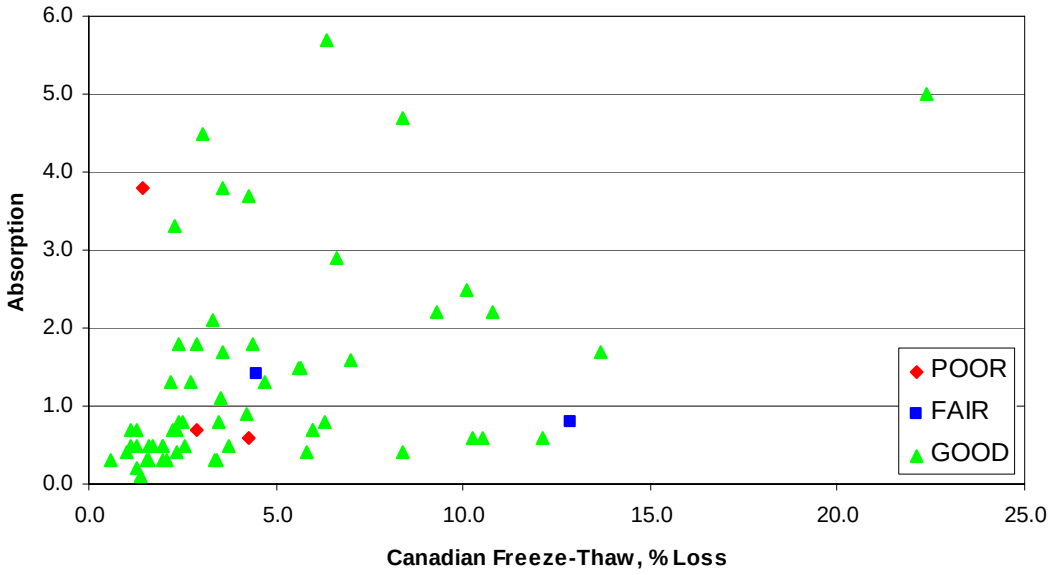

Figure D.30: Absorption vs. Canadian Freeze-Thaw Soundness

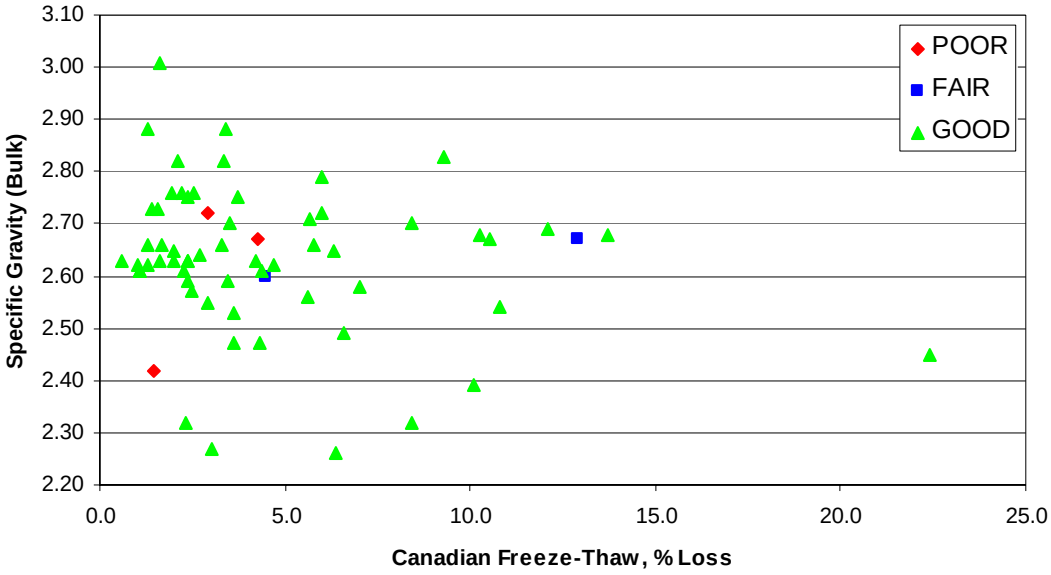

Figure D.31: Specific Gravity (Bulk) vs. Canadian Freeze-Thaw Soundness

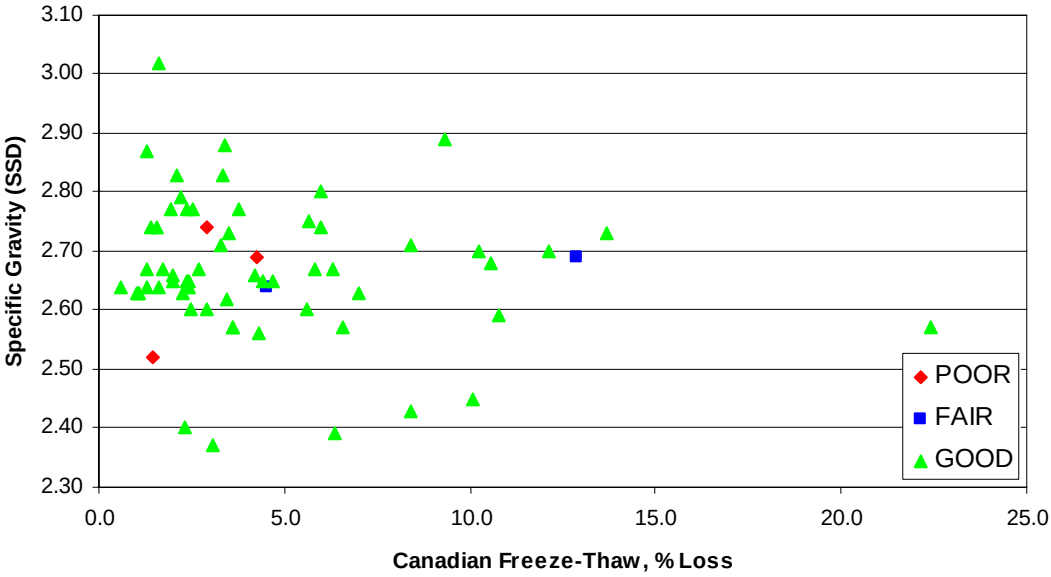

Figure D.32: Specific Gravity (SSD) vs. Canadian Freeze-Thaw Soundness

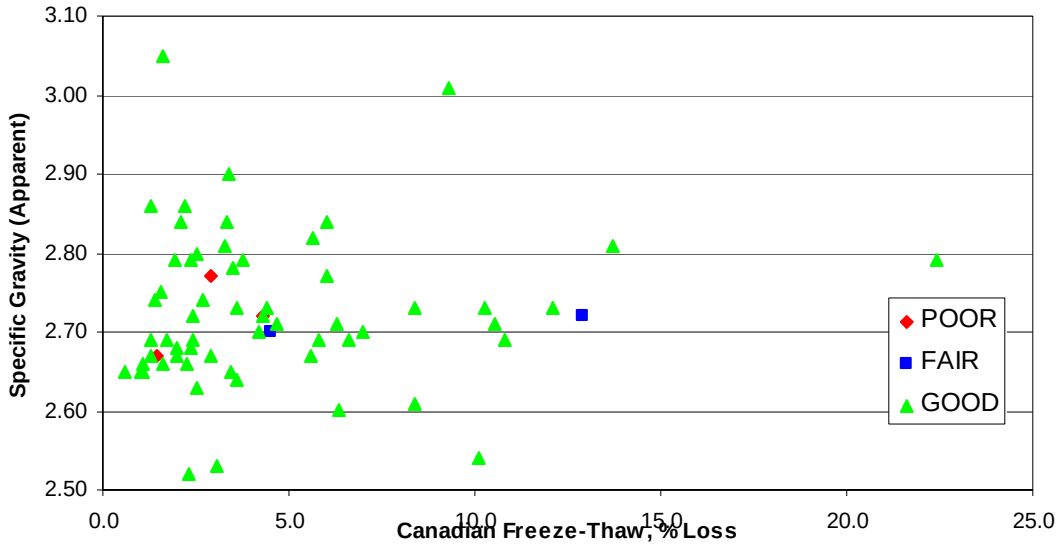

Figure D.33: Specific Gravity (Apparent) vs. Canadian Freeze-Thaw Soundness

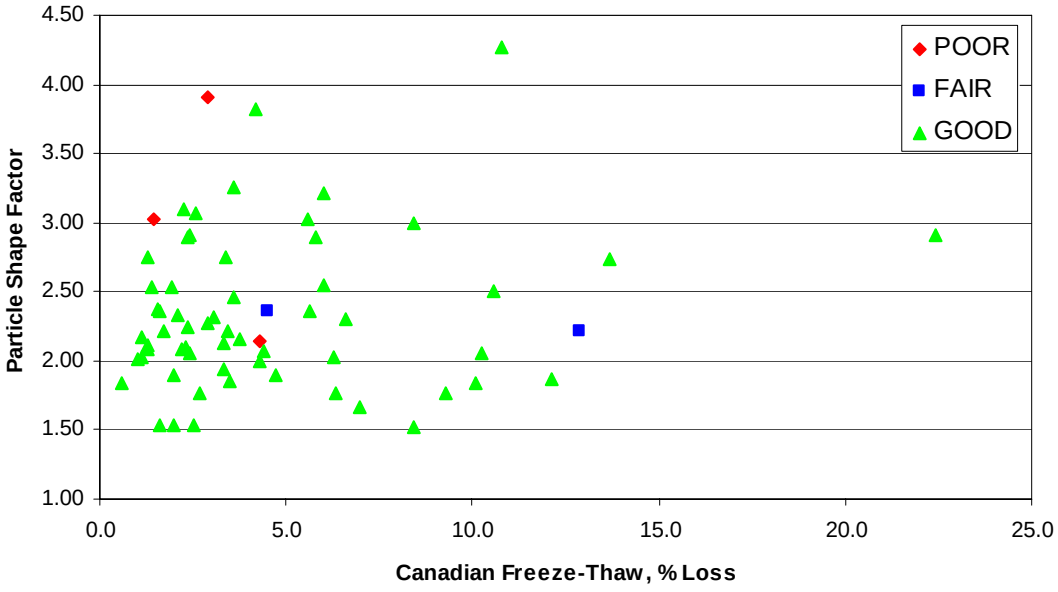

Figure D.34: Particle Shape Factor vs. Canadian Freeze-Thaw Soundness

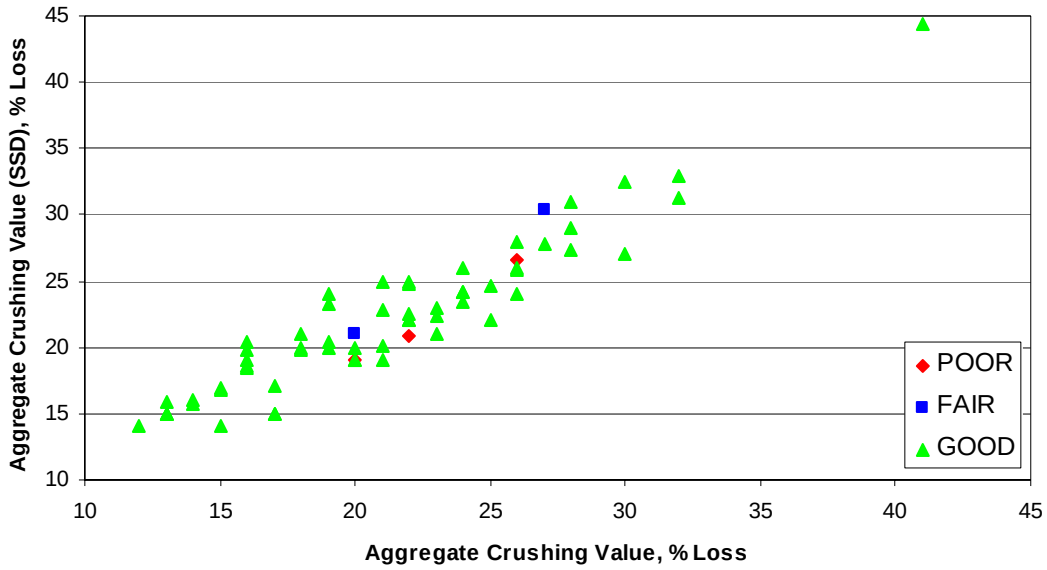

Figure D.35: Aggregate Crushing Value (SSD) vs. Aggregate Crushing Value

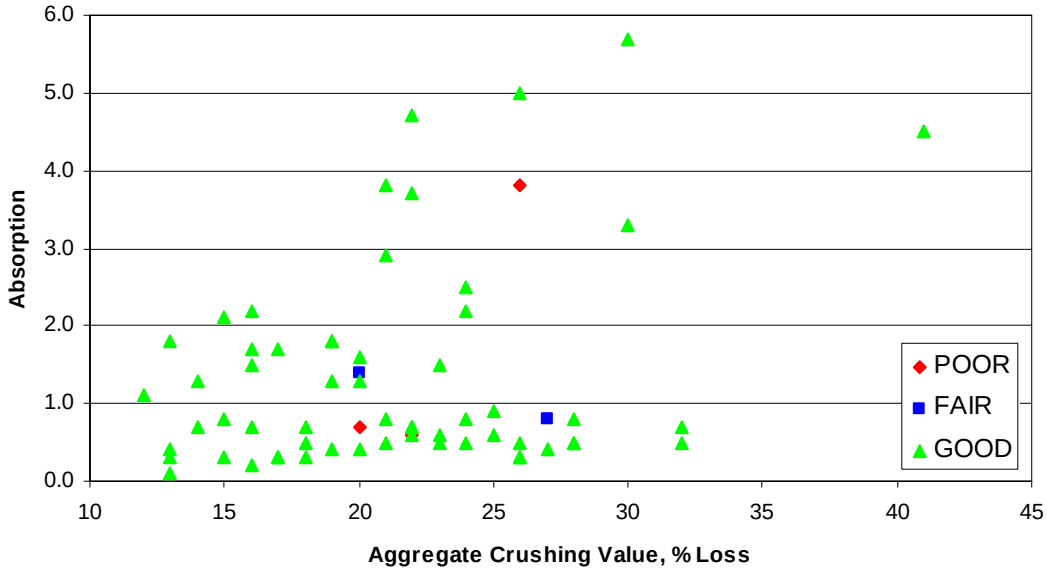

Figure D.36: Absorption vs. Aggregate Crushing Value

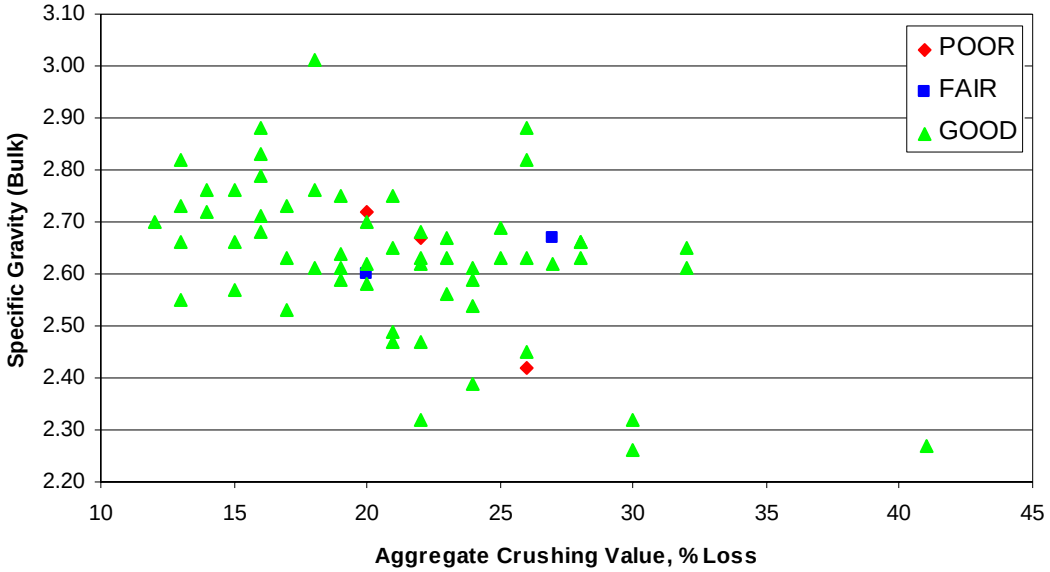

Figure D.37: Specific Gravity (Bulk) vs. Aggregate Crushing Value

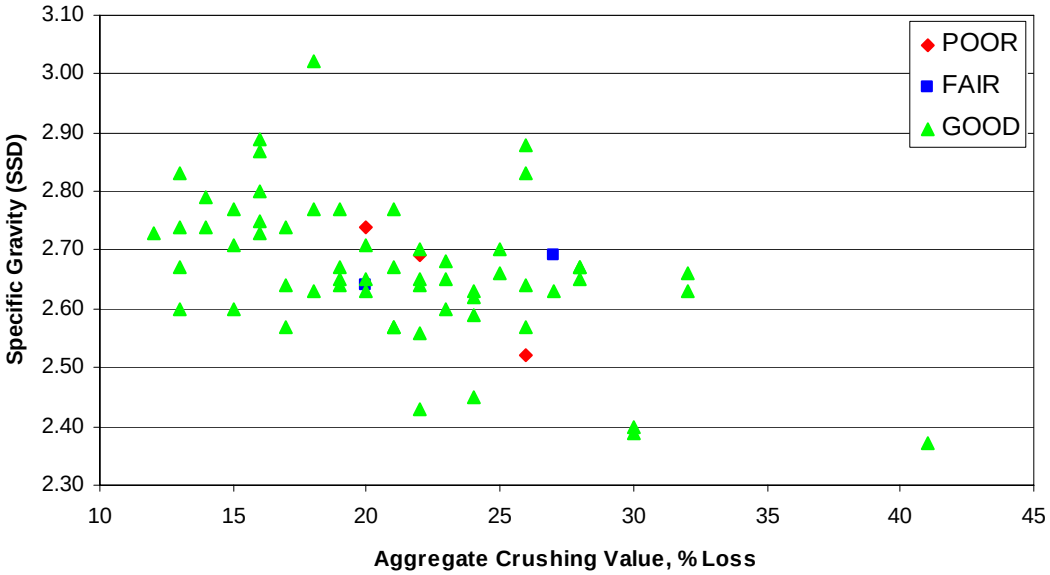

Figure D.38: Specific Gravity (SSD) vs. Aggregate Crushing Value

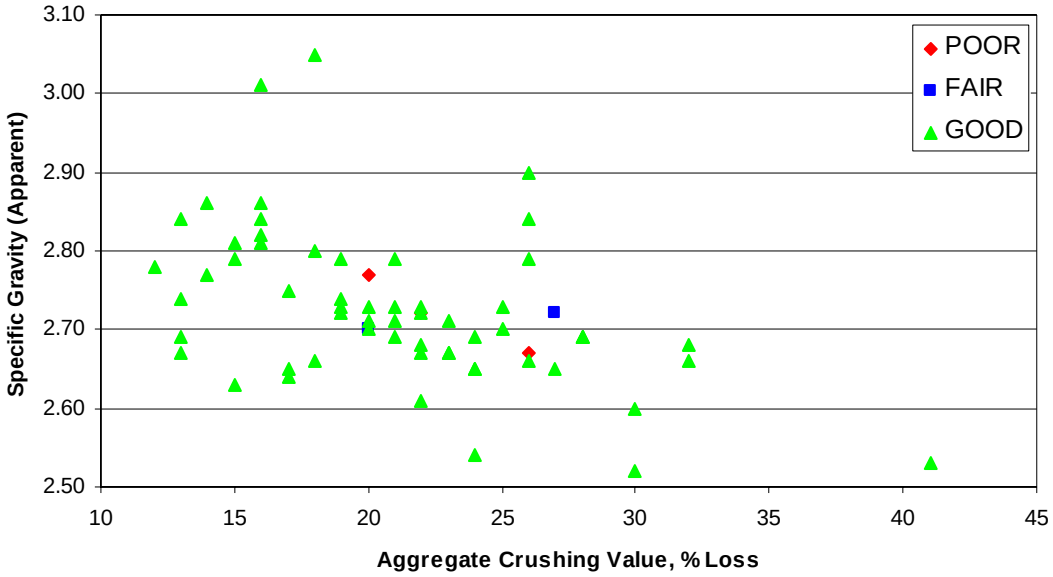

Figure D.39: Specific Gravity (Apparent) vs. Aggregate Crushing Value

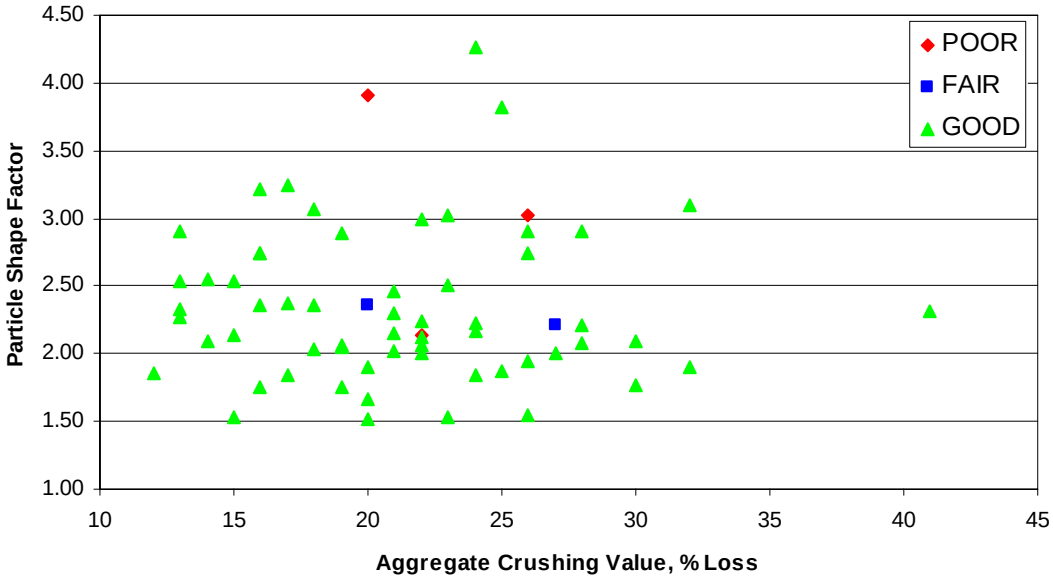

Figure D.40: Particle Shape Factor vs. Aggregate Crushing Value

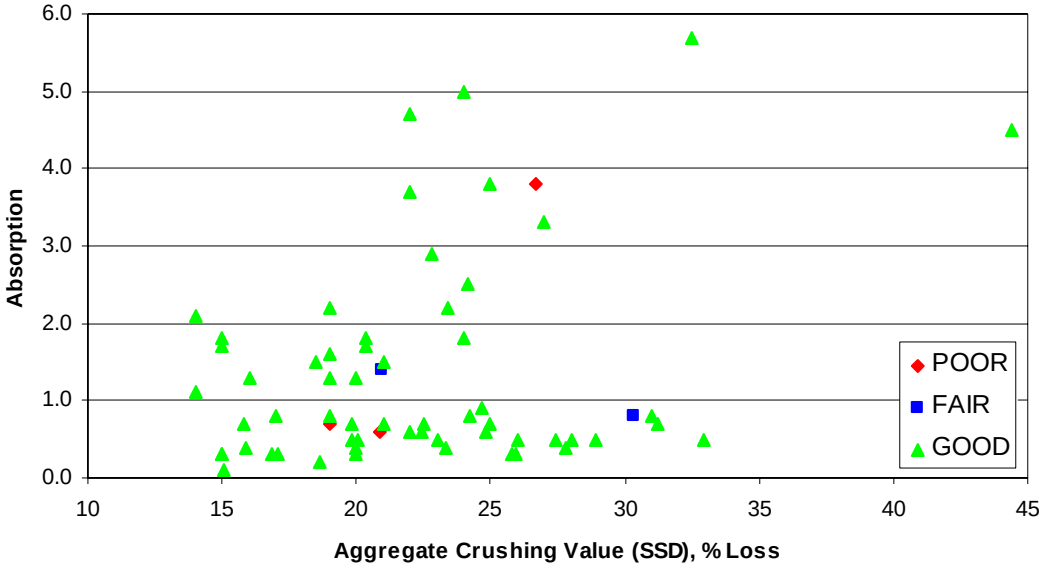

Figure D.41: Absorption vs. Aggregate Crushing Value (SSD)

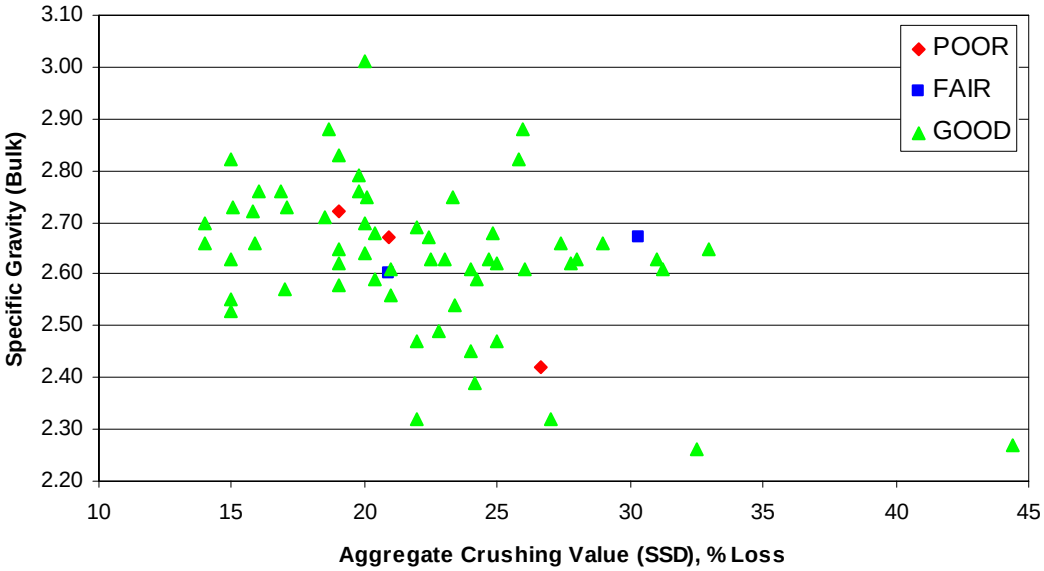

Figure D.42: Specific Gravity (Bulk) vs. Aggregate Crushing Value (SSD)

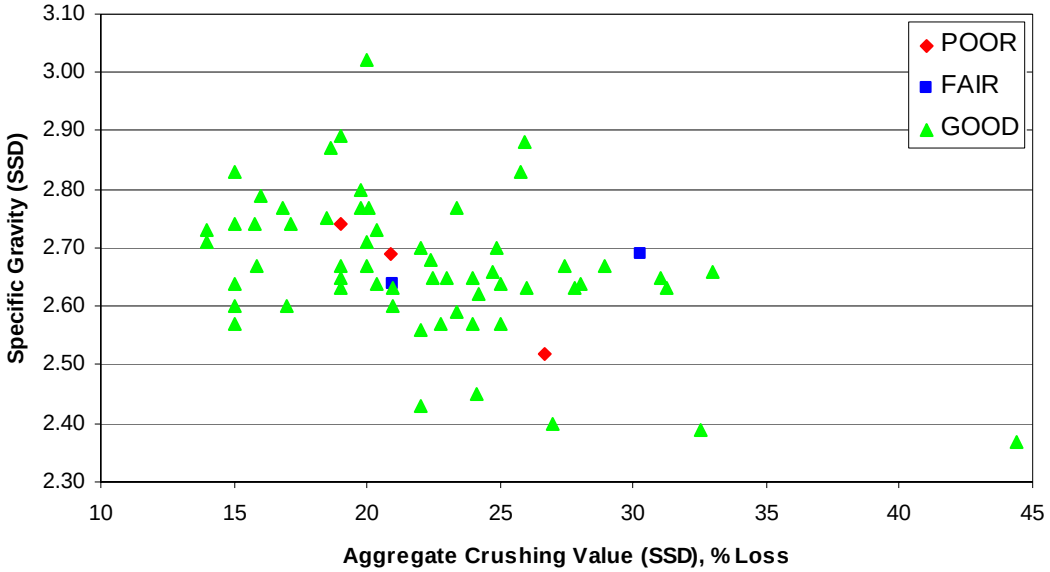

Figure D.43: Specific Gravity (SSD) vs. Aggregate Crushing Value (SSD)

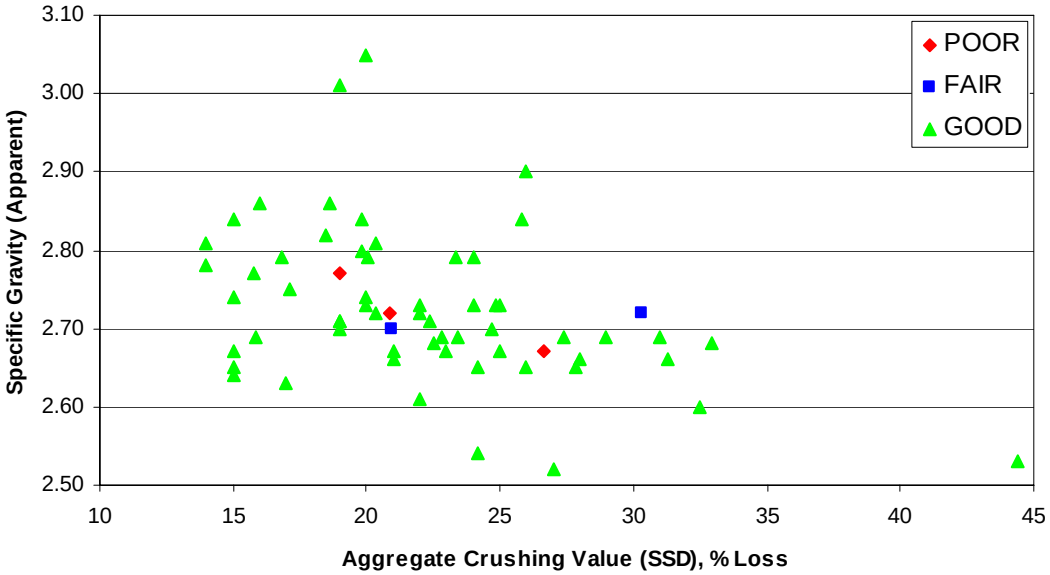

Figure D.44: Specific Gravity (Apparent) vs. Aggregate Crushing Value (SSD)

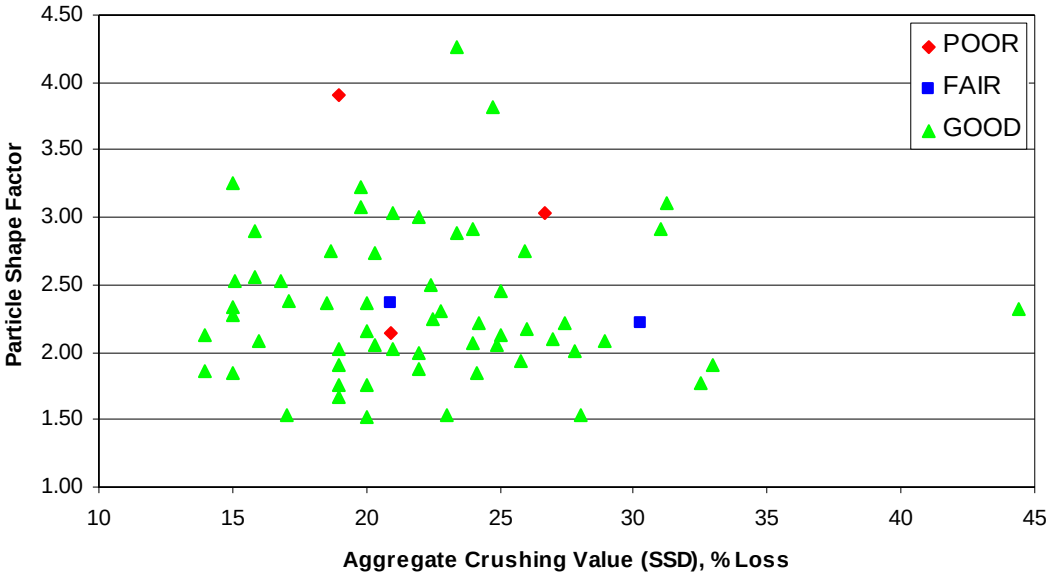

Figure D.45: Particle Shape Factor vs. Aggregate Crushing Value (SSD)

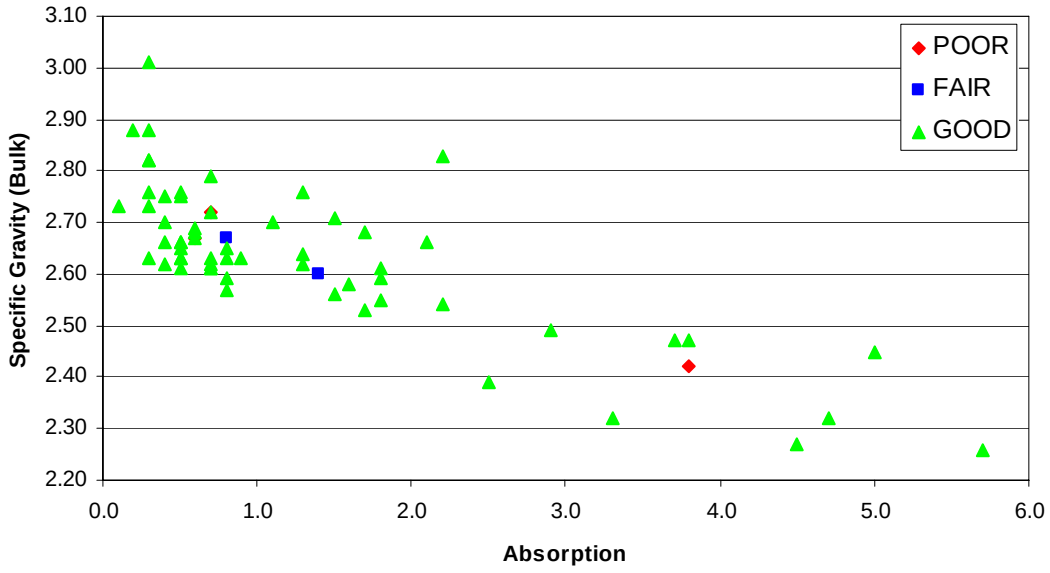

Figure D.46: Specific Gravity (Bulk) vs. Absorption

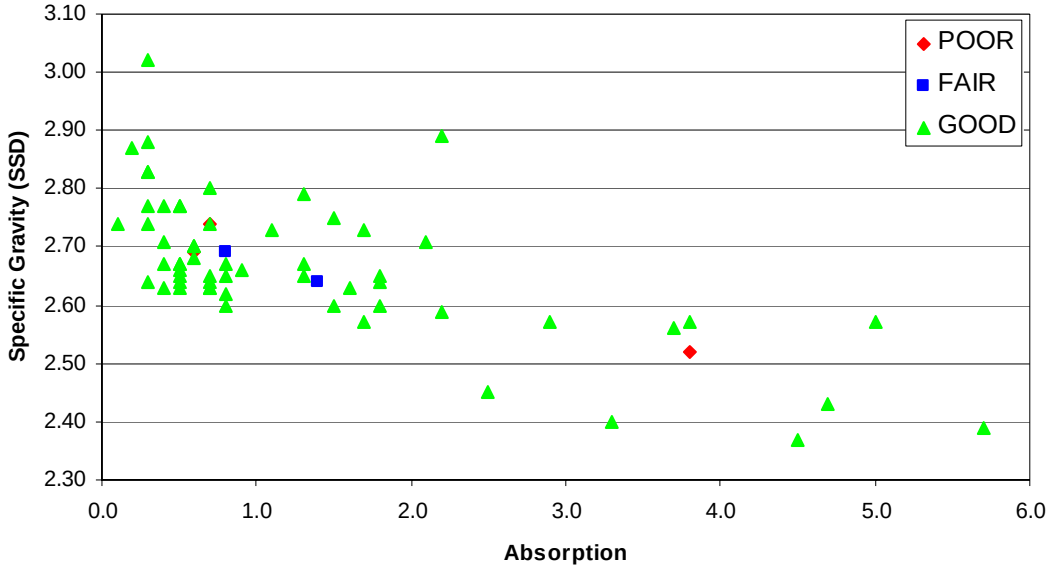

Figure D.47: Specific Gravity (SSD) vs. Absorption

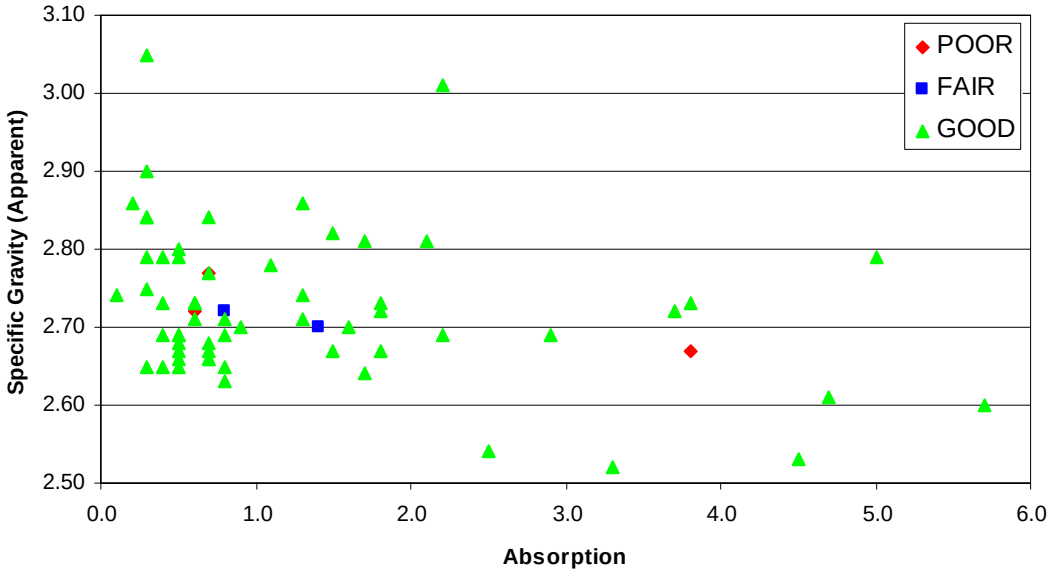

Figure D.48: Specific Gravity (Apparent) vs. Absorption

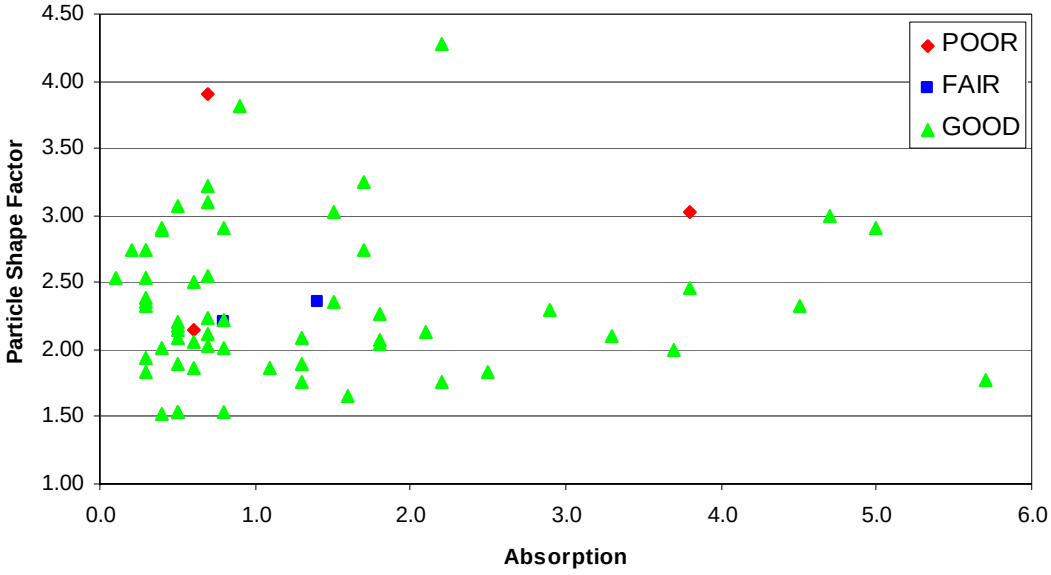

Figure D.49: Particle Shape Factor vs. Absorption

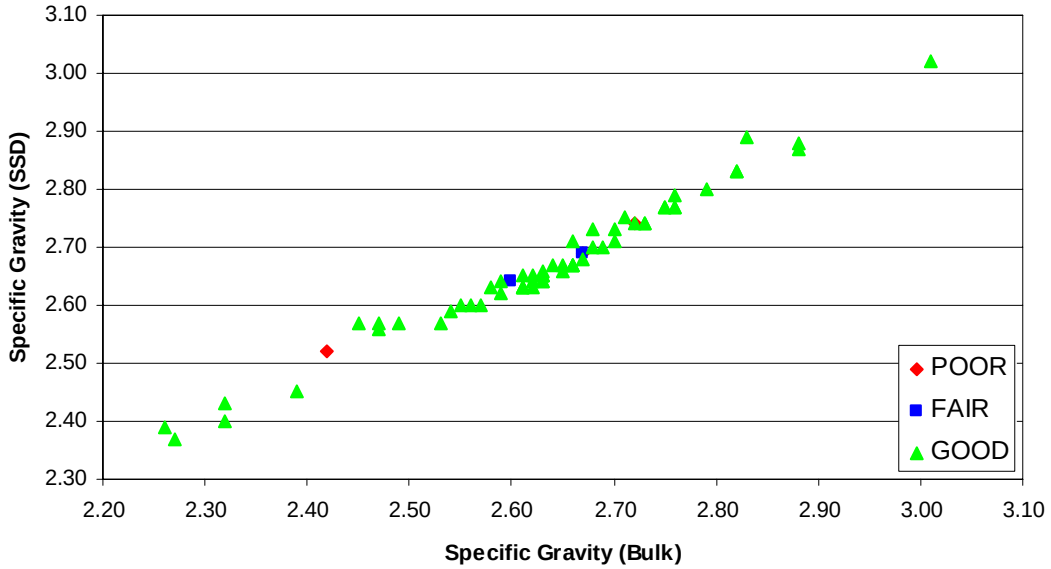

Figure D.50: Specific Gravity (SSD) vs. Specific Gravity (Bulk)

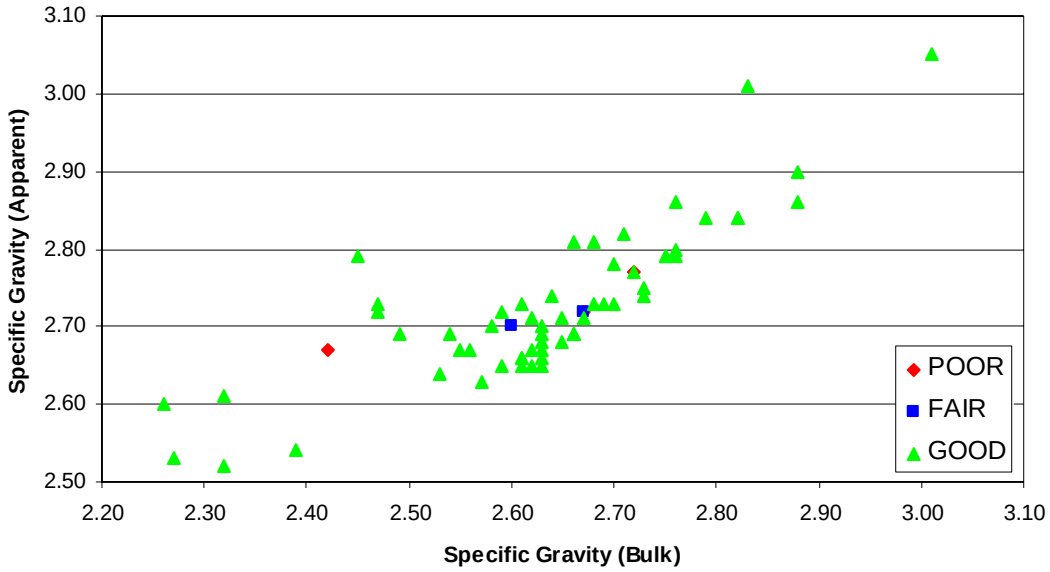

Figure D.51: Specific Gravity (Apparent) vs. Specific Gravity (Bulk)

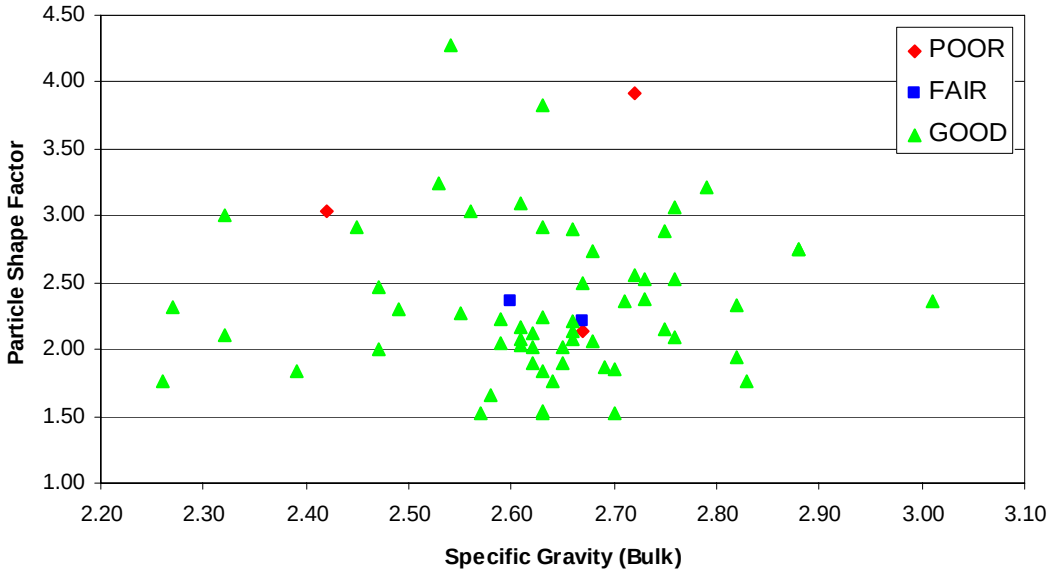

Figure D.52: Particle Shape Factor vs. Specific Gravity (Bulk)

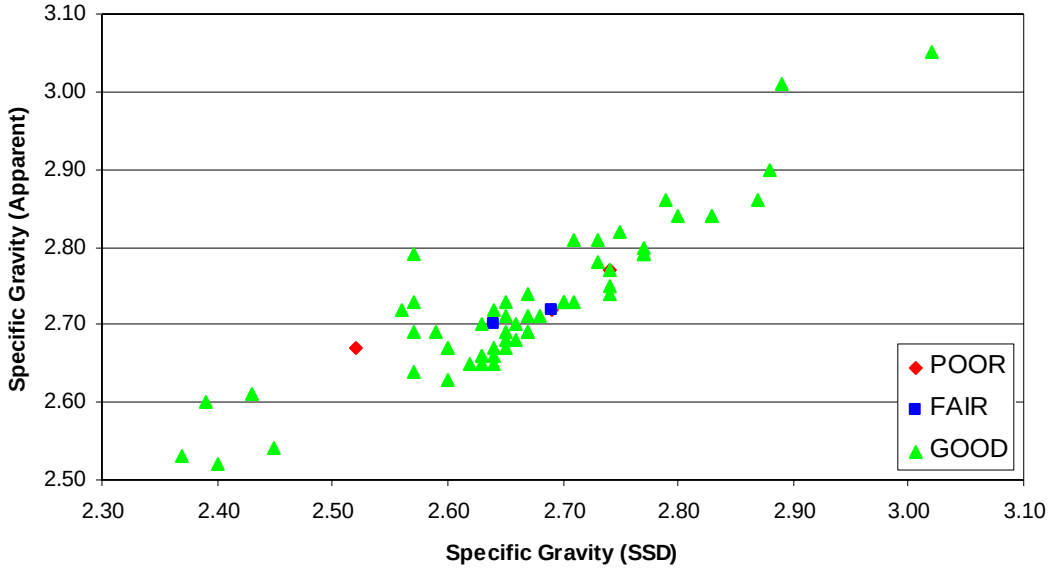

Figure D.53: Specific Gravity (Apparent) vs. Specific Gravity (SSD)

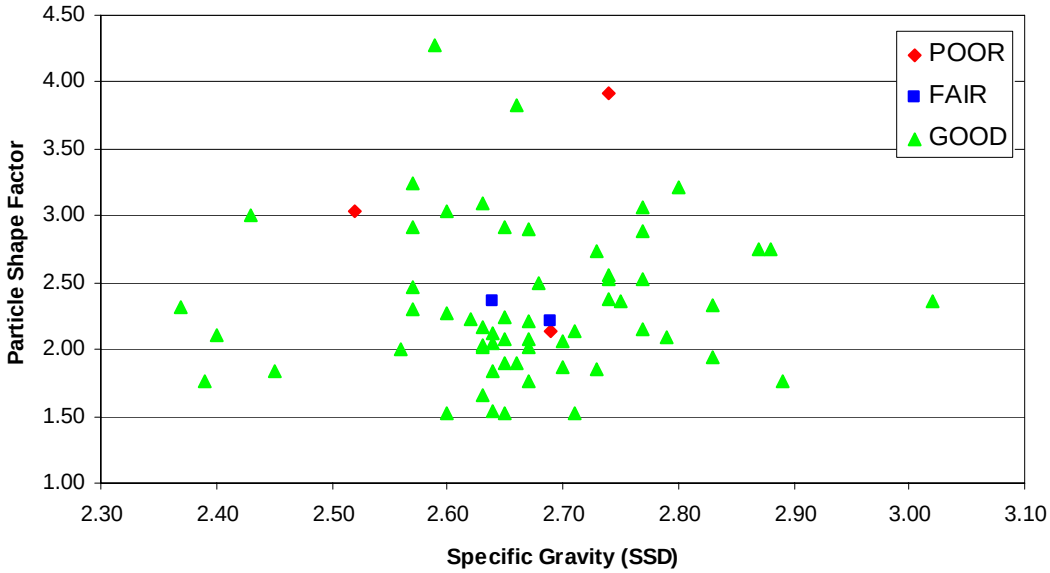

Figure D.54: Particle Shape Factor vs. Specific Gravity (SSD)

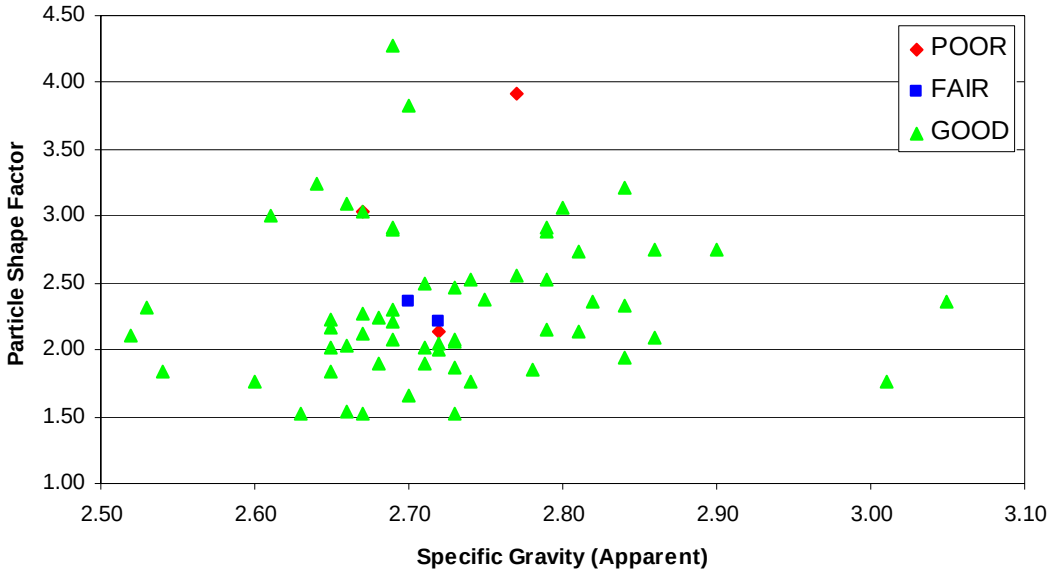

Figure D.55: Particle Shape Factor vs. Specific Gravity (Apparent)

Appendix E: Test Correlation Graphs for the Full Data Set

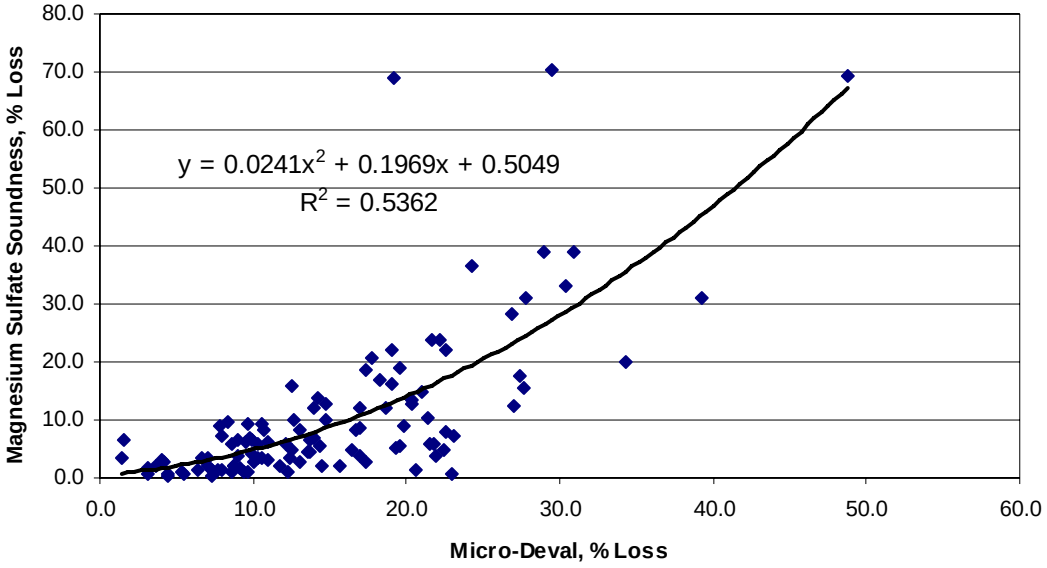

Figure E.1: Magnesium Sulfate Soundness vs. Micro-Deval

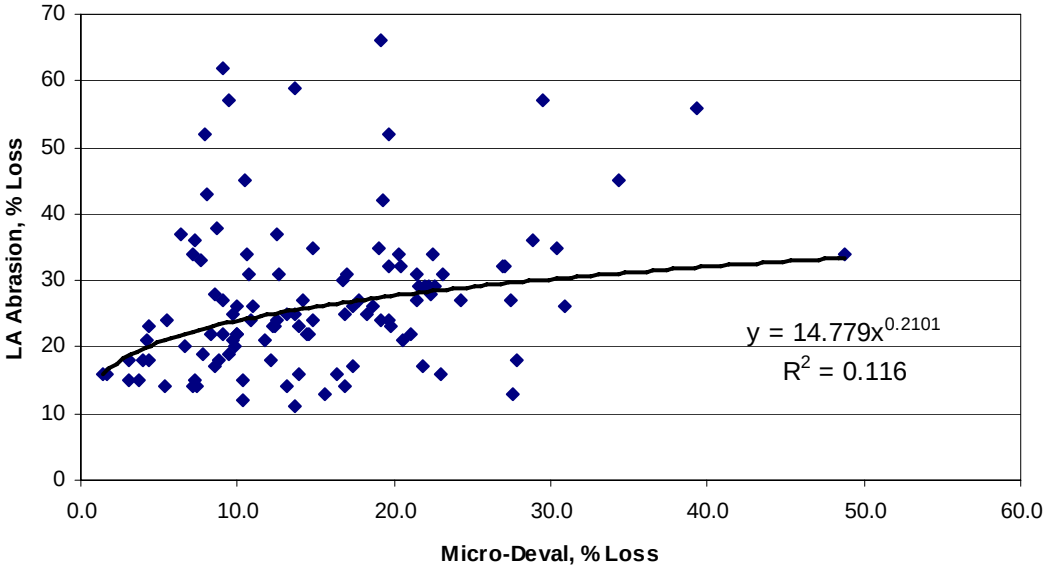

Figure E.2: L.A. Abrasion vs. Micro-Deval

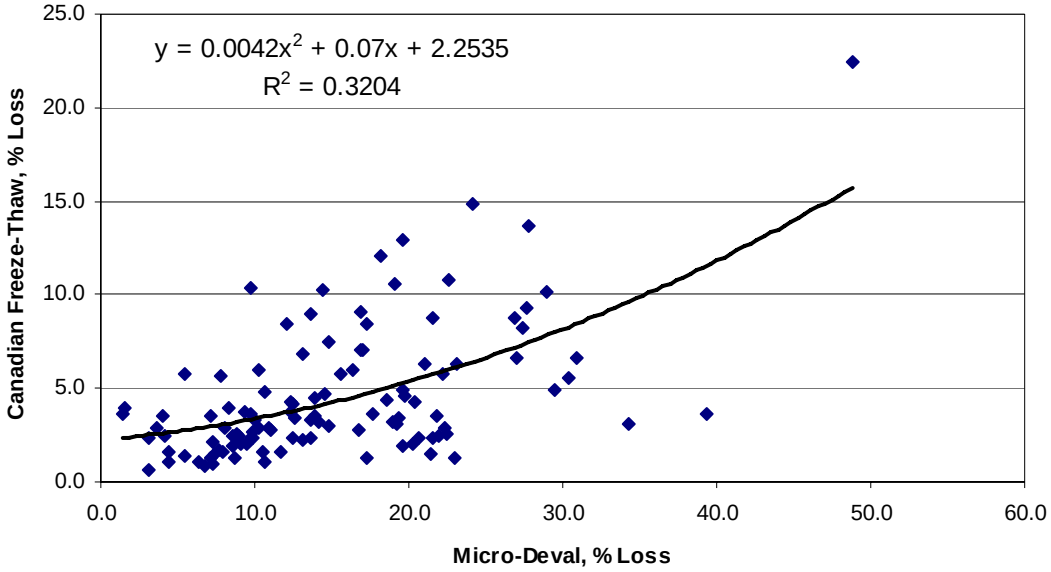

Figure E.3: Canadian Freeze-Thaw vs. Micro-Deval

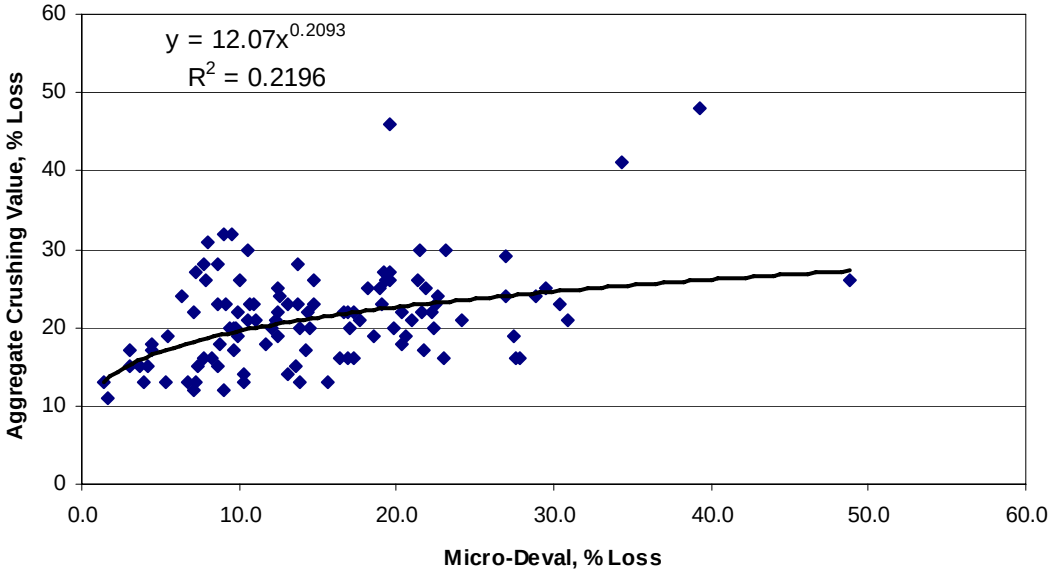

Figure E.4: Aggregate Crushing Value vs. Micro-Deval

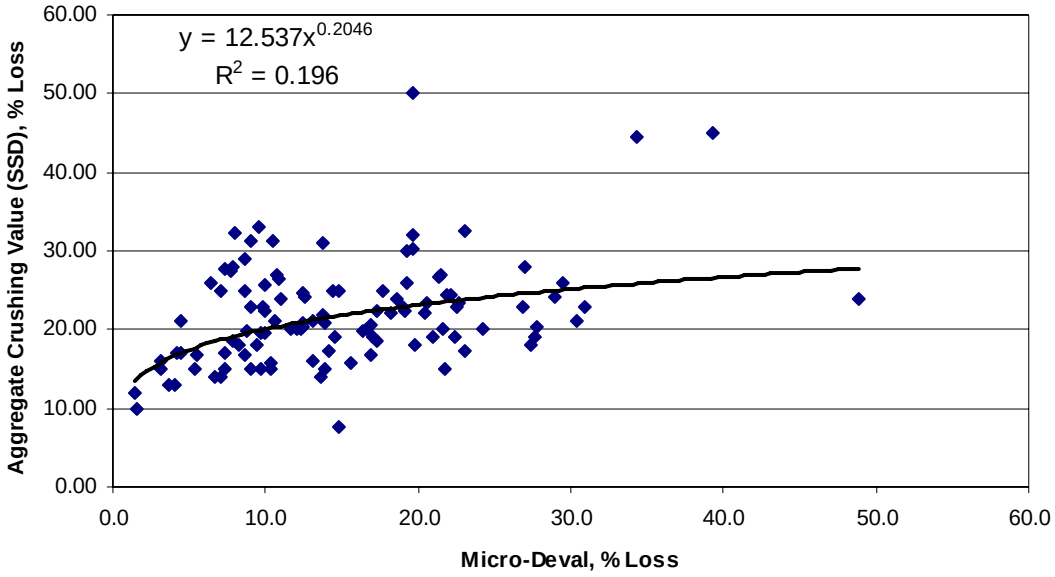

Figure E.5: Aggregate Crushing Value (SSD) vs. Micro-Deval

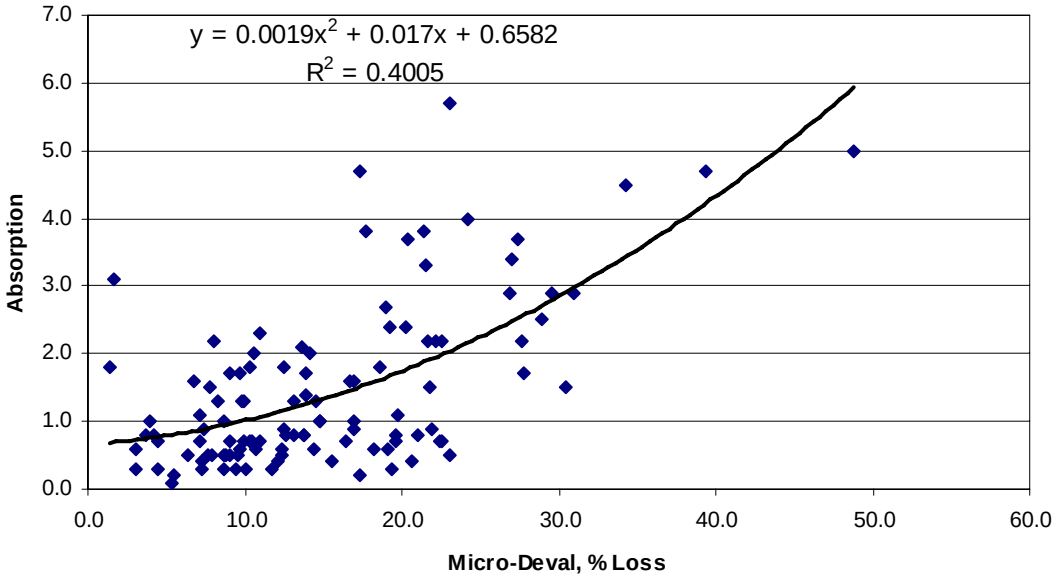

Figure E.6: Absorption vs. Micro-Deval

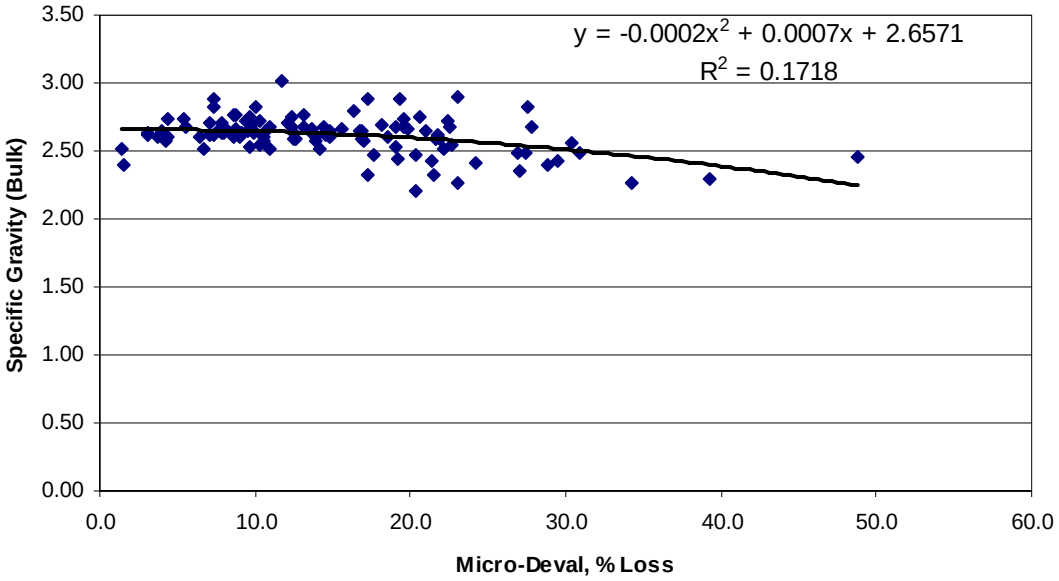

Figure E.7: Specific Gravity (Bulk) vs. Micro-Deval

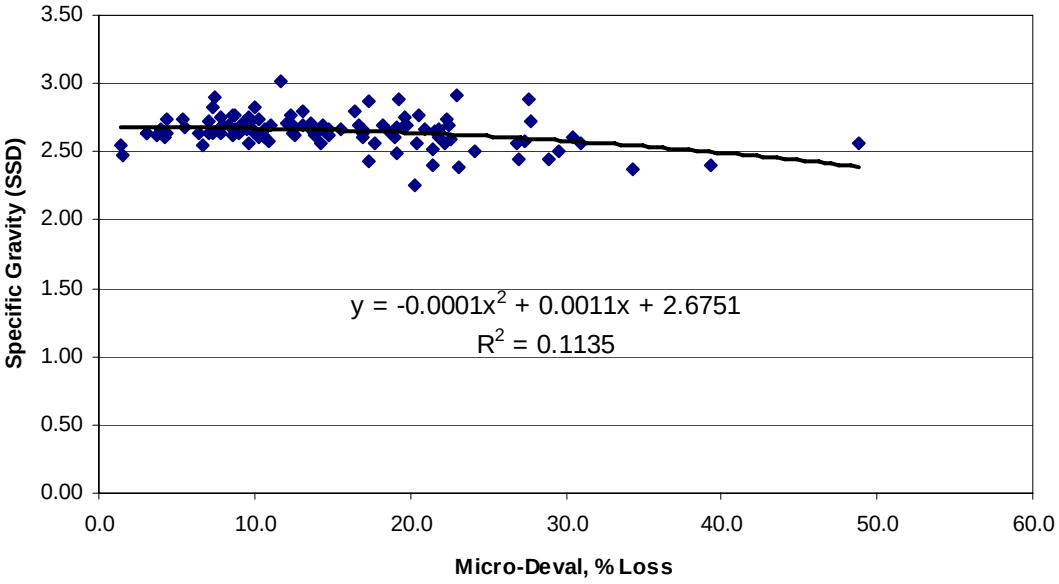

Figure E.8: Specific Gravity (SSD) vs. Micro-Deval

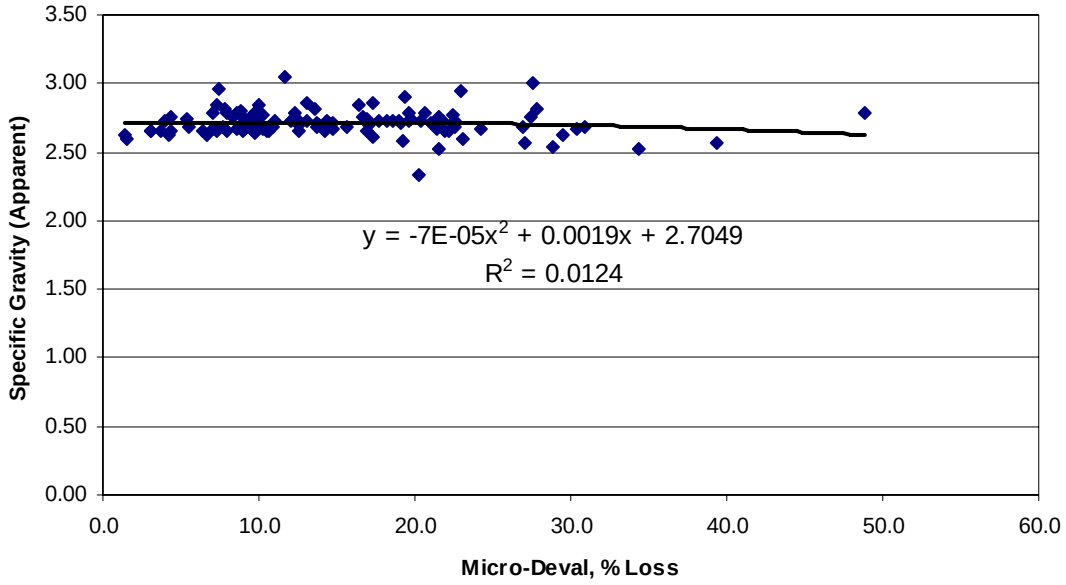

Figure E.9: Specific Gravity (Apparent) vs. Micro-Deval

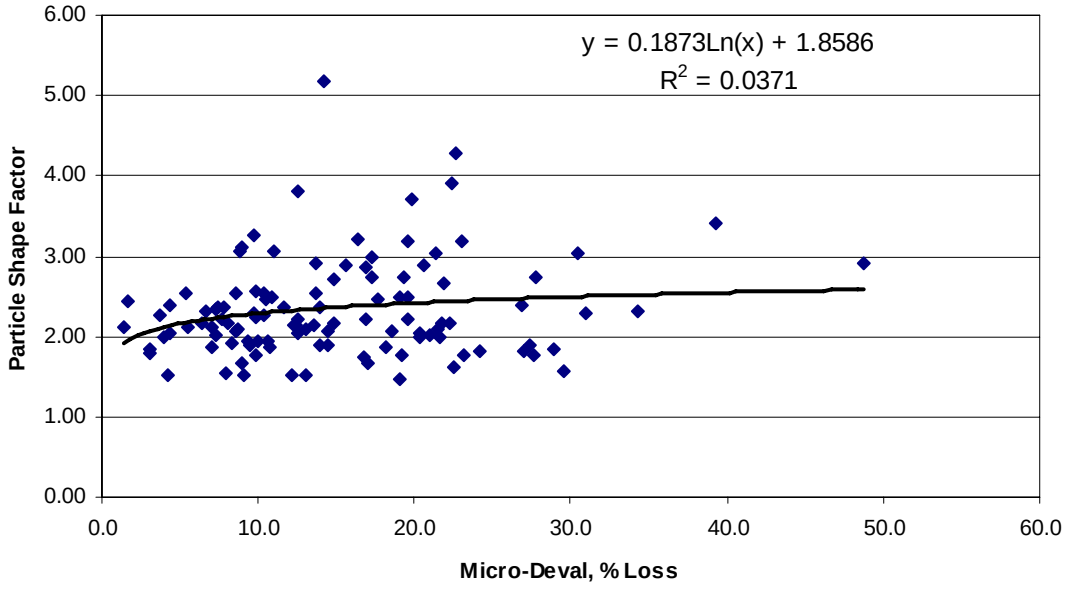

Figure E.10: Particle Shape Factor vs. Micro-Deval

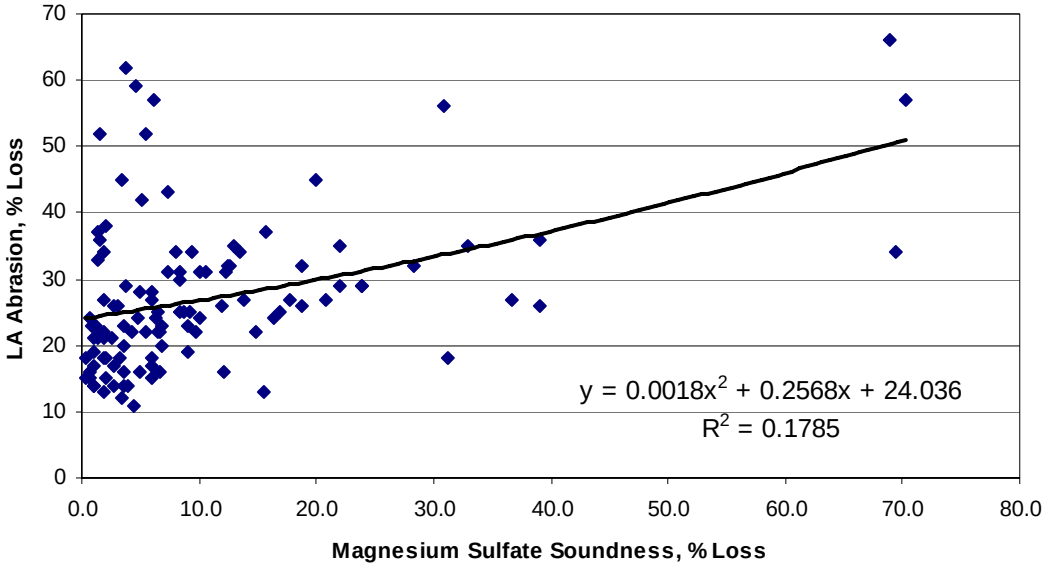

Figure E.11: L.A. Abrasion vs. Magnesium Sulfate Soundness

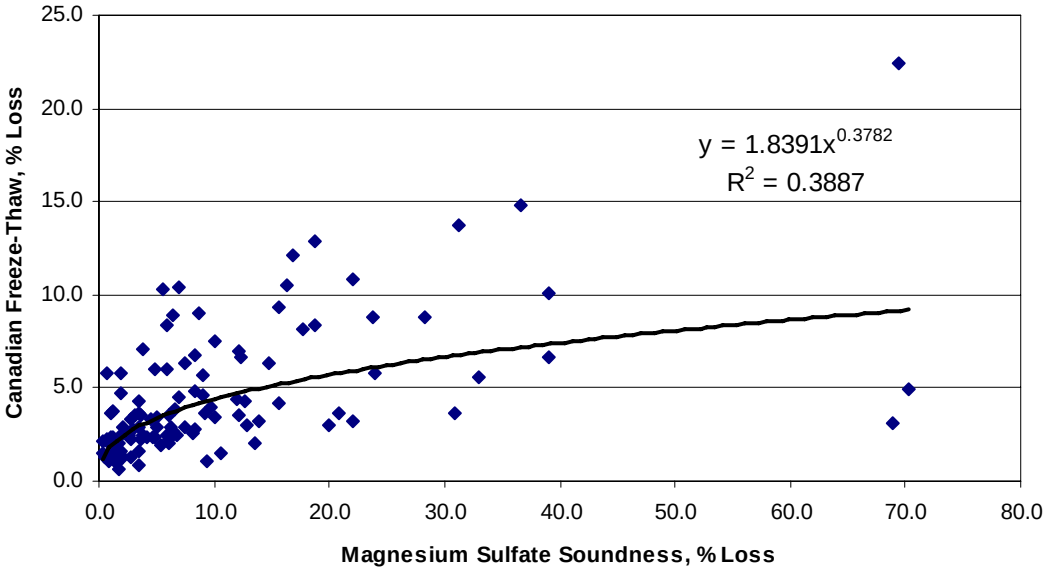

Figure E.12: Canadian Freeze-Thaw vs. Magnesium Sulfate Soundness

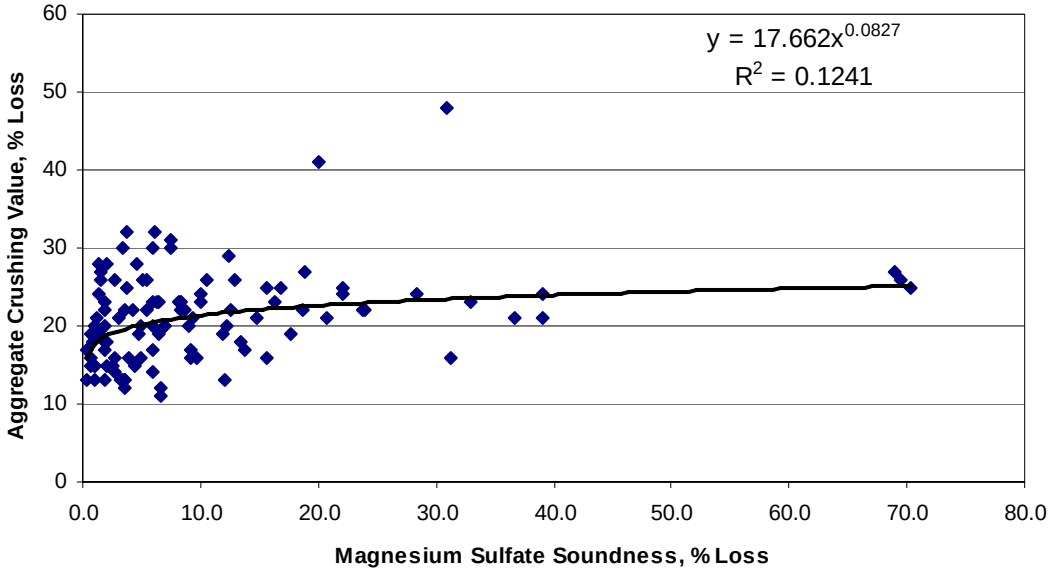

Figure E.13: Aggregate Crushing Value vs. Magnesium Sulfate Soundness

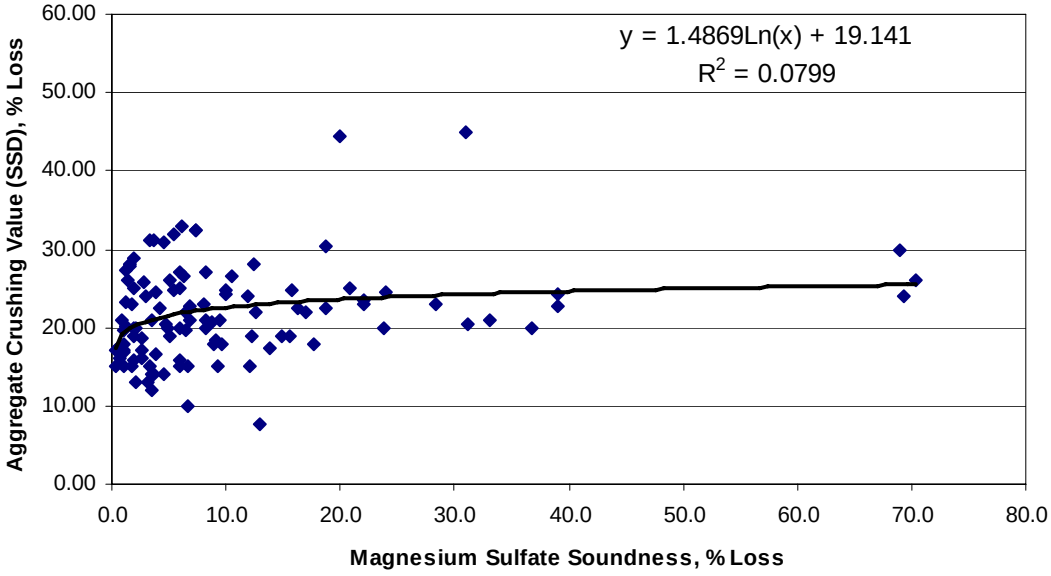

Figure E.14: Aggregate Crushing Value (SSD) vs. Magnesium Sulfate Soundness

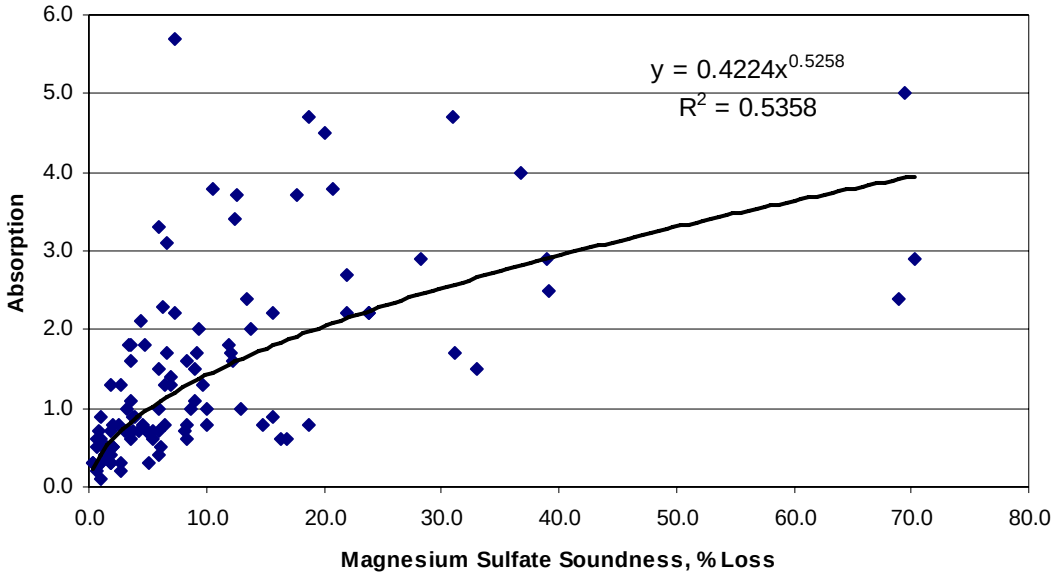

Figure E.15: Absorption vs. Magnesium Sulfate Soundness

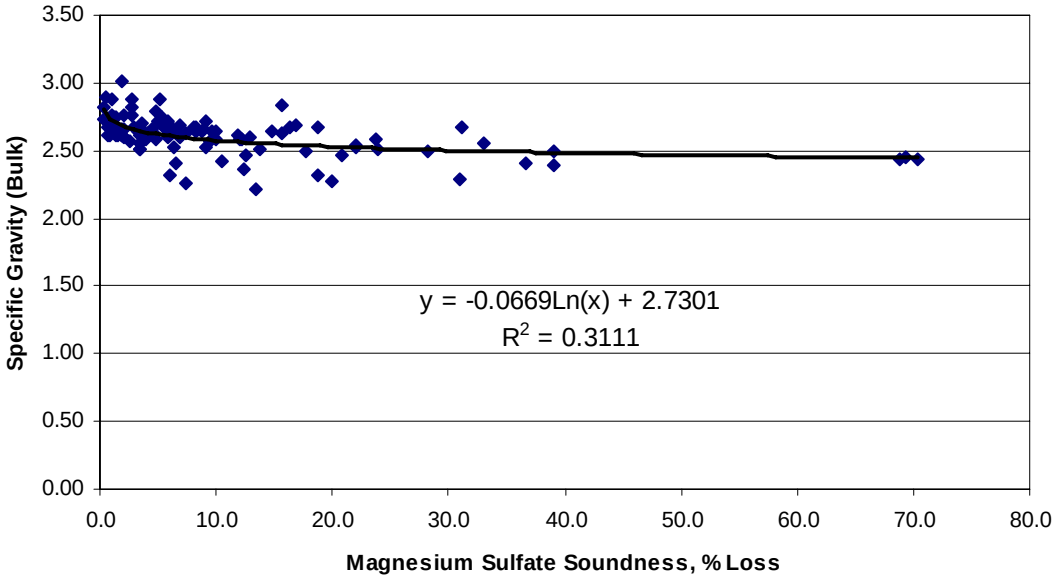

Figure E.16: Specific Gravity (Bulk) vs. Magnesium Sulfate Soundness

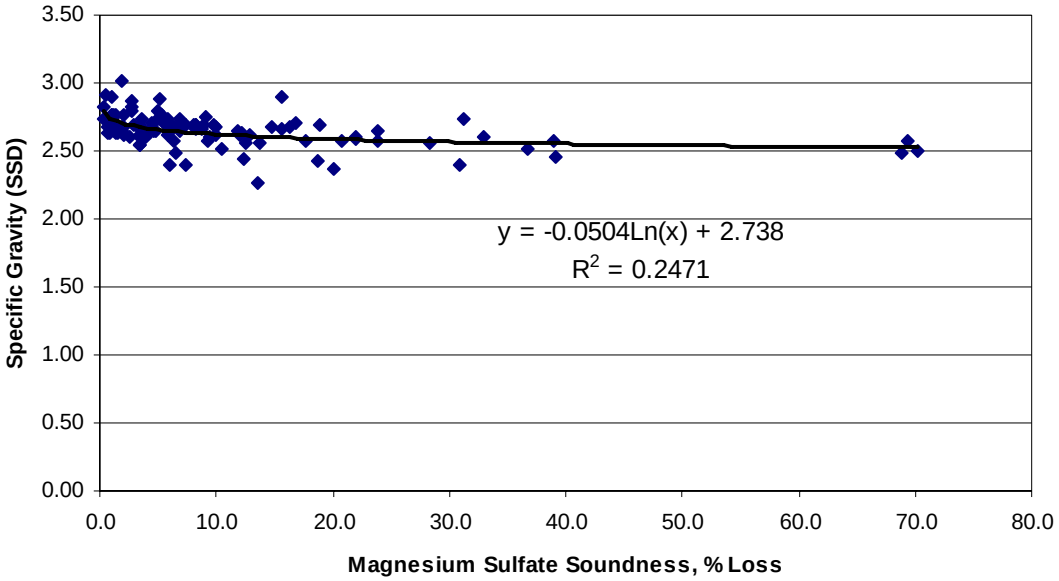

Figure E.17: Specific Gravity (SSD) vs. Magnesium Sulfate Soundness

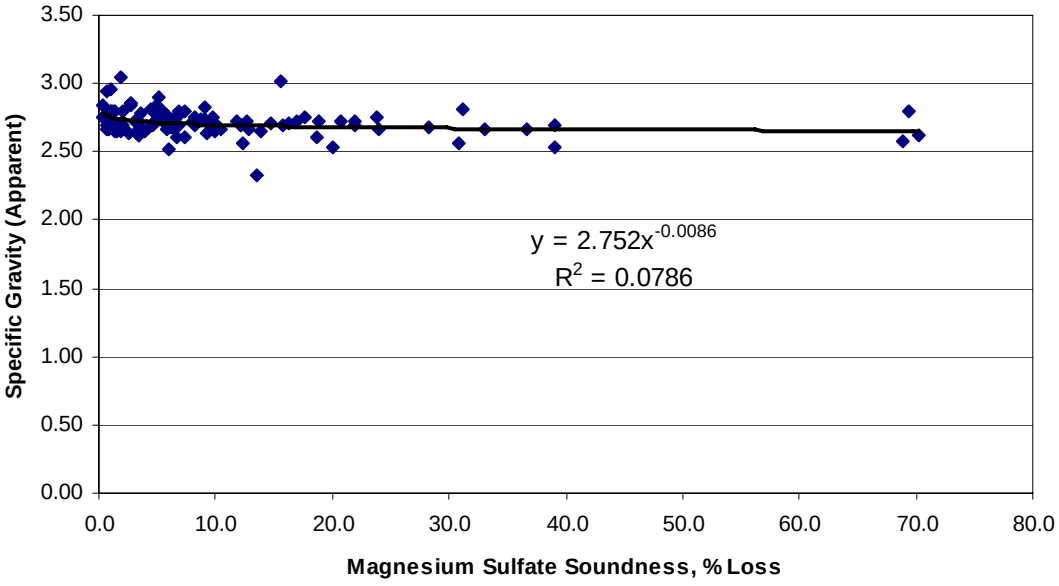

Figure E.18: Specific Gravity (Apparent) vs. Magnesium Sulfate Soundness

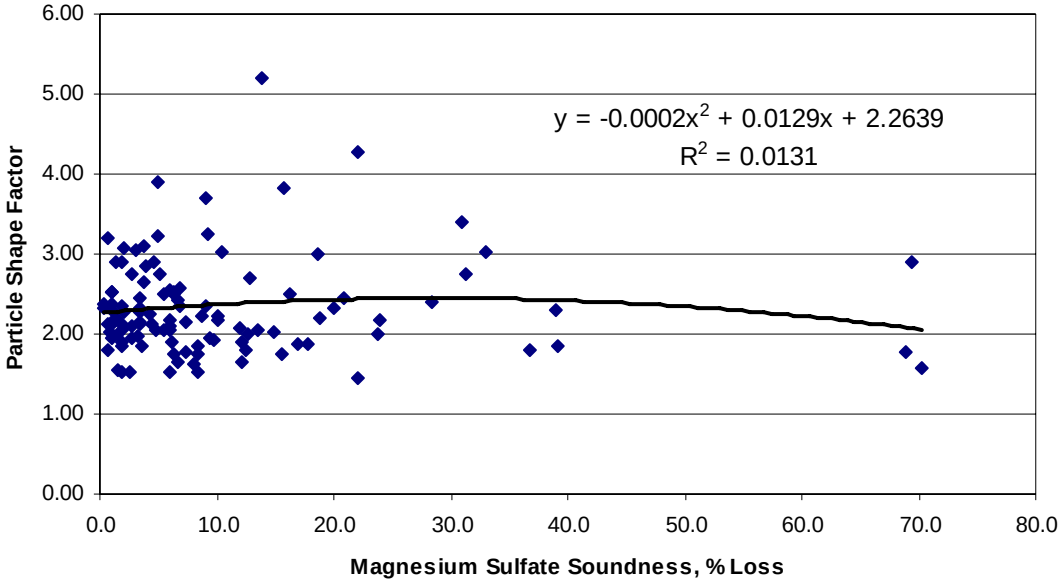

Figure E.19: Particle Shape Factor vs. Magnesium Sulfate Soundness

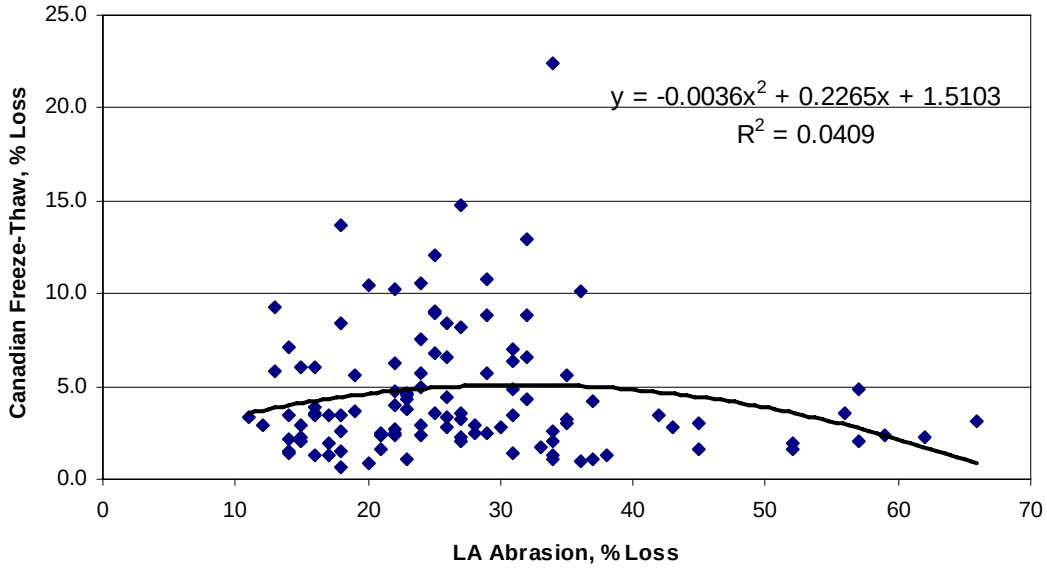

Figure E.20: Canadian Freeze-Thaw vs. L.A. Abrasion

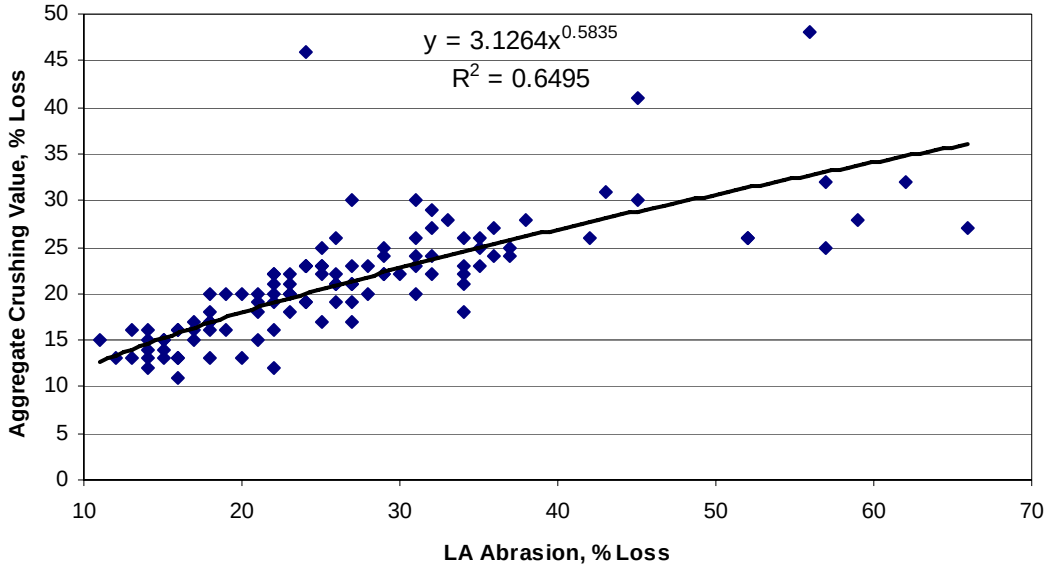

Figure E.21: Aggregate Crushing Value vs. L.A. Abrasion

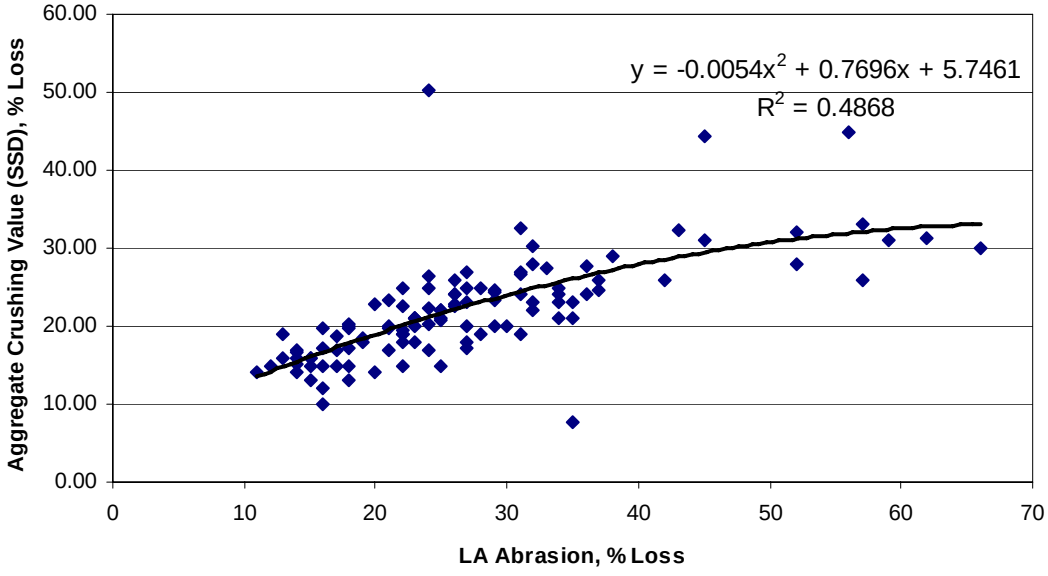

Figure E.22: Aggregate Crushing Value (SSD) vs. L.A. Abrasion

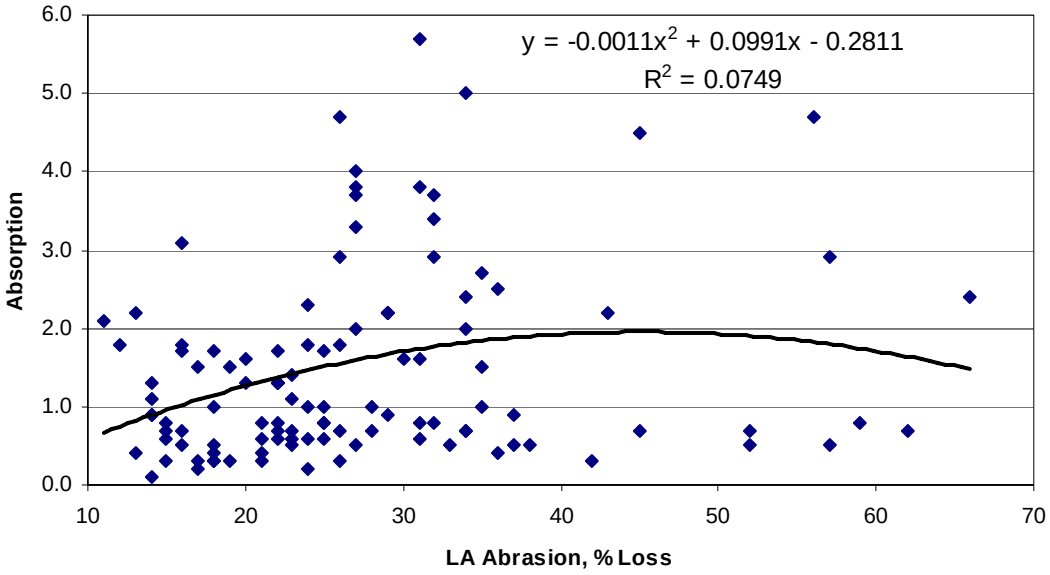

Figure E.23: Absorption vs. L.A. Abrasion

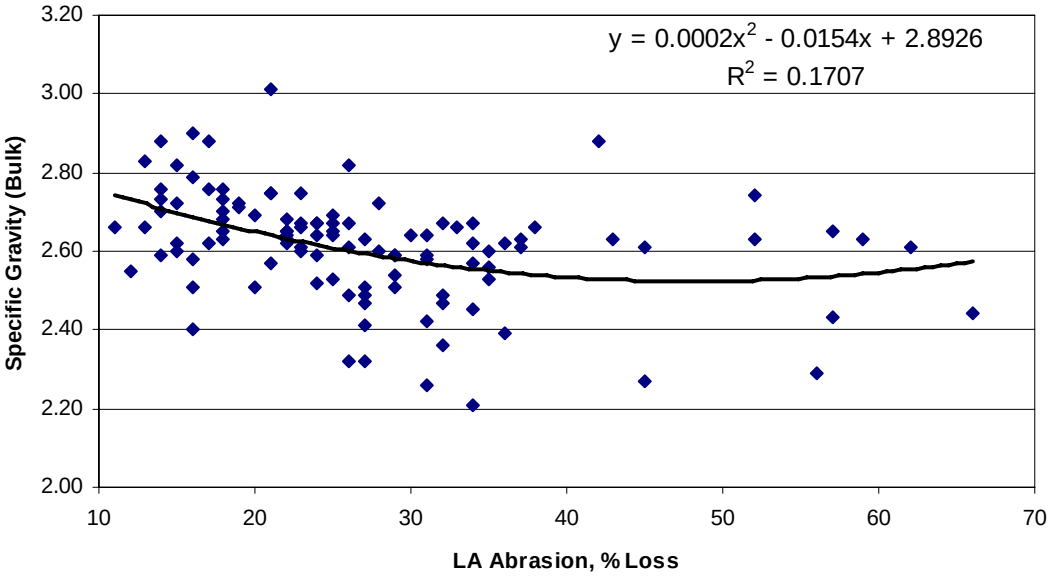

Figure E.24: Specific Gravity (Bulk) vs. L.A. Abrasion

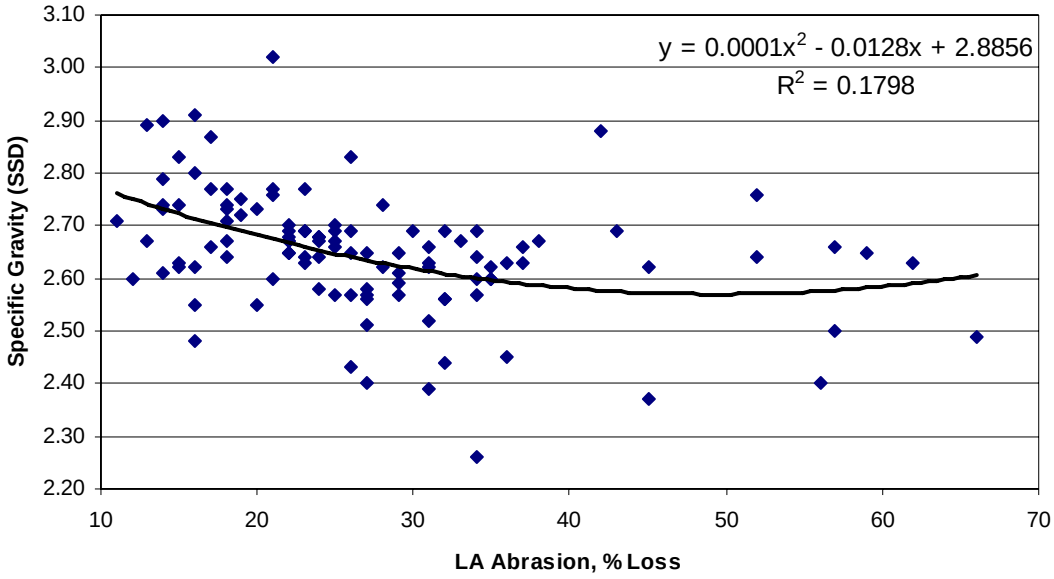

Figure E.25: Specific Gravity (SSD) vs. L.A. Abrasion

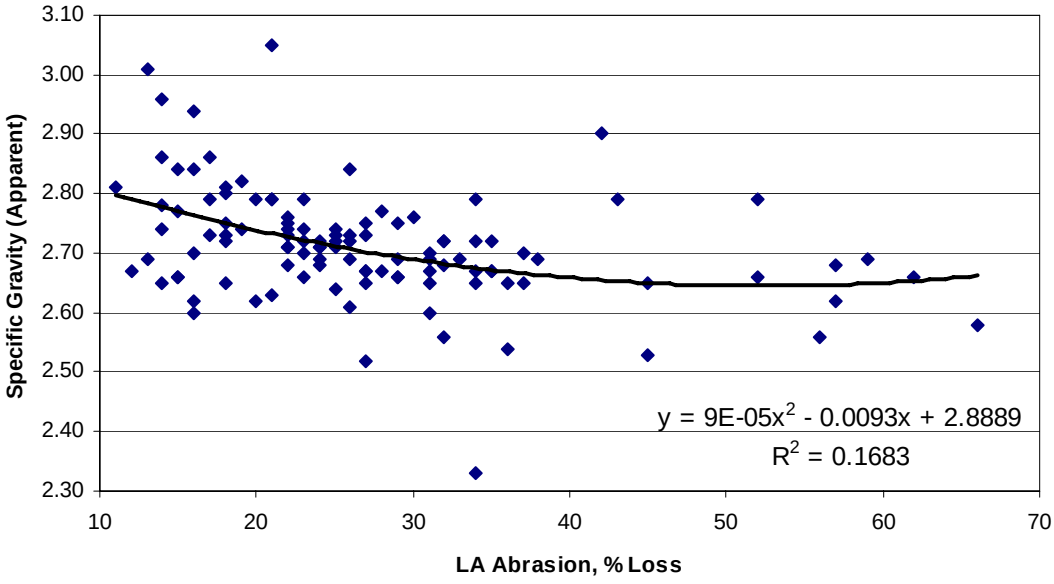

Figure E.26: Specific Gravity (Apparent) vs. L.A. Abrasion

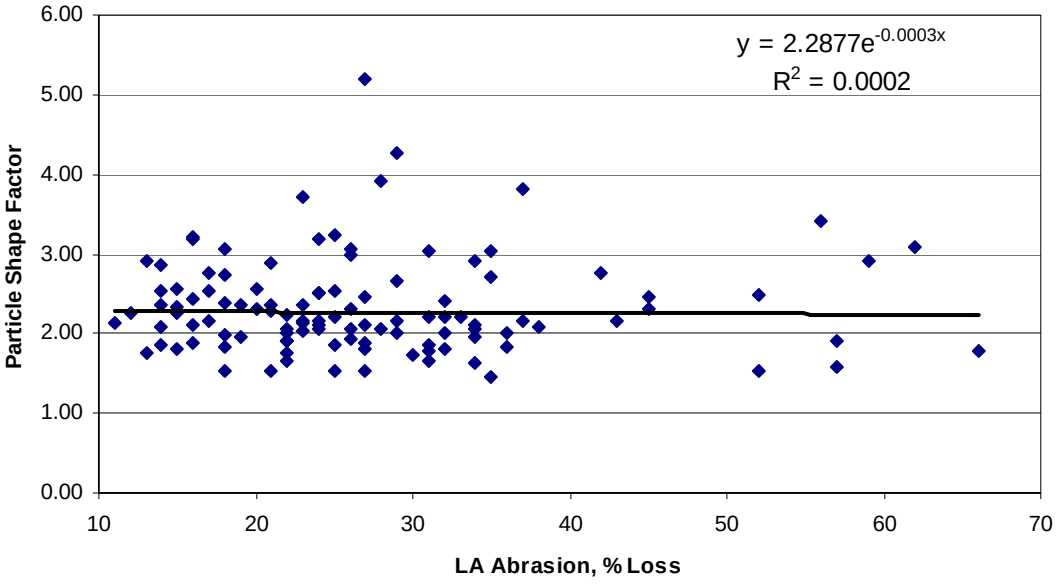

Figure E.27: Particle Shape Factor vs. L.A. Abrasion

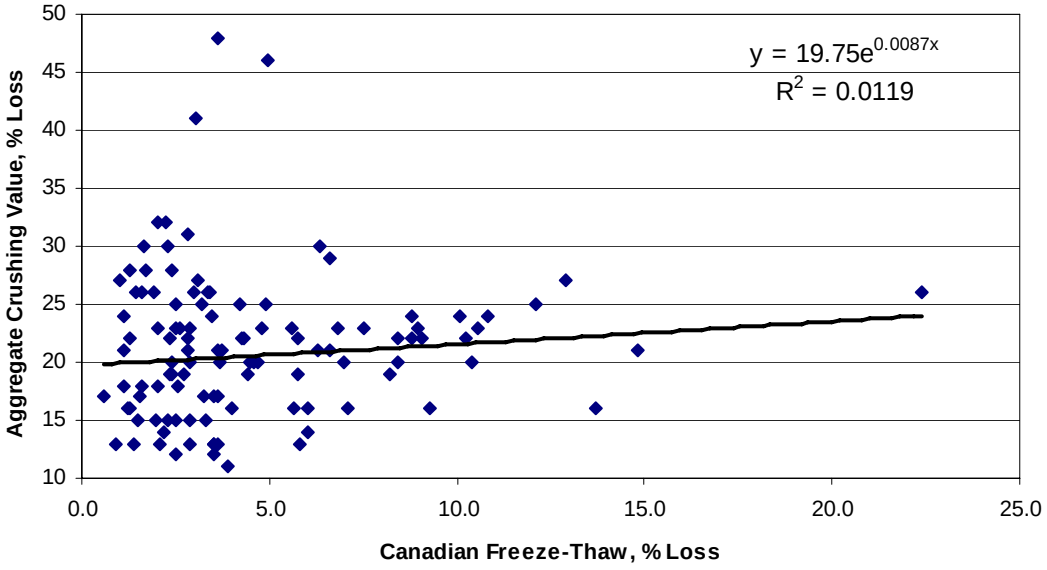

Figure E.28: Aggregate Crushing Value vs. Canadian Freeze-Thaw

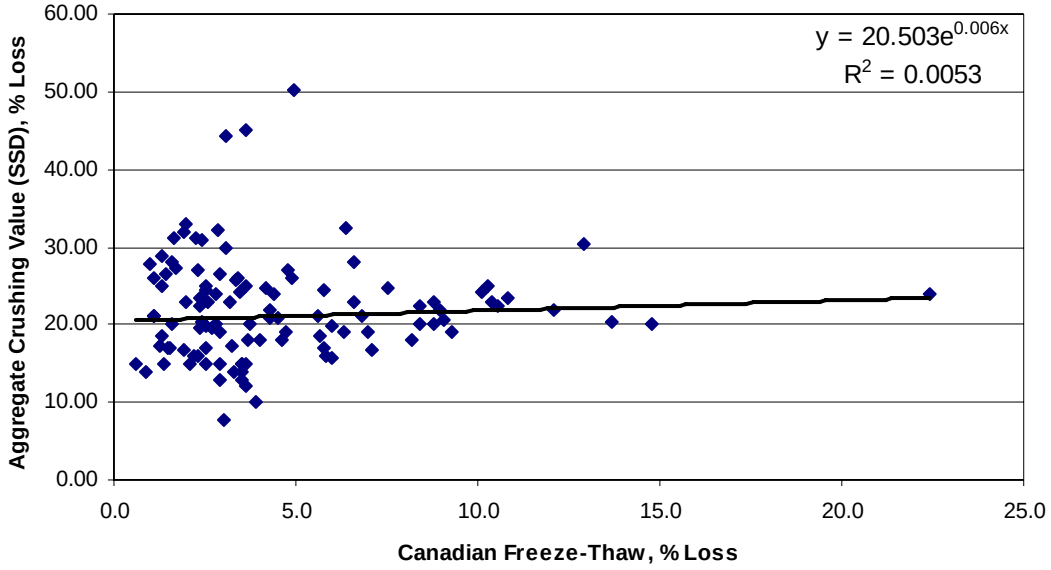

Figure E.29: Aggregate Crushing Value (SSD) vs. Canadian Freeze-Thaw

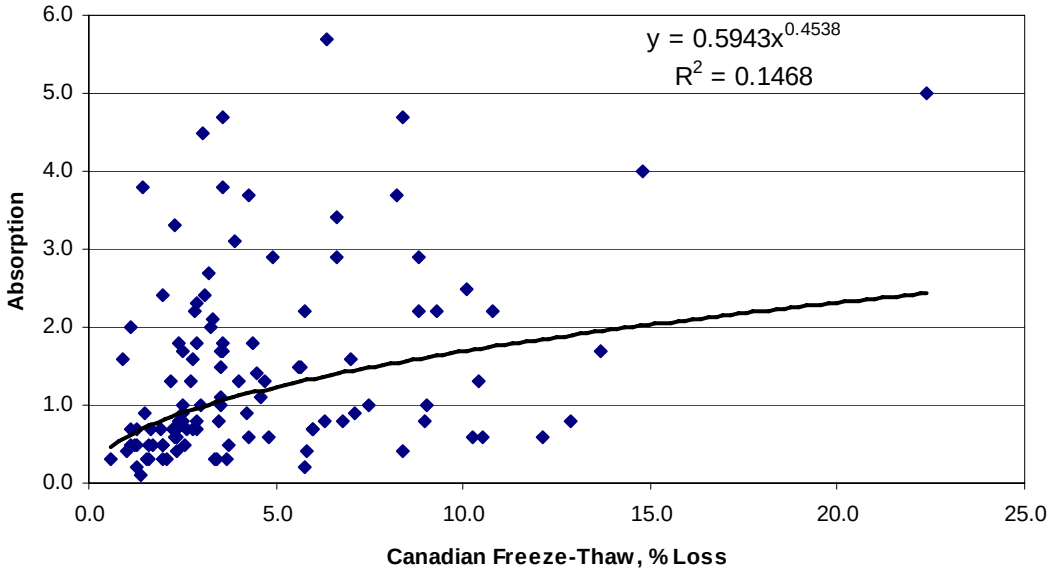

Figure E.30: Absorption vs. Canadian Freeze-Thaw

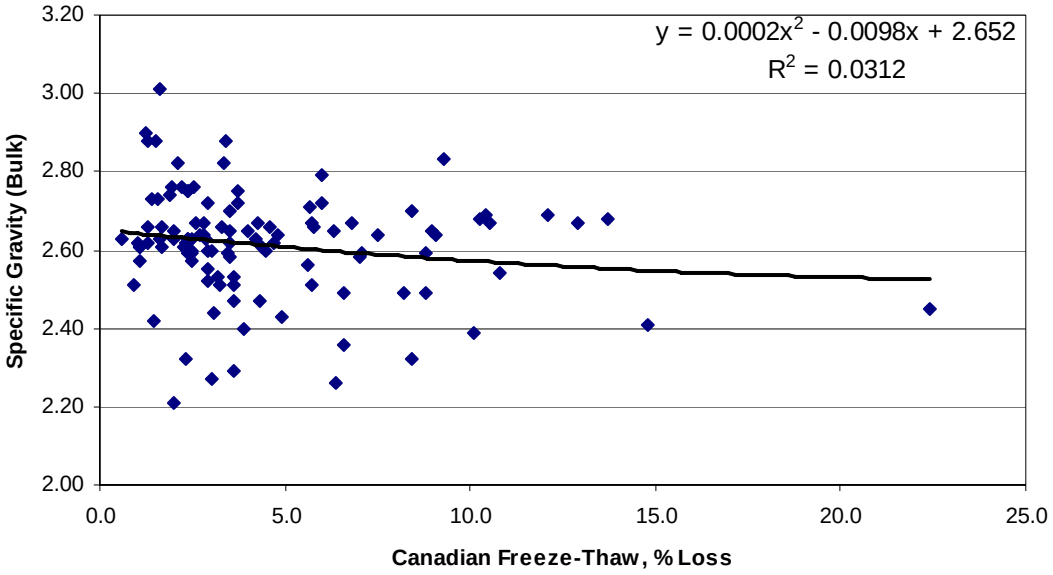

Figure E.31: Specific Gravity (Bulk) vs. Canadian Freeze-Thaw

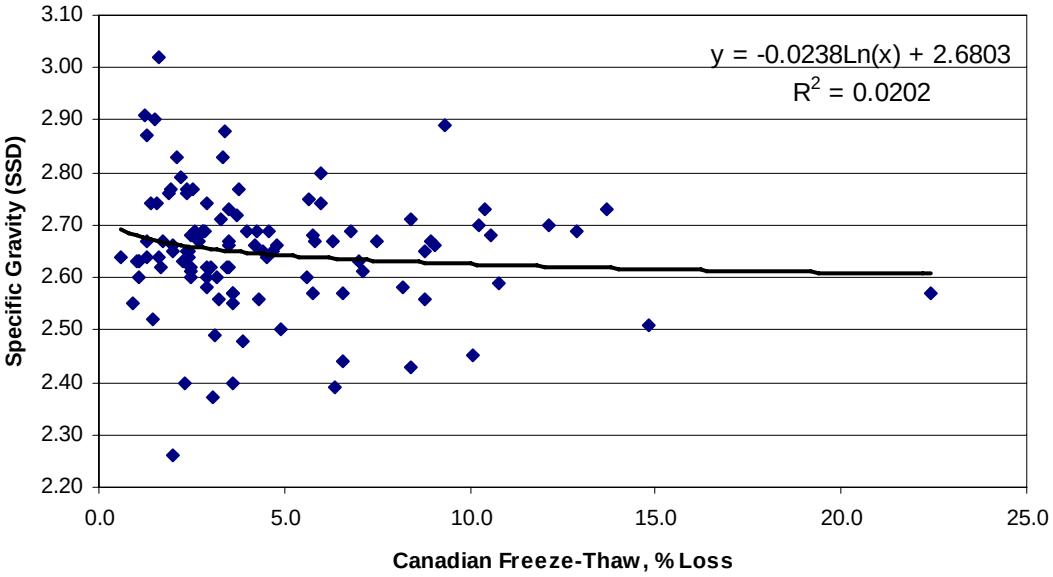

Figure E.32: Specific Gravity (SSD) vs. Canadian Freeze-Thaw

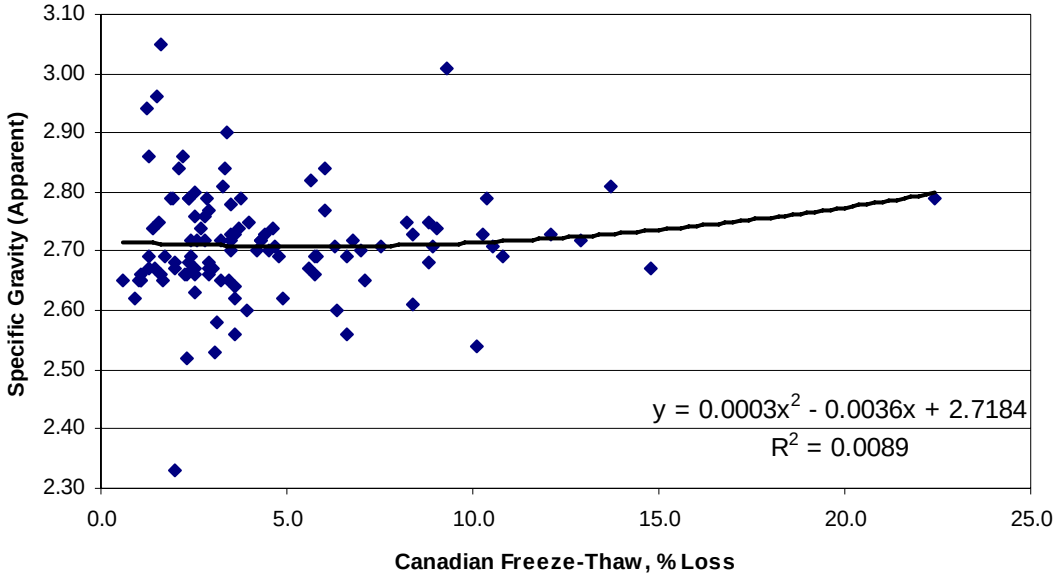

Figure E.33: Specific Gravity (Apparent) vs. Canadian Freeze-Thaw

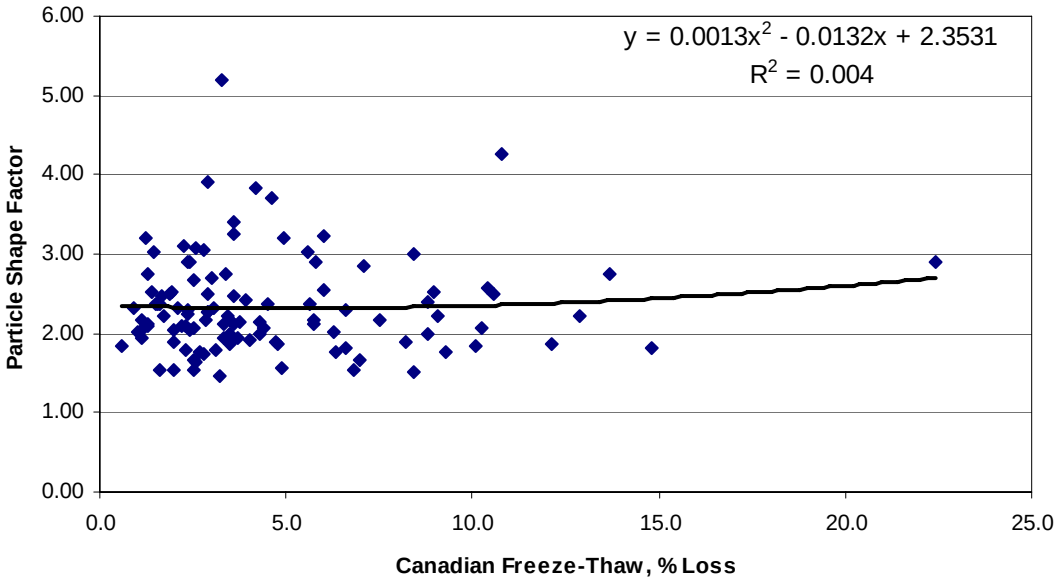

Figure E.34: Particle Shape Factor vs. Canadian Freeze-Thaw

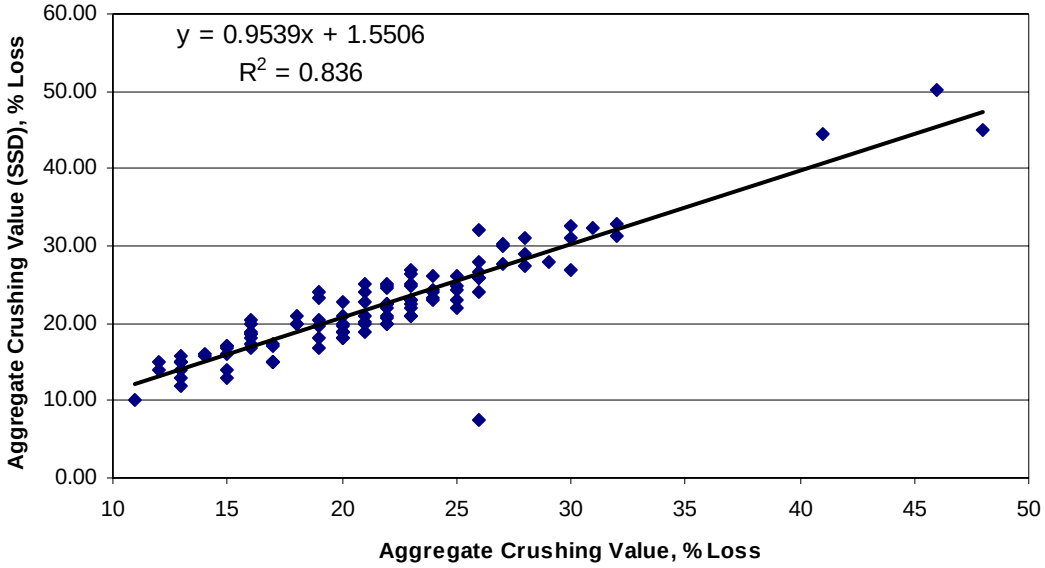

Figure E.35: Aggregate Crushing Value (SSD) vs. Aggregate Crushing Value

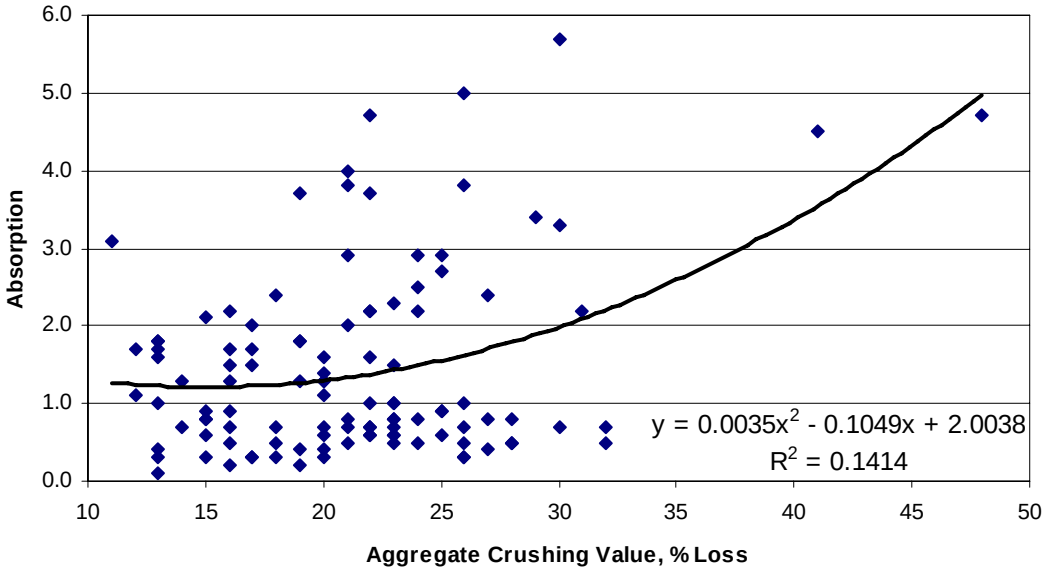

Figure E.36: Absorption vs. Aggregate Crushing Value

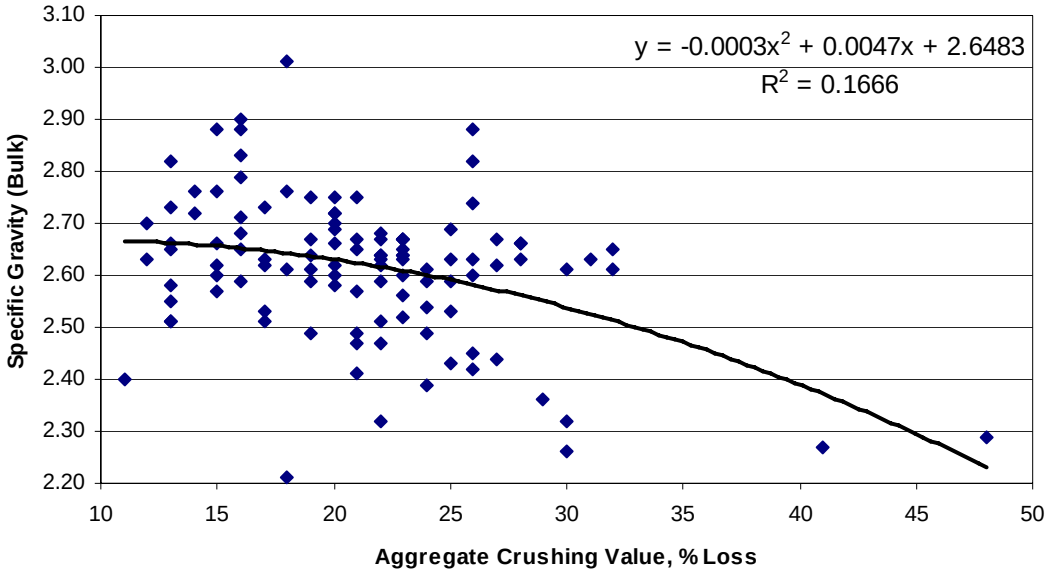

Figure E.37: Specific Gravity (Bulk) vs. Aggregate Crushing Value

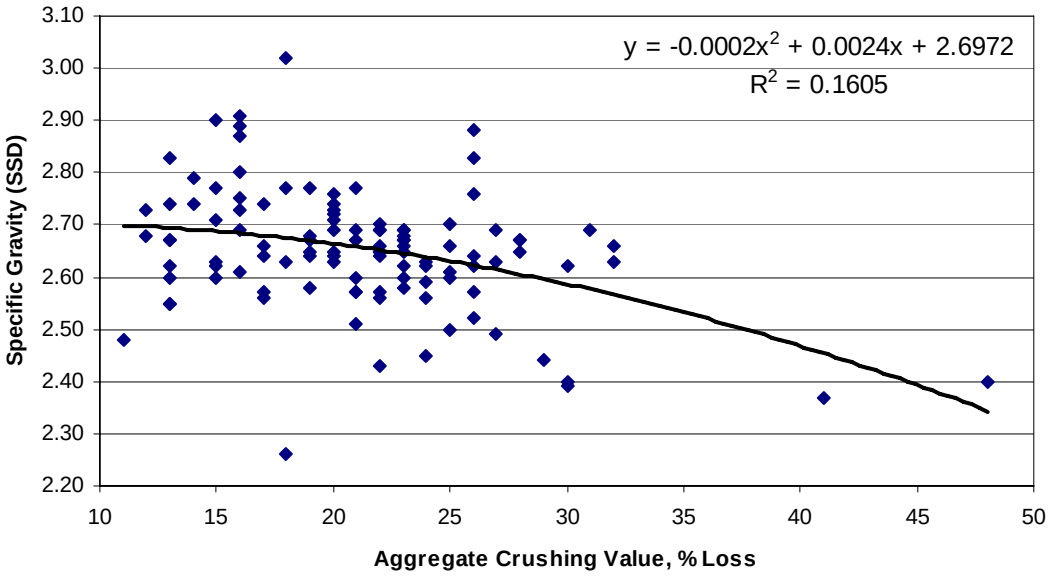

Figure E.38: Specific Gravity (SSD) vs. Aggregate Crushing Value

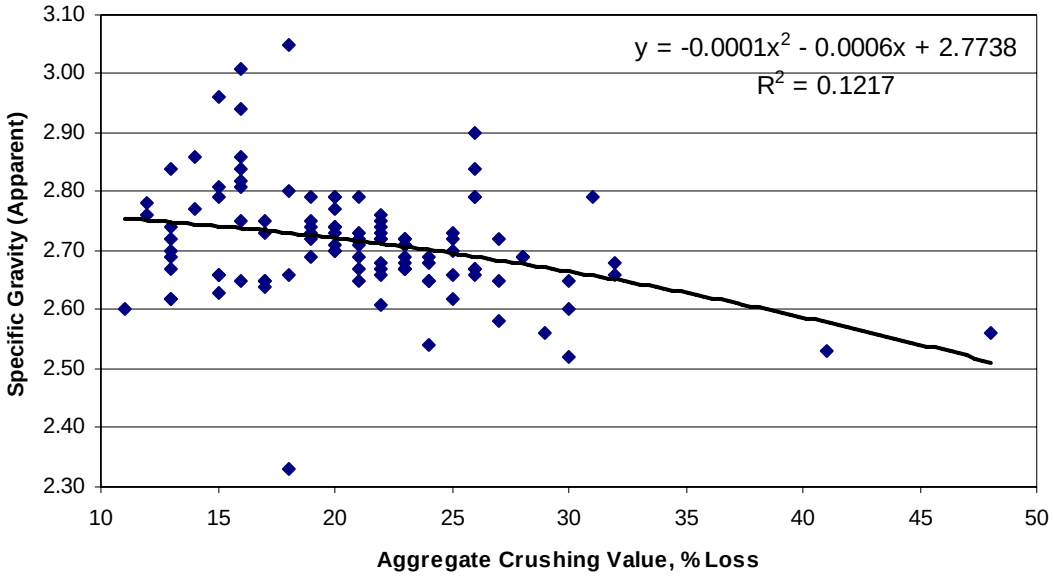

Figure E.39: Specific Gravity (Apparent) vs. Aggregate Crushing Value

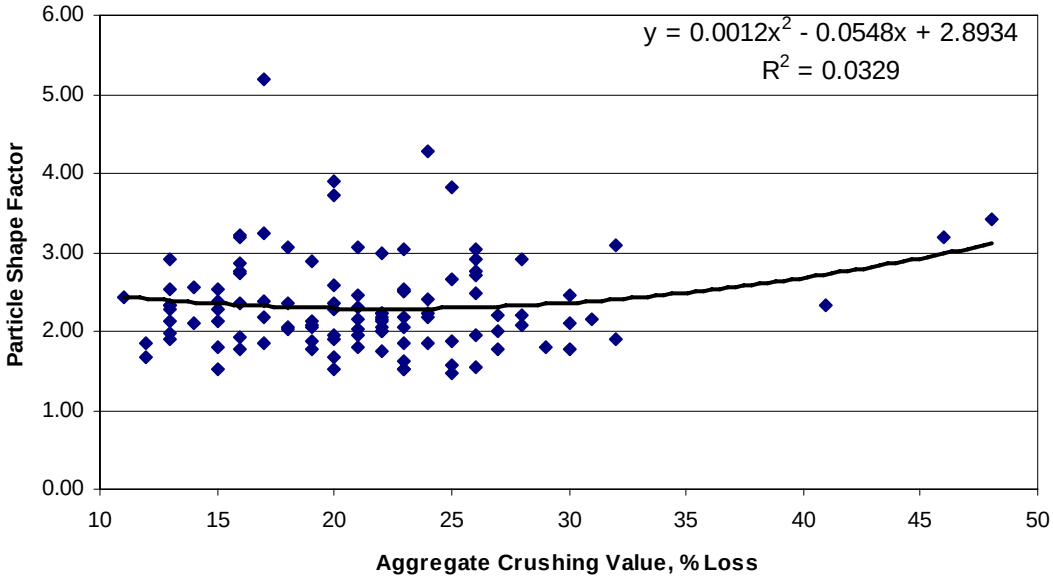

Figure E.40: Particle Shape Factor vs. Aggregate Crushing Value

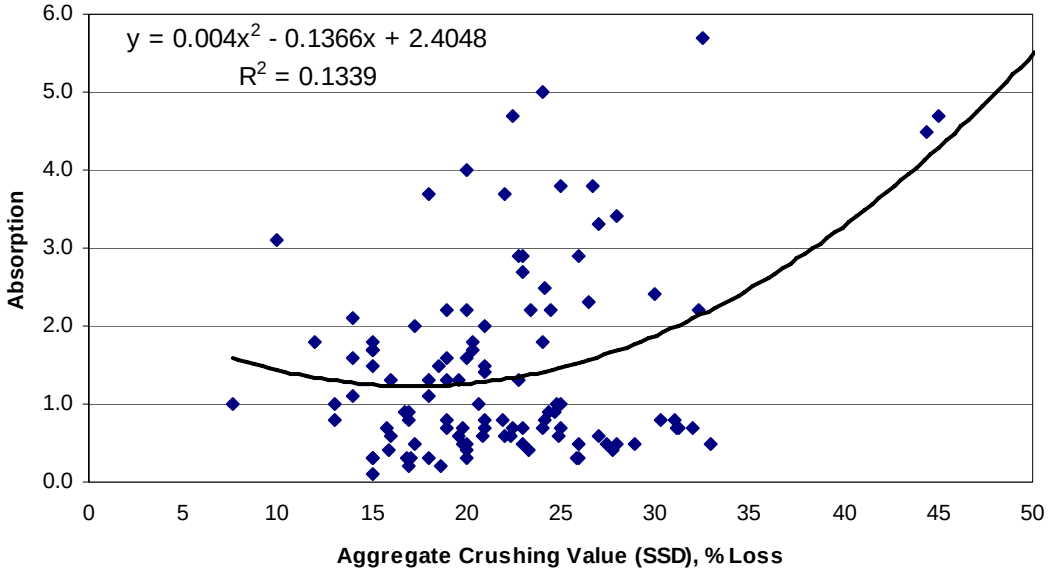

Figure E.41: Absorption vs. Aggregate Crushing Value (SSD)

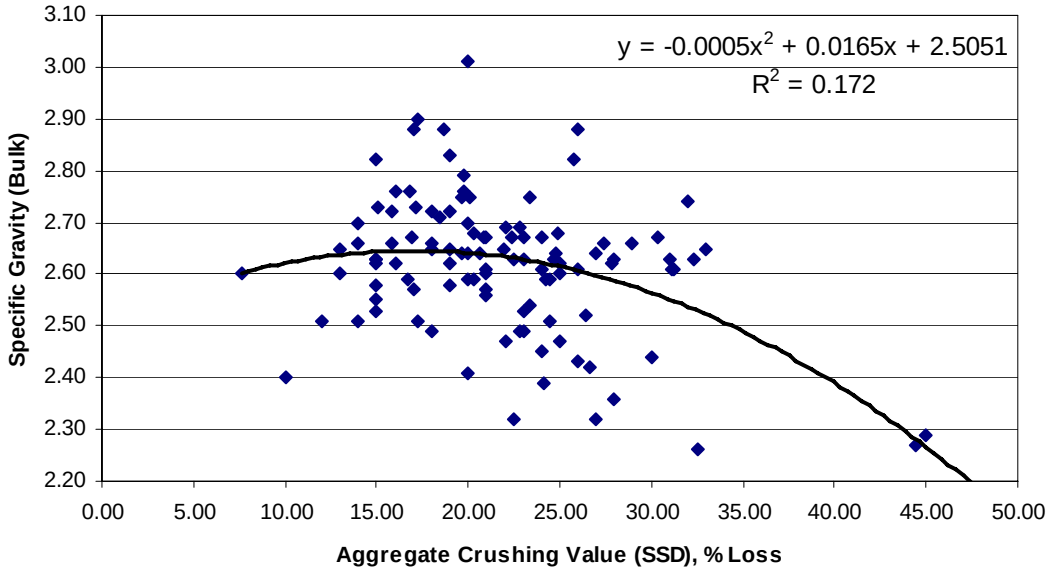

Figure E.42: Specific Gravity (Bulk) vs. Aggregate Crushing Value (SSD)

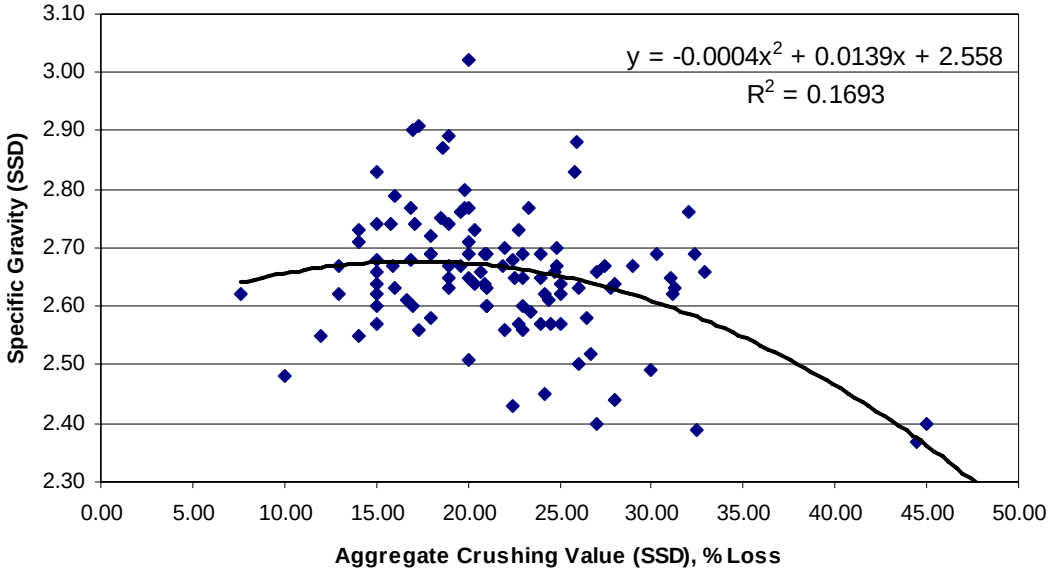

Figure E.43: Specific Gravity (SSD) vs. Aggregate Crushing Value (SSD)

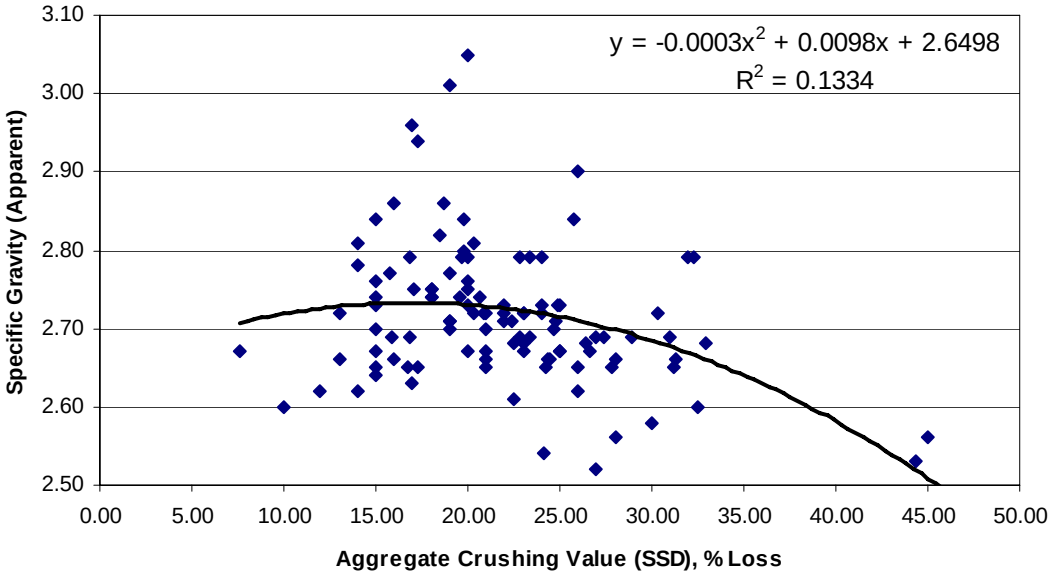

Figure E.44: Specific Gravity (Apparent) vs. Aggregate Crushing Value (SSD)

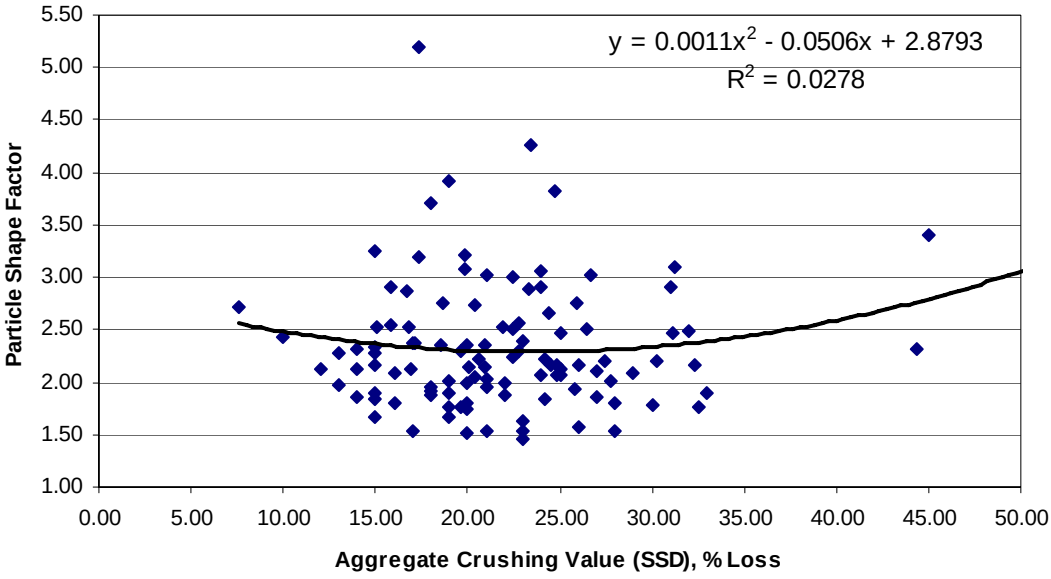

Figure E.45: Particle Shape Factor vs. Aggregate Crushing Value (SSD)

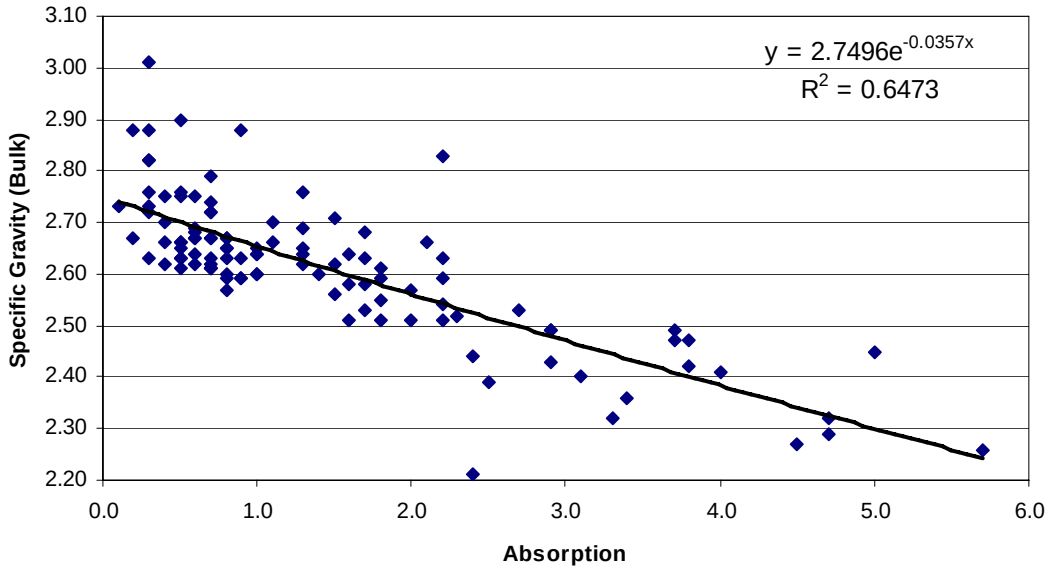

Figure E.46: Specific Gravity (Bulk) vs. Absorption

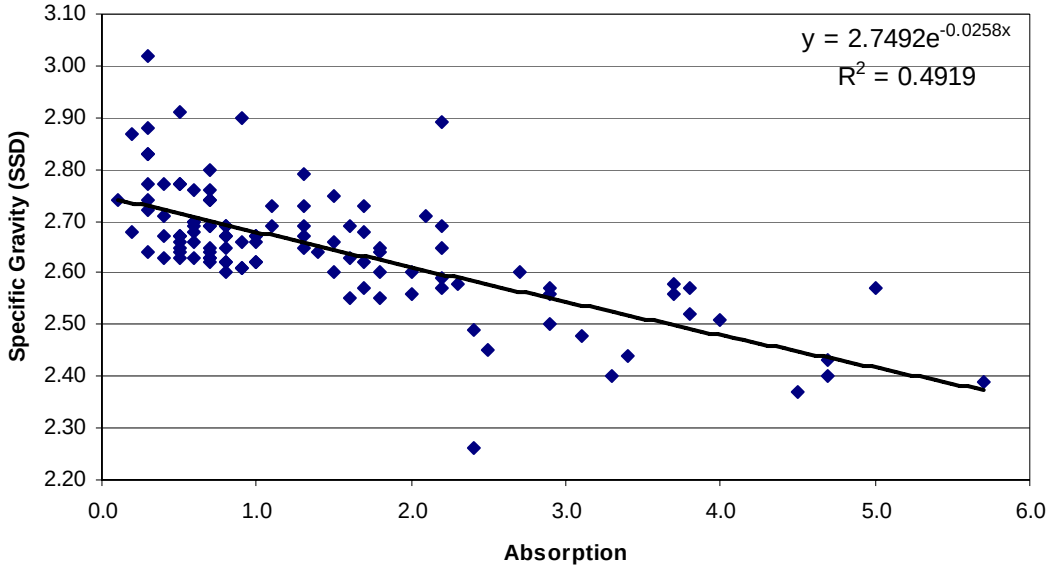

Figure E.47: Specific Gravity (SSD) vs. Absorption

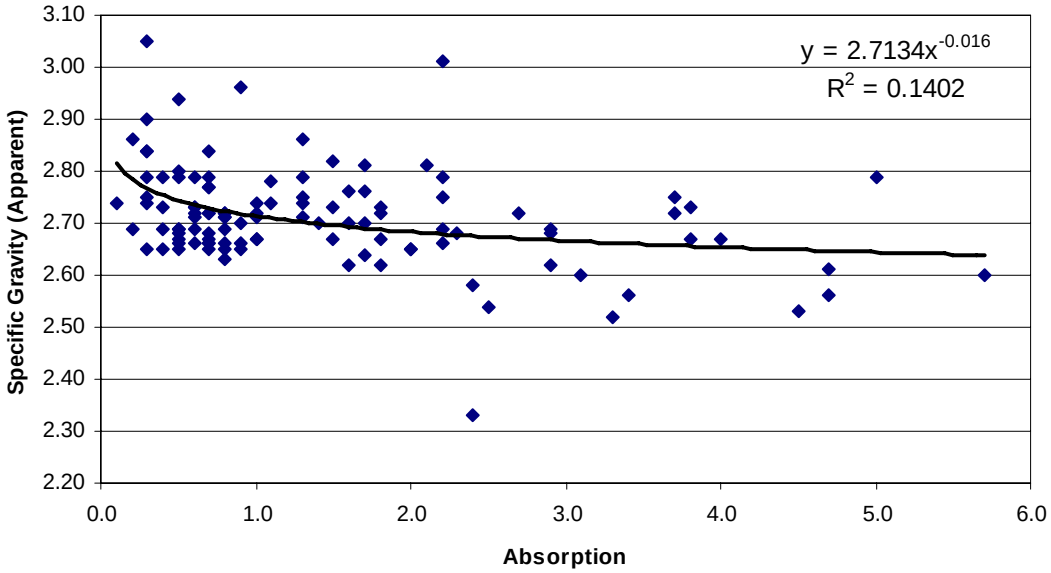

Figure E.48: Specific Gravity (Apparent) vs. Absorption

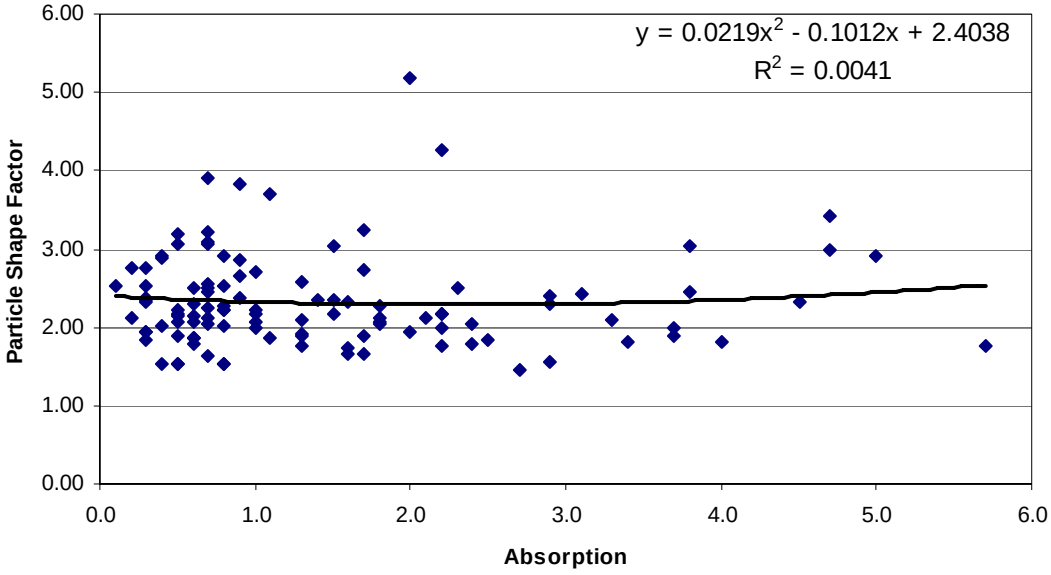

Figure E.49: Particle Shape Factor vs. Absorption

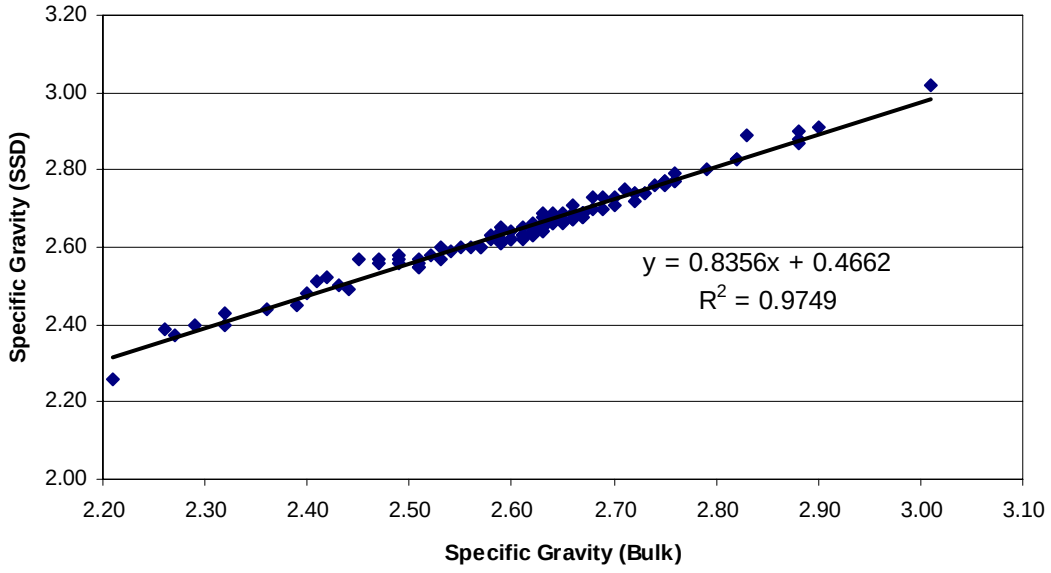

Figure E.50: Specific Gravity (SSD) vs. Specific Gravity (Bulk)

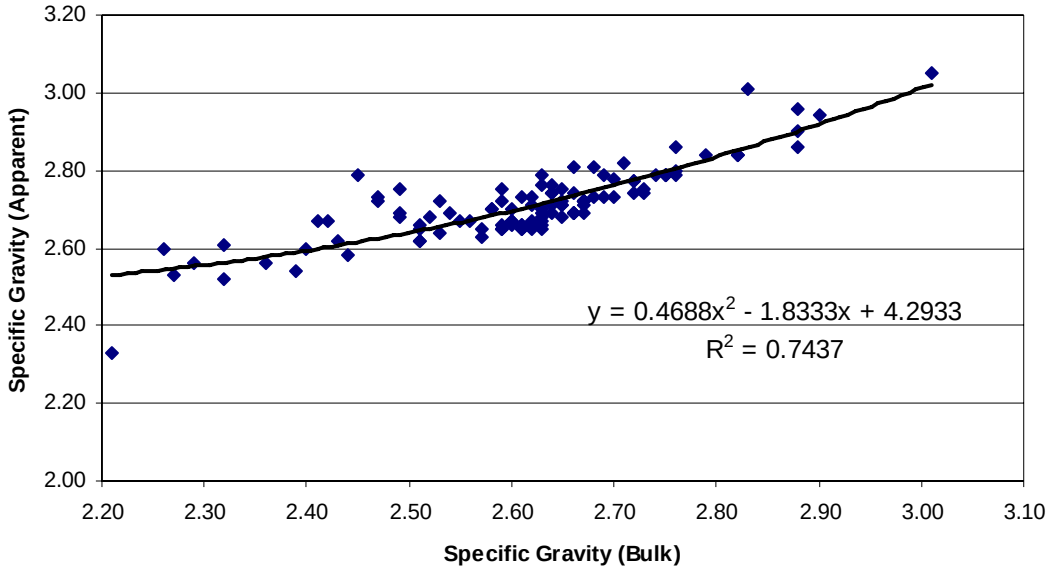

Figure E.51: Specific Gravity (Apparent) vs. Specific Gravity (Bulk)

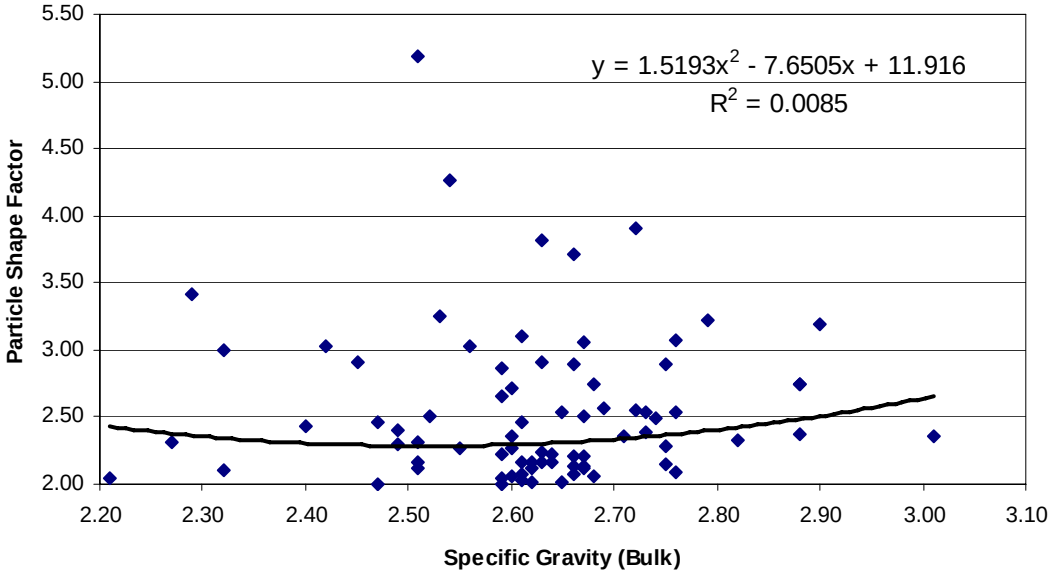

Figure E.52: Particle Shape Factor vs. Specific Gravity (Bulk)

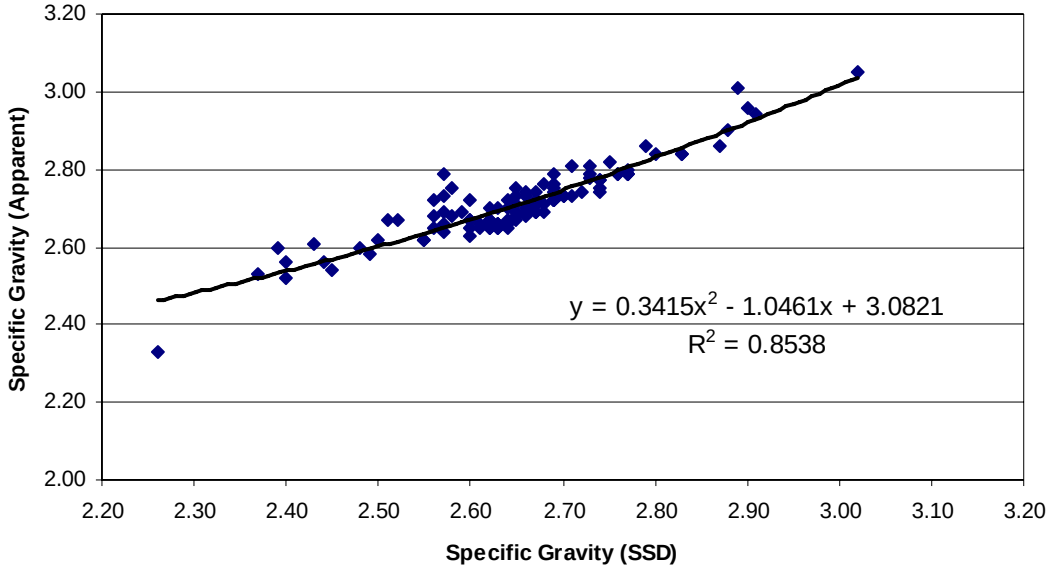

Figure E.53: Specific Gravity (Apparent) vs. Specific Gravity (SSD)

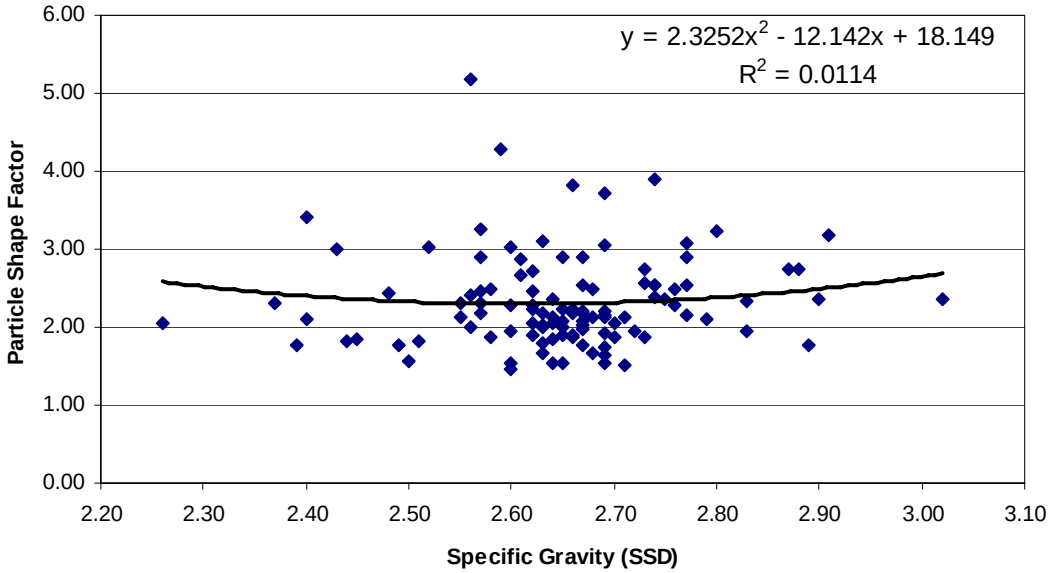

Figure E.54: Particle Shape Factor vs. Specific Gravity (SSD)

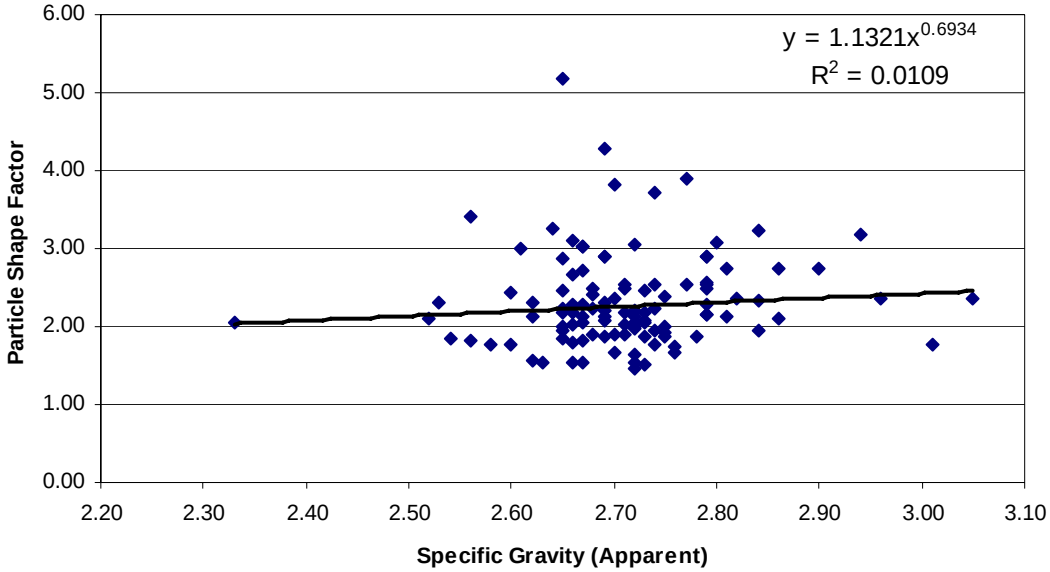

Figure E.55: Particle Shape Factor vs. Specific Gravity (Apparent)

Appendix F: Test Correlation Graphs for the Partial Data Set I

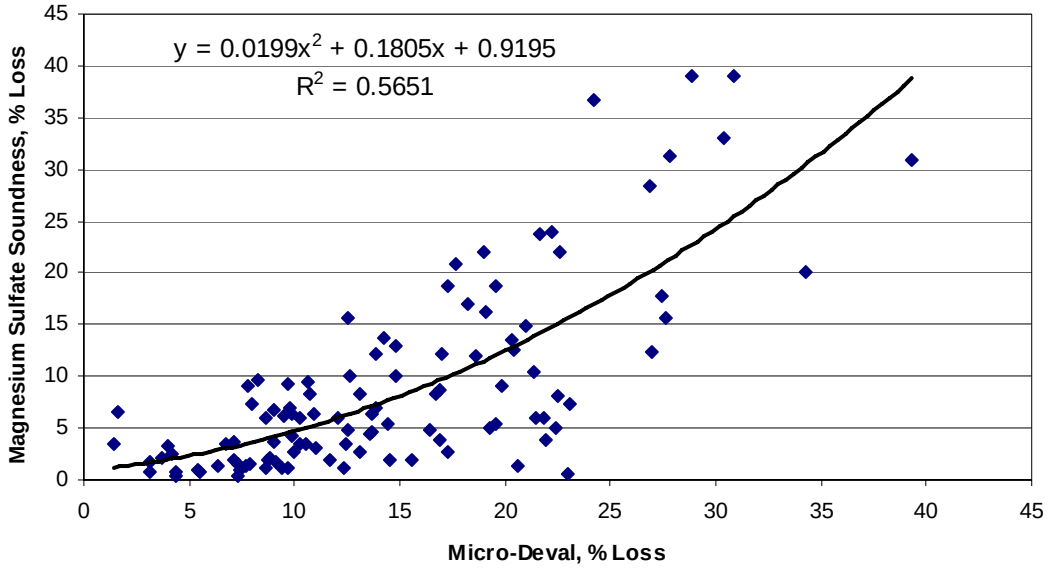

Figure F.1: Magnesium Sulfate Soundness vs. Micro-Deval

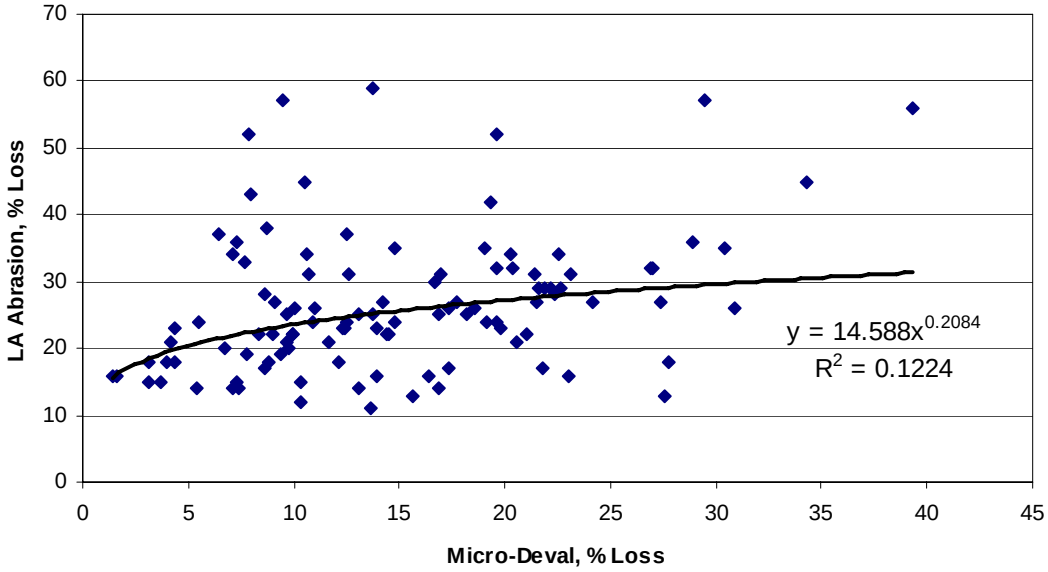

Figure F.2: L.A. Abrasion vs. Micro-Deval

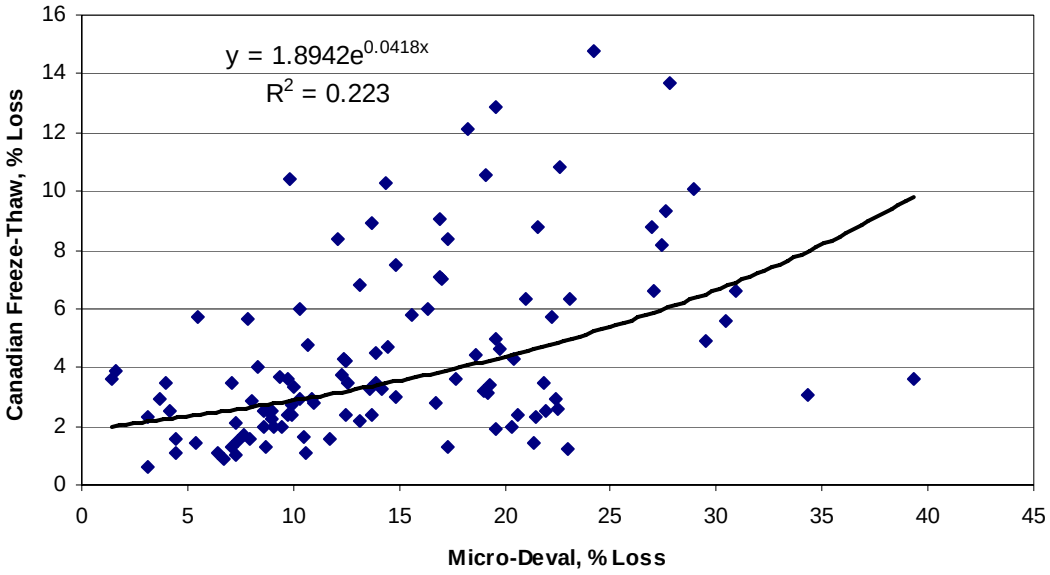

Figure F.3: Canadian Freeze-Thaw vs. Micro-Deval

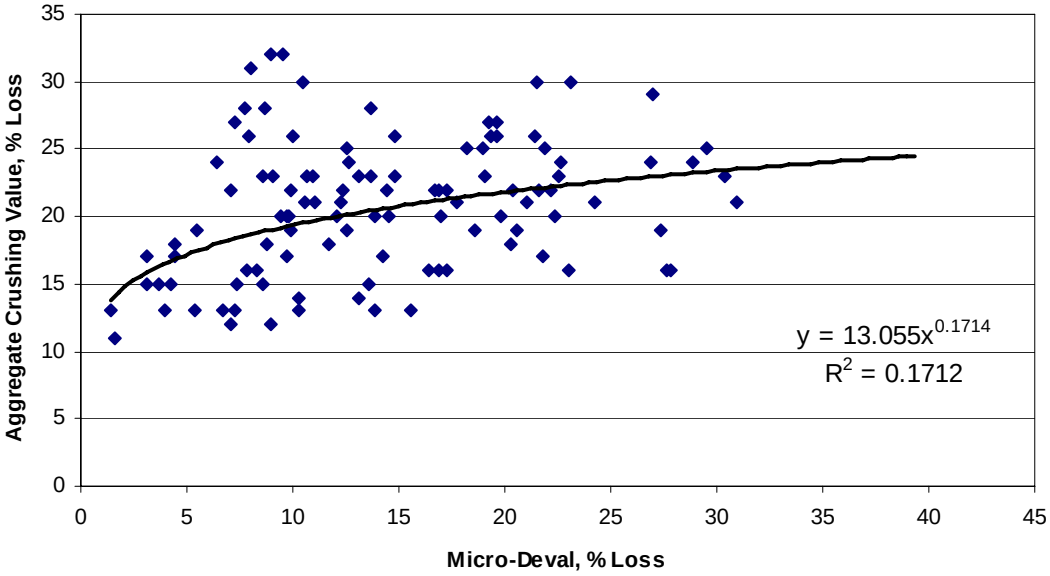

Figure F.4: Aggregate Crushing Value vs. Micro-Deval

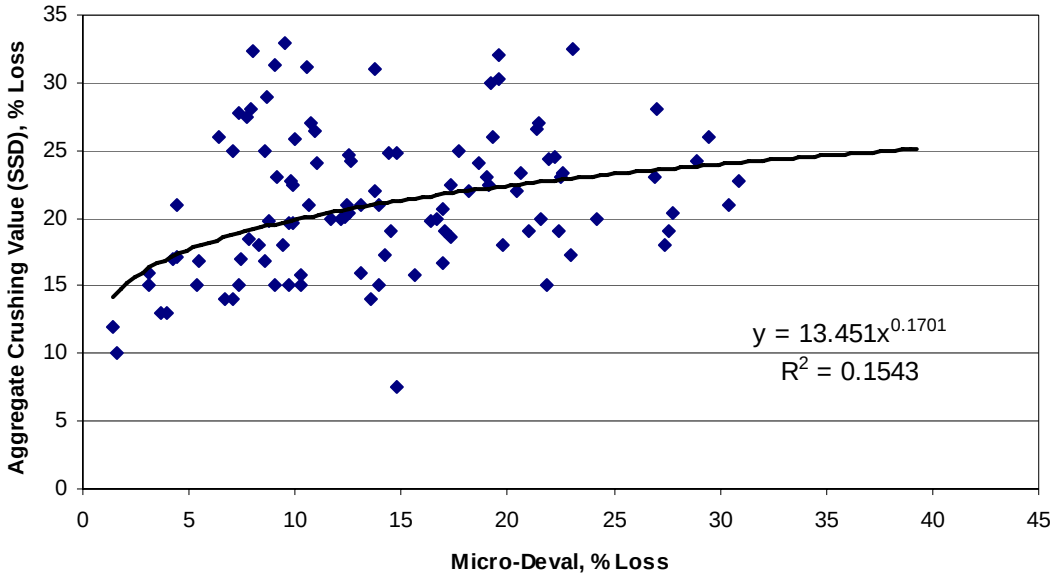

Figure F.5: Aggregate Crushing Value (SSD) vs. Micro-Deval

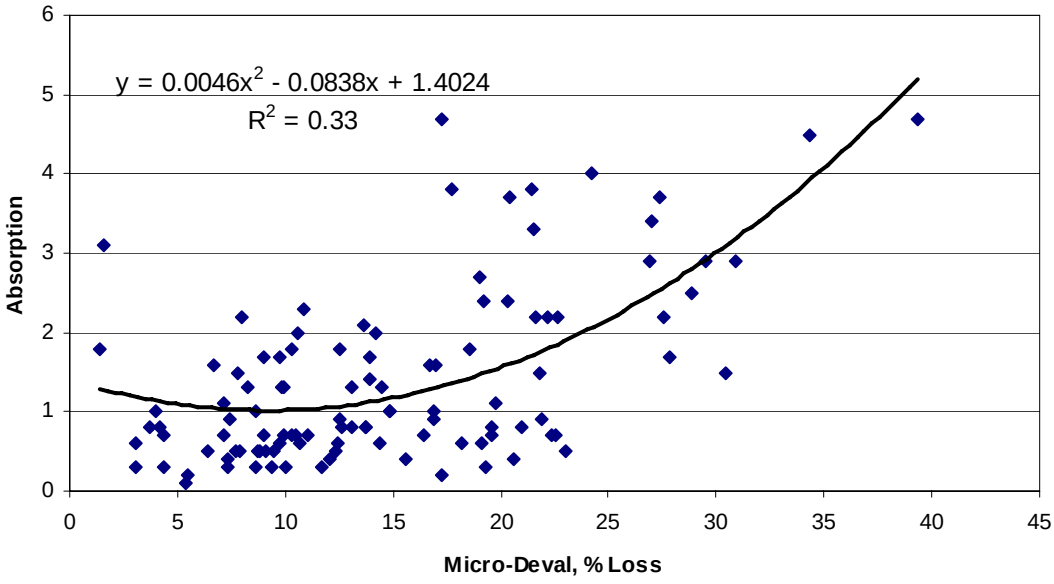

Figure F.6: Absorption vs. Micro-Deval

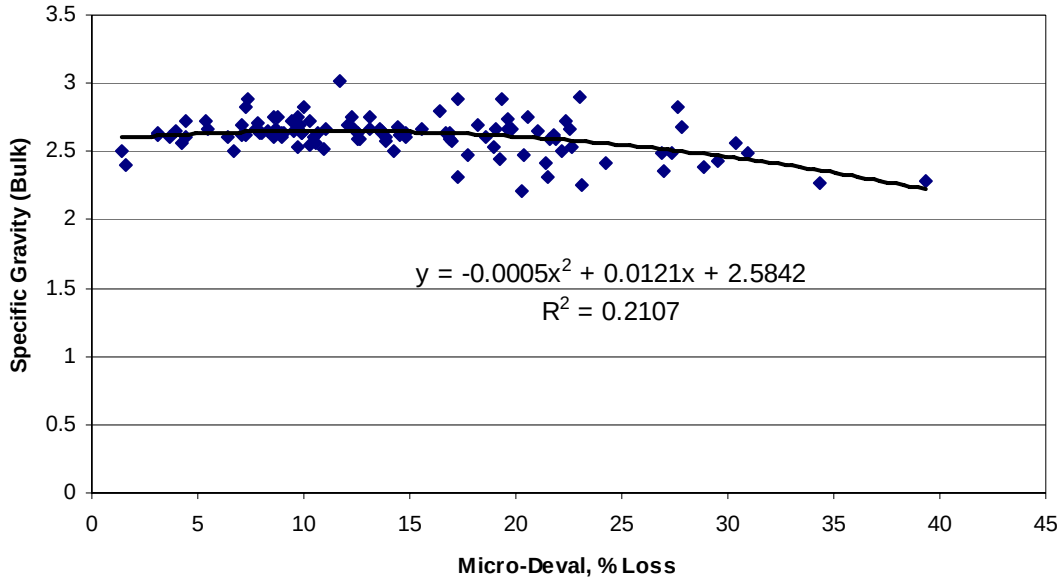

Figure F.7: Specific Gravity (Bulk) vs. Micro-Deval

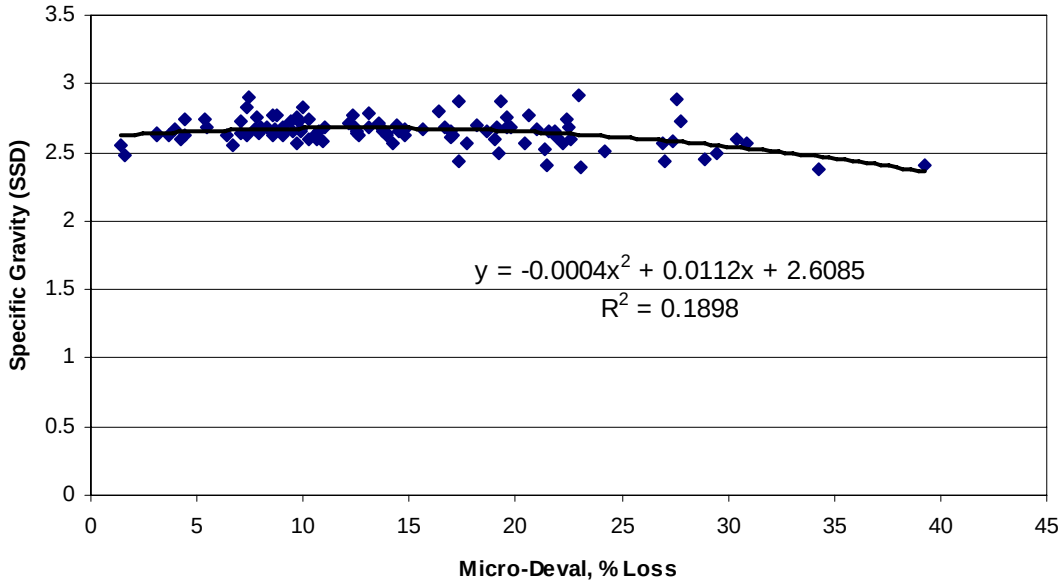

Figure F.8: Specific Gravity (SSD) vs. Micro-Deval

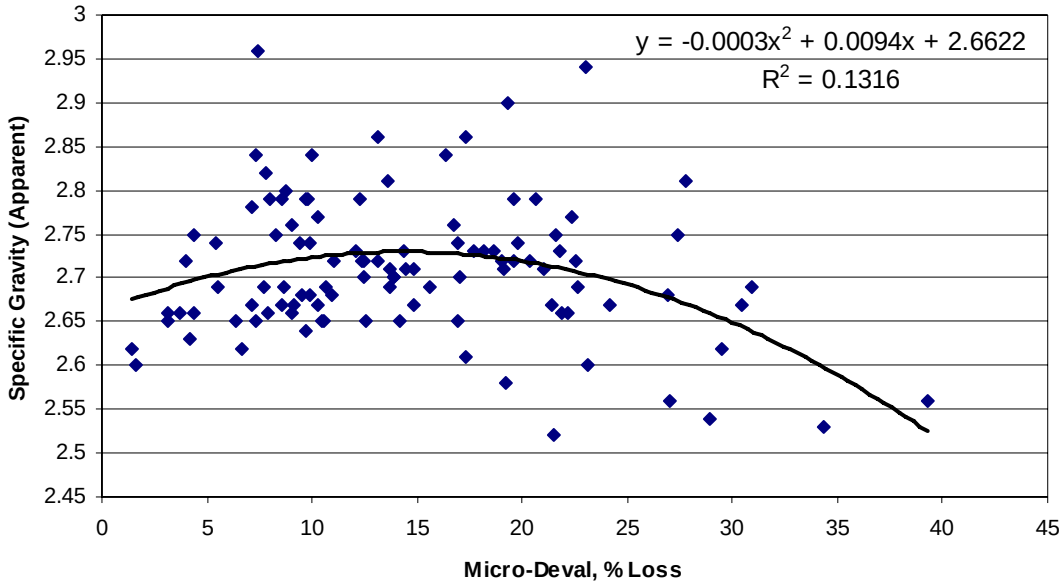

Figure F.9: Specific Gravity (Apparent) vs. Micro-Deval

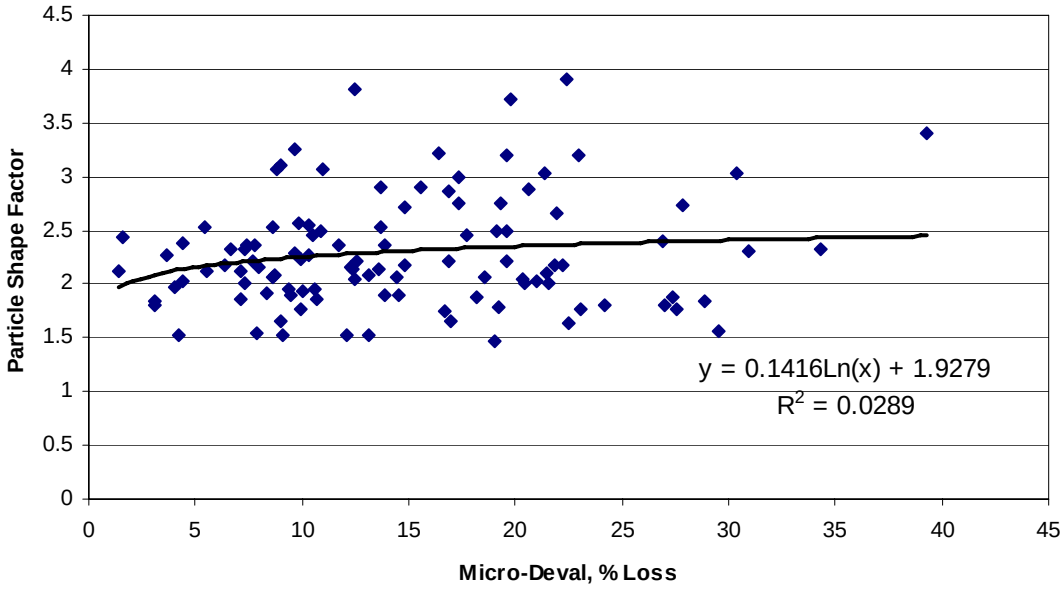

Figure F.10: Particle Shape Factor vs. Micro-Deval

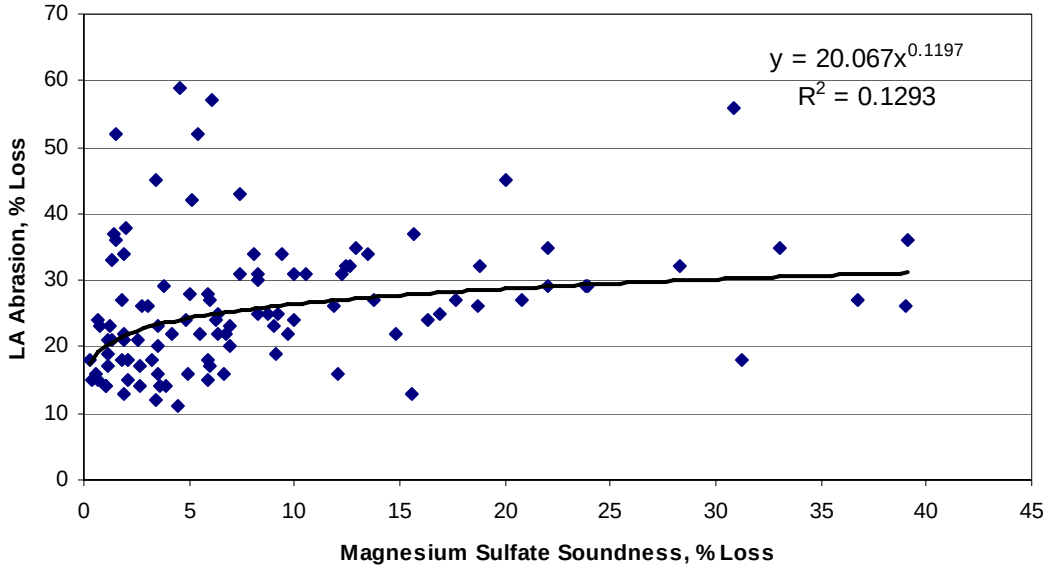

Figure F.11: L.A. Abrasion vs. Magnesium Sulfate Soundness

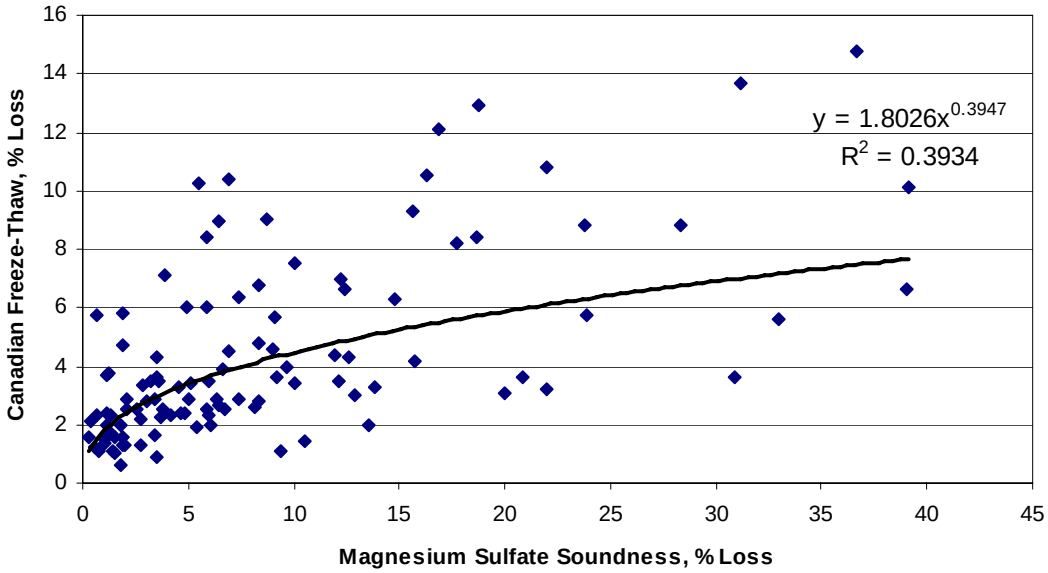

Figure F.12: Canadian Freeze-Thaw vs. Magnesium Sulfate Soundness

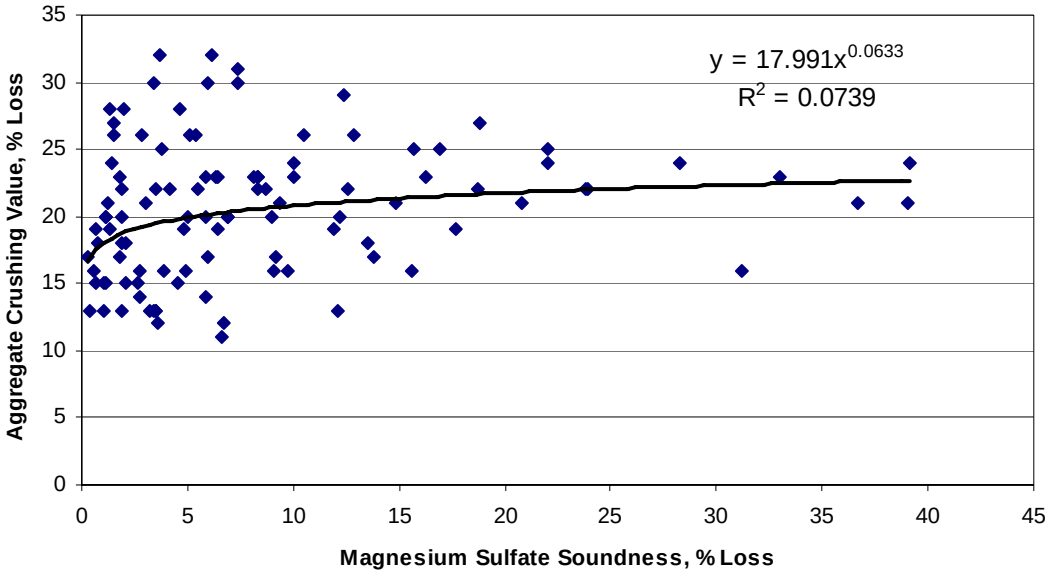

Figure F.13: Aggregate Crushing Value vs. Magnesium Sulfate Soundness

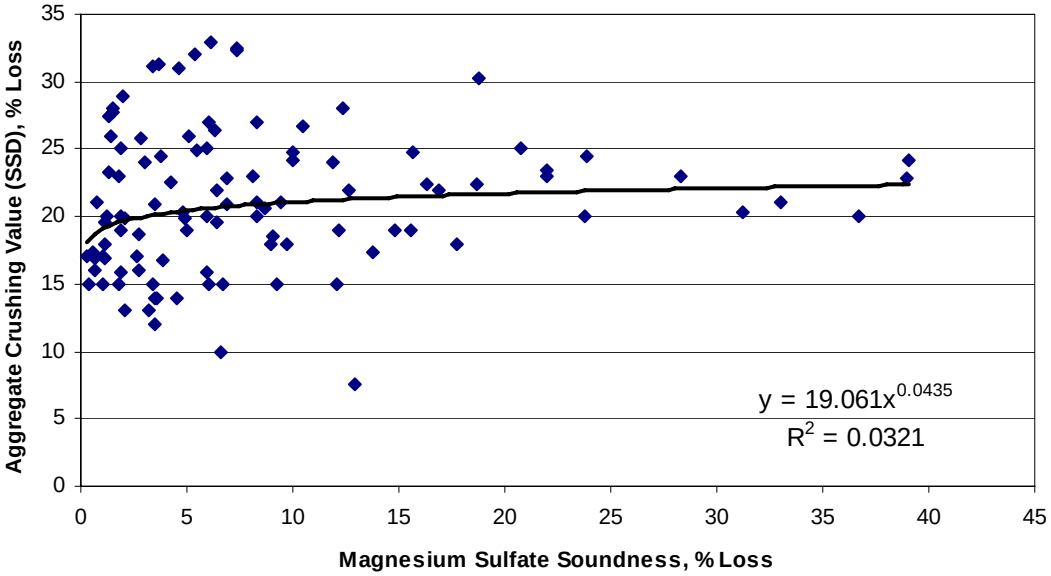

Figure F.14: Aggregate Crushing Value (SSD) vs. Magnesium Sulfate Soundness

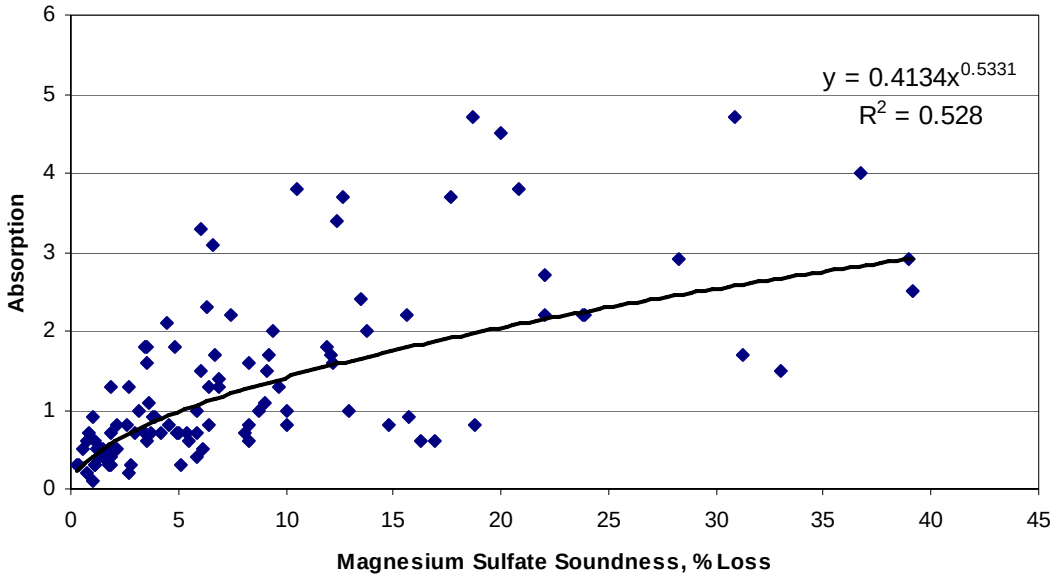

Figure F.15: Absorption vs. Magnesium Sulfate Soundness

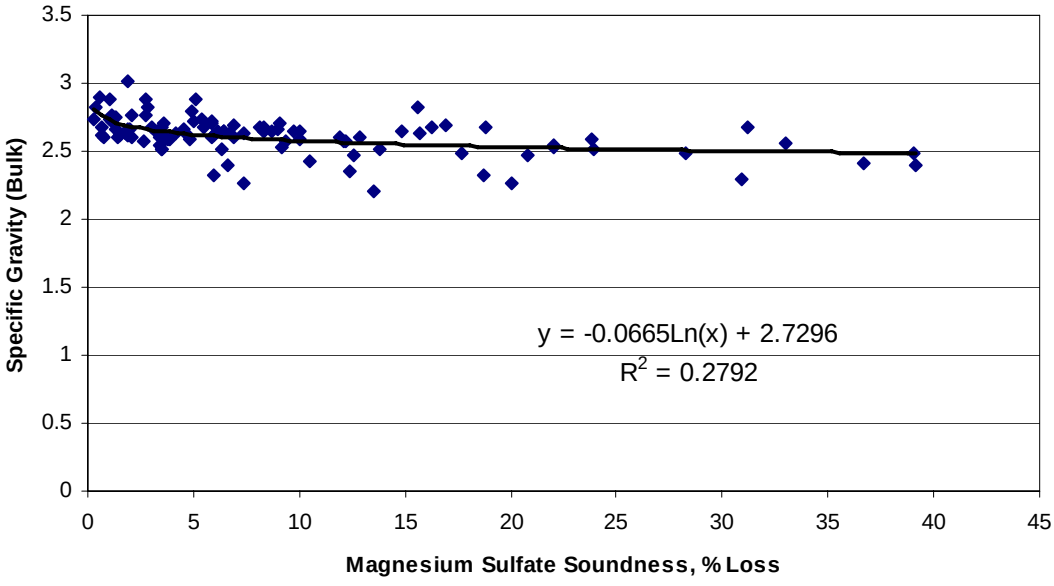

Figure F.16: Specific Gravity (Bulk) vs. Magnesium Sulfate Soundness

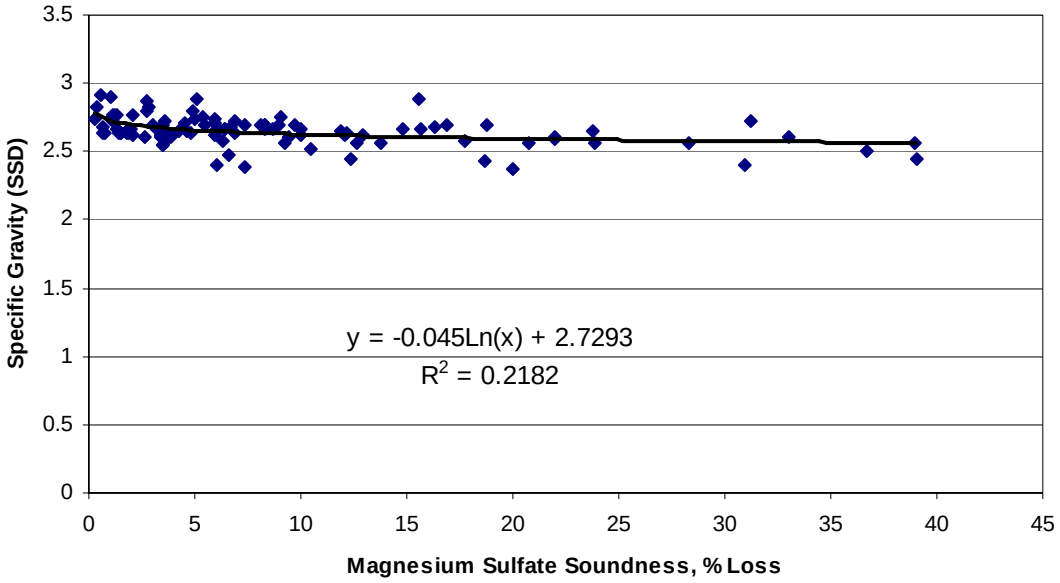

Figure F.17: Specific Gravity (SSD) vs. Magnesium Sulfate Soundness

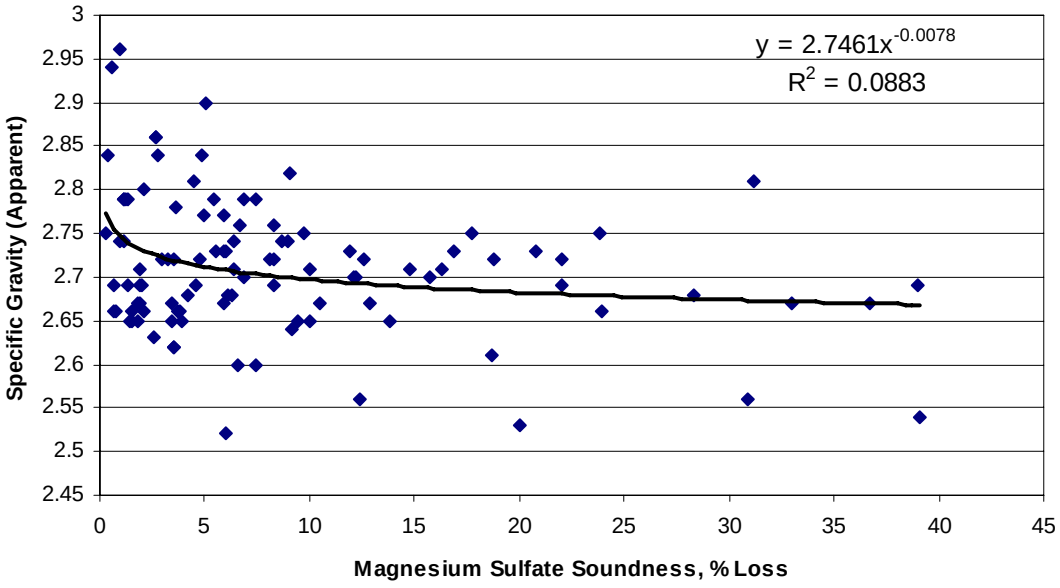

Figure F.18: Specific Gravity (Apparent) vs. Magnesium Sulfate Soundness

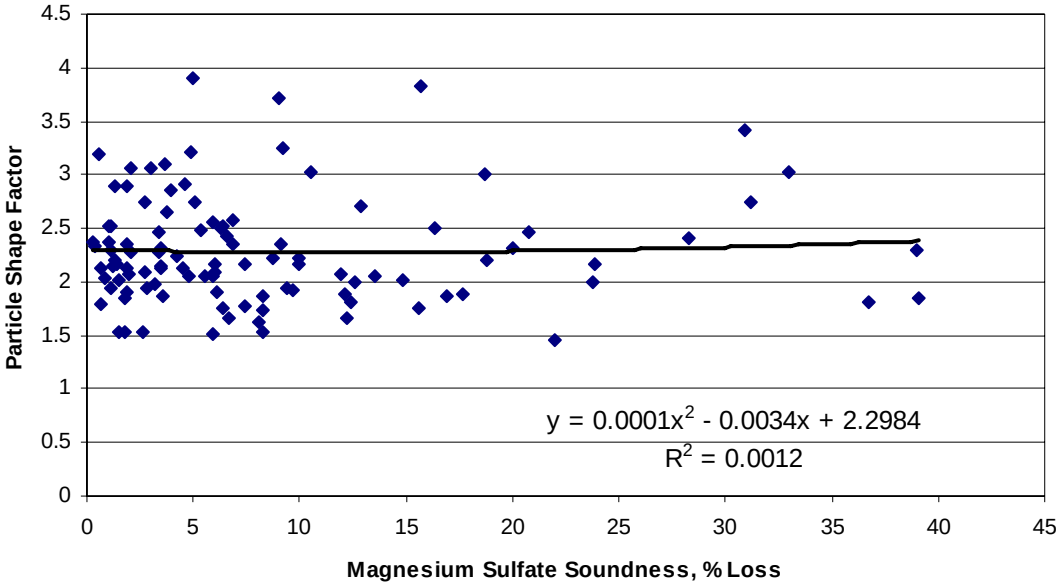

Figure F.19: Particle Shape Factor vs. Magnesium Sulfate Soundness

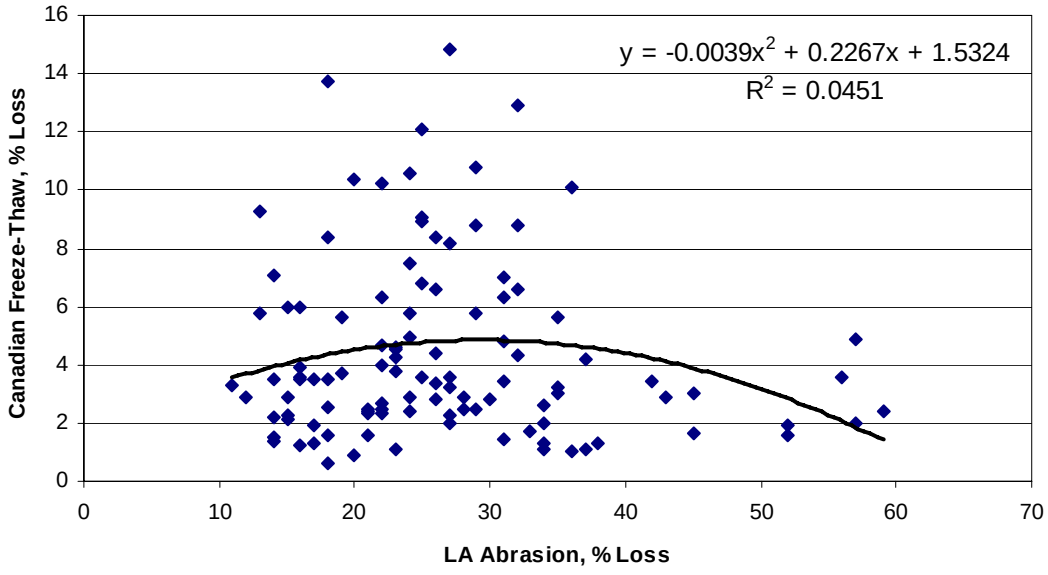

Figure F.20: Canadian Freeze-Thaw vs. L.A. Abrasion

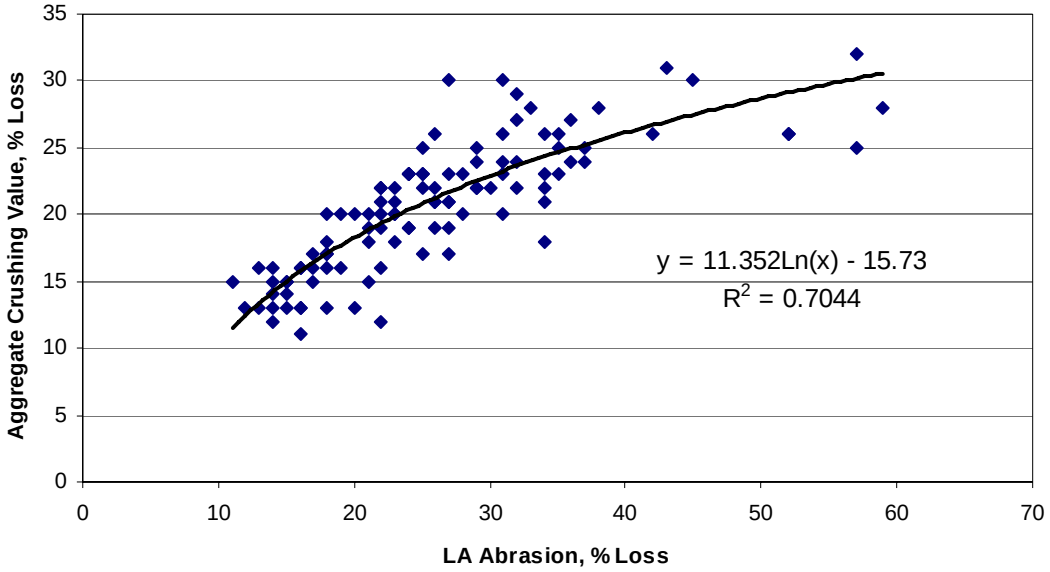

Figure F.21: Aggregate Crushing Value vs. L.A. Abrasion

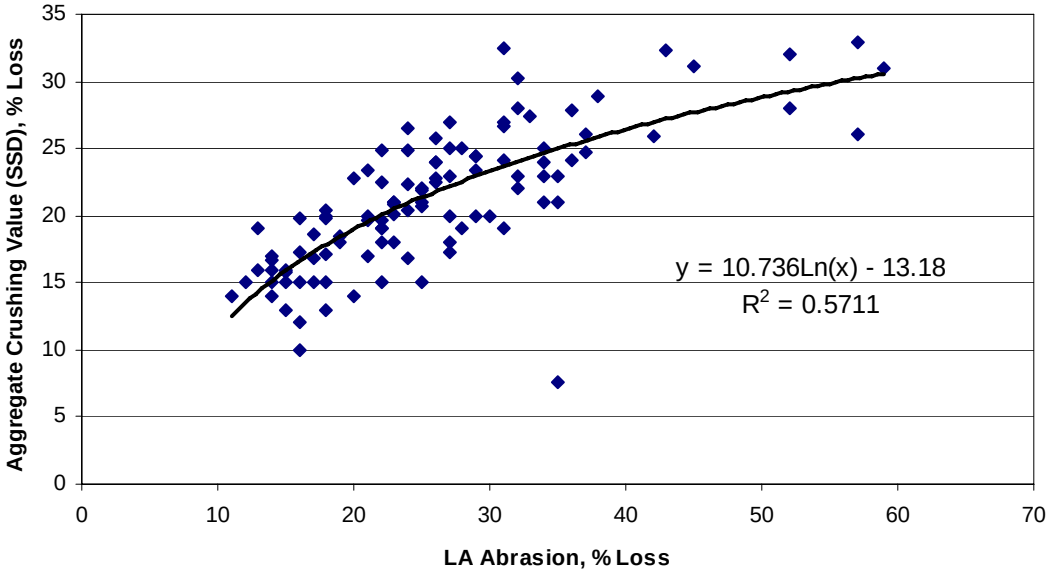

Figure F.22: Aggregate Crushing Value (SSD) vs. L.A. Abrasion

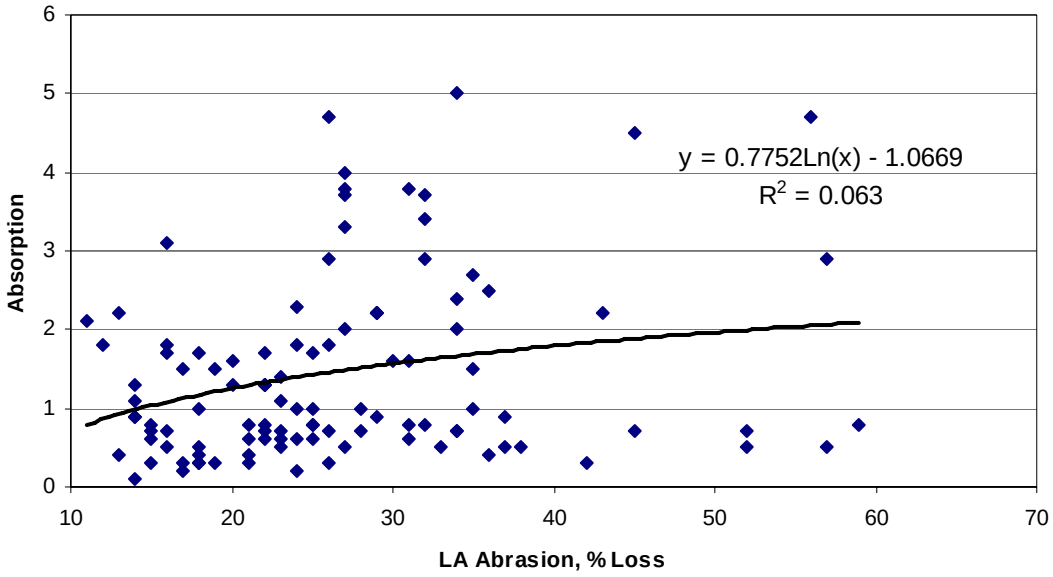

Figure F.23: Absorption vs. L.A. Abrasion

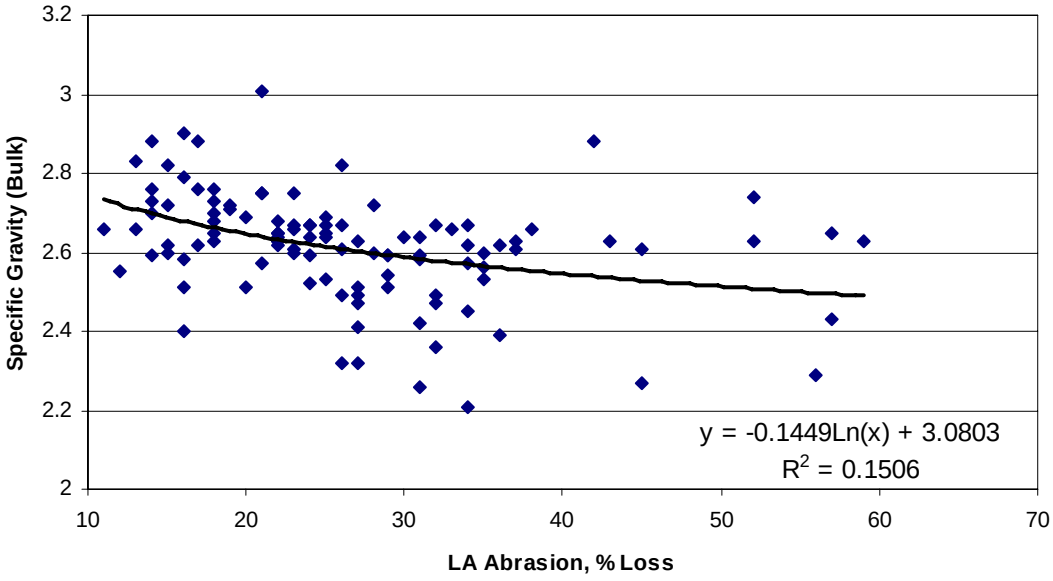

Figure F.24: Specific Gravity (Bulk) vs. L.A. Abrasion

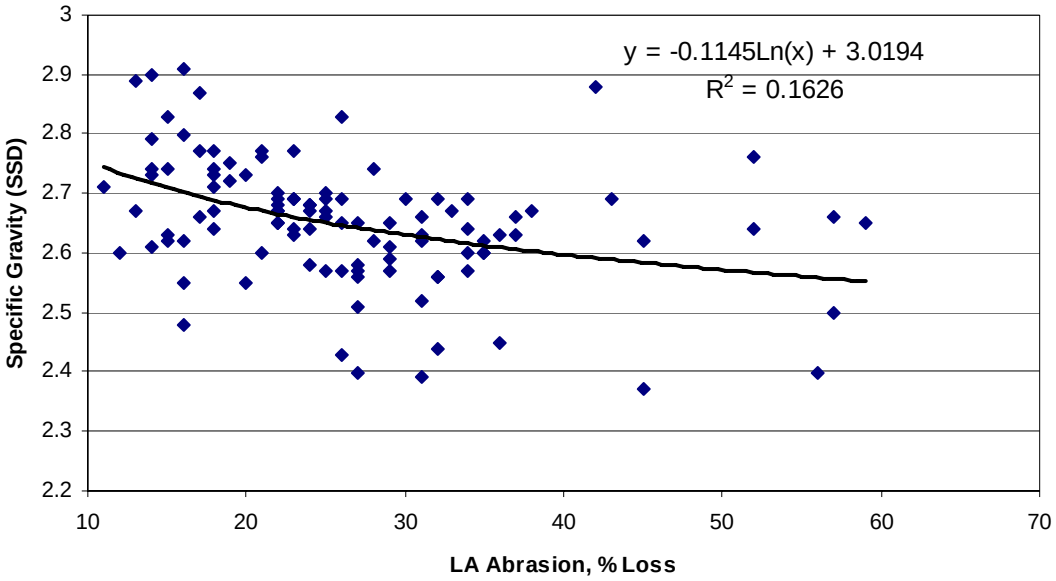

Figure F.25: Specific Gravity (SSD) vs. L.A. Abrasion

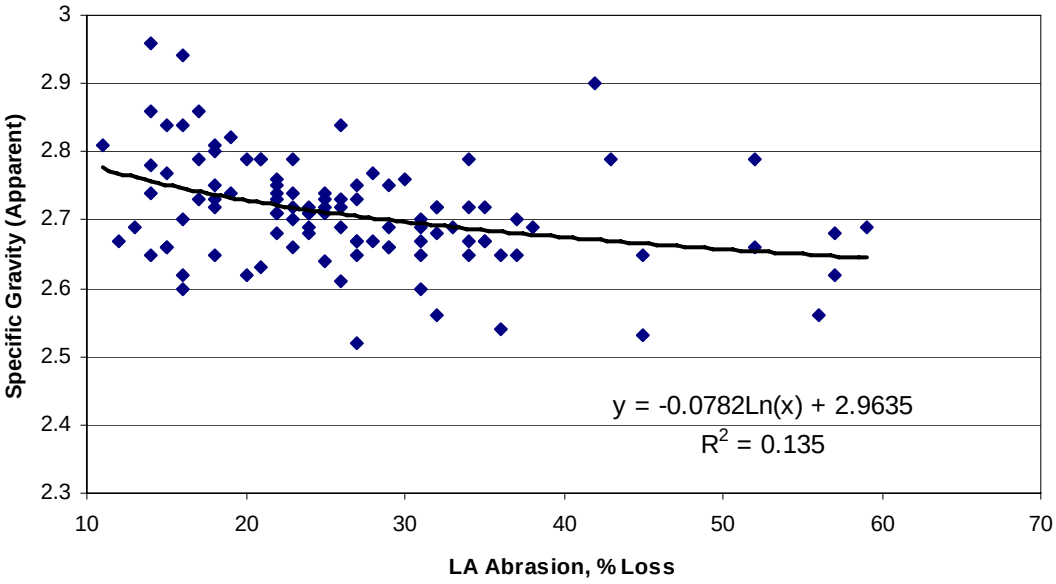

Figure F.26: Specific Gravity (Apparent) vs. L.A. Abrasion

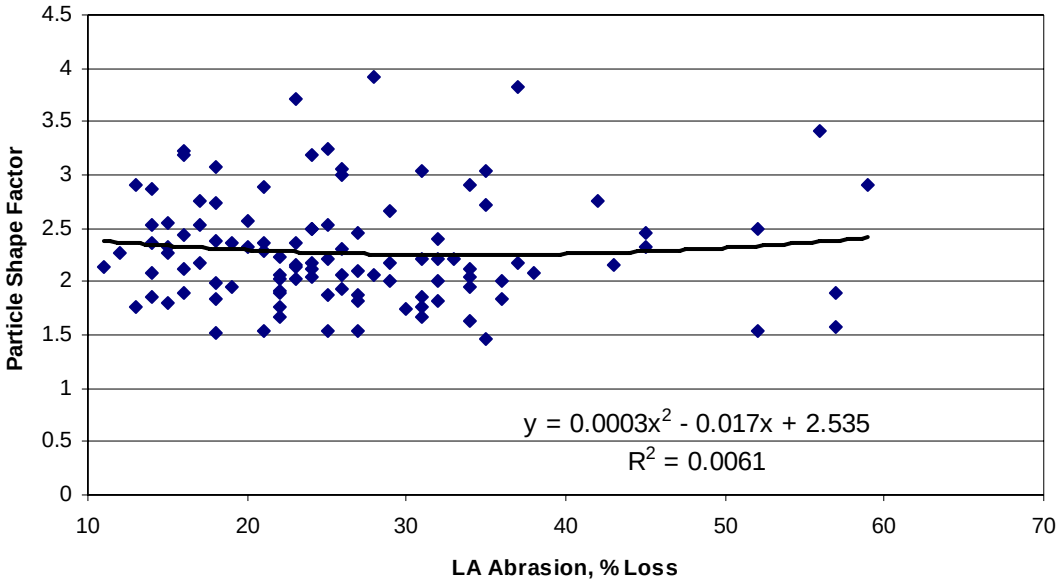

Figure F.27: Particle Shape Factor vs. L.A. Abrasion

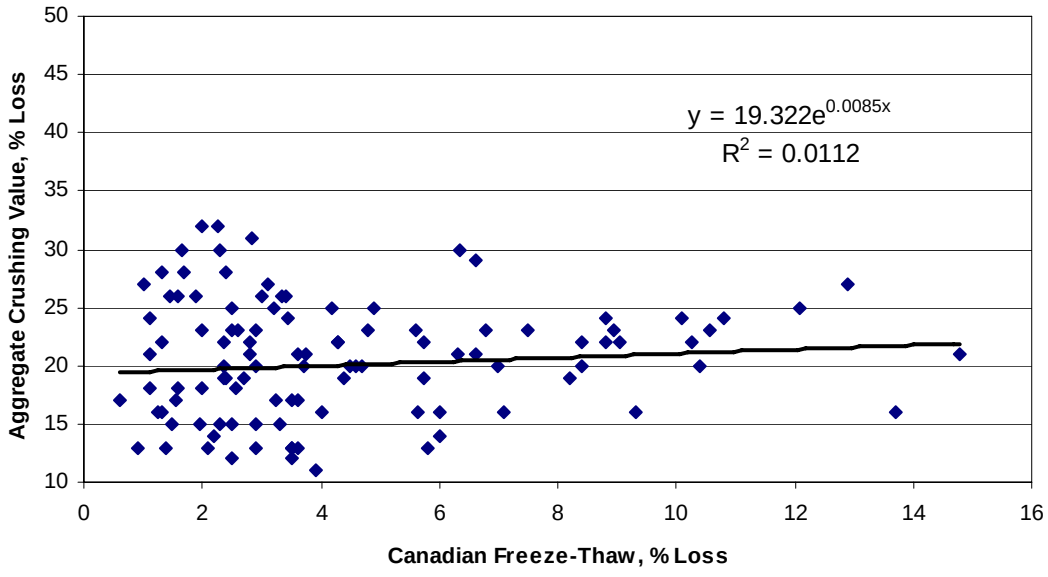

Figure F.28: Aggregate Crushing Value vs. Canadian Freeze-Thaw

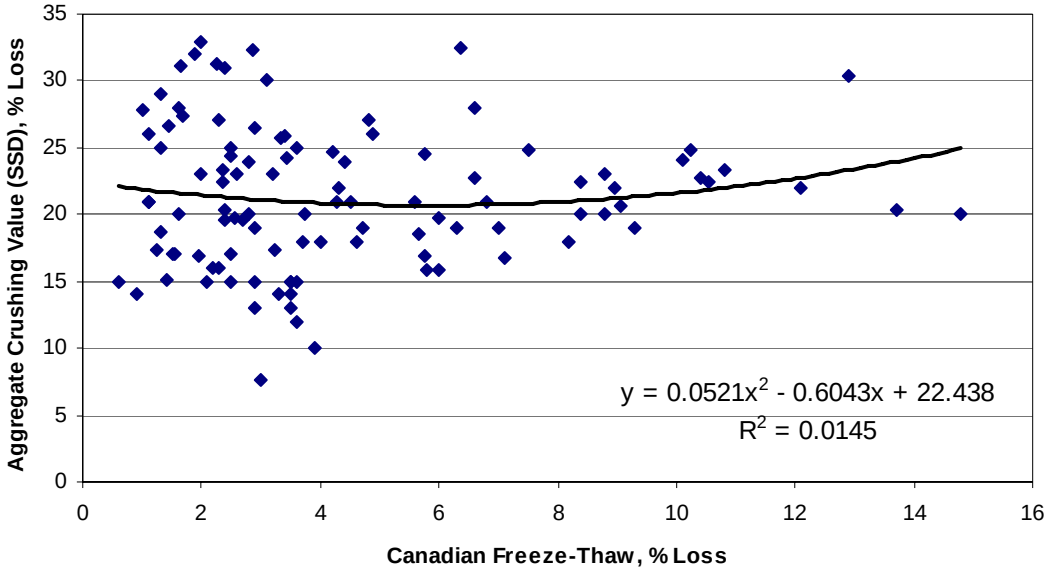

Figure F.29: Aggregate Crushing Value (SSD) vs. Canadian Freeze-Thaw

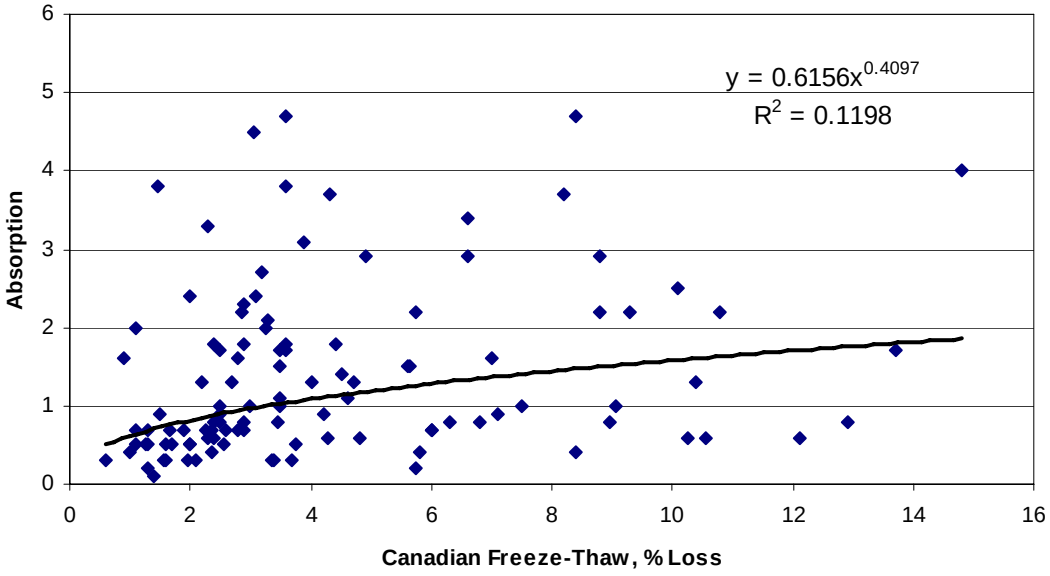

Figure F.30: Absorption vs. Canadian Freeze-Thaw

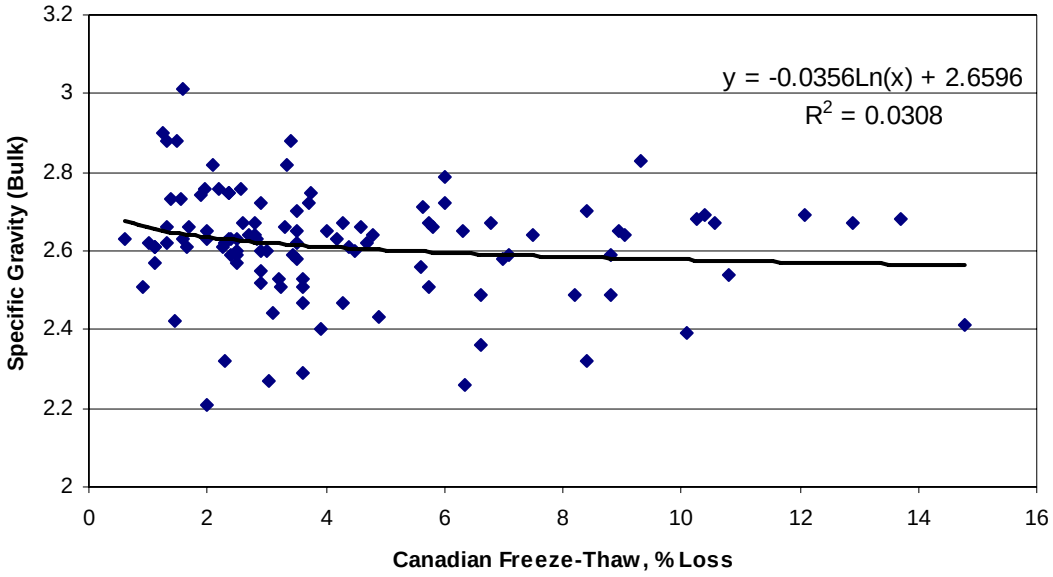

Figure F.31: Specific Gravity (Bulk) vs. Canadian Freeze-Thaw

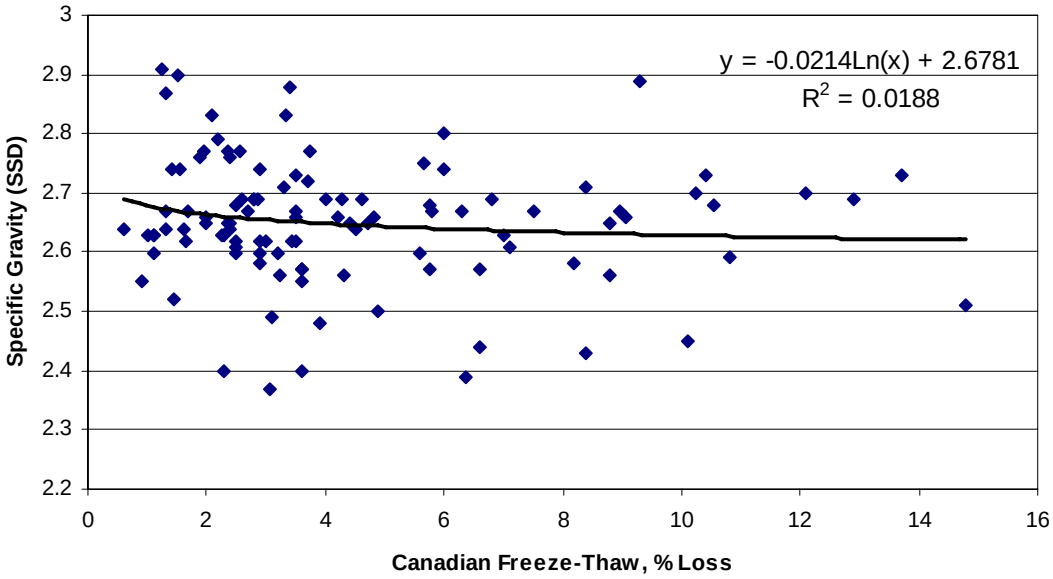

Figure F.32: Specific Gravity (SSD) vs. Canadian Freeze-Thaw

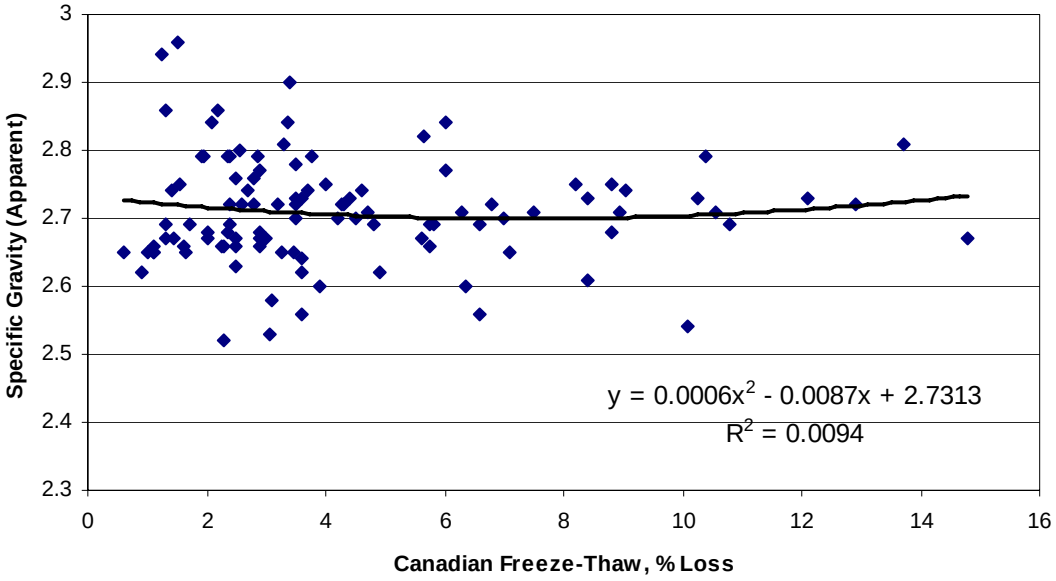

Figure F.33: Specific Gravity (Apparent) vs. Canadian Freeze-Thaw

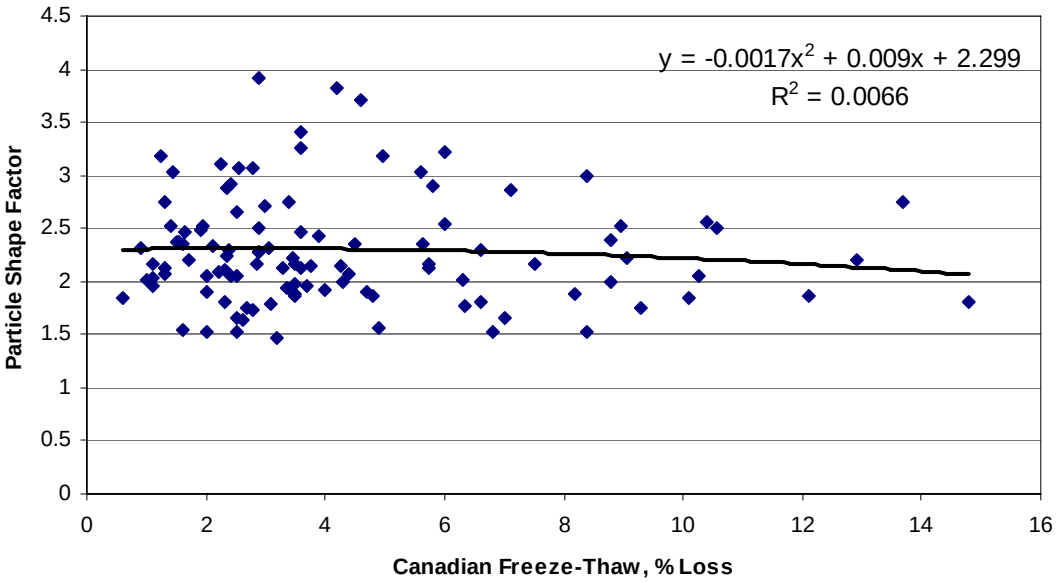

Figure F.34: Particle Shape Factor vs. Canadian Freeze-Thaw

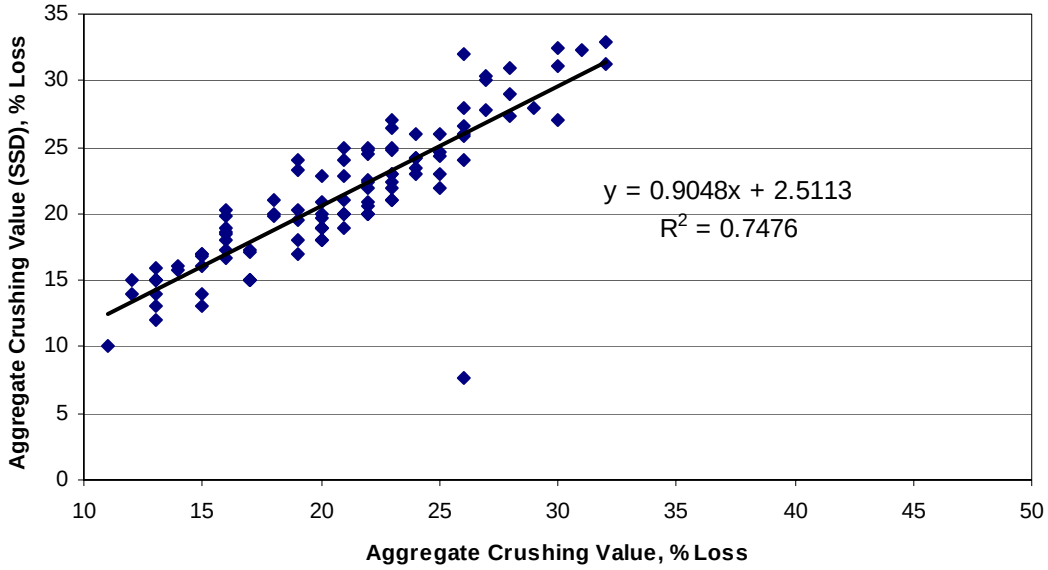

Figure F.35: Aggregate Crushing Value (SSD) vs. Aggregate Crushing Value

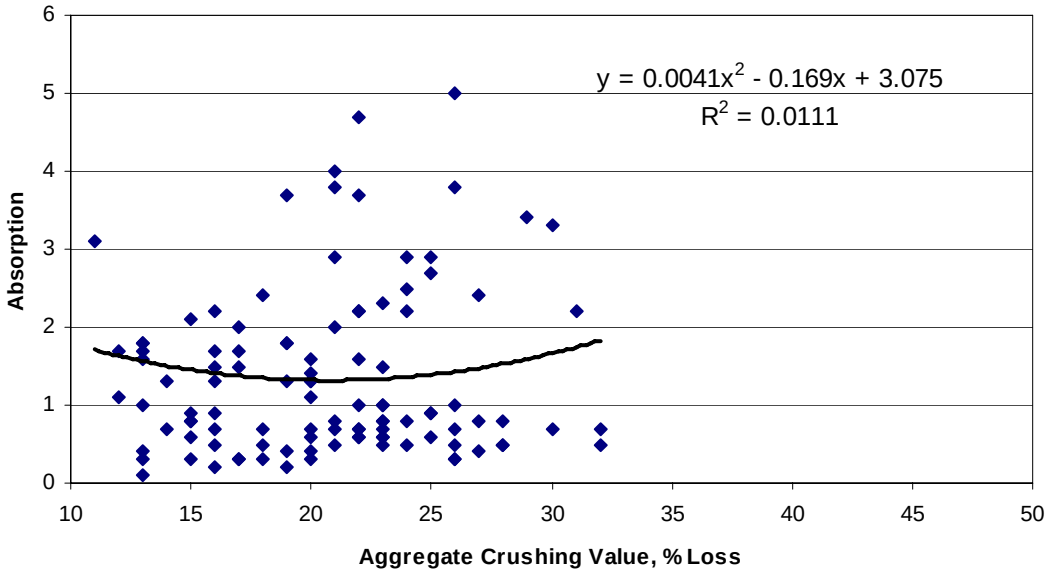

Figure F.36: Absorption vs. Aggregate Crushing Value

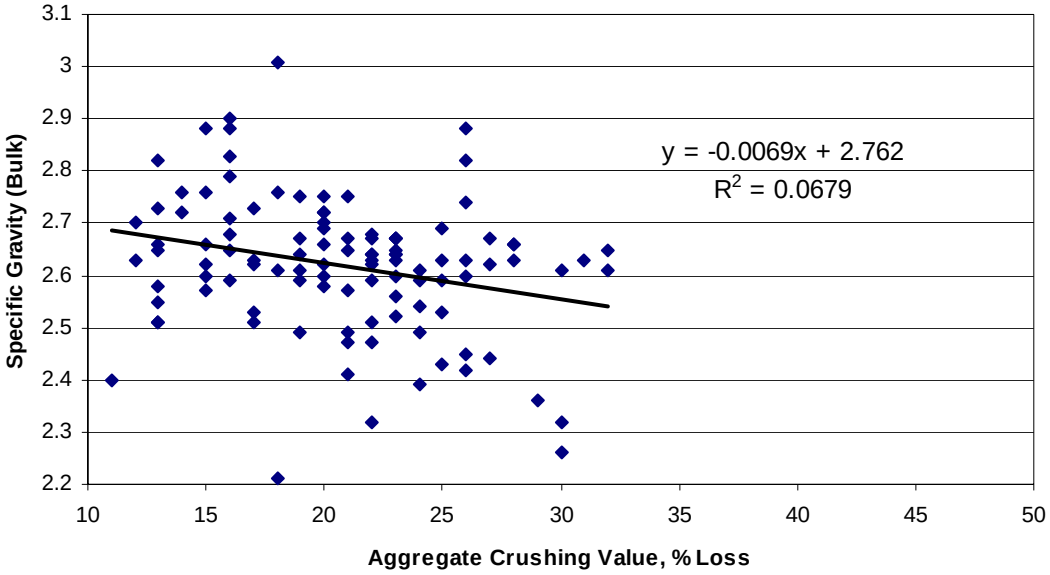

Figure F.37: Specific Gravity (Bulk) vs. Aggregate Crushing Value

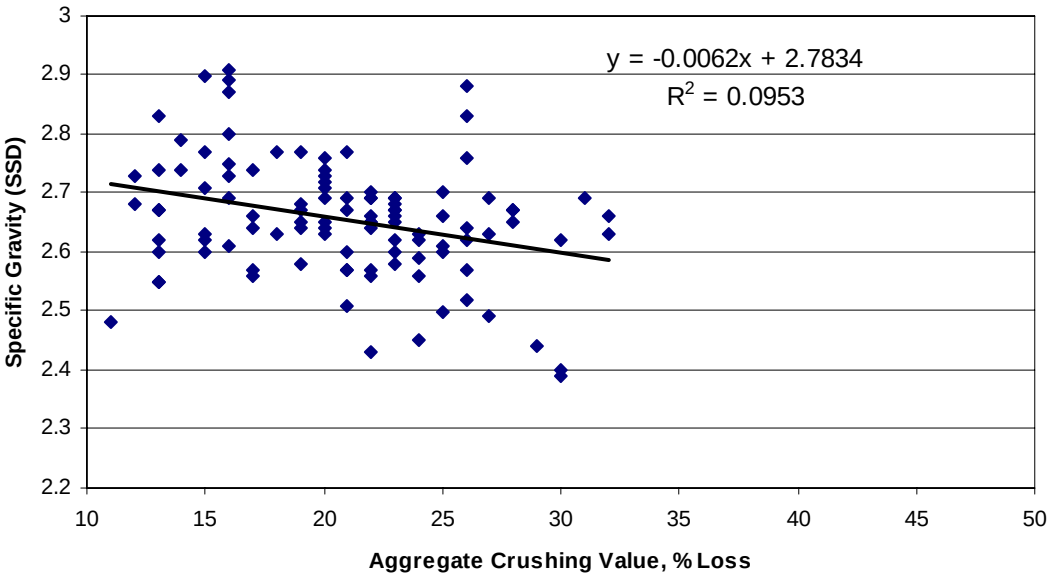

Figure F.38: Specific Gravity (SSD) vs. Aggregate Crushing Value

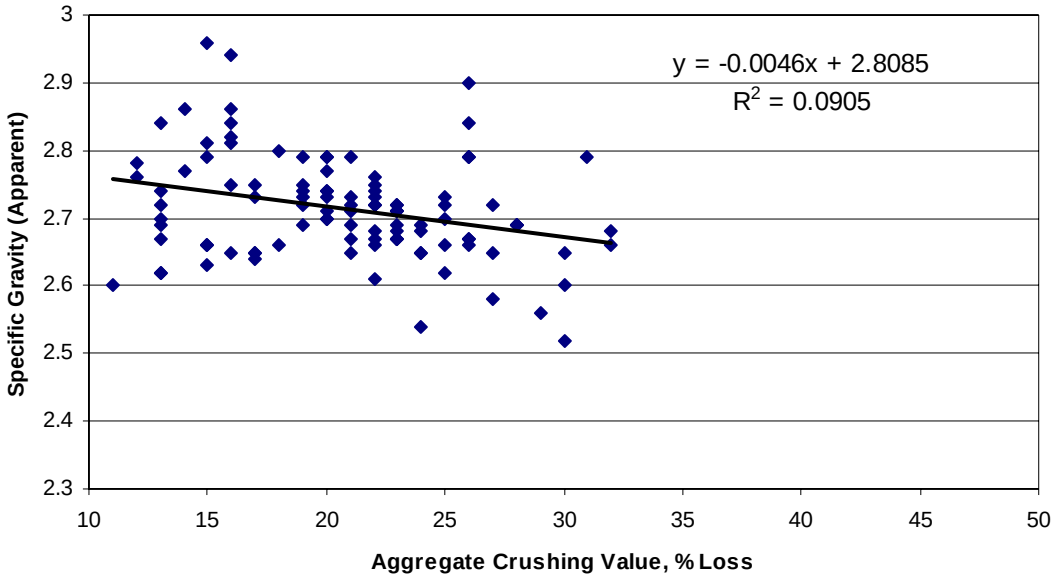

Figure F.39: Specific Gravity (Apparent) vs. Aggregate Crushing Value

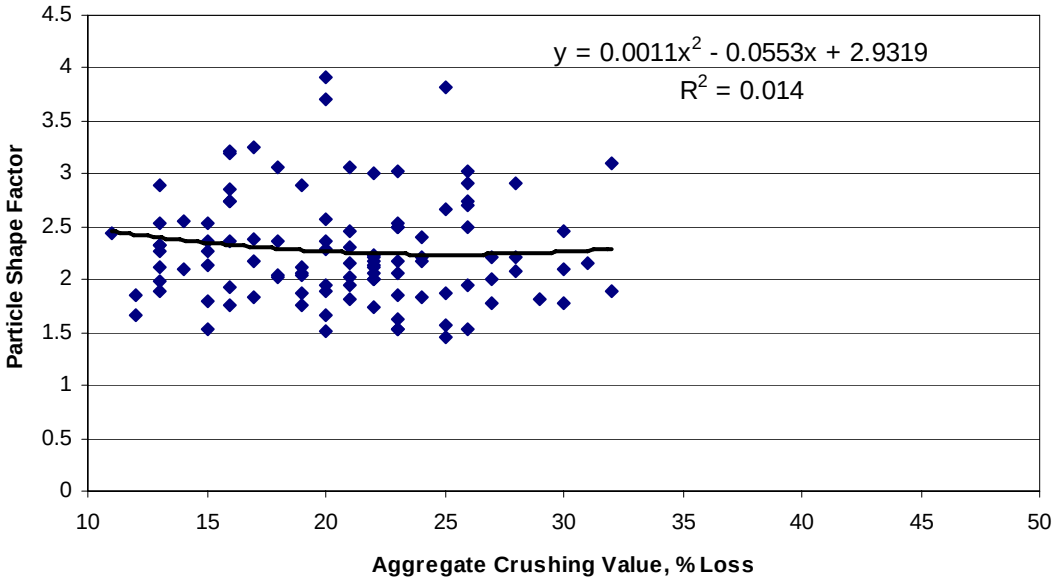

Figure F.40: Particle Shape Factor vs. Aggregate Crushing Value

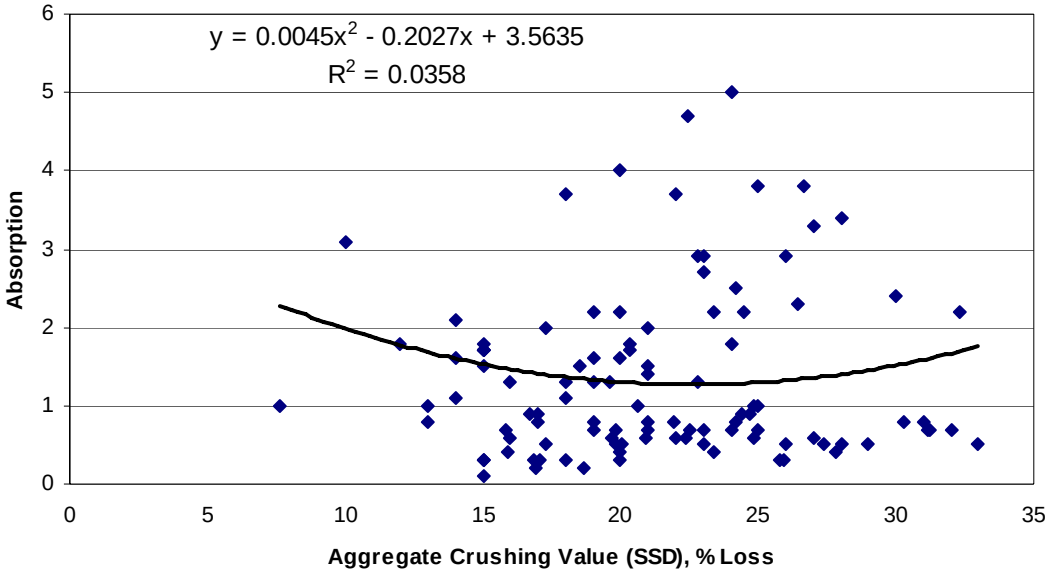

Figure F.41: Absorption vs. Aggregate Crushing Value (SSD)

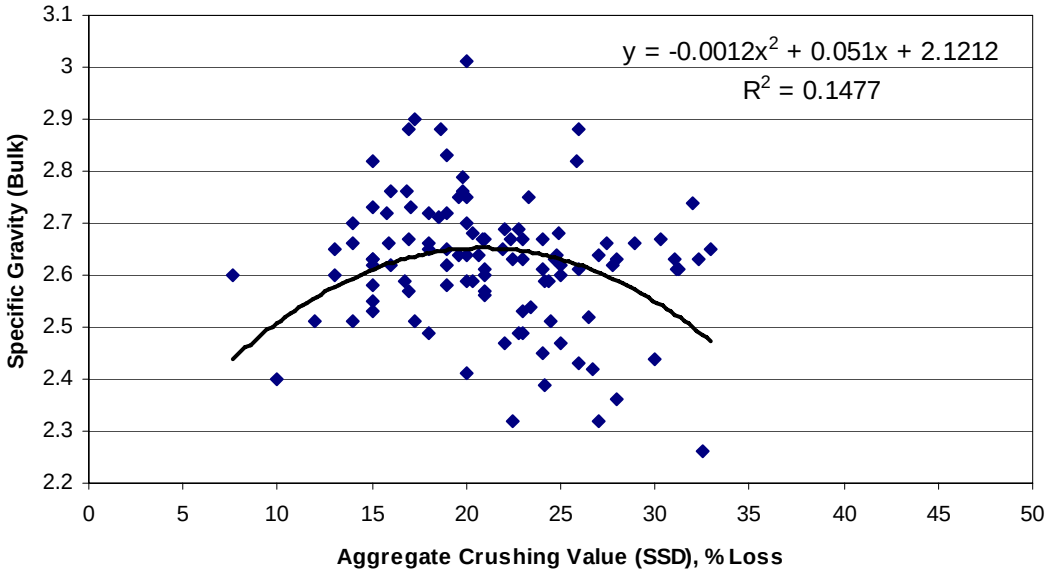

Figure F.42: Specific Gravity (Bulk) vs. Aggregate Crushing Value (SSD)

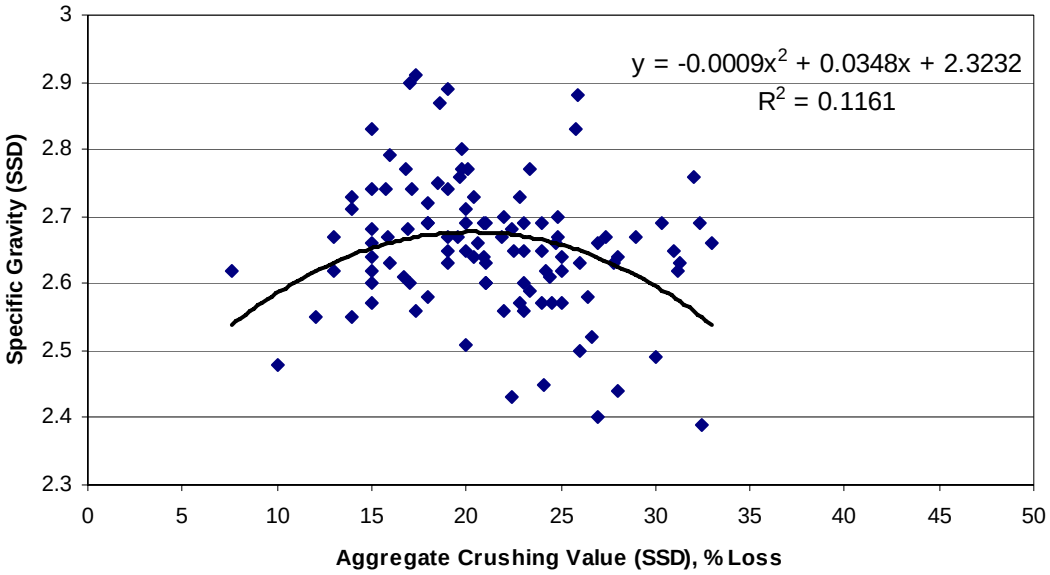

Figure F.43: Specific Gravity (SSD) vs. Aggregate Crushing Value (SSD)

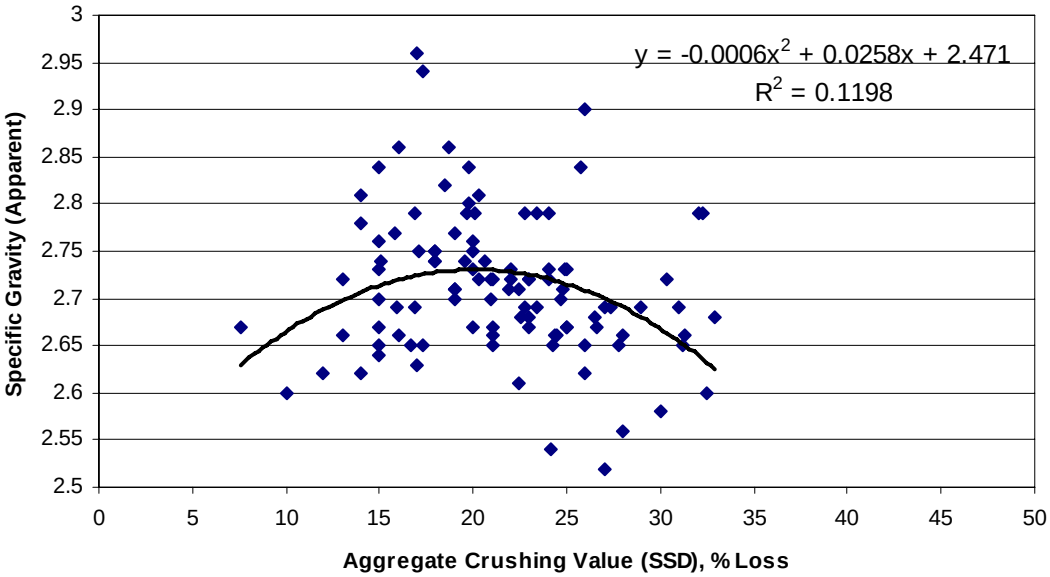

Figure F.44: Specific Gravity (Apparent) vs. Aggregate Crushing Value (SSD)

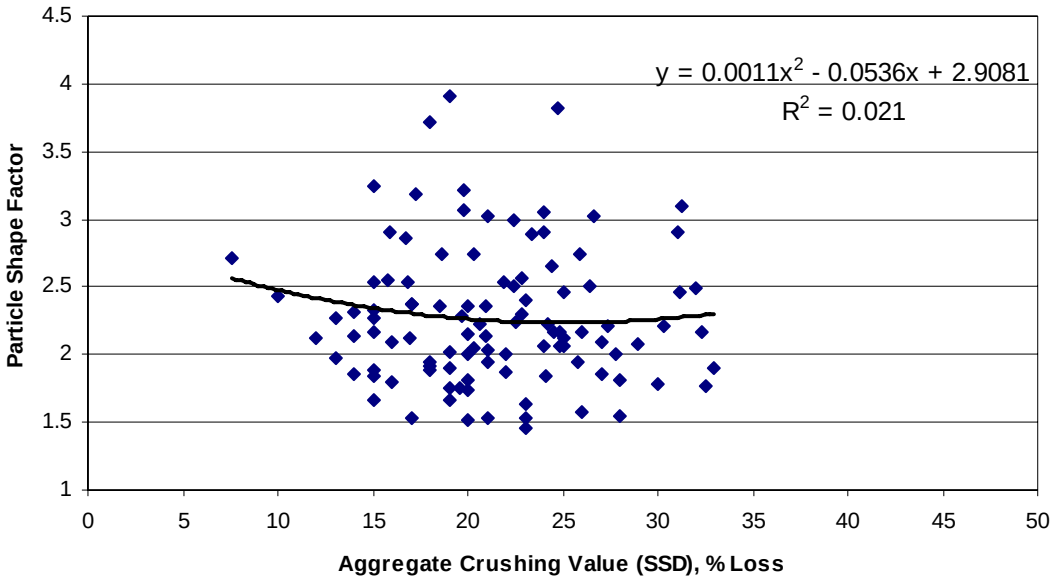

Figure F.45: Particle Shape Factor vs. Aggregate Crushing Value (SSD)

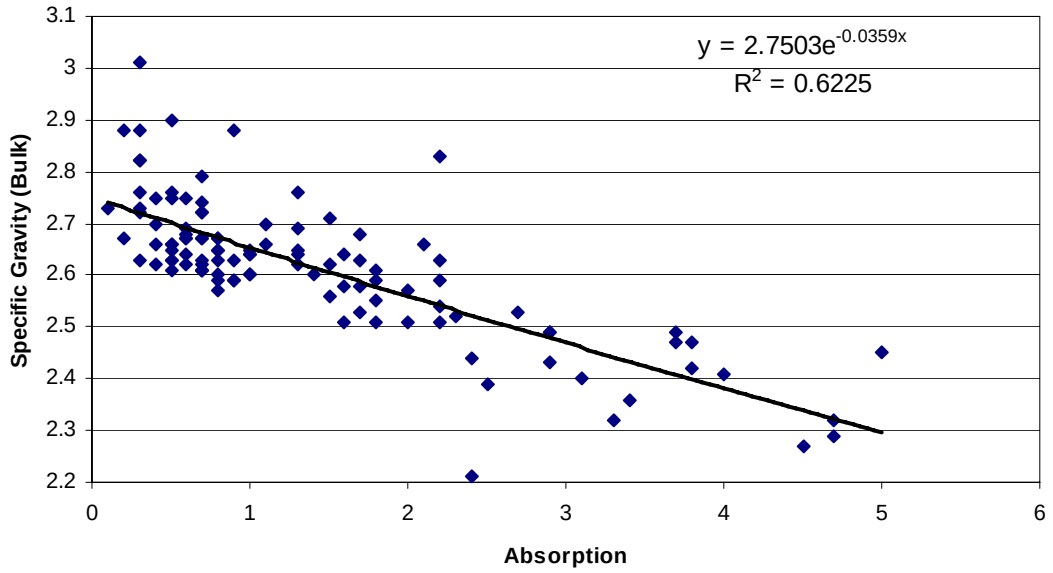

Figure F.46: Specific Gravity (Bulk) vs. Absorption

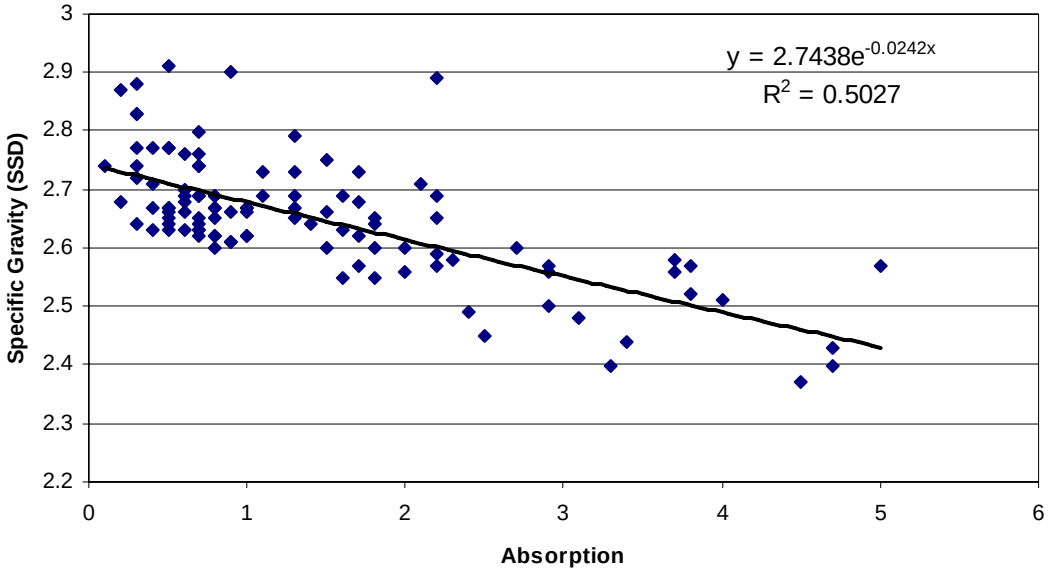

Figure F.47: Specific Gravity (SSD) vs. Absorption

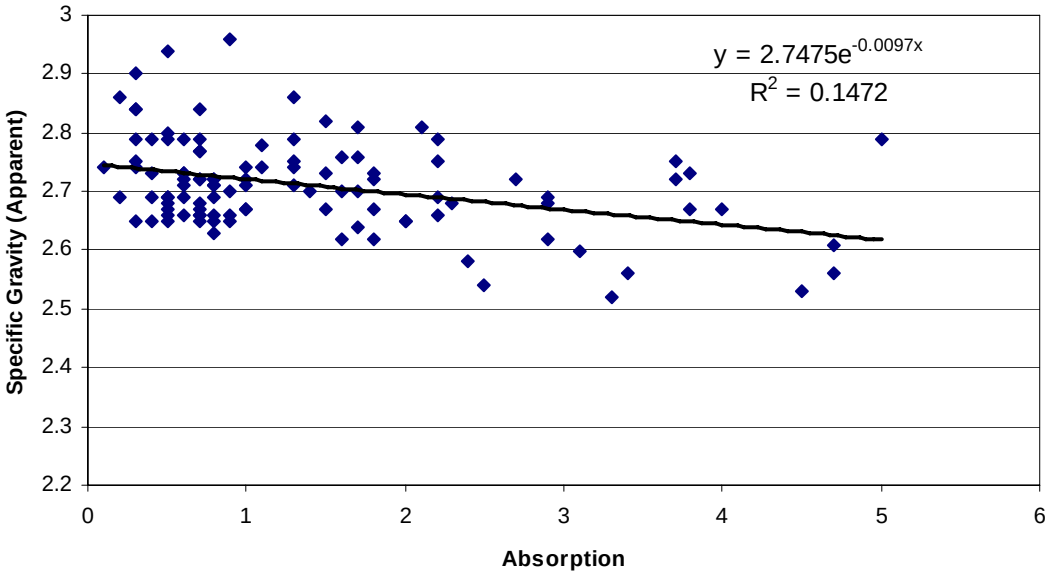

Figure F.48: Specific Gravity (Apparent) vs. Absorption

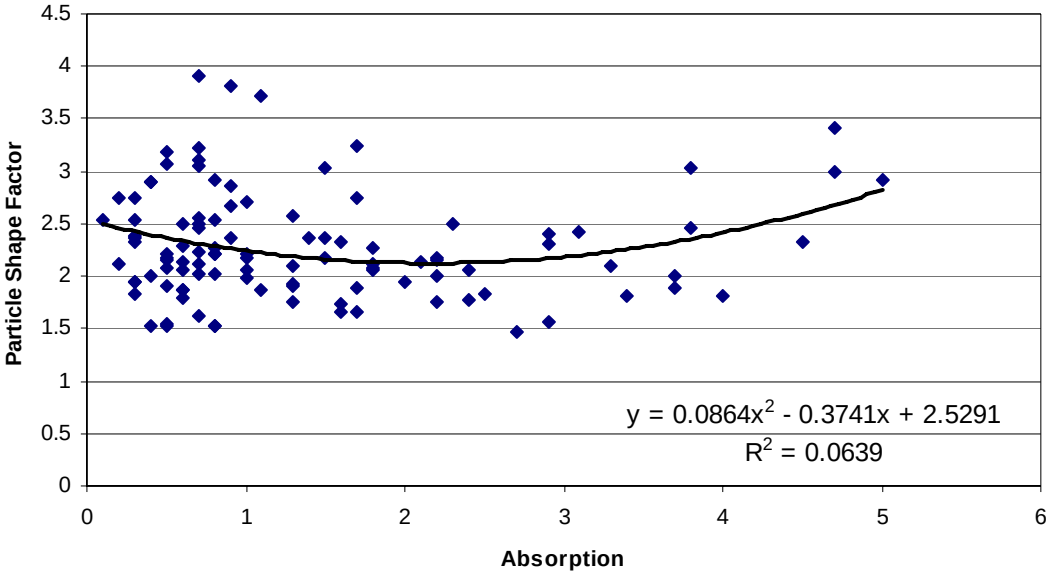

Figure F.49: Particle Shape Factor vs. Absorption

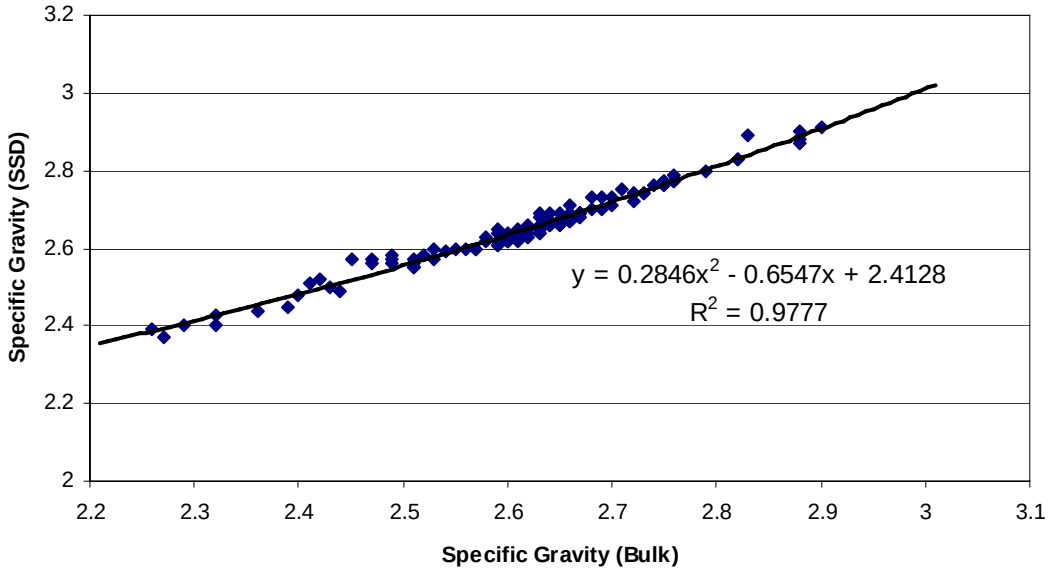

Figure F.50: Specific Gravity (SSD) vs. Specific Gravity (Bulk)

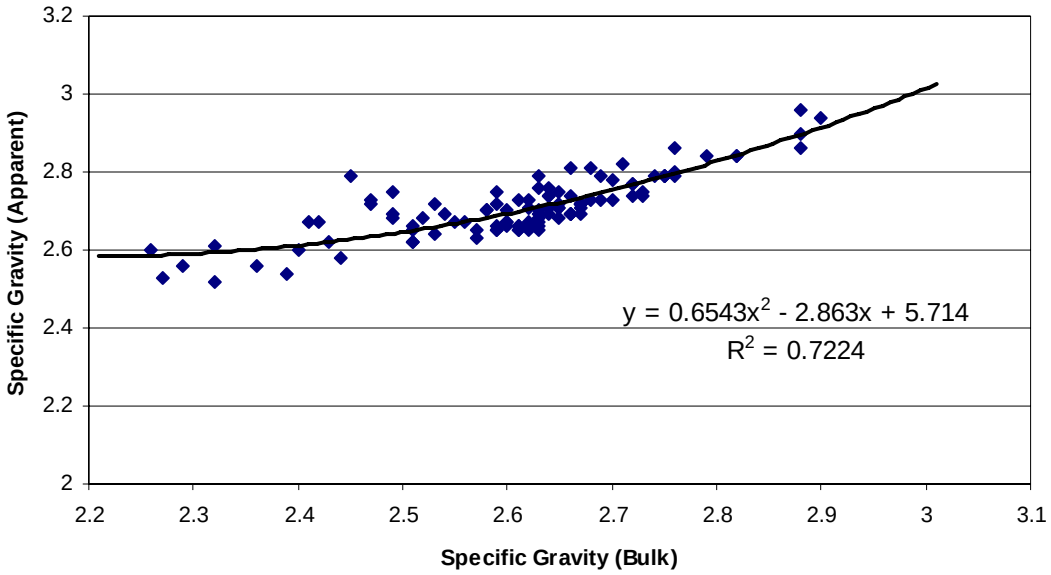

Figure F.51: Specific Gravity (Apparent) vs. Specific Gravity (Bulk)

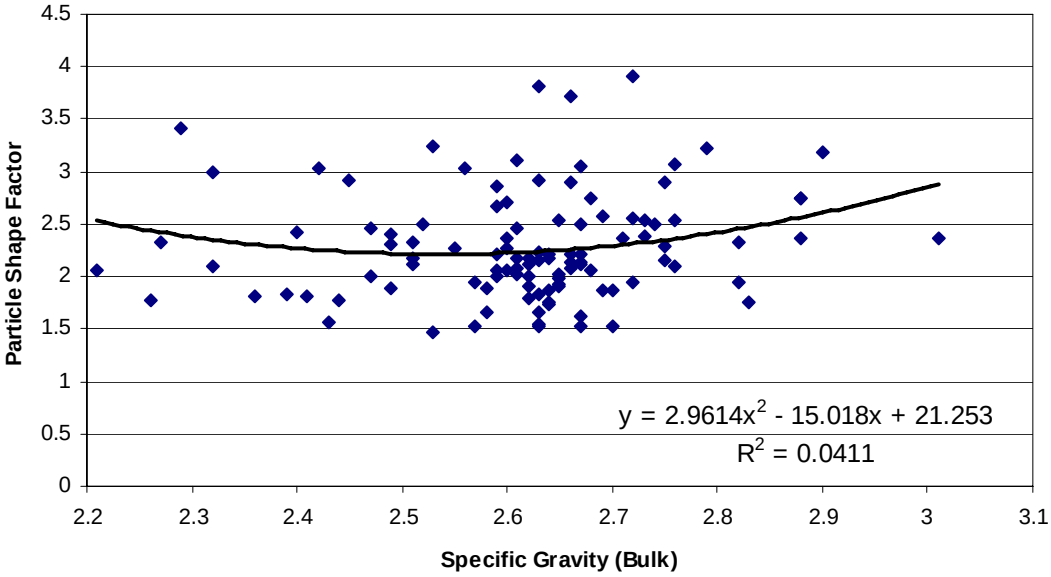

Figure F.52: Particle Shape Factor vs. Specific Gravity (Bulk)

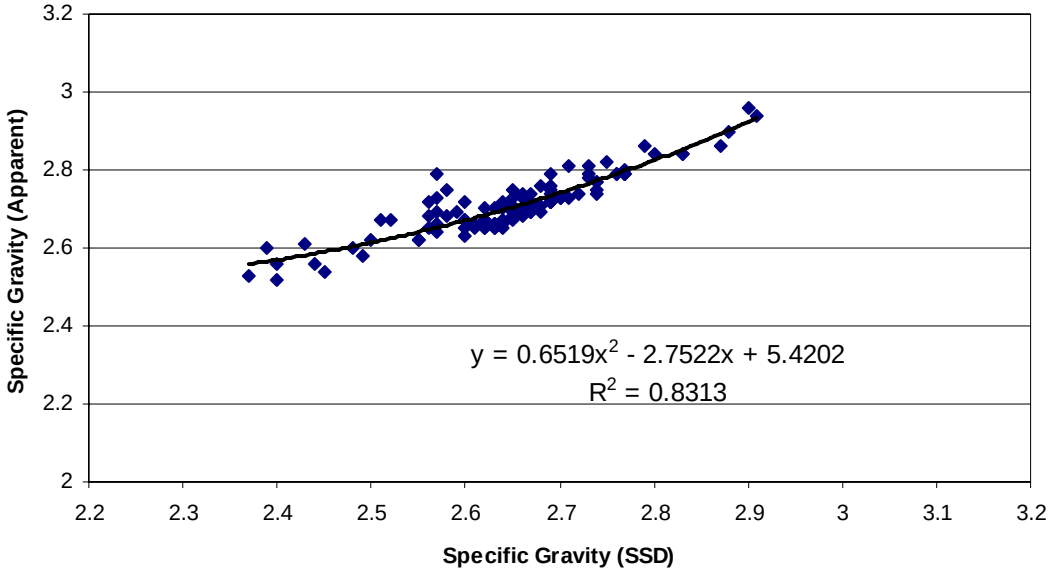

Figure F.53: Specific Gravity (Apparent) vs. Specific Gravity (SSD)

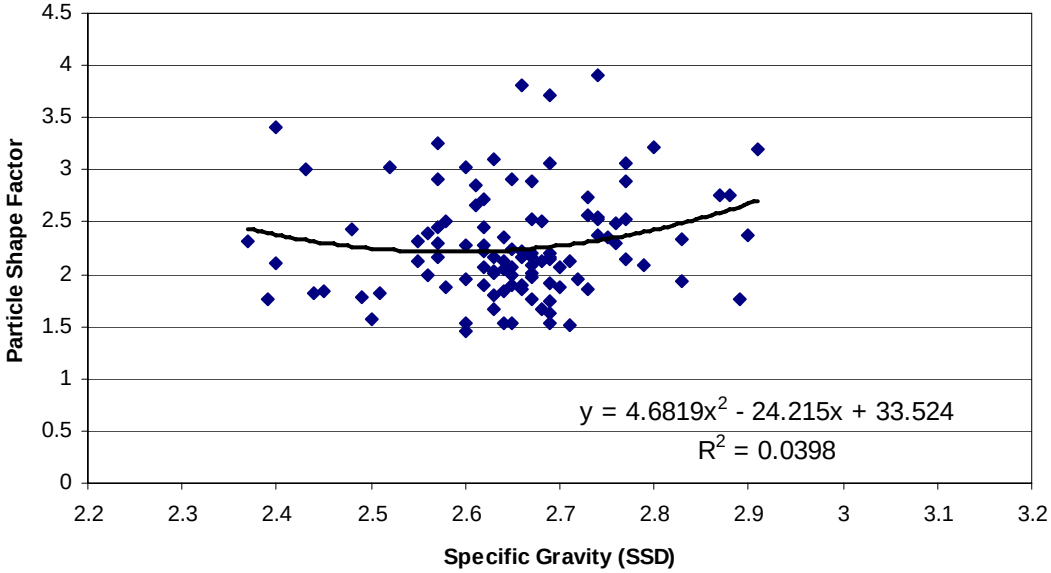

Figure F.54: Particle Shape Factor vs. Specific Gravity (SSD)

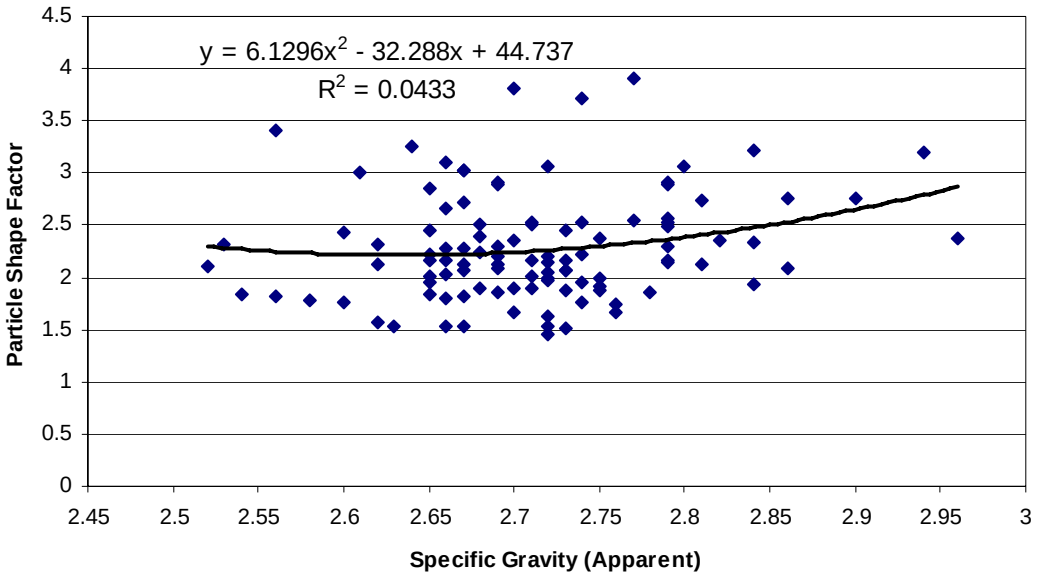

Figure F.55: Particle Shape Factor vs. Specific Gravity (Apparent)

Appendix G: Test Correlation Graphs for the Partial Data Set II

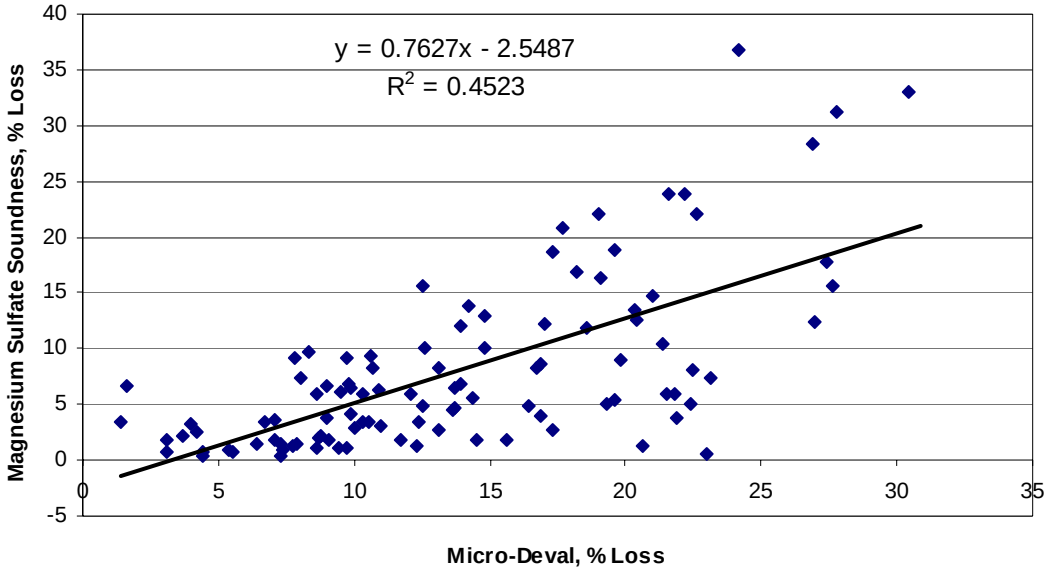

Figure G.1: Magnesium Sulfate Soundness vs. Micro-Deval

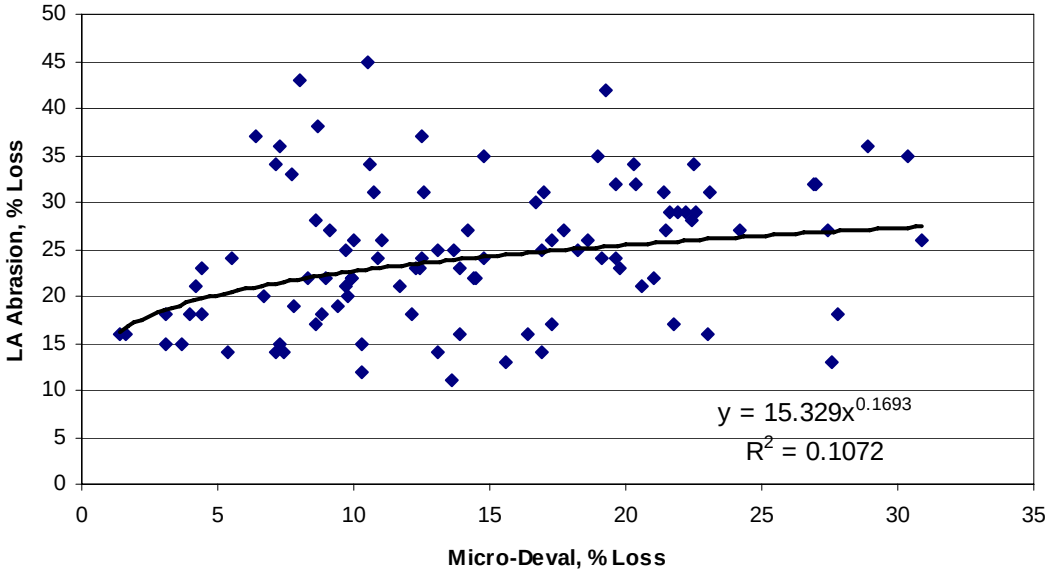

Figure G.2: L.A. Abrasion vs. Micro-Deval

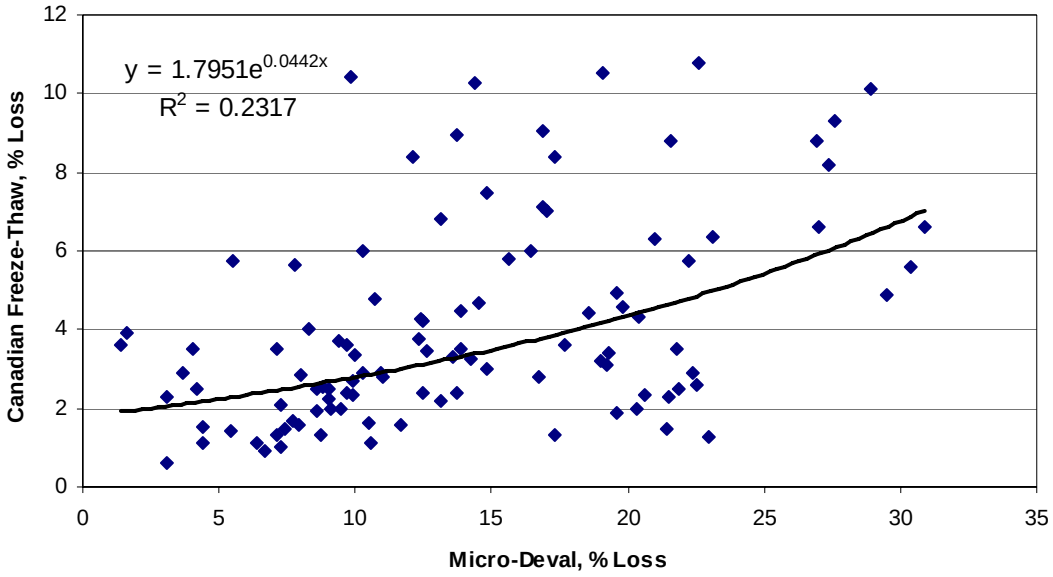

Figure G.3: Canadian Freeze-Thaw vs. Micro-Deval

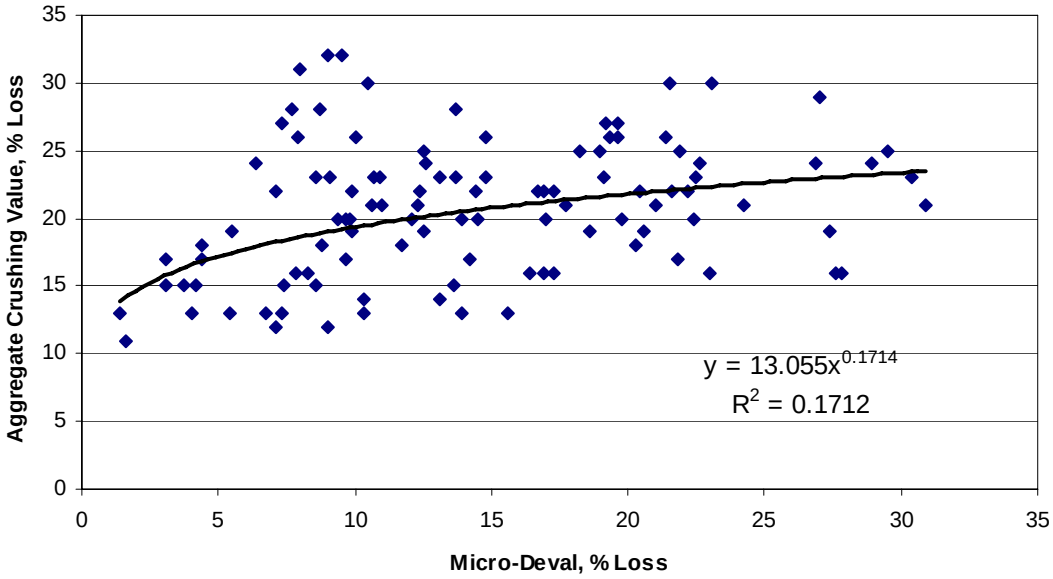

Figure G.4: Aggregate Crushing Value vs. Micro-Deval

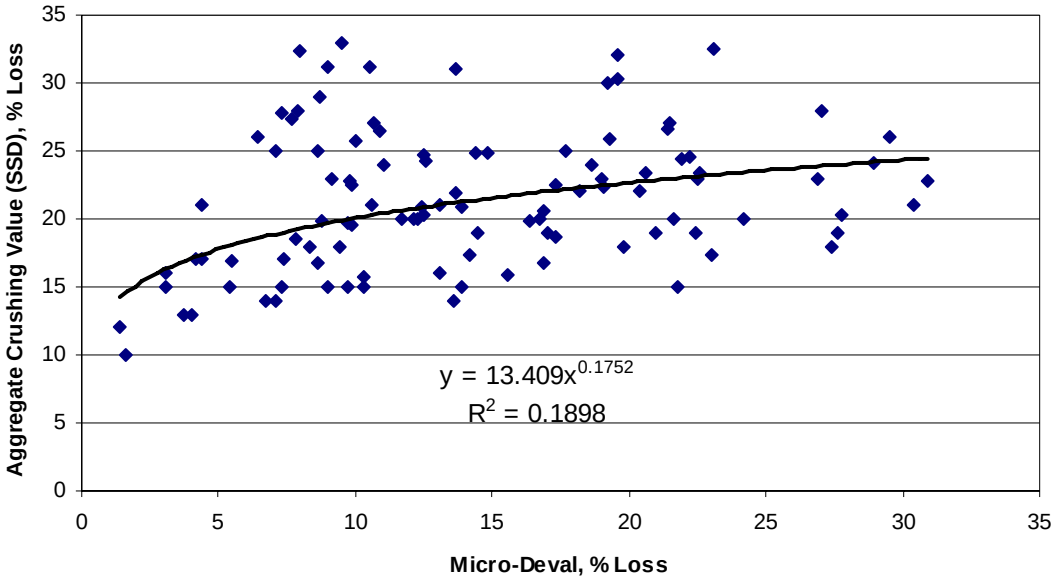

Figure G.5: Aggregate Crushing Value (SSD) vs. Micro-Deval

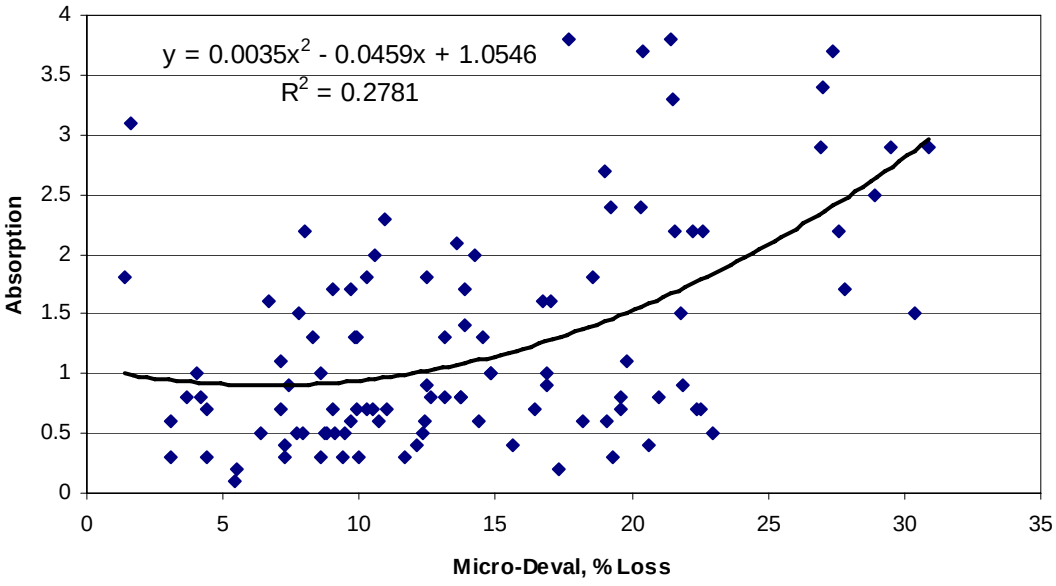

Figure G.6: Absorption vs. Micro-Deval

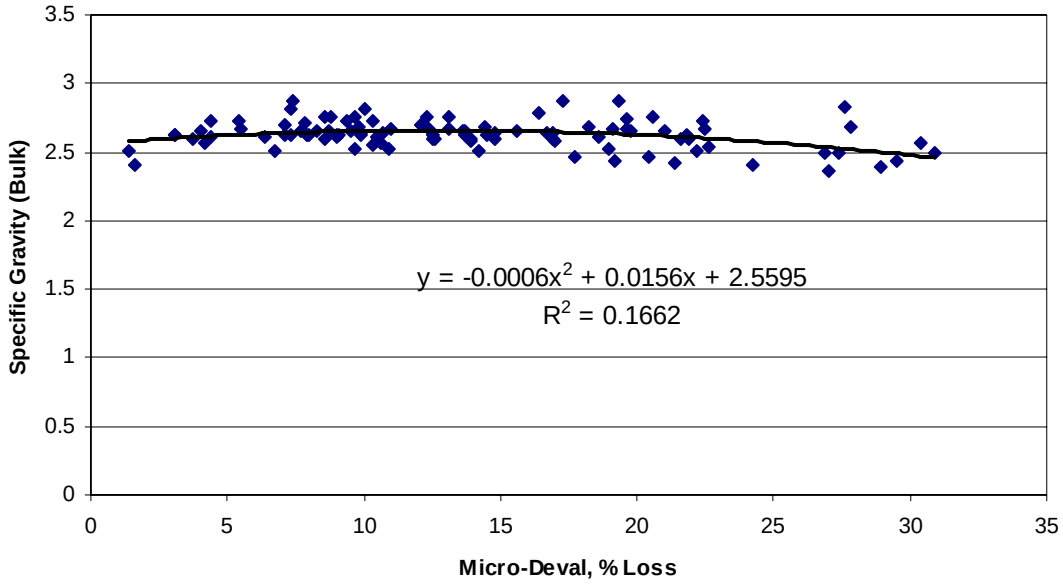

Figure G.7: Specific Gravity (Bulk) vs. Micro-Deval

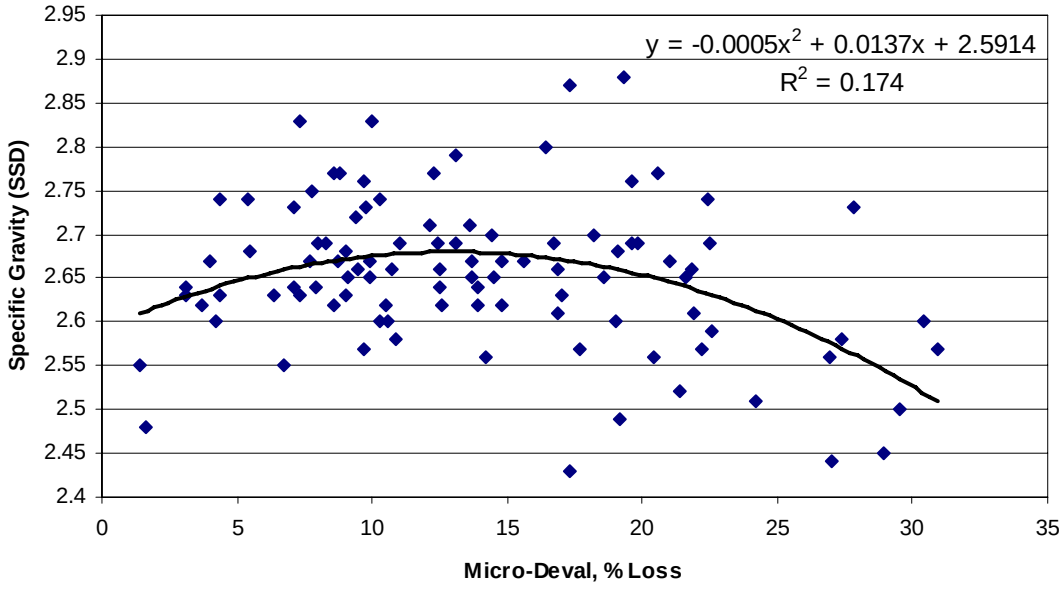

Figure G.8: Specific Gravity (SSD) vs. Micro-Deval

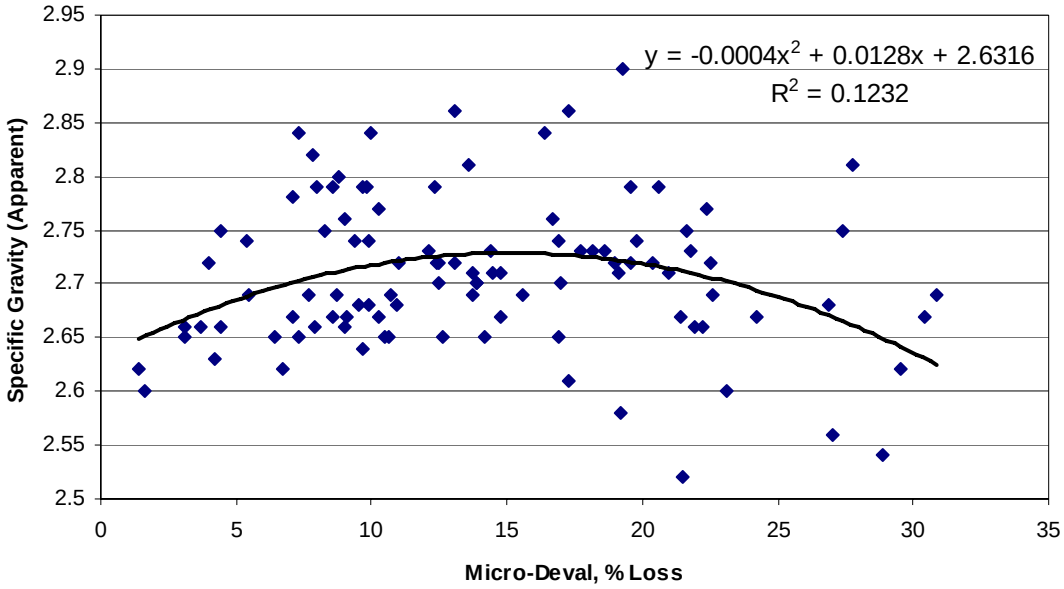

Figure G.9: Specific Gravity (Apparent) vs. Micro-Deval

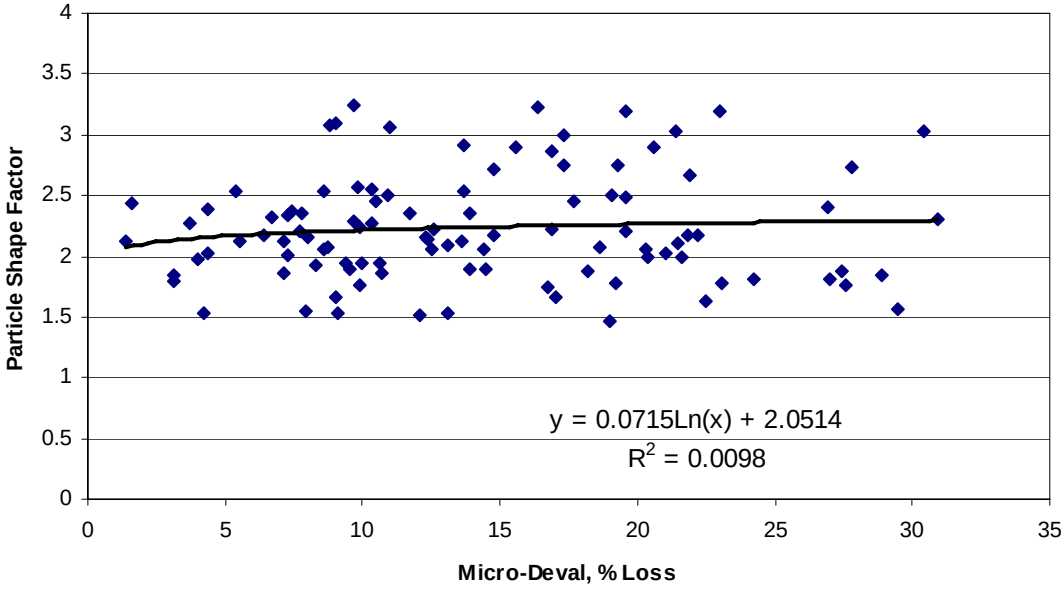

Figure G.10: Particle Shape Factor vs. Micro-Deval

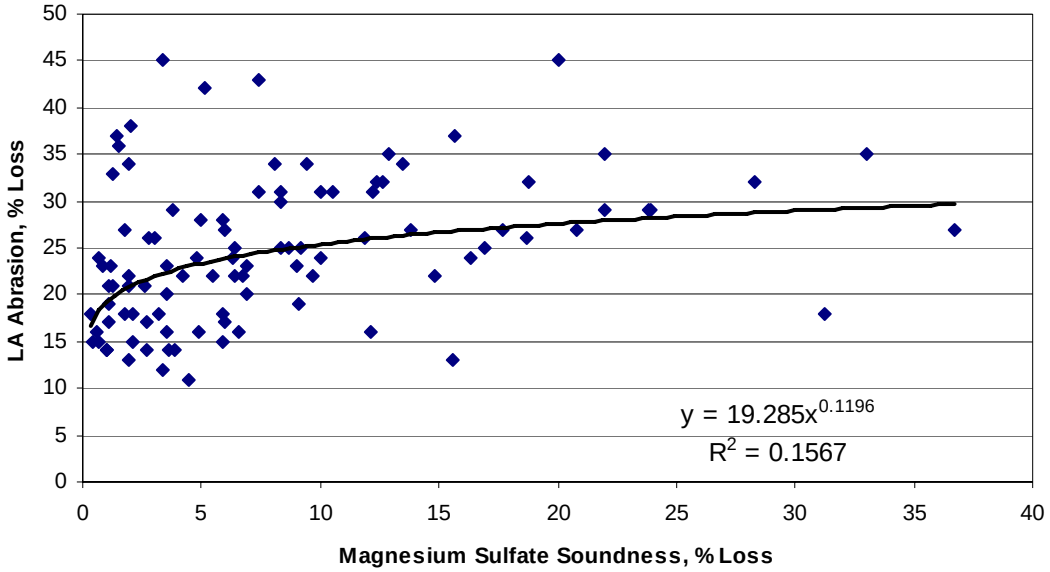

Figure G.11: L.A. Abrasion vs. Magnesium Sulfate Soundness

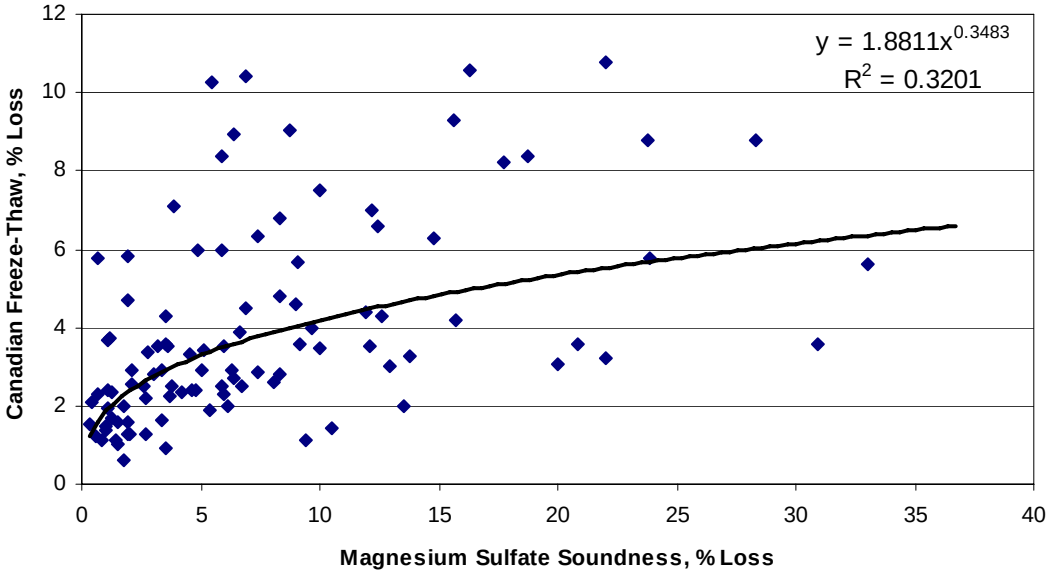

Figure G.12: Canadian Freeze-Thaw vs. Magnesium Sulfate Soundness

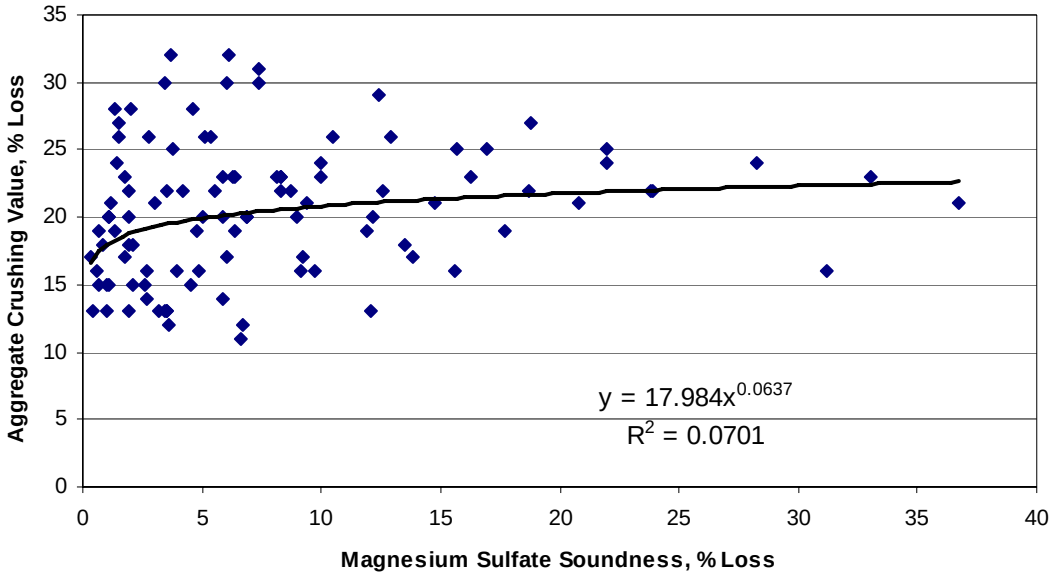

Figure G.13: Aggregate Crushing Value vs. Magnesium Sulfate Soundness

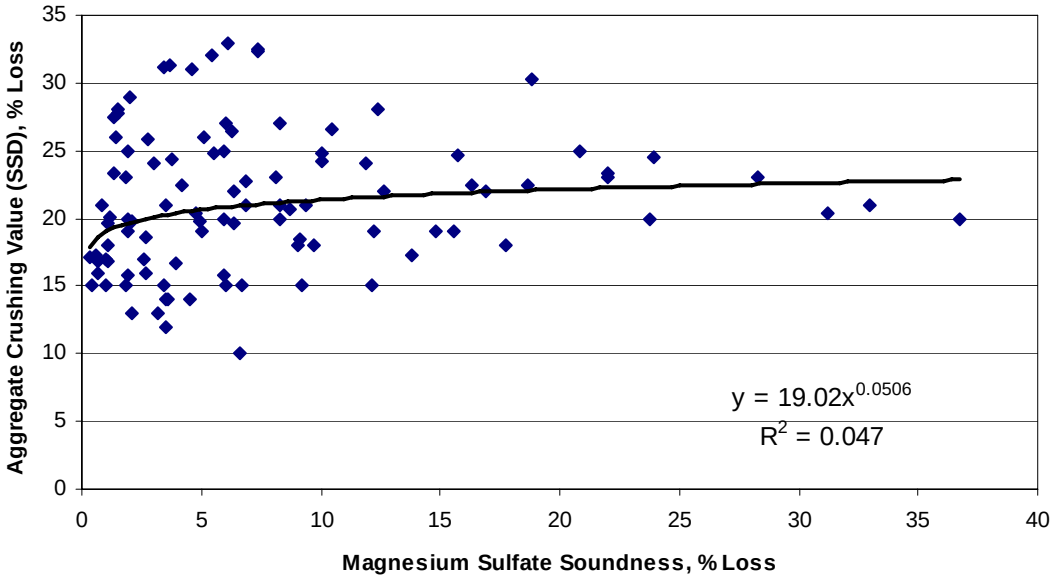

Figure G.14: Aggregate Crushing Value (SSD) vs. Magnesium Sulfate Soundness

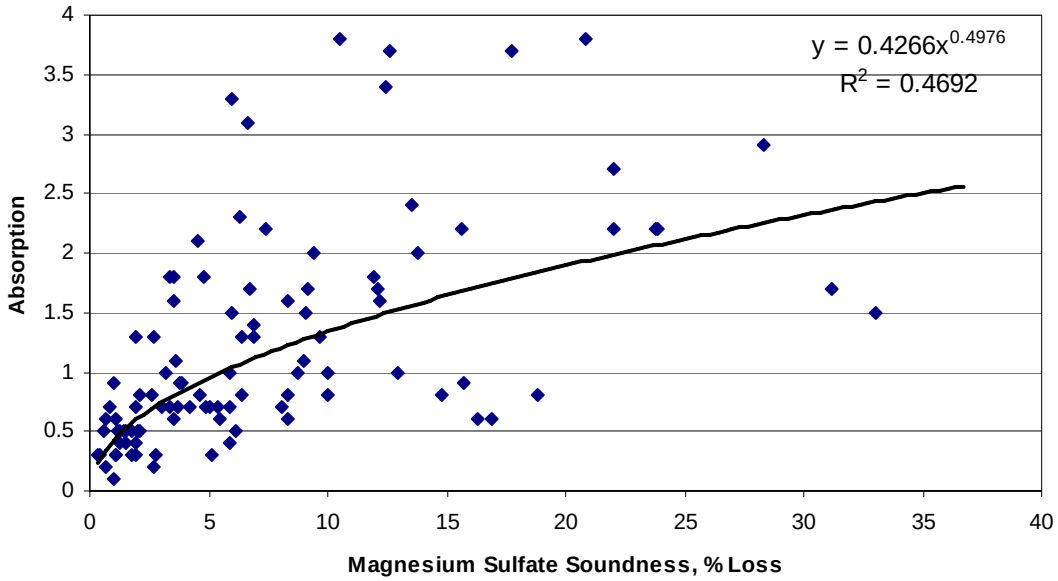

Figure G.15: Absorption vs. Magnesium Sulfate Soundness

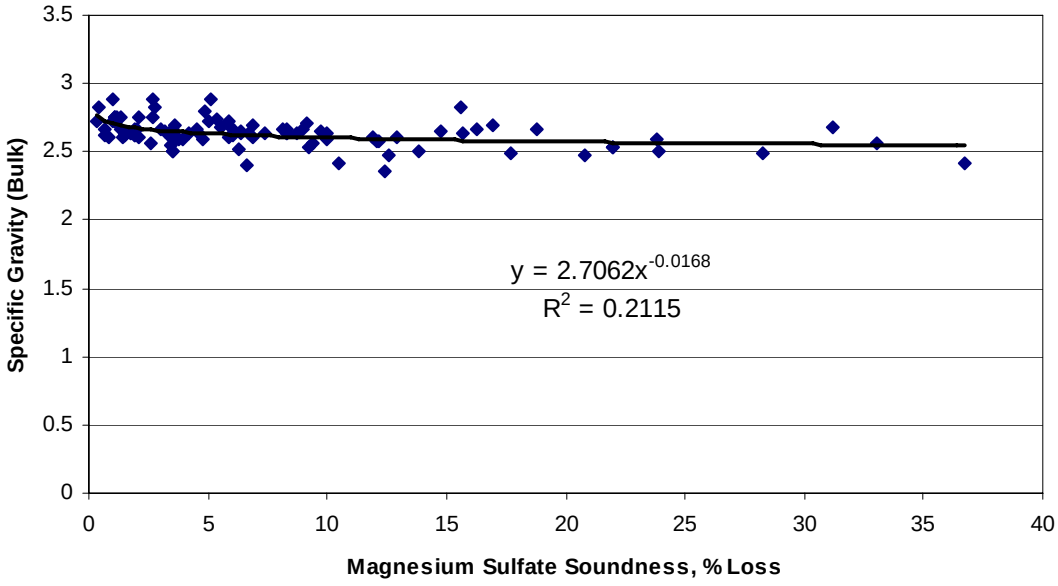

Figure G.16: Specific Gravity (Bulk) vs. Magnesium Sulfate Soundness

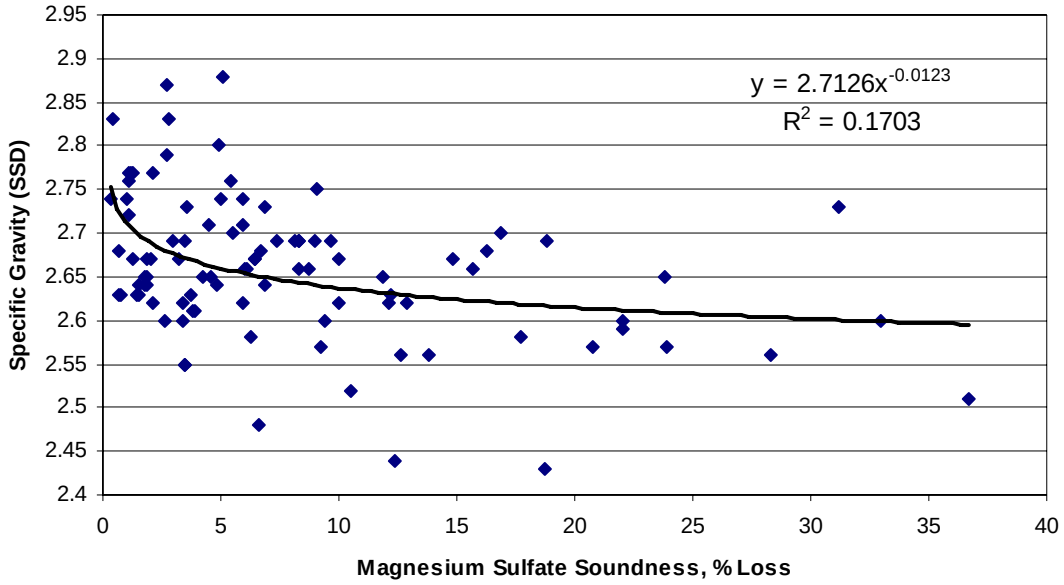

Figure G.17: Specific Gravity (SSD) vs. Magnesium Sulfate Soundness

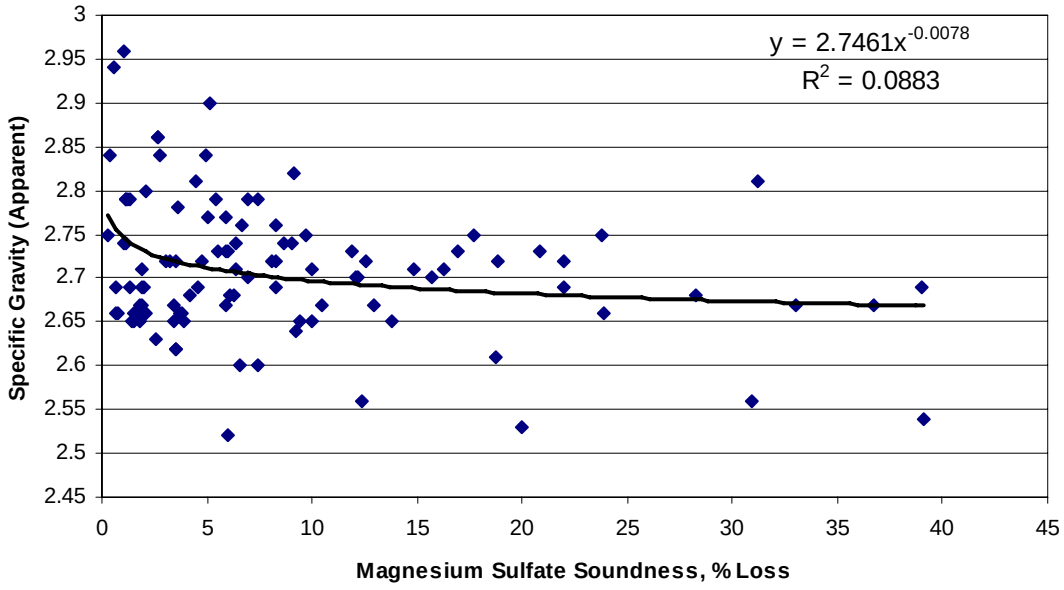

Figure G.18: Specific Gravity (Apparent) vs. Magnesium Sulfate Soundness

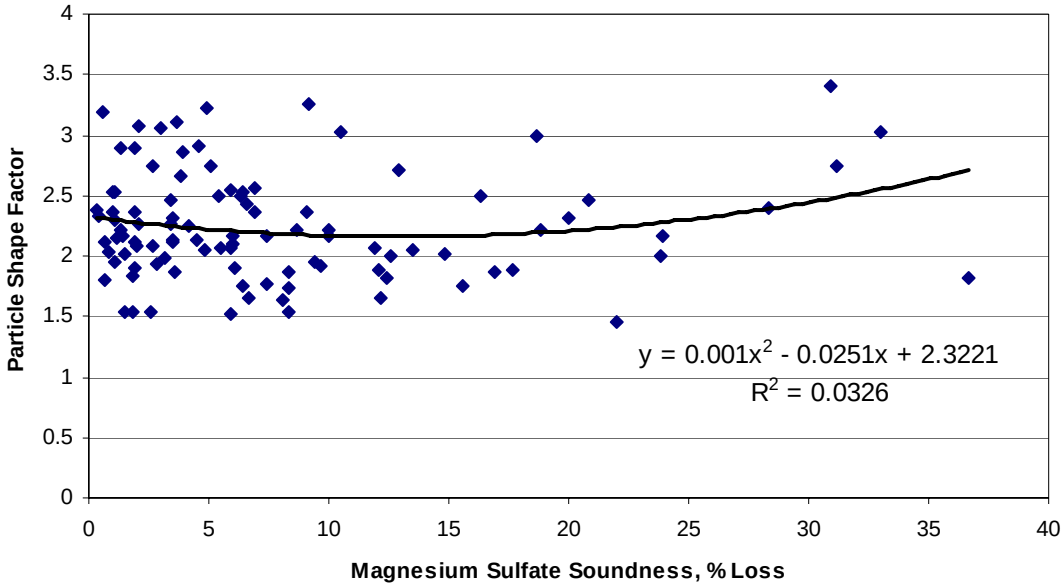

Figure G.19: Particle Shape Factor vs. Magnesium Sulfate Soundness

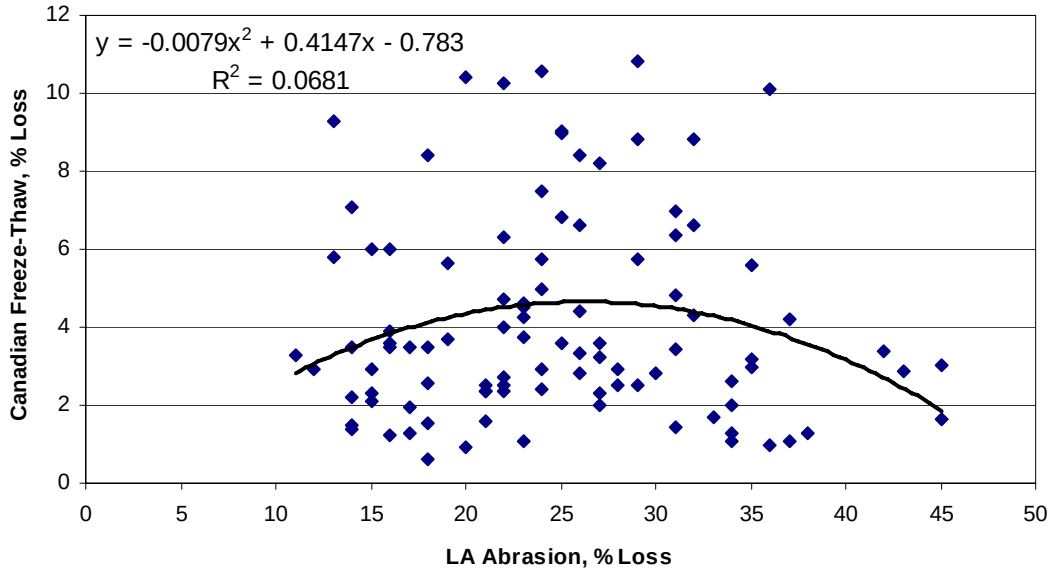

Figure G.20: Canadian Freeze-Thaw vs. L.A. Abrasion

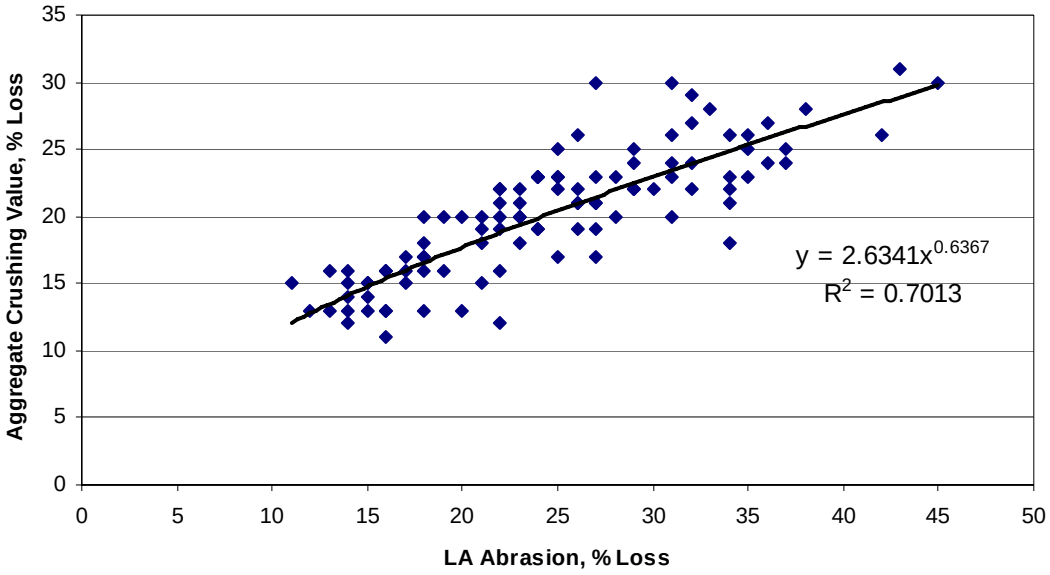

Figure G.21: Aggregate Crushing Value vs. L.A. Abrasion

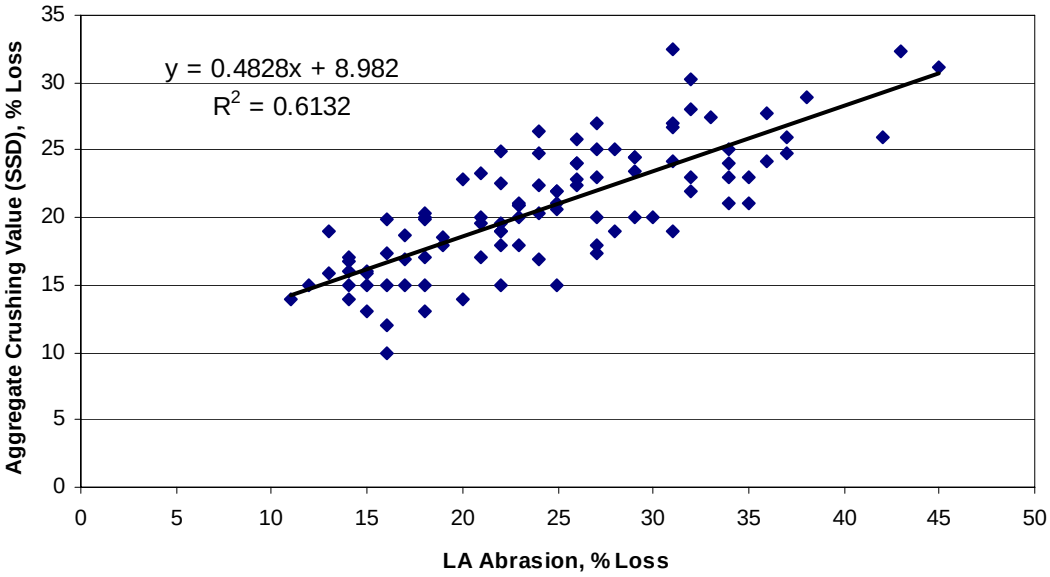

Figure G.22: Aggregate Crushing Value (SSD) vs. L.A. Abrasion

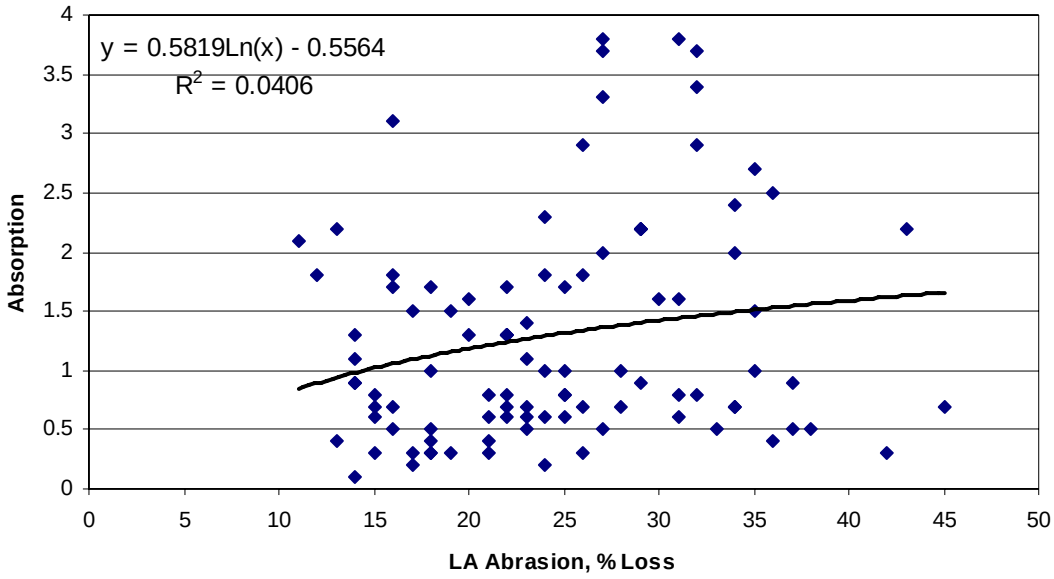

Figure G.23: Absorption vs. L.A. Abrasion

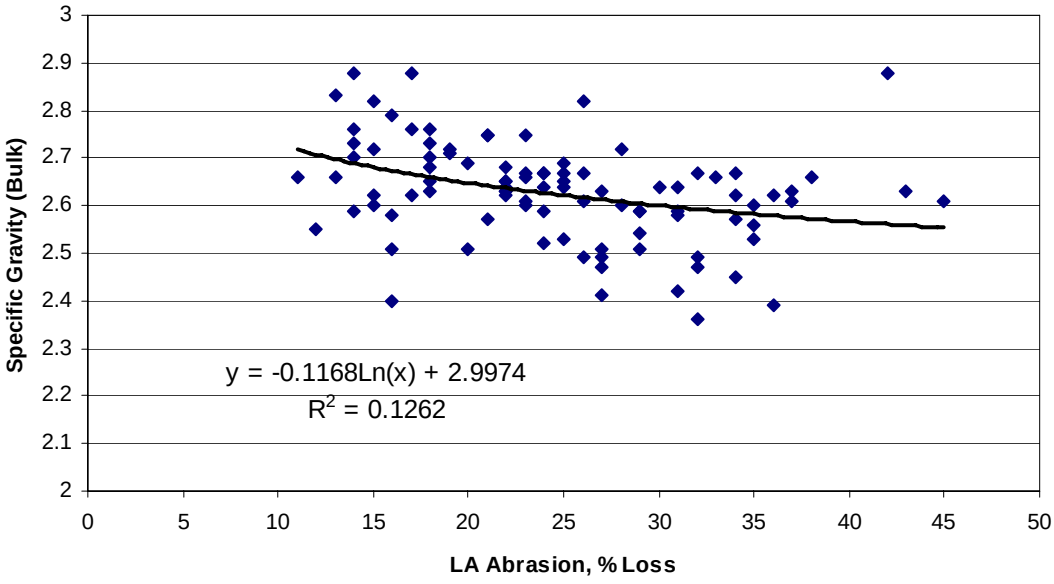

Figure G.24: Specific Gravity (Bulk) vs. L.A. Abrasion

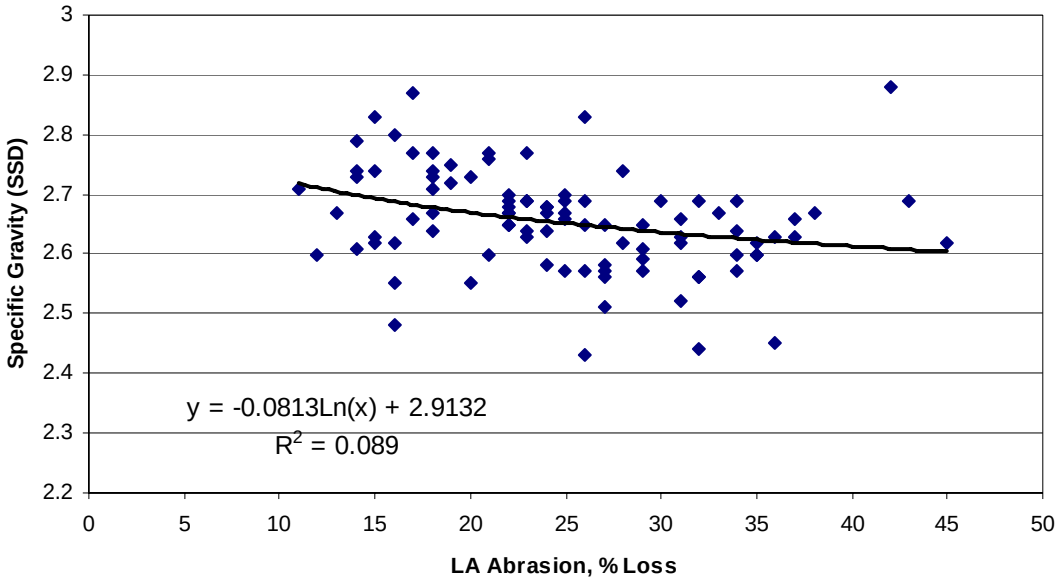

Figure G.25: Specific Gravity (SSD) vs. L.A. Abrasion

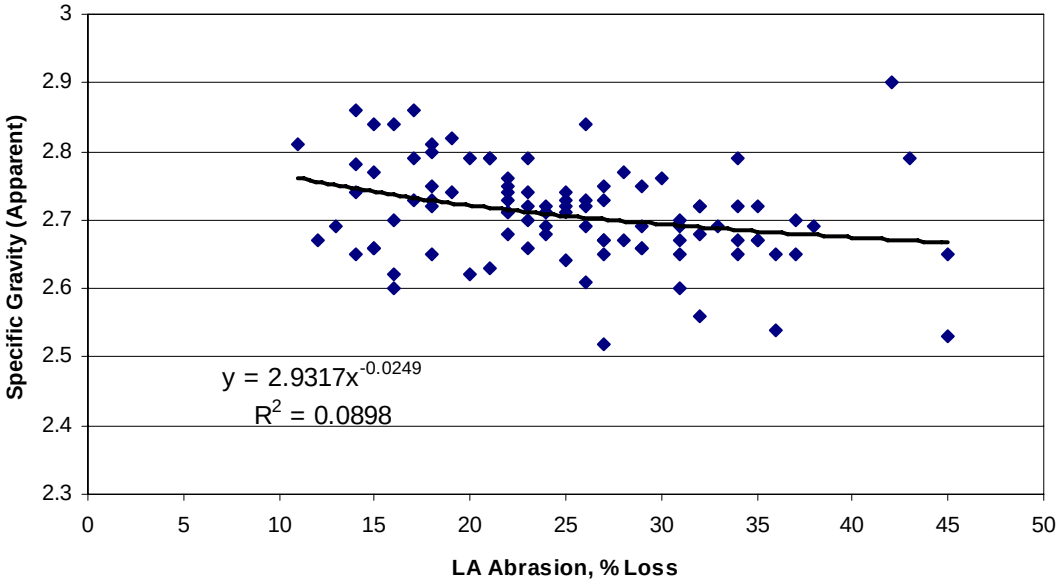

Figure G.26: Specific Gravity (Apparent) vs. L.A. Abrasion

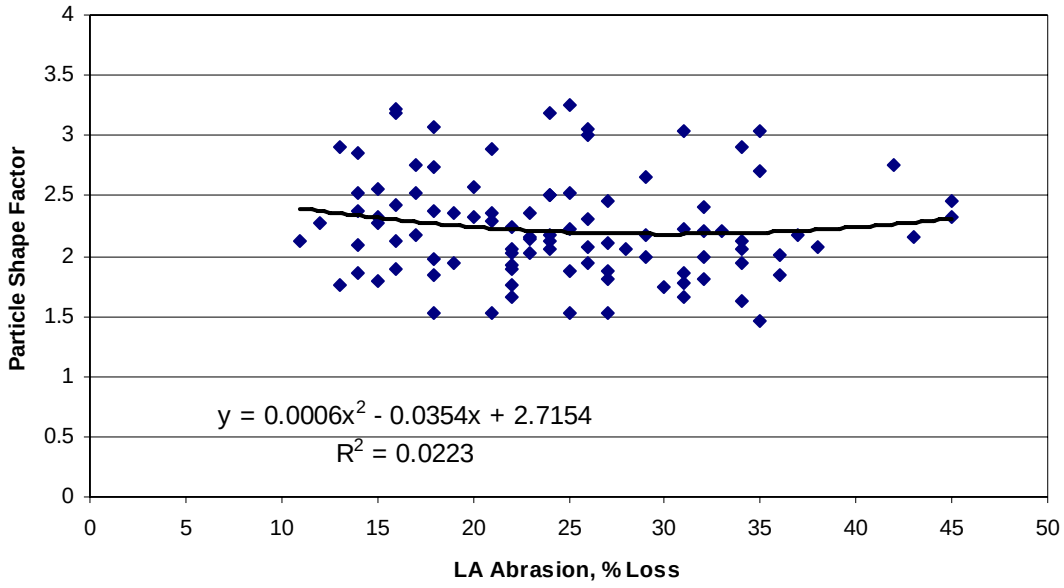

Figure G.27: Particle Shape Factor vs. L.A. Abrasion

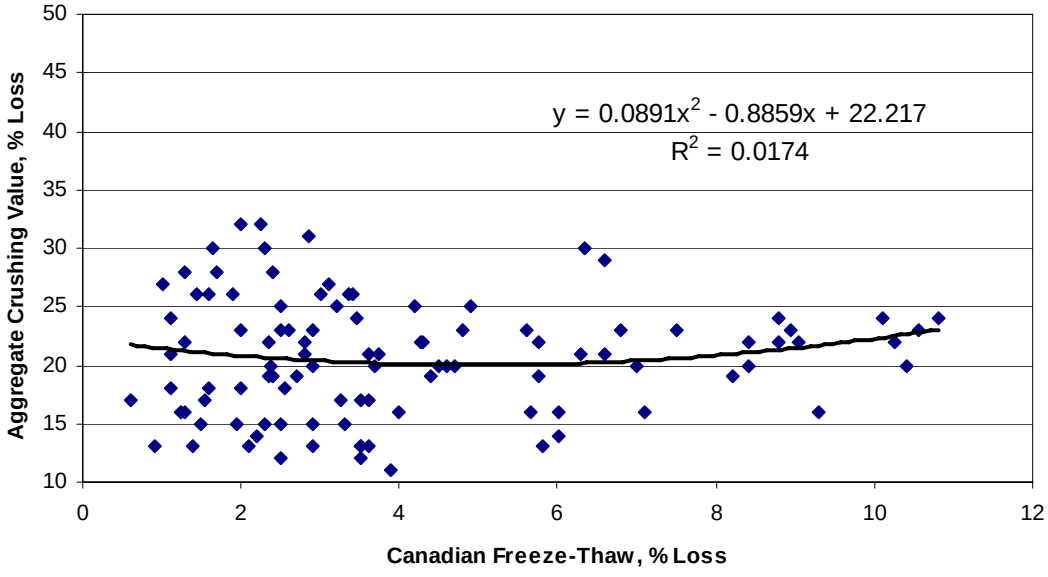

Figure G.28: Aggregate Crushing Value vs. Canadian Freeze-Thaw

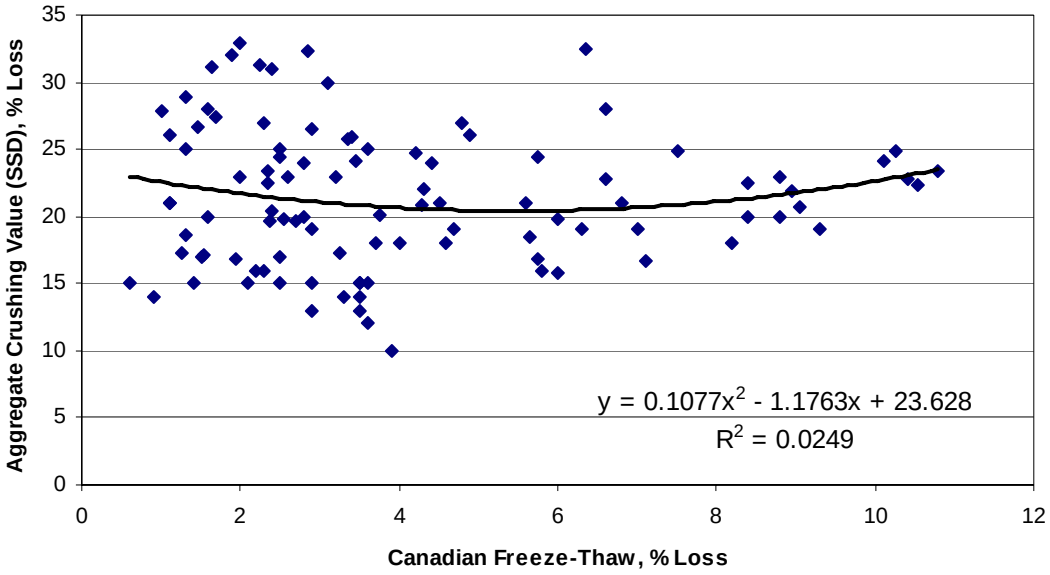

Figure G.29: Aggregate Crushing Value (SSD) vs. Canadian Freeze-Thaw

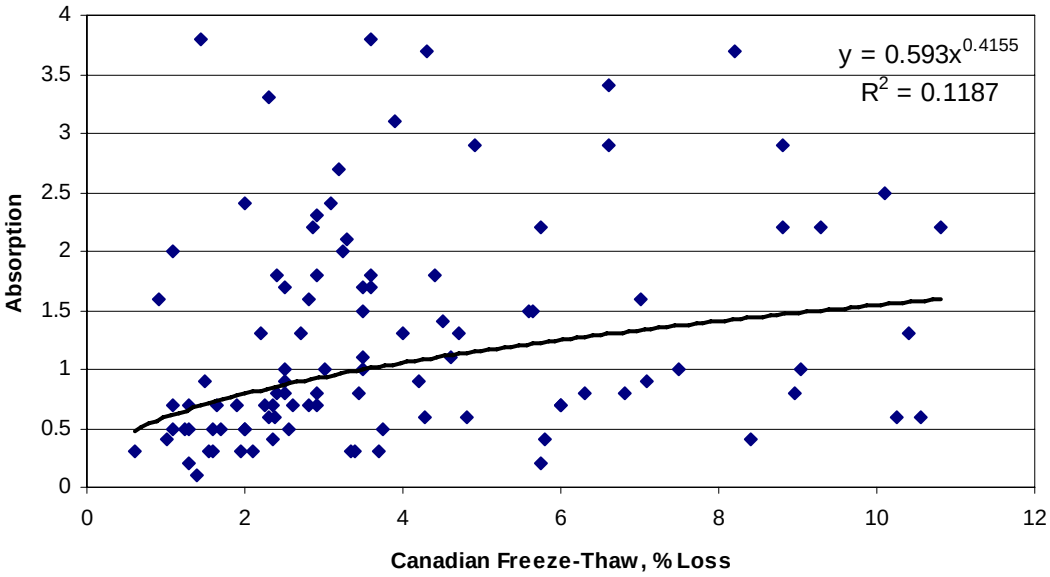

Figure G.30: Absorption vs. Canadian Freeze-Thaw

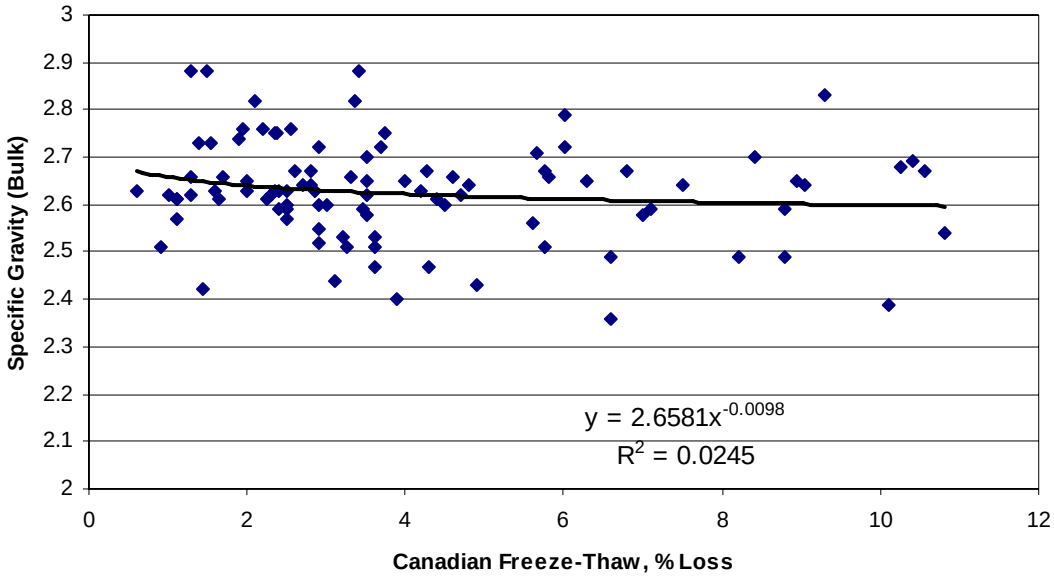

Figure G.31: Specific Gravity (Bulk) vs. Canadian Freeze-Thaw

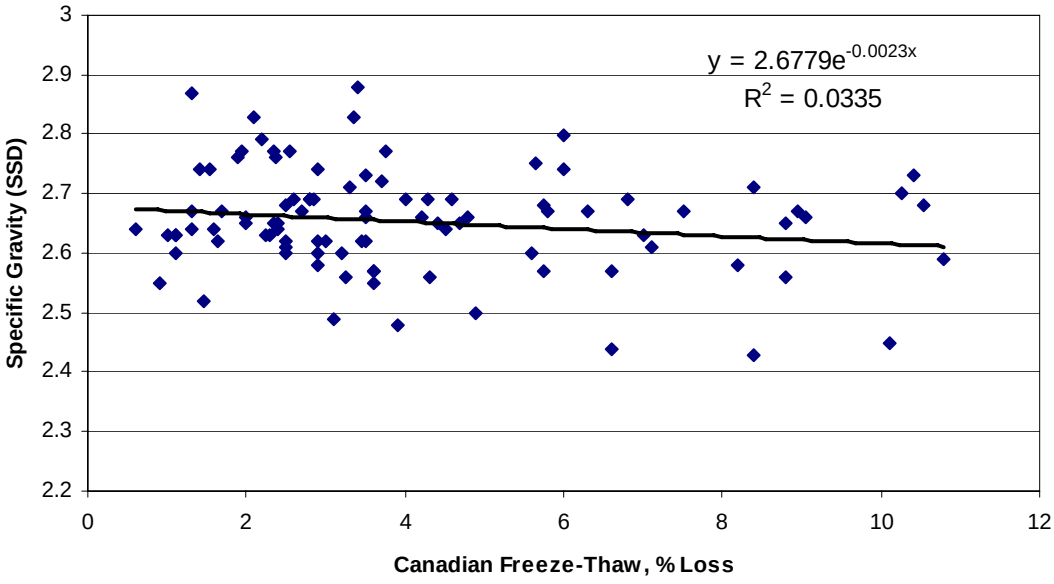

Figure G.32: Specific Gravity (SSD) vs. Canadian Freeze-Thaw

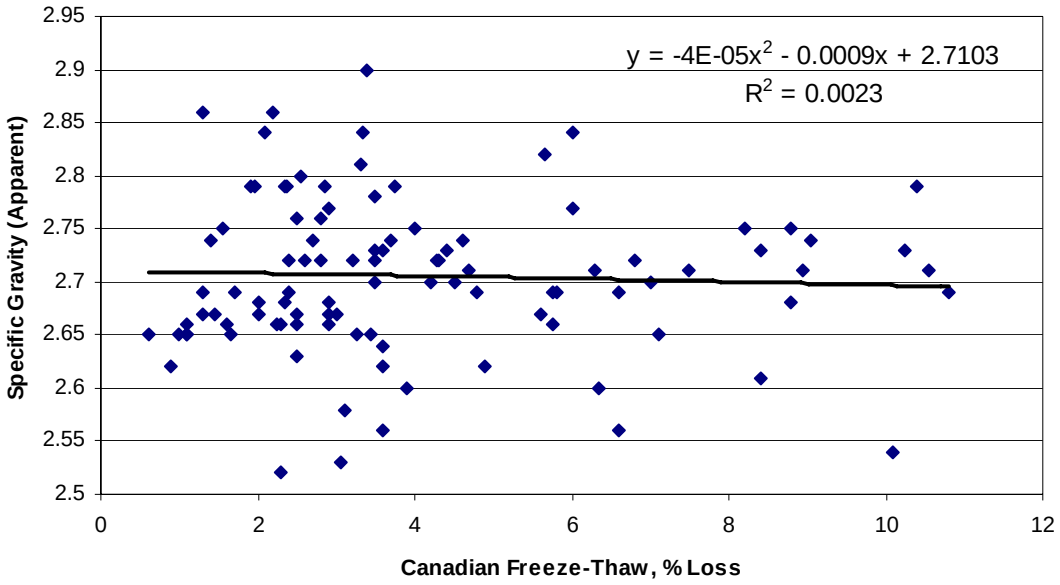

Figure G.33: Specific Gravity (Apparent) vs. Canadian Freeze-Thaw

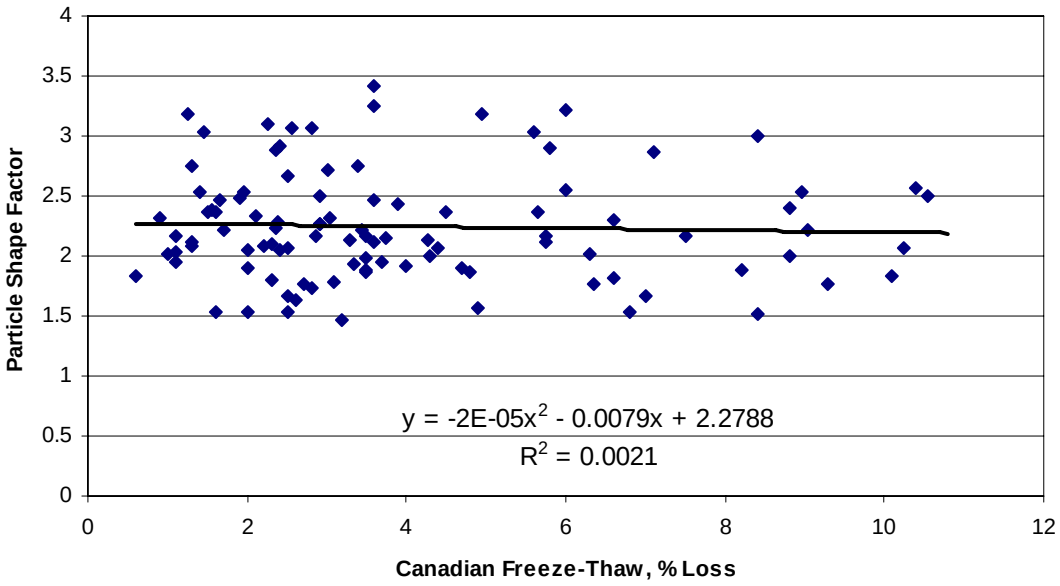

Figure G.34: Particle Shape Factor vs. Canadian Freeze-Thaw

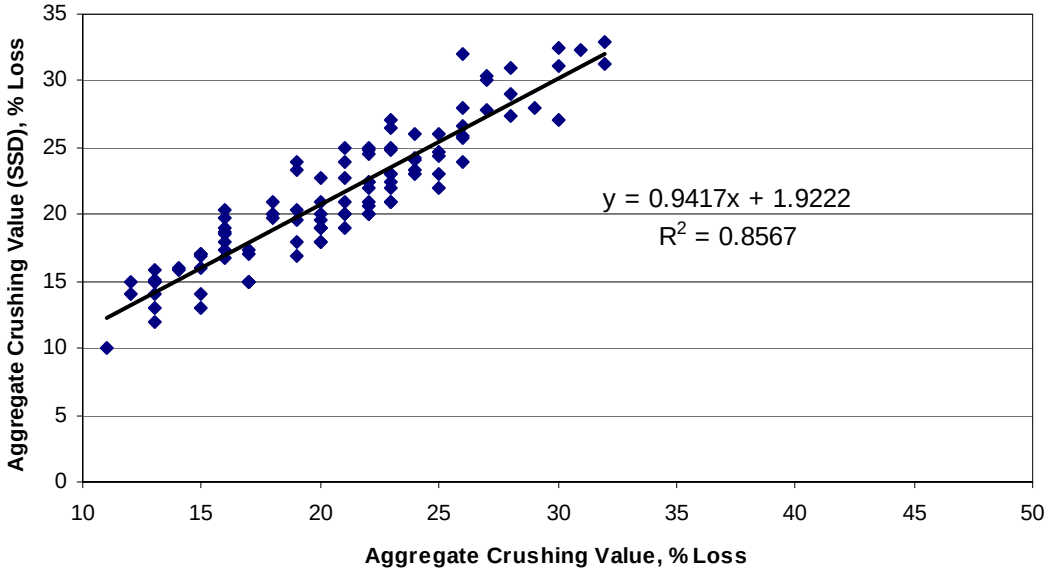

Figure G.35: Aggregate Crushing Value (SSD) vs. Aggregate Crushing Value

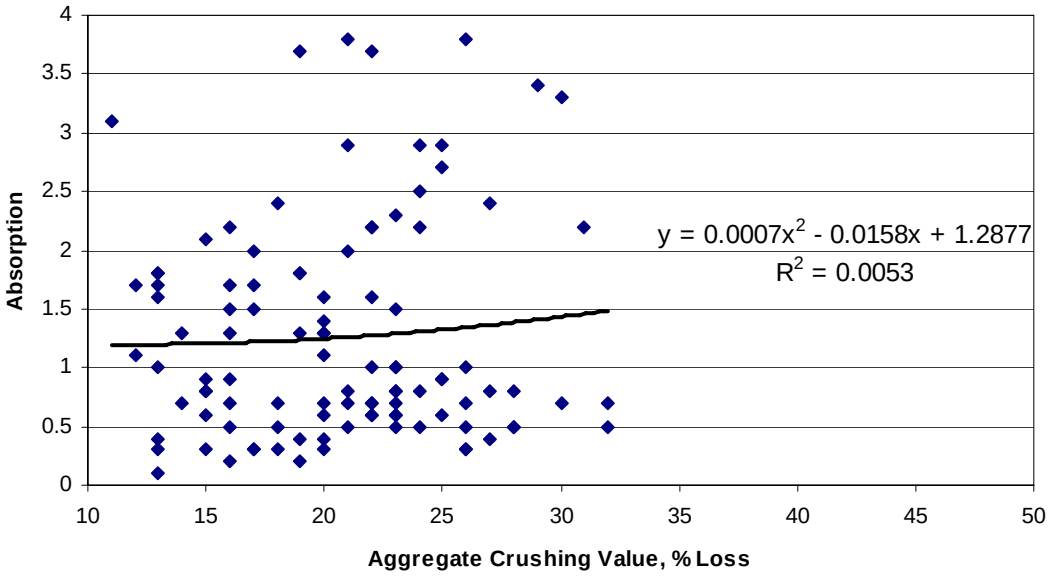

Figure G.36: Absorption vs. Aggregate Crushing Value

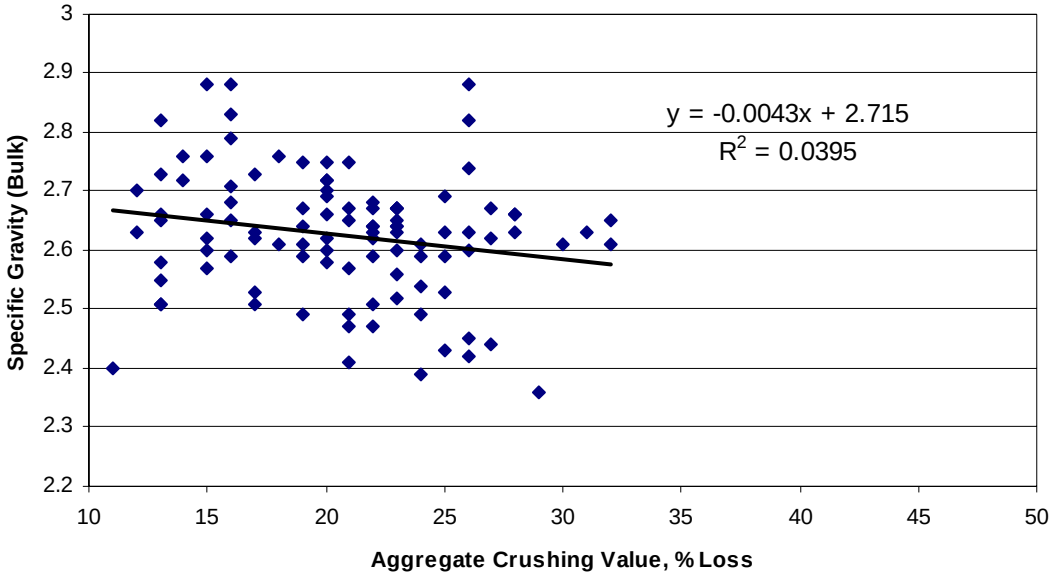

Figure G.37: Specific Gravity (Bulk) vs. Aggregate Crushing Value

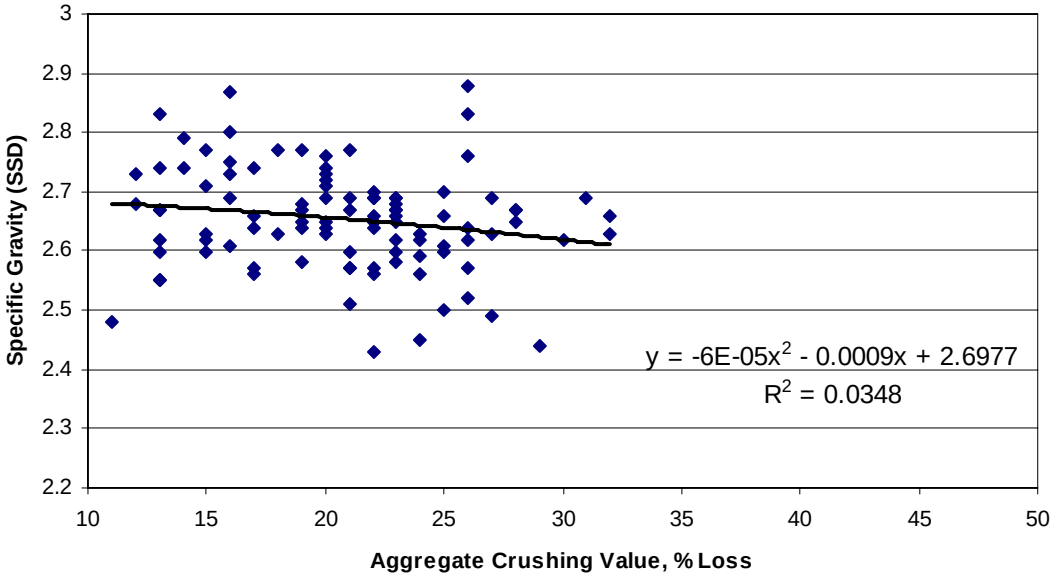

Figure G.38: Specific Gravity (SSD) vs. Aggregate Crushing Value

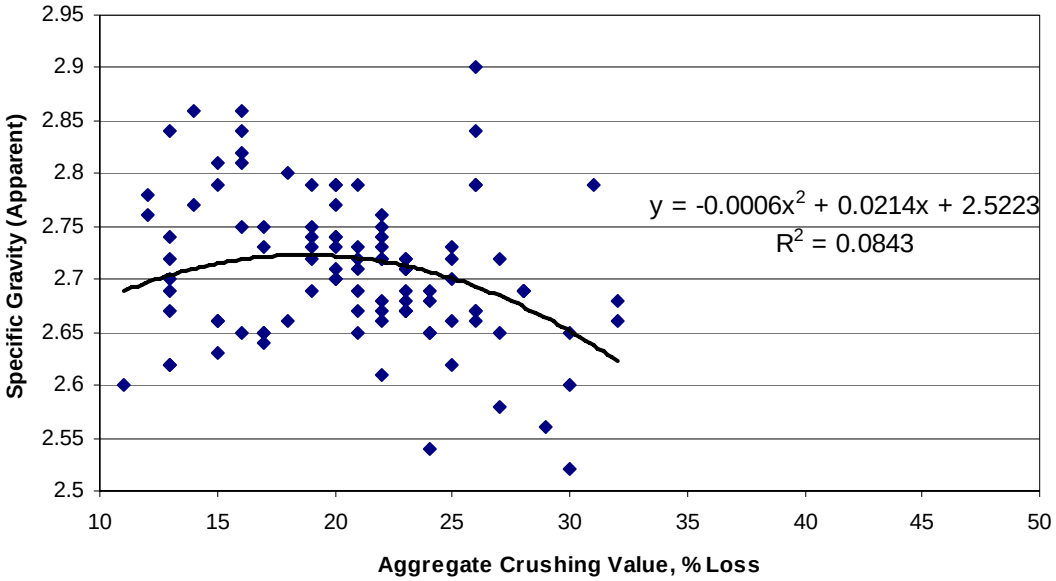

Figure G.39: Specific Gravity (Apparent) vs. Aggregate Crushing Value

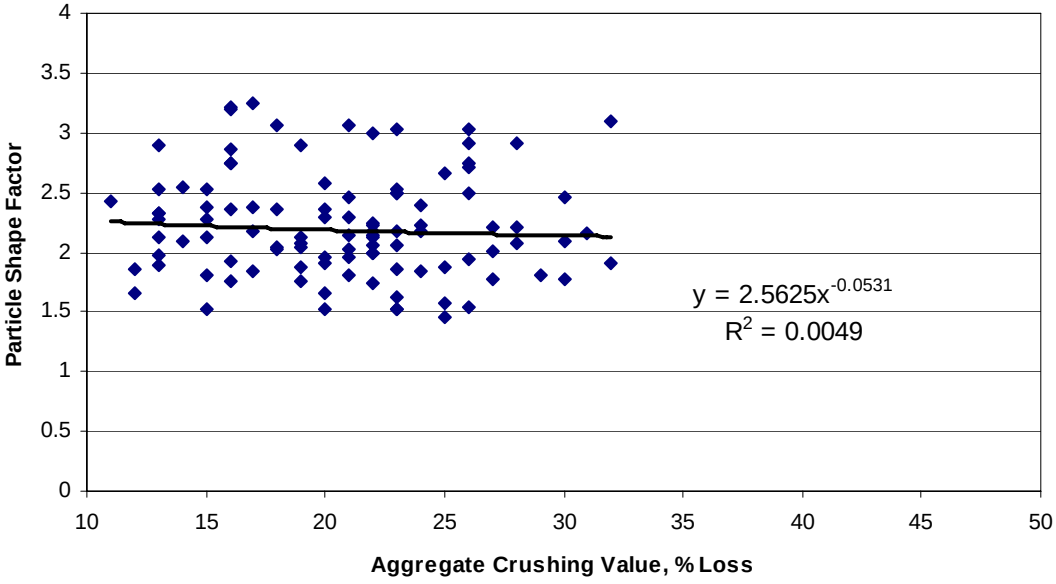

Figure G.40: Particle Shape Factor vs. Aggregate Crushing Value

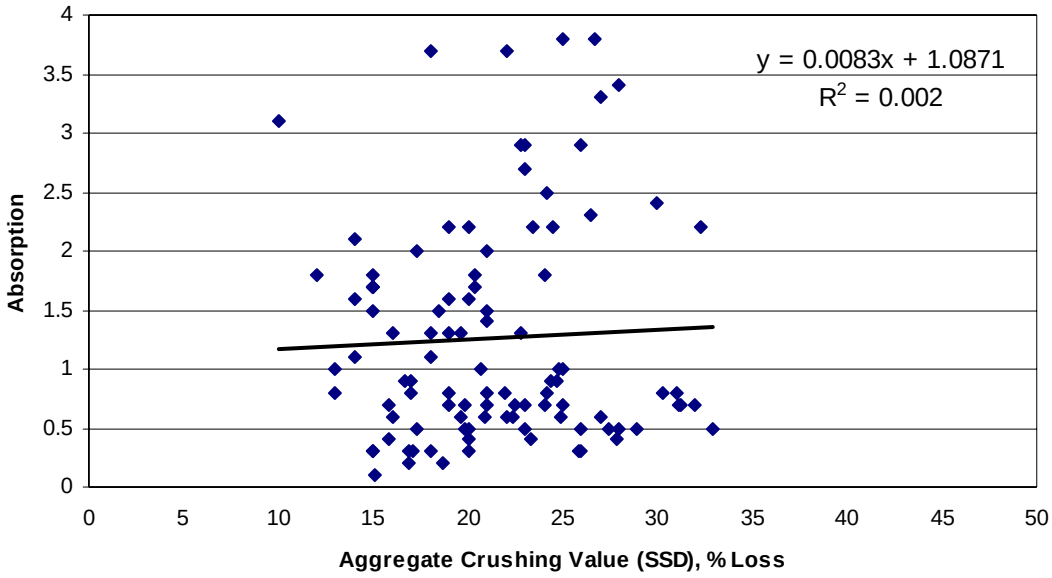

Figure G.41: Absorption vs. Aggregate Crushing Value (SSD)

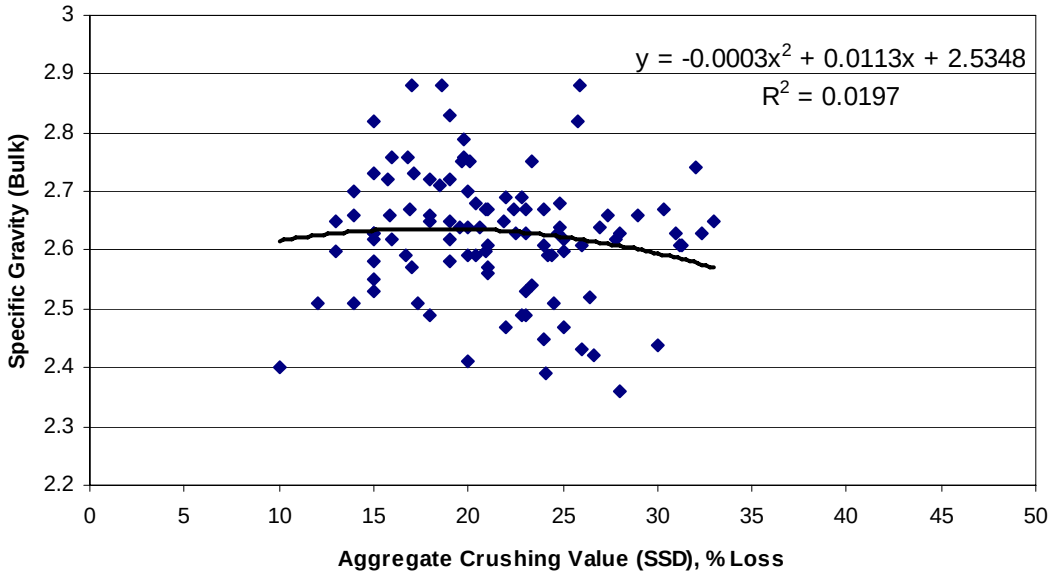

Figure G.42: Specific Gravity (Bulk) vs. Aggregate Crushing Value (SSD)

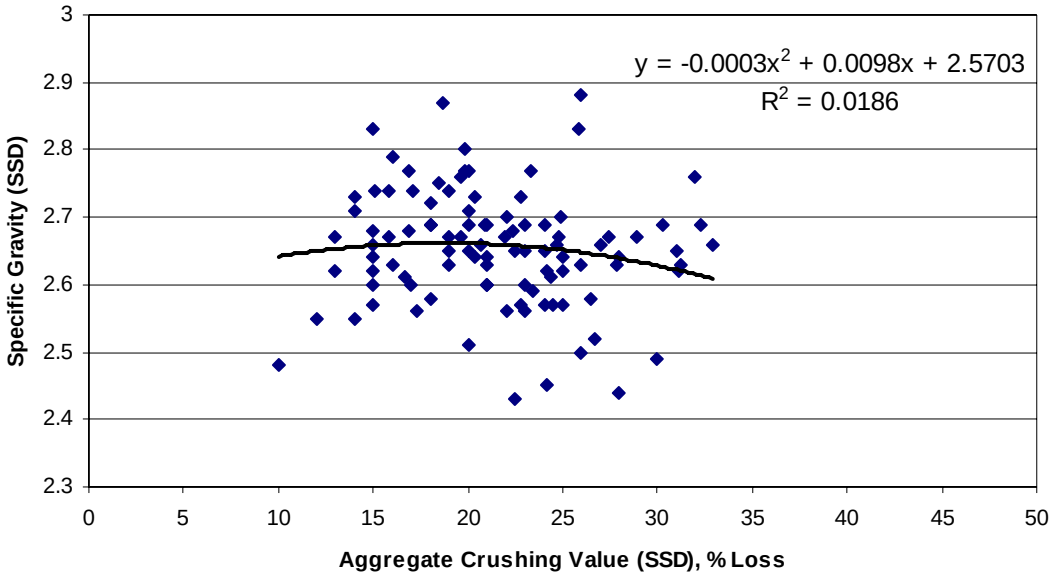

Figure G.43: Specific Gravity (SSD) vs. Aggregate Crushing Value (SSD)

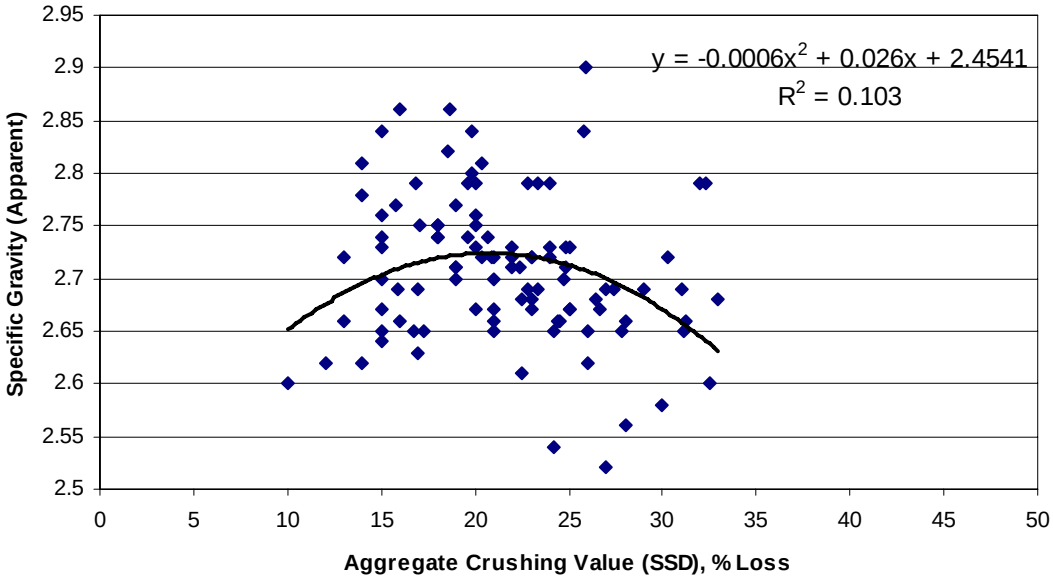

Figure G.44: Specific Gravity (Apparent) vs. Aggregate Crushing Value (SSD)

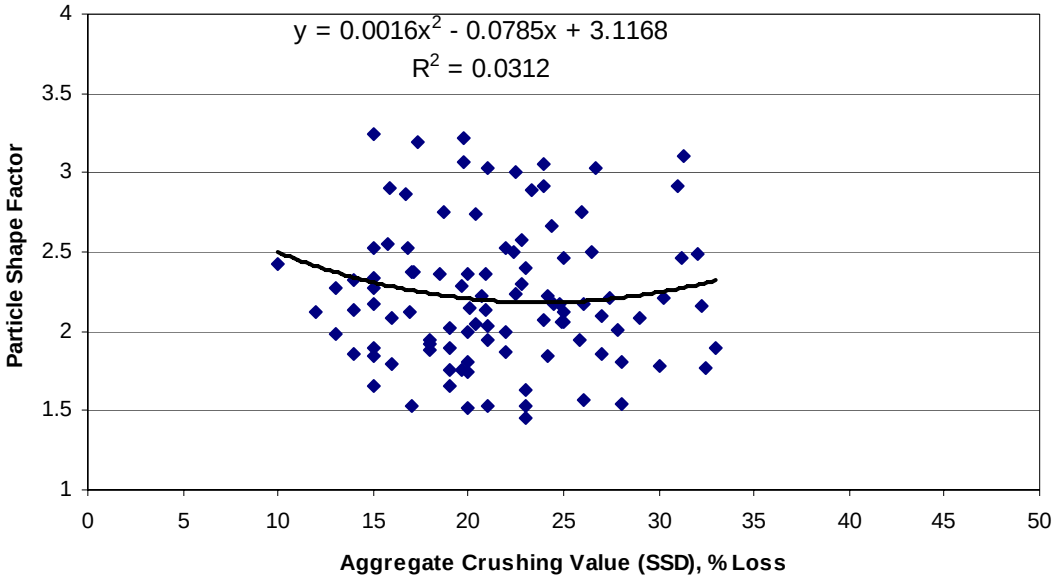

Figure G.45: Particle Shape Factor vs. Aggregate Crushing Value (SSD)

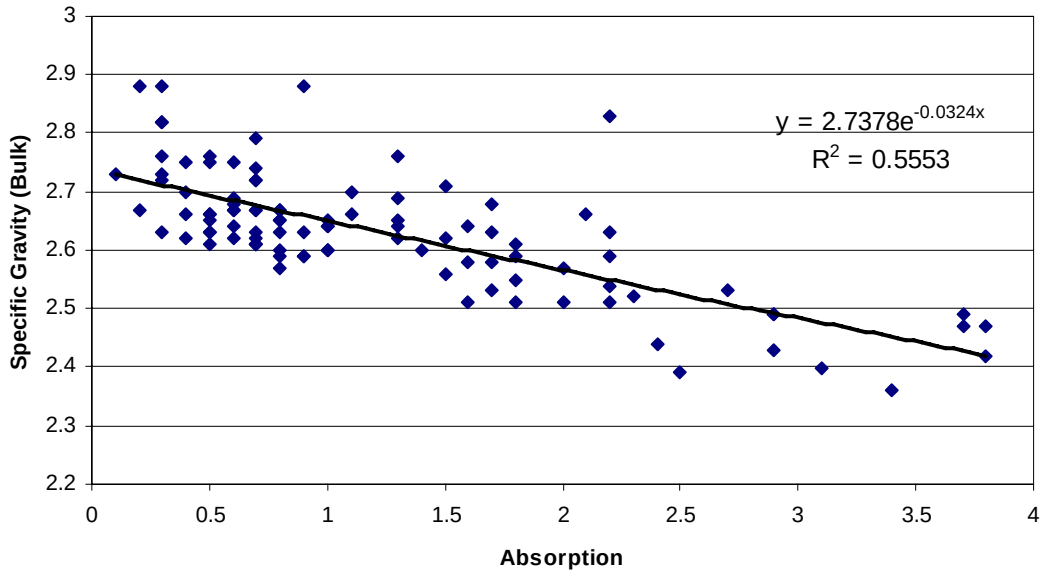

Figure G.46: Specific Gravity (Bulk) vs. Absorption

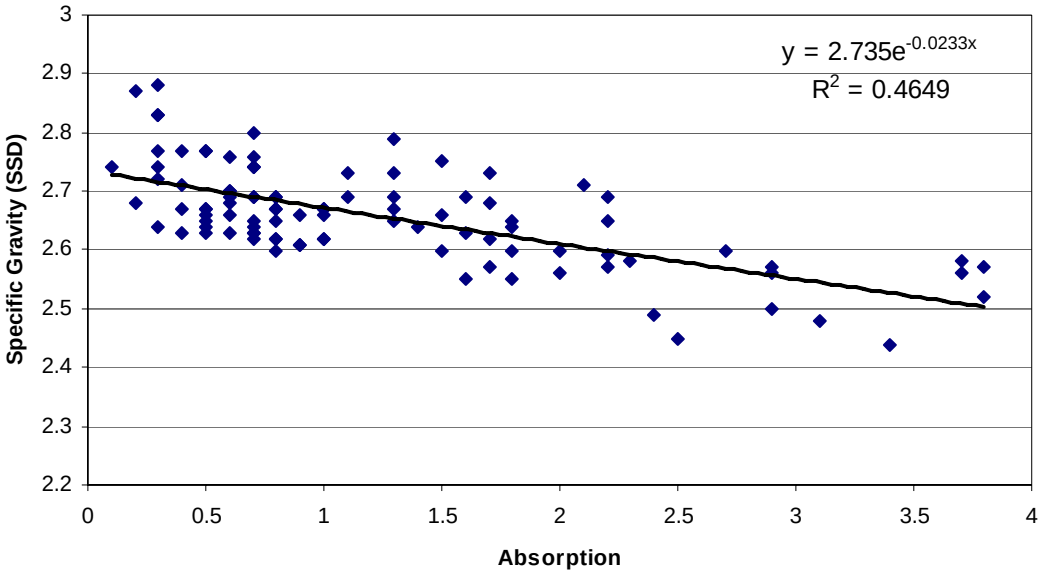

Figure G.47: Specific Gravity (SSD) vs. Absorption

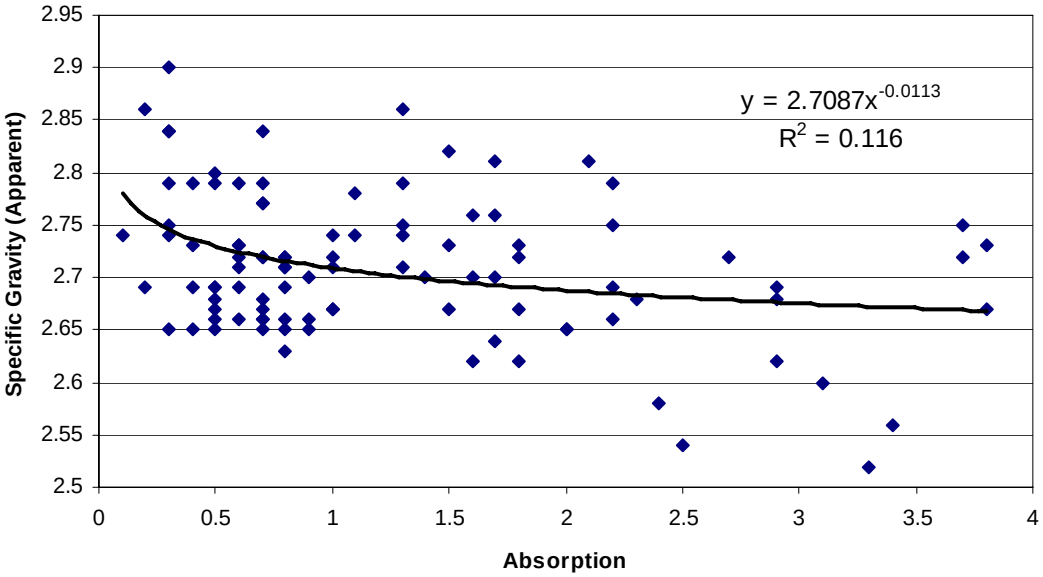

Figure G.48: Specific Gravity (Apparent) vs. Absorption

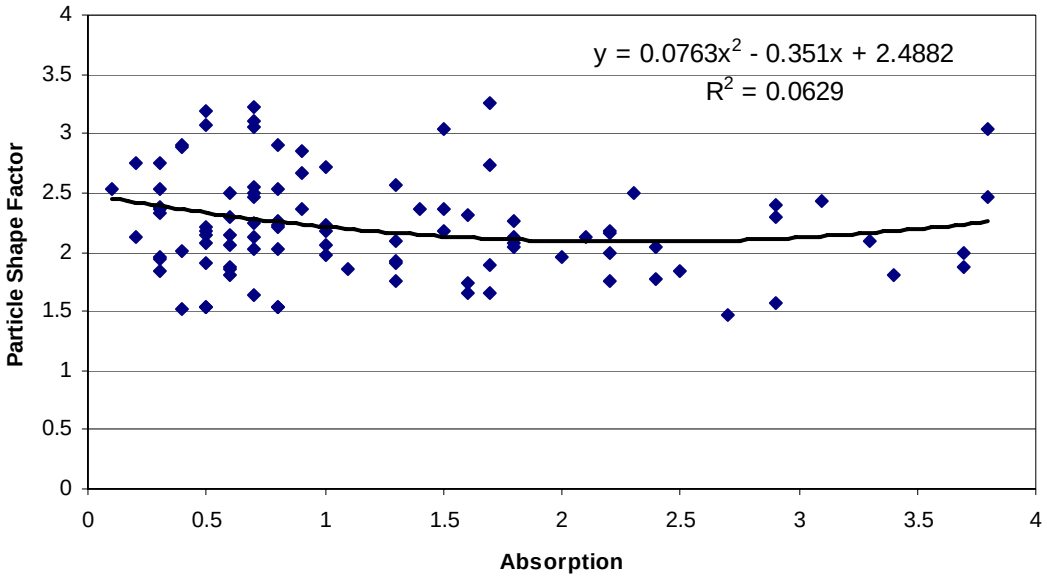

Figure G.49: Particle Shape Factor vs. Absorption

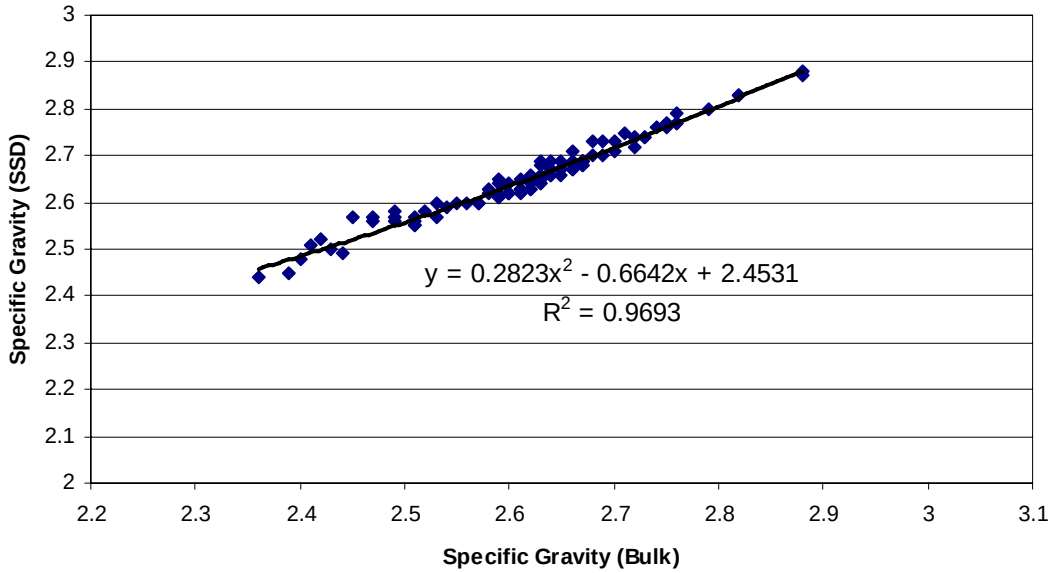

Figure G.50: Specific Gravity (SSD) vs. Specific Gravity (Bulk)

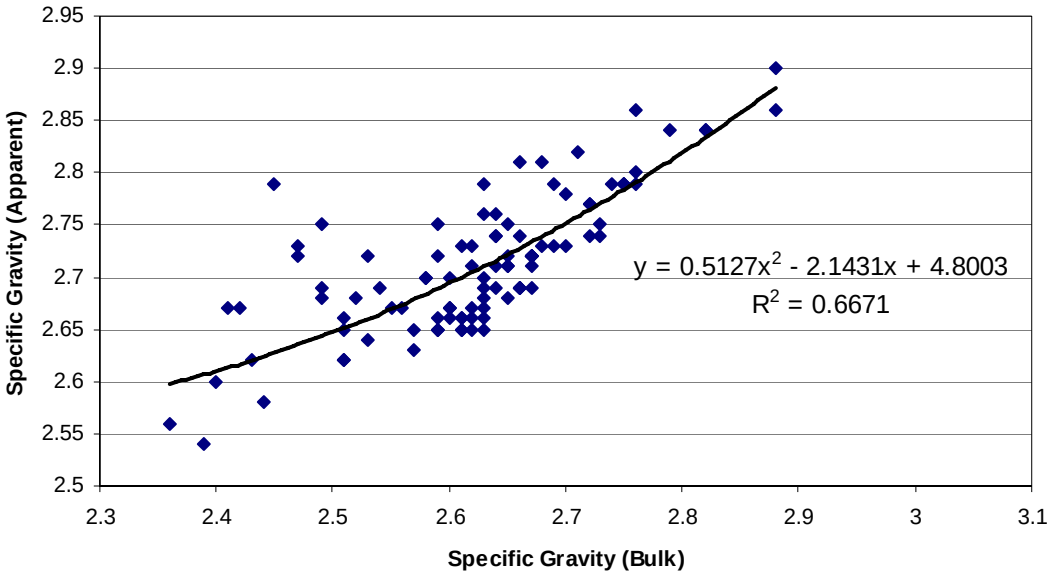

Figure G.51: Specific Gravity (Apparent) vs. Specific Gravity (Bulk)

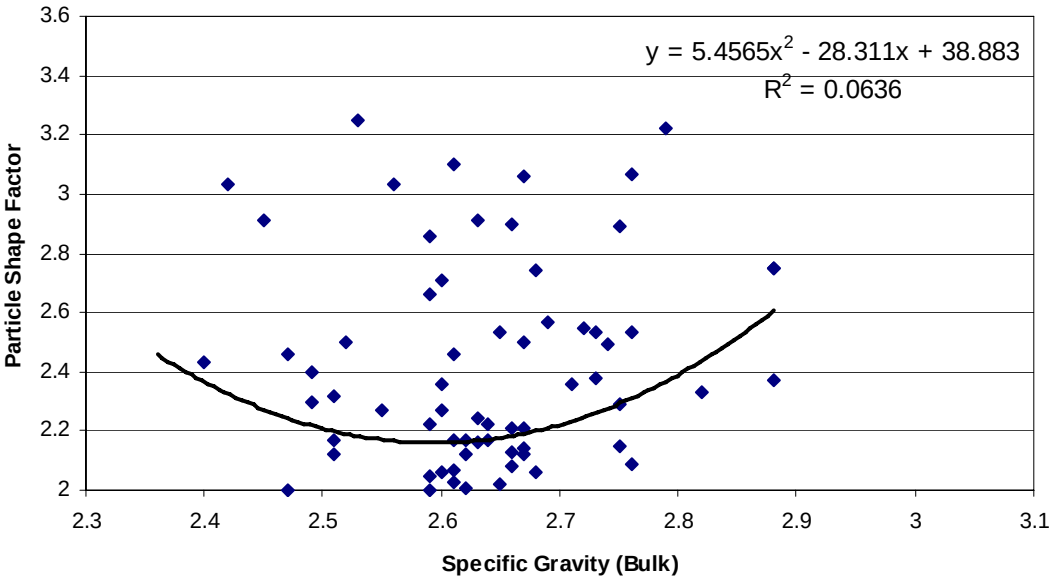

Figure G.52: Particle Shape Factor vs. Specific Gravity (Bulk)

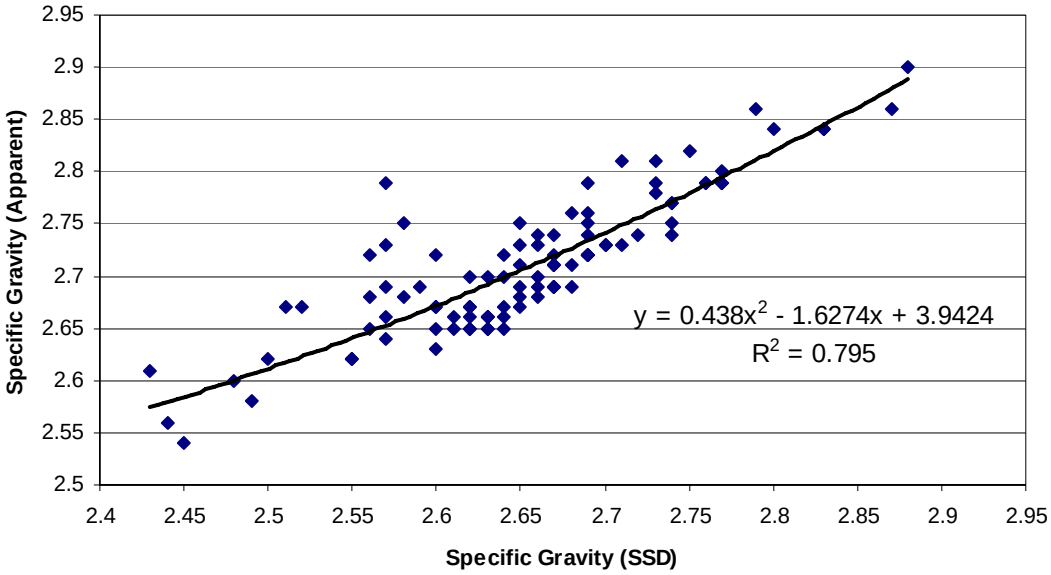

Figure G.53: Specific Gravity (Apparent) vs. Specific Gravity (SSD)

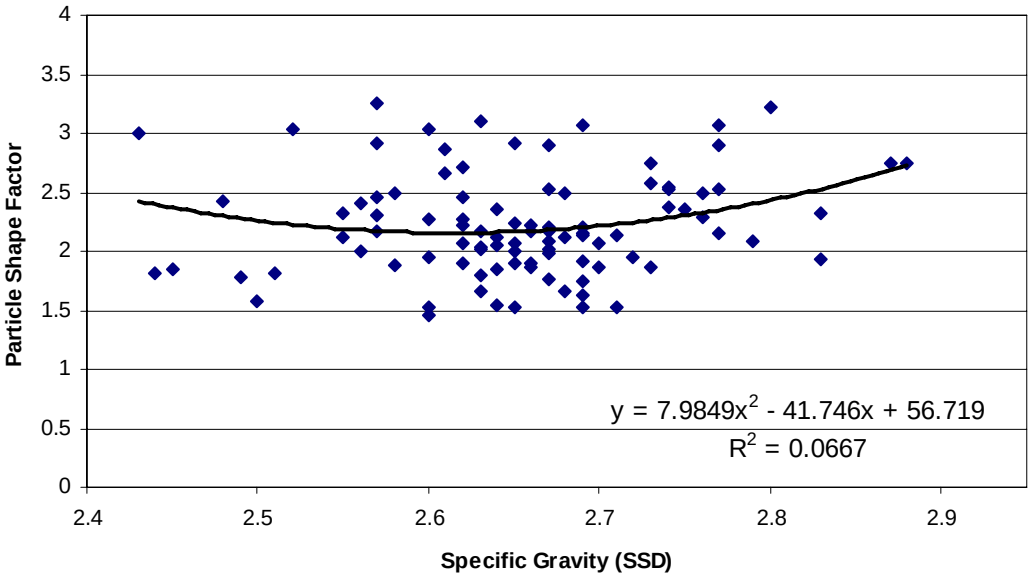

Figure G.54: Particle Shape Factor vs. Specific Gravity (SSD)

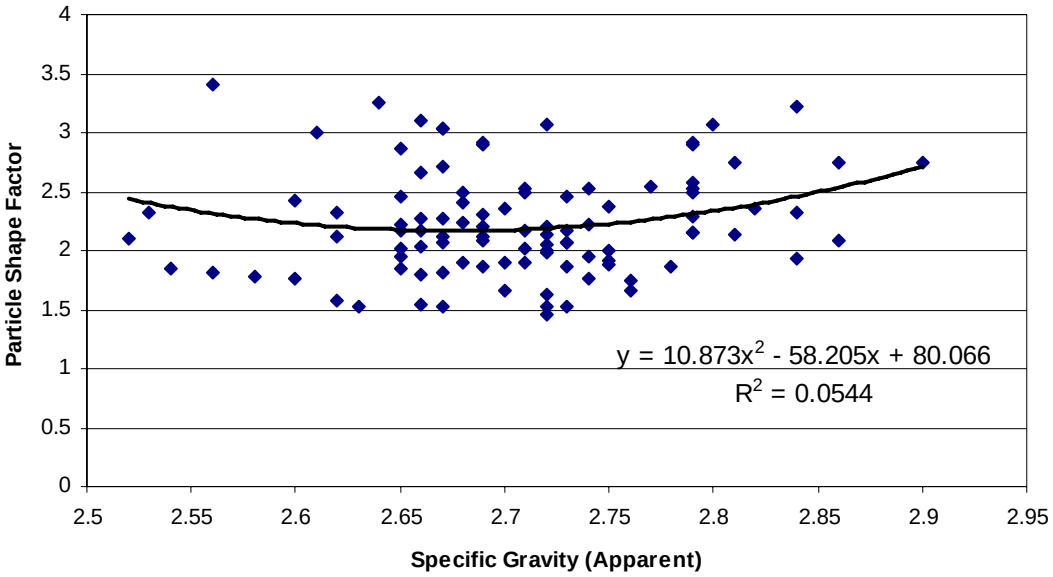

Figure G.55: Particle Shape Factor vs. Specific Gravity (Apparent)

Appendix H: Test Correlation Tables for Full Data Set, Partial Data Set I, and Partial Data Set II

ID #	MD	MSS	LAA	CFT	ACV	WCV	ABS	SG_{BULK}	SG_{SSD}	SG_{APP}	PSF
AB-1	17.0	12.2	31	7.0	20	19.00	1.6	2.58	2.63	2.70	1.66
AL-1	19.2	68.9	66	3.1	27	30.00	2.4	2.44	2.49	2.58	1.78
AL-2	29.5	70.3	57	4.9	25	26.00	2.9	2.43	2.50	2.62	1.57
AL-3	22.2	23.9	29	5.8	22	24.50	2.2	2.51	2.57	2.66	2.17
AL-4	9.7	1.1	21	2.4	20	19.65	0.6	2.75	2.76	2.79	2.29
AL-5	11.0	3.0	26	2.8	21	24.00	0.7	2.67	2.69	2.72	3.06
AZ-1	13.1	2.7	14	2.2	14	16.00	1.3	2.76	2.79	2.86	2.09
AZ-2	27.6	15.6	13	9.3	16	19.00	2.2	2.83	2.89	3.01	1.76
AZ-3	4.2	2.6	21	2.5	15	17.00	0.8	2.57	2.60	2.63	1.53
AZ-4	7.1	3.6	14	3.5	12	14.00	1.1	2.70	2.73	2.78	1.86
BC-1	10.3	5.9	15	6.0	14	15.80	0.7	2.72	2.74	2.77	2.55
BC-2	12.6	10.0	31	3.5	24	24.20	0.8	2.59	2.62	2.65	2.22
DE-1	8.8	2.1	18	2.6	18	19.80	0.5	2.76	2.77	2.80	3.07
DE-2	8.6	1.1	17	2.0	15	16.83	0.3	2.76	2.77	2.79	2.53
DE-3	9.1	1.8	27	2.0	23	23.00	0.5	2.63	2.65	2.67	1.53
DE-4	16.9	3.9	14	7.1	16	16.70	0.9	2.59	2.61	2.65	2.86
FL-1	27.0	12.4	32	6.6	29	28.00	3.4	2.36	2.44	2.56	1.81
GA-1	7.3	0.4	15	2.1	13	15.00	0.3	2.82	2.83	2.84	2.33
GA-2	13.7	4.6	59	2.4	28	31.00	0.8	2.63	2.65	2.69	2.91
GA-3	9.0	3.7	62	2.3	32	31.25	0.7	2.61	2.63	2.66	3.10
GA-4	9.5	6.1	57	2.0	32	32.95	0.5	2.65	2.66	2.68	1.90
GA-5	6.4	1.4	37	1.1	24	26.00	0.5	2.61	2.63	2.65	2.17
GA-6	7.9	1.5	52	1.6	26	28.00	0.5	2.63	2.64	2.66	1.54
IN-1	48.8	69.4	34	22.4	26	24.00	5.0	2.45	2.57	2.79	2.91
KS-1	19.6		24	5.0	46	50.15					3.19
KS-2	14.8	12.9	35	3.0	26	7.60	1.0	2.60	2.62	2.67	2.71
LA-1	3.1	0.7	15	2.3	15	16.00	0.6	2.62	2.63	2.66	1.80
LA-2	21.5	6.0	27	2.3	30	27.00	3.3	2.32	2.40	2.52	2.10
MB-1	21.4	10.5	31	1.5	26	26.65	3.8	2.42	2.52	2.67	3.03
MB-2	7.8	9.1	19	5.7	16	18.50	1.5	2.71	2.75	2.82	2.36
MB-3	12.5	4.8	24	2.4	19	20.35	1.8	2.59	2.64	2.72	2.05
MD-1	11.7	1.9	21	1.6	18	20.00	0.3	3.01	3.02	3.05	2.36
MD-2	15.6	1.9	13	5.8	13	15.87	0.4	2.66	2.67	2.69	2.90
MD-3	19.3	5.1	42	3.4	26	25.93	0.3	2.88	2.88	2.90	2.75
MD-4	22.5	8.1	34	2.6	23	23.00	0.7	2.67	2.69	2.72	1.63
ME-1	10.5	3.4	45	1.7	30	31.15	0.7	2.61	2.62	2.65	2.46
ME-2	23.0	0.6	16	1.3	16	17.30	0.5	2.90	2.91	2.94	3.19
ME-3	19.8	9.0	23	4.6	20	18.00	1.1	2.66	2.69	2.74	3.71
MN-1	19.0	22.0	35	3.2	25	23.00	2.7	2.53	2.60	2.72	1.46
MN-2	4.4	0.3	18	1.6	17	17.10	0.3	2.73	2.74	2.75	2.38
MO-1	13.7	6.4	25	9.0	23	21.93	0.8	2.65	2.67	2.71	2.53
MO-2	21.9	3.8	29	2.5	25	24.40	0.9	2.59	2.61	2.66	2.66
MO-3	9.8	6.9	20	10.4	20	22.80	1.3	2.69	2.73	2.79	2.57
MO-4	13.1	8.3	25	6.8	23	21.00	0.8	2.67	2.69	2.72	1.53
MO-5	14.8	10.0	24	7.5	23	24.80	1.0	2.64	2.67	2.71	2.17
MO-6	16.9	8.7	25	9.1	22	20.65	1.0	2.64	2.66	2.74	2.22

MO-7	21.6	23.8	29	8.8	22	20.00	2.2	2.59	2.65	2.75	2.00
MS-1	1.6	6.6	16	3.9	11	10.00	3.1	2.40	2.48	2.60	2.43
MS-2	1.4	3.5	16	3.6	13	12.00	1.8	2.51	2.55	2.62	2.12
NB-1	16.4	4.9	16	6.0	16	19.80	0.7	2.79	2.80	2.84	3.22
NC-1	7.3	1.5	36	1.0	27	27.80	0.4	2.62	2.63	2.65	2.01
NC-2	17.3	2.7	17	1.3	16	18.65	0.2	2.88	2.87	2.86	2.75
NC-3	20.6	1.3	21	2.4	19	23.35	0.4	2.75	2.77	2.79	2.89
NC-4	34.3	20.0	45	3.1	41	44.40	4.5	2.27	2.37	2.53	2.32
ND-1	4.0	3.2	18	3.5	13	13.00	1.0	2.65	2.67	2.72	1.98
ND-2	24.2	36.7	27	14.8	21	20.00	4.0	2.41	2.51	2.67	1.81
ND-3	3.7	2.1	15	2.9	15	13.00	0.8	2.60	2.62	2.66	2.27
ND-4	8.3	9.7	22	4.0	16	18.00	1.3	2.65	2.69	2.75	1.92
NE-1	26.9	28.3	32	8.8	24	23.00	2.9	2.49	2.56	2.68	2.40
NM-1	8.0	7.4	43	2.9	31	32.30	2.2	2.63	2.69	2.79	2.16
NM-2	21.0	14.8	22	6.3	21	19.00	0.8	2.65	2.67	2.71	2.02
NM-3	23.1	7.4	31	6.4	30	32.50	5.7	2.26	2.39	2.60	1.77
NM-4	9.9	4.2	22	2.4	22	22.50	0.7	2.63	2.65	2.68	2.24
NM-5	5.5	0.7	24	5.8	19	16.90	0.2	2.67	2.68	2.69	2.12
NV-1	10.3	3.4	12	2.9	13	15.00	1.8	2.55	2.60	2.67	2.27
NV-2	13.6	4.5	11	3.3	15	14.00	2.1	2.66	2.71	2.81	2.13
NV-3	12.3	1.2	23	3.8	21	20.05	0.5	2.75	2.77	2.79	2.15
NY-1	13.9	12.1	16	3.5	13	15.00	1.7	2.58	2.62	2.70	1.89
NY-2	7.4	1.0	14	1.5	15	17.00	0.9	2.88	2.90	2.96	2.37
NY-3	9.4	1.1	19	3.7	20	18.00	0.3	2.72	2.72	2.74	1.95
NY-4	21.8	6.0	17	3.5	17	15.00	1.5	2.62	2.66	2.73	2.17
NY-5	30.9	39.0	26	6.6	21	22.80	2.9	2.49	2.57	2.69	2.30
OH-1	12.1	5.9	18	8.4	20	20.00	0.4	2.70	2.71	2.73	1.52
OH-2	18.2	16.9	25	12.1	25	22.00	0.6	2.69	2.70	2.73	1.87
OH-3	14.4	5.5	22	10.3	22	24.85	0.6	2.68	2.70	2.73	2.06
OH-4	27.4	17.7	27	8.2	19	18.00	3.7	2.49	2.58	2.75	1.88
OH-5	17.7	20.8	27	3.6	21	25.00	3.8	2.47	2.57	2.73	2.46
OH-6	20.4	12.6	32	4.3	22	22.00	3.7	2.47	2.56	2.72	2.00
OH-7	9.0	6.7	22	2.5	12	15.00	1.7	2.63	2.68	2.76	1.66
OH-8	18.6	11.9	26	4.4	19	24.00	1.8	2.61	2.65	2.73	2.07
ON-1	19.1	16.3	24	10.6	23	22.40	0.6	2.67	2.68	2.71	2.50
ON-2	7.7	1.3	33	1.7	28	27.40	0.5	2.66	2.67	2.69	2.21
ON-3	8.7	2.0	38	1.3	28	28.95	0.5	2.66	2.67	2.69	2.08
ON-4	5.4	1.0	14	1.4	13	15.05	0.1	2.73	2.74	2.74	2.53
ON-5	13.9	6.9	23	4.5	20	20.95	1.4	2.60	2.64	2.70	2.36
ON-6	28.9	39.1	36	10.1	24	24.15	2.5	2.39	2.45	2.54	1.84
ON-7	12.5	15.7	37	4.2	25	24.70	0.9	2.63	2.66	2.70	3.82
ON-8	10.0	2.8	26	3.4	26	25.80	0.3	2.82	2.83	2.84	1.94
ON-10	19.6	18.8	32	12.9	27	30.30	0.8	2.67	2.69	2.72	2.21
ON-11	9.9	6.4	22	2.7	19	19.60	1.3	2.64	2.67	2.74	1.76
ON-12	17.3	18.7	26	8.4	22	22.45	4.7	2.32	2.43	2.61	3.00
ON-13	27.8	31.2	18	13.7	16	20.35	1.7	2.68	2.73	2.81	2.74
OR-1	10.9	6.3	24	2.9	23	26.45	2.3	2.52	2.58	2.68	2.50
QC-1	10.7	8.3	31	4.8	23	27.00	0.6	2.64	2.66	2.69	1.86

SC-1	4.4	0.8	23	1.1	18	21.00	0.7	2.61	2.63	2.66	2.03
SC-2	19.6	5.4	52	1.9	26	32.00	0.7	2.74	2.76	2.79	2.49
SC-3	39.3	30.9	56	3.6	48	45.00	4.7	2.29	2.40	2.56	3.41
SD-1	22.6	22.0	29	10.8	24	23.40	2.2	2.54	2.59	2.69	4.27
SD-2	3.1	1.8	18	0.6	17	15.00	0.3	2.63	2.64	2.65	1.84
TN-1	10.6	9.4	34	1.1	21	21.00	2.0	2.57	2.60	2.65	1.95
TN-2	14.2	13.8	27	3.3	17	17.30	2.0	2.51	2.56	2.65	5.19
TX-2	20.3	13.5	34	2.0	18		2.4	2.21	2.26	2.33	2.05
TX-3	12.4	3.5	23	4.3	22	20.90	0.6	2.67	2.69	2.72	2.14
UT-1	16.7	8.3	30	2.8	22	20.00	1.6	2.64	2.69	2.76	1.74
UT-2	6.7	3.5	20	0.9	13	14.00	1.6	2.51	2.55	2.62	2.32
VT-1	22.4	5.0	28	2.9	20	19.00	0.7	2.72	2.74	2.77	3.91
VT-2	7.1	1.9	34	1.3	22	25.00	0.7	2.62	2.64	2.67	2.12
WA-1	8.6	5.9	28	2.5	23	25.00	1.0	2.60	2.62	2.67	2.06
WV-1	14.5	1.9	22	4.7	20	19.00	1.3	2.62	2.65	2.71	1.90
WV-2	9.7	9.2	25	3.6	17	15.00	1.7	2.53	2.57	2.64	3.25
WV-3	30.4	33.0	35	5.6	23	21.00	1.5	2.56	2.60	2.67	3.03

Table H.1: Full Data Set

ID #	MD	MSS	LAA	CFT	ACV	WCV	ABS	SG_{BULK}	SG_{SSD}	SG_{APP}	PSF
AB-1	17	12.2	31	7	20	19	1.6	2.58	2.63	2.7	1.66
AL-1	19.2			3.1	27	30	2.4	2.44	2.49	2.58	1.78
AL-2	29.5		57	4.9	25	26	2.9	2.43	2.5	2.62	1.57
AL-3	22.2	23.9	29	5.75	22	24.5	2.2	2.51	2.57	2.66	2.17
AL-4	9.7	1.1	21	2.375	20	19.65	0.6	2.75	2.76	2.79	2.29
AL-5	11	3	26	2.8	21	24	0.7	2.67	2.69	2.72	3.06
AZ-1	13.1	2.7	14	2.2	14	16	1.3	2.76	2.79	2.86	2.09
AZ-2	27.6	15.6	13	9.3	16	19	2.2	2.83	2.89		1.76
AZ-3	4.2	2.6	21	2.5	15	17	0.8	2.57	2.6	2.63	1.53
AZ-4	7.1	3.6	14	3.5	12	14	1.1	2.7	2.73	2.78	1.86
BC-1	10.3	5.9	15	6	14	15.8	0.7	2.72	2.74	2.77	2.55
BC-2	12.6	10	31	3.45	24	24.2	0.8	2.59	2.62	2.65	2.22
DE-1	8.8	2.1	18	2.55	18	19.8	0.5	2.76	2.77	2.8	3.07
DE-2	8.6	1.1	17	1.95	15	16.833	0.3	2.76	2.77	2.79	2.53
DE-3	9.1	1.8	27	2	23	23	0.5	2.63	2.65	2.67	1.53
DE-4	16.9	3.9	14	7.1	16	16.7	0.9	2.59	2.61	2.65	2.86
FL-1	27	12.4	32	6.6	29	28	3.4	2.36	2.44	2.56	1.81
GA-1	7.3	0.4	15	2.1	13	15	0.3	2.82	2.83	2.84	2.33
GA-2	13.7	4.6	59	2.4	28	31	0.8	2.63	2.65	2.69	2.91
GA-3	9	3.7		2.25	32	31.25	0.7	2.61	2.63	2.66	3.1
GA-4	9.5	6.1	57	2	32	32.95	0.5	2.65	2.66	2.68	1.9
GA-5	6.4	1.4	37	1.1	24	26	0.5	2.61	2.63	2.65	2.17
GA-6	7.9	1.5	52	1.6	26	28	0.5	2.63	2.64	2.66	1.54
IN-1			34		26	24	5	2.45	2.57	2.79	2.91
KS-1	19.6		24	4.95							3.19
KS-2	14.8	12.9	35	3	26	7.6	1	2.6	2.62	2.67	2.71
LA-1	3.1	0.7	15	2.3	15	16	0.6	2.62	2.63	2.66	1.8
LA-2	21.5	6	27	2.3	30	27	3.3	2.32	2.4	2.52	2.1
MB-1	21.4	10.5	31	1.45	26	26.65	3.8	2.42	2.52	2.67	3.03
MB-2	7.8	9.1	19	5.65	16	18.5	1.5	2.71	2.75	2.82	2.36
MB-3	12.5	4.8	24	2.4	19	20.35	1.8	2.59	2.64	2.72	2.05
MD-1	11.	1.9	21	1.6	18	20	0.3	3.01			2.36

	7										
MD-2	15.6	1.9	13	5.8	13	15.867	0.4	2.66	2.67	2.69	2.9
MD-3	19.3	5.1	42	3.4	26	25.933	0.3	2.88	2.88	2.9	2.75
MD-4	22.5	8.1	34	2.6	23	23	0.7	2.67	2.69	2.72	1.63
ME-1	10.5	3.4	45	1.65	30	31.15	0.7	2.61	2.62	2.65	2.46
ME-2	23	0.6	16	1.25	16	17.3	0.5	2.9	2.91	2.94	3.19
ME-3	19.8	9	23	4.6	20	18	1.1	2.66	2.69	2.74	3.71
MN-1	19	22	35	3.2	25	23	2.7	2.53	2.6	2.72	1.46
MN-2	4.4	0.3	18	1.55	17	17.1	0.3	2.73	2.74	2.75	2.38
MO-1	13.7	6.4	25	8.95	23	21.933	0.8	2.65	2.67	2.71	2.53
MO-2	21.9	3.8	29	2.5	25	24.4	0.9	2.59	2.61	2.66	2.66
MO-3	9.8	6.9	20	10.4	20	22.8	1.3	2.69	2.73	2.79	2.57
MO-4	13.1	8.3	25	6.8	23	21	0.8	2.67	2.69	2.72	1.53
MO-5	14.8	10	24	7.5	23	24.8	1	2.64	2.67	2.71	2.17
MO-6	16.9	8.7	25	9.05	22	20.65	1	2.64	2.66	2.74	2.22
MO-7	21.6	23.8	29	8.8	22	20	2.2	2.59	2.65	2.75	2
MS-1	1.6	6.6	16	3.9	11	10	3.1	2.4	2.48	2.6	2.43
MS-2	1.4	3.5	16	3.6	13	12	1.8	2.51	2.55	2.62	2.12
NB-1	16.4	4.9	16	6	16	19.8	0.7	2.79	2.8	2.84	3.22
NC-1	7.3	1.5	36	1	27	27.8	0.4	2.62	2.63	2.65	2.01
NC-2	17.3	2.7	17	1.3	16	18.65	0.2	2.88	2.87	2.86	2.75
NC-3	20.6	1.3	21	2.35	19	23.35	0.4	2.75	2.77	2.79	2.89
NC-4	34.3	20	45	3.05			4.5	2.27	2.37	2.53	2.32
ND-1	4	3.2	18	3.5	13	13	1	2.65	2.67	2.72	1.98
ND-2	24.2	36.7	27	14.8	21	20	4	2.41	2.51	2.67	1.81
ND-3	3.7	2.1	15	2.9	15	13	0.8	2.6	2.62	2.66	2.27
ND-4	8.3	9.7	22	4	16	18	1.3	2.65	2.69	2.75	1.92
NE-1	26.9	28.3	32	8.8	24	23	2.9	2.49	2.56	2.68	2.4
NM-1	8	7.4	43	2.85	31	32.3	2.2	2.63	2.69	2.79	2.16
NM-2	21	14.8	22	6.3	21	19	0.8	2.65	2.67	2.71	2.02
NM-3	23.1	7.4	31	6.35	30	32.5		2.26	2.39	2.6	1.77
NM-4	9.9	4.2	22	2.35	22	22.5	0.7	2.63	2.65	2.68	2.24
NM-5	5.5	0.7	24	5.75	19	16.9	0.2	2.67	2.68	2.69	2.12

NV-1	10.3	3.4	12	2.9	13	15	1.8	2.55	2.6	2.67	2.27
NV-2	13.6	4.5	11	3.3	15	14	2.1	2.66	2.71	2.81	2.13
NV-3	12.3	1.2	23	3.75	21	20.05	0.5	2.75	2.77	2.79	2.15
NY-1	13.9	12.1	16	3.5	13	15	1.7	2.58	2.62	2.7	1.89
NY-2	7.4	1	14	1.5	15	17	0.9	2.88	2.9	2.96	2.37
NY-3	9.4	1.1	19	3.7	20	18	0.3	2.72	2.72	2.74	1.95
NY-4	21.8	6	17	3.5	17	15	1.5	2.62	2.66	2.73	2.17
NY-5	30.9	39	26	6.6	21	22.8	2.9	2.49	2.57	2.69	2.3
OH-1	12.1	5.9	18	8.4	20	20	0.4	2.7	2.71	2.73	1.52
OH-2	18.2	16.9	25	12.1	25	22	0.6	2.69	2.7	2.73	1.87
OH-3	14.4	5.5	22	10.25	22	24.85	0.6	2.68	2.7	2.73	2.06
OH-4	27.4	17.7	27	8.2	19	18	3.7	2.49	2.58	2.75	1.88
OH-5	17.7	20.8	27	3.6	21	25	3.8	2.47	2.57	2.73	2.46
OH-6	20.4	12.6	32	4.3	22	22	3.7	2.47	2.56	2.72	2
OH-7	9	6.7	22	2.5	12	15	1.7	2.63	2.68	2.76	1.66
OH-8	18.6	11.9	26	4.4	19	24	1.8	2.61	2.65	2.73	2.07
ON-1	19.1	16.3	24	10.55	23	22.4	0.6	2.67	2.68	2.71	2.5
ON-2	7.7	1.3	33	1.7	28	27.4	0.5	2.66	2.67	2.69	2.21
ON-3	8.7	2	38	1.3	28	28.95	0.5	2.66	2.67	2.69	2.08
ON-4	5.4	1	14	1.4	13	15.05	0.1	2.73	2.74	2.74	2.53
ON-5	13.9	6.9	23	4.5	20	20.95	1.4	2.6	2.64	2.7	2.36
ON-6	28.9	39.1	36	10.1	24	24.15	2.5	2.39	2.45	2.54	1.84
ON-7	12.5	15.7	37	4.2	25	24.7	0.9	2.63	2.66	2.7	3.82
ON-8	10	2.8	26	3.35	26	25.8	0.3	2.82	2.83	2.84	1.94
ON-10	19.6	18.8	32	12.9	27	30.3	0.8	2.67	2.69	2.72	2.21
ON-11	9.9	6.4	22	2.7	19	19.6	1.3	2.64	2.67	2.74	1.76
ON-12	17.3	18.7	26	8.4	22	22.45	4.7	2.32	2.43	2.61	3
ON-13	27.8	31.2	18	13.7	16	20.35	1.7	2.68	2.73	2.81	2.74
OR-1	10.9	6.3	24	2.9	23	26.45	2.3	2.52	2.58	2.68	2.5

QC-1	10.7	8.3	31	4.8	23	27	0.6	2.64	2.66	2.69	1.86
SC-1	4.4	0.8	23	1.1	18	21	0.7	2.61	2.63	2.66	2.03
SC-2	19.6	5.4	52	1.9	26	32	0.7	2.74	2.76	2.79	2.49
SC-3	39.3	30.9	56	3.6			4.7	2.29	2.4	2.56	3.41
SD-1	22.6	22	29	10.8	24	23.4	2.2	2.54	2.59	2.69	
SD-2	3.1	1.8	18	0.6	17	15	0.3	2.63	2.64	2.65	1.84
TN-1	10.6	9.4	34	1.1	21	21	2	2.57	2.6	2.65	1.95
TN-2	14.2	13.8	27	3.25	17	17.3	2	2.51	2.56	2.65	
TX-2	20.3	13.5	34	2	18		2.4	2.21			2.05
TX-3	12.4	3.5	23	4.275	22	20.9	0.6	2.67	2.69	2.72	2.14
UT-1	16.7	8.3	30	2.8	22	20	1.6	2.64	2.69	2.76	1.74
UT-2	6.7	3.5	20	0.9	13	14	1.6	2.51	2.55	2.62	2.32
VT-1	22.4	5	28	2.9	20	19	0.7	2.72	2.74	2.77	3.91
VT-2	7.1	1.9	34	1.3	22	25	0.7	2.62	2.64	2.67	2.12
WA-1	8.6	5.9	28	2.5	23	25	1	2.6	2.62	2.67	2.06
WV-1	14.5	1.9	22	4.7	20	19	1.3	2.62	2.65	2.71	1.9
WV-2	9.7	9.2	25	3.6	17	15	1.7	2.53	2.57	2.64	3.25
WV-3	30.4	33	35	5.6	23	21	1.5	2.56	2.6	2.67	3.03

Table H.2: Partial Data Set I

ID #	MD	MSS	LAA	CFT	ACV	WCV	ABS	SG_{BULK}	SG_{SSD}	SG_{APP}	PSF
AB-1	17	12.2	31	7	20	19	1.6	2.58	2.63	2.7	1.66
AL-1	19.2			3.1	27	30	2.4	2.44	2.49	2.58	1.78
AL-2	29.5			4.9	25	26	2.9	2.43	2.5	2.62	1.57
AL-3	22.2	23.9	29	5.75	22	24.5	2.2	2.51	2.57	2.66	2.17
AL-4	9.7	1.1	21	2.375	20	19.65	0.6	2.75	2.76	2.79	2.29
AL-5	11	3	26	2.8	21	24	0.7	2.67	2.69	2.72	3.06
AZ-1	13.1	2.7	14	2.2	14	16	1.3	2.76	2.79	2.86	2.09
AZ-2	27.6	15.6	13	9.3	16	19	2.2	2.83			1.76
AZ-3	4.2	2.6	21	2.5	15	17	0.8	2.57	2.6	2.63	1.53
AZ-4	7.1	3.6	14	3.5	12	14	1.1	2.7	2.73	2.78	1.86
BC-1	10.3	5.9	15	6	14	15.8	0.7	2.72	2.74	2.77	2.55
BC-2	12.6	10	31	3.45	24	24.2	0.8	2.59	2.62	2.65	2.22
DE-1	8.8	2.1	18	2.55	18	19.8	0.5	2.76	2.77	2.8	3.07
DE-2	8.6	1.1	17	1.95	15	16.833	0.3	2.76	2.77	2.79	2.53
DE-3	9.1	1.8	27	2	23	23	0.5	2.63	2.65	2.67	1.53
DE-4	16.9	3.9	14	7.1	16	16.7	0.9	2.59	2.61	2.65	2.86
FL-1	27	12.4	32	6.6	29	28	3.4	2.36	2.44	2.56	1.81
GA-1	7.3	0.4	15	2.1	13	15	0.3	2.82	2.83	2.84	2.33
GA-2	13.7	4.6		2.4	28	31	0.8	2.63	2.65	2.69	2.91
GA-3	9	3.7		2.25	32	31.25	0.7	2.61	2.63	2.66	3.1
GA-4	9.5	6.1		2	32	32.95	0.5	2.65	2.66	2.68	1.9
GA-5	6.4	1.4	37	1.1	24	26	0.5	2.61	2.63	2.65	2.17
GA-6	7.9	1.5		1.6	26	28	0.5	2.63	2.64	2.66	1.54
IN-1			34		26	24		2.45	2.57	2.79	2.91
KS-1	19.6		24	4.95							3.19
KS-2	14.8	12.9	35	3	26		1	2.6	2.62	2.67	2.71
LA-1	3.1	0.7	15	2.3	15	16	0.6	2.62	2.63	2.66	1.8
LA-2	21.5	6	27	2.3	30	27	3.3			2.52	2.1
MB-1	21.4	10.5	31	1.45	26	26.65	3.8	2.42	2.52	2.67	3.03
MB-2	7.8	9.1	19	5.65	16	18.5	1.5	2.71	2.75	2.82	2.36
MB-3	12.5	4.8	24	2.4	19	20.35	1.8	2.59	2.64	2.72	2.05
MD-1	11.7	1.9	21	1.6	18	20	0.3				2.36
MD-2	15.6	1.9	13	5.8	13	15.867	0.4	2.66	2.67	2.69	2.9
MD-3	19.3	5.1	42	3.4	26	25.933	0.3	2.88	2.88	2.9	2.75
MD-4	22.5	8.1	34	2.6	23	23	0.7	2.67	2.69	2.72	1.63
ME-1	10.5	3.4	45	1.65	30	31.15	0.7	2.61	2.62	2.65	2.46
ME-2	23	0.6	16	1.25	16	17.3	0.5				3.19
ME-3	19.8	9	23	4.6	20	18	1.1	2.66	2.69	2.74	
MN-1	19	22	35	3.2	25	23	2.7	2.53	2.6	2.72	1.46
MN-2	4.4	0.3	18	1.55	17	17.1	0.3	2.73	2.74	2.75	2.38
MO-1	13.7	6.4	25	8.95	23	21.933	0.8	2.65	2.67	2.71	2.53
MO-2	21.9	3.8	29	2.5	25	24.4	0.9	2.59	2.61	2.66	2.66
MO-3	9.8	6.9	20	10.4	20	22.8	1.3	2.69	2.73	2.79	2.57
MO-4	13.1	8.3	25	6.8	23	21	0.8	2.67	2.69	2.72	1.53
MO-5	14.8	10	24	7.5	23	24.8	1	2.64	2.67	2.71	2.17

MO-6	16.9	8.7	25	9.05	22	20.65	1	2.64	2.66	2.74	2.22
MO-7	21.6	23.8	29	8.8	22	20	2.2	2.59	2.65	2.75	2
MS-1	1.6	6.6	16	3.9	11	10	3.1	2.4	2.48	2.6	2.43
MS-2	1.4	3.5	16	3.6	13	12	1.8	2.51	2.55	2.62	2.12
NB-1	16.4	4.9	16	6	16	19.8	0.7	2.79	2.8	2.84	3.22
NC-1	7.3	1.5	36	1	27	27.8	0.4	2.62	2.63	2.65	2.01
NC-2	17.3	2.7	17	1.3	16	18.65	0.2	2.88	2.87	2.86	2.75
NC-3	20.6	1.3	21	2.35	19	23.35	0.4	2.75	2.77	2.79	2.89
NC-4		20	45	3.05						2.53	2.32
ND-1	4	3.2	18	3.5	13	13	1	2.65	2.67	2.72	1.98
ND-2	24.2	36.7	27		21	20		2.41	2.51	2.67	1.81
ND-3	3.7	2.1	15	2.9	15	13	0.8	2.6	2.62	2.66	2.27
ND-4	8.3	9.7	22	4	16	18	1.3	2.65	2.69	2.75	1.92
NE-1	26.9	28.3	32	8.8	24	23	2.9	2.49	2.56	2.68	2.4
NM-1	8	7.4	43	2.85	31	32.3	2.2	2.63	2.69	2.79	2.16
NM-2	21	14.8	22	6.3	21	19	0.8	2.65	2.67	2.71	2.02
NM-3	23.1	7.4	31	6.35	30	32.5				2.6	1.77
NM-4	9.9	4.2	22	2.35	22	22.5	0.7	2.63	2.65	2.68	2.24
NM-5	5.5	0.7	24	5.75	19	16.9	0.2	2.67	2.68	2.69	2.12
NV-1	10.3	3.4	12	2.9	13	15	1.8	2.55	2.6	2.67	2.27
NV-2	13.6	4.5	11	3.3	15	14	2.1	2.66	2.71	2.81	2.13
NV-3	12.3	1.2	23	3.75	21	20.05	0.5	2.75	2.77	2.79	2.15
NY-1	13.9	12.1	16	3.5	13	15	1.7	2.58	2.62	2.7	1.89
NY-2	7.4	1	14	1.5	15	17	0.9	2.88			2.37
NY-3	9.4	1.1	19	3.7	20	18	0.3	2.72	2.72	2.74	1.95
NY-4	21.8	6	17	3.5	17	15	1.5	2.62	2.66	2.73	2.17
NY-5	30.9		26	6.6	21	22.8	2.9	2.49	2.57	2.69	2.3
OH-1	12.1	5.9	18	8.4	20	20	0.4	2.7	2.71	2.73	1.52
OH-2	18.2	16.9	25		25	22	0.6	2.69	2.7	2.73	1.87
OH-3	14.4	5.5	22	10.25	22	24.85	0.6	2.68	2.7	2.73	2.06
OH-4	27.4	17.7	27	8.2	19	18	3.7	2.49	2.58	2.75	1.88
OH-5	17.7	20.8	27	3.6	21	25	3.8	2.47	2.57	2.73	2.46
OH-6	20.4	12.6	32	4.3	22	22	3.7	2.47	2.56	2.72	2
OH-7	9	6.7	22	2.5	12	15	1.7	2.63	2.68	2.76	1.66
OH-8	18.6	11.9	26	4.4	19	24	1.8	2.61	2.65	2.73	2.07
ON-1	19.1	16.3	24	10.55	23	22.4	0.6	2.67	2.68	2.71	2.5
ON-2	7.7	1.3	33	1.7	28	27.4	0.5	2.66	2.67	2.69	2.21
ON-3	8.7	2	38	1.3	28	28.95	0.5	2.66	2.67	2.69	2.08
ON-4	5.4	1	14	1.4	13	15.05	0.1	2.73	2.74	2.74	2.53
ON-5	13.9	6.9	23	4.5	20	20.95	1.4	2.6	2.64	2.7	2.36
ON-6	28.9		36	10.1	24	24.15	2.5	2.39	2.45	2.54	1.84
ON-7	12.5	15.7	37	4.2	25	24.7	0.9	2.63	2.66	2.7	
ON-8	10	2.8	26	3.35	26	25.8	0.3	2.82	2.83	2.84	1.94
ON-10	19.6	18.8	32		27	30.3	0.8	2.67	2.69	2.72	2.21
ON-11	9.9	6.4	22	2.7	19	19.6	1.3	2.64	2.67	2.74	1.76
ON-12	17.3	18.7	26	8.4	22	22.45			2.43	2.61	3
ON-13	27.8	31.2	18		16	20.35	1.7	2.68	2.73	2.81	2.74
OR-1	10.9	6.3	24	2.9	23	26.45	2.3	2.52	2.58	2.68	2.5

QC-1	10.7	8.3	31	4.8	23	27	0.6	2.64	2.66	2.69	1.86
SC-1	4.4	0.8	23	1.1	18	21	0.7	2.61	2.63	2.66	2.03
SC-2	19.6	5.4		1.9	26	32	0.7	2.74	2.76	2.79	2.49
SC-3		30.9		3.6						2.56	3.41
SD-1	22.6	22	29	10.8	24	23.4	2.2	2.54	2.59	2.69	
SD-2	3.1	1.8	18	0.6	17	15	0.3	2.63	2.64	2.65	1.84
TN-1	10.6	9.4	34	1.1	21	21	2	2.57	2.6	2.65	1.95
TN-2	14.2	13.8	27	3.25	17	17.3	2	2.51	2.56	2.65	
TX-2	20.3	13.5	34	2	18		2.4				2.05
TX-3	12.4	3.5	23	4.275	22	20.9	0.6	2.67	2.69	2.72	2.14
UT-1	16.7	8.3	30	2.8	22	20	1.6	2.64	2.69	2.76	1.74
UT-2	6.7	3.5	20	0.9	13	14	1.6	2.51	2.55	2.62	2.32
VT-1	22.4	5	28	2.9	20	19	0.7	2.72	2.74	2.77	
VT-2	7.1	1.9	34	1.3	22	25	0.7	2.62	2.64	2.67	2.12
WA-1	8.6	5.9	28	2.5	23	25	1	2.6	2.62	2.67	2.06
WV-1	14.5	1.9	22	4.7	20	19	1.3	2.62	2.65	2.71	1.9
WV-2	9.7	9.2	25	3.6	17	15	1.7	2.53	2.57	2.64	3.25
WV-3	30.4	33	35	5.6	23	21	1.5	2.56	2.6	2.67	3.03

Table H.3: Partial Data Set II

The vita has been removed from the reformatted version of this document.